POLYTECHNIQUE MONTRÉAL

affiliée à l'Université de Montréal

Transience of Bank Filtration in Snowmelt-dominated Basins: from Tracer-based Characterization to Monitoring and Operational Strategies

JANIE MASSE-DUFRESNE

Département des génies civil, géologique et des mines

Thèse présentée en vue de l'obtention du diplôme de *Philosophiæ Doctor*

Génie minéral

Novembre 2021

© Janie Masse-Dufresne, 2021.

POLYTECHNIQUE MONTRÉAL

affiliée à l'Université de Montréal

Cette thèse intitulée:

Transience of Bank Filtration in Snowmelt-dominated Basins: from Tracer-based Characterization to Monitoring and Operational Strategies

Présentée par **Janie MASSE-DUFRESNE**

en vue de l'obtention du diplôme de *Philosophiæ Doctor*

a été dûment acceptée par le jury d'examen constitué de :

Françoise BICHAI, Ph.D, présidente
Paul BAUDRON, Ph.D, membre et directeur de recherche
Florent BARBECOT, Ph.D, membre et codirecteur de recherche
Philippe PASQUIER, Ph.D, membre et codirecteur de recherche
Janek GRESKOWIAK, Ph.D, membre externe
Patrick LACHASSAGNE, Ph.D, membre

DEDICATION

To my family

À ma famille

ACKNOWLEDGEMENTS

English version

Many thanks to my supervisor, Paul Baudron, for sparking my curiosity for hydrogeochemistry, providing my very first research opportunity during an internship in 2015, and encouraging me to fast-tracking to a doctoral program. Thank you for creating a welcoming work environment favourable to exchange and creativity. Thank you for facilitating the planning and execution of more than 60 field campaigns during which you showed me your confidence by letting me discover a variety of hydrogeochemical and isotopic tools. Thanks for the flexibility you gave me in defining the objectives of my project. Thank you for your contagious enthusiasm towards all the data, graphs and ideas that I presented to you during our working meetings. Thank you for your support and impressive availability during the many "sprints" that punctuated my doctoral journey. I am grateful for the countless advices that, all together, allowed me to grow as a person and as a researcher in this field. Thank you for having encouraged me to seize different opportunities (conferences, teaching, student supervision) that made me discover the richness of an academic career.

Thanks to my two co-directors Florent Barbecot and Philippe Pasquier for your involvement in this project. I would like to thank Florent for your 1001 "outside the box" ideas (and questions!) that contributed not only positively to this project, but also to my academic training. Thank you for your empathy, your reassuring listening and your advices in the moments when I needed a confidence boost. Philippe, thank you for your rigorous and honest look at my project. Thank you for sharing your expertise and your passion for hydrogeology and geothermal energy. Thank you for encouraging me to develop my numerical modeling skills. Thank you also for your support in planning the timelines for the completion of my thesis. Paul, Florent and Philippe, you have all played an important and complementary role in my PhD journey. Consistent with your personal convictions, you have shown me that there are as many successful role models in research as there are researchers.

Thanks to Matthieu Menou, Francis Proteau-Bédard, Benoit Barbeau and John Gibson for collaborating on this work. Matthieu Menou and Francis Proteau-Bédard, thank you for conducting the initial field campaigns and laboratory analyses. Benoit Barbeau, thank you for your

participation in this project. Your expertise in water treatment has greatly helped me direct my work to ensure concrete benefits for the municipal partner. Thanks to John Gibson for your help in developing the stable isotope mass balance model. Learning from your expertise was a true privilege.

I warmly thank the graduate students who have offered me support and friendship along the way. Thanks to the G2H students at Polytechnique, Marc Patenaude, Coralie Pontoreau, Maximilien Delestre, Francis Proteau-Bédard, Sabine Veuille, with whom I shared days (and many discussions) in the office and in the field under all weather conditions, on foot or by pedalo! Thanks to Léo Cerclet for the exchange of ideas, the contagious laughter, the coffee breaks, and the cross-country skiing (and all other sports). Thanks to the students at UQAM, Guillaume Meyzonnat, Alexandra Mattei, Rachid Barry, Djak Aimé Djongon, with whom I shared weekly meetings for several years and during which I was able to broaden my horizons, thanks to each of your critical reviews of scientific articles on hydrogeology-related topics. A special thanks to Karine Lefebvre, Laurence Labelle and Coralie Pontoreau who shared with me and helped motivate more than 150 "co-working" sessions on *Zoom* during the pandemic.

Thanks to Jérôme Leroy, Manon Leduc, Gabriel St-Jean at Polytechnique for your precious support in the preparation of the field campaigns, the assistance in the orders of material and the realization of the geochemical analyses. Thank you also for your generous advice and all the discussions concerning good practices in the laboratory and in the field. Thanks to Marina Tcaci and Jean-François Hélie at UQAM for your help with isotopic analyses.

Thanks to Dominique Claveau-Mallet for your precious advices and suggestions for the preparation of my application files for various grants. Your discipline inspire me a lot!

Thanks to NSERC and the Town of Sainte-Marthe-sur-le-Lac for co-funding this project. I sincerely thank the employees of the Town and the treatment plant for facilitating access to the study site and the database.

Warm thanks to my roommates, Arielle, Mick, Jade, Coralie and Jean-Simon, for bringing so much joy day-to-day. Preparing dinner, doing the dishes, shoveling the snow in winter will never be as much fun as with you! Thank you also for your help with the transport of soda bottles for my field campaigns and the endless laughter during those evenings! Thank you to all my friends, Jean-

Simon, Camille, Jean-François, Émilie, who generously accompanied me in the field, even in the winter under a freezing wind!

Already thanked as a roommate and friend, thank you one last time to Jean-Simon, my lover, my accomplice. Thank you for supporting me in my choice to pursue a doctorate thesis. Thank you for all the good dinners after the fieldwork and lab days. Thank you for your calmness and all the comfort you gave me during moments of doubt!

The last word goes to my big family. A warm thank you to the members of the Dufresne family for having improvised themselves as an audience on a beautiful Sunday afternoon to practice my pre-doctoral exam. Thank you to the members of the Masse family for encouraging me since the beginning of my long academic journey (and when I arrived in The Big City!). Thank you all for your curiosity about science. It is always a pleasure to discuss my passions with you! Thanks to my parents, Dominique and Pierre, who have greatly inspired and encouraged me to follow my passions for as long as I can remember! Mom, thank you for all the confidence and pride (often exaggerated!) you have in me. Dad, I am sure you would have shared the same feelings and enjoyed reading this thesis. I am honoured that I am now working in the same field as you did. You will always be with me! Love you!

Traduction française

Merci à mon directeur de recherche, Paul Baudron, pour avoir su éveiller ma curiosité pour l'hydrogéochimie, offert ma toute première opportunité en recherche à l'occasion d'un stage en 2015 et encouragé à passer au doctorat. Merci plus particulièrement pour avoir créé un environnement de travail accueillant, propice aux échanges et à la créativité. Merci pour avoir facilité la planification et le déroulement de plus de 60 campagnes de terrain au cours desquelles tu m'as témoigné ta confiance en me laissant découvrir toute une palette d'outils d'hydrogéochimie et isotopiques. Merci aussi pour toute la flexibilité que tu m'as laissé dans la définition des objectifs de mon projet. Merci pour ton enthousiasme contagieux envers toutes les données, les graphiques et les idées que je t'ai présenté lors de nos réunions de travail. Merci pour ton soutien et ton impressionnante disponibilité durant les nombreux « sprints » qui ont ponctué mon parcours doctoral. Je suis reconnaissante pour les innombrables conseils qui, petit à petit, m'ont permis de grandir en tant que personne et chercheuse dans ce domaine. Merci de m'avoir autant encouragée à saisir différentes opportunités (conférences, enseignement, encadrement d'étudiants) qui m'ont fait découvrir la richesse d'une carrière académique.

Merci à mes deux co-directeurs Florent Barbecot et Philippe Pasquier pour votre implication dans ce projet. Merci plus particulièrement à Florent pour tes 1001 idées « outside the box » (et questions!) qui ont contribué non seulement de façon positive à ce projet, mais également à ma formation académique. Merci pour ton empathie, ton écoute rassurante et tes conseils dans les moments où j'ai eu besoin d'un « boost » de confiance en soi. Philippe, merci pour ton regard rigoureux et honnête sur mon projet. Merci pour avoir partagé ton expertise et ta passion pour l'hydrogéologie et la géothermie. Merci pour m'avoir encouragé à développer mes habilités de modélisation numérique. Merci aussi pour ton support dans la planification des échéanciers pour l'achèvement de ma thèse. Paul, Florent et Philippe, vous avez tous joué un rôle important et complémentaire au cours de mon cheminement au doctorat. Fidèles à vos valeurs, vous m'avez démontré qu'il existe autant de modèles de réussite en recherche qu'il y a de chercheurs.

Merci à Matthieu Menou, Francis Proteau-Bédard, Benoit Barbeau et John Gibson pour avoir collaboré à ce travail. Matthieu Menou et Francis Proteau-Bédard, merci pour avoir mené les premières campagnes de terrain et analyses au laboratoire. Benoit Barbeau, merci pour ta participation dans ce projet. Ton expertise en traitement de l'eau m'a grandement aidé à orienter

mes travaux pour assurer des retombées concrètes pour le partenaire municipal. Thanks to John Gibson for your help in developing the stable isotope mass balance model. Learning from your expertise was a true privilege.

Je remercie chaleureusement les étudiants que j'ai côtoyé et qui m'ont offert support et amitié tout au long de ce parcours. Merci aux étudiants du G2H à Polytechnique, Marc Patenaude, Coralie Pontoreau, Maximilien Delestre, Francis Proteau-Bédard, Sabine Veuille, avec qui j'ai partagé des journées (et bien des discussions) au bureau et sur le terrain sous toutes les conditions météo, à pieds ou en pédalo! Merci à Léo Cerclet pour les échanges d'idées, les rires contagieux, les pauses-cafés et les sorties de ski de fond (et tous les autres sports). Merci aux étudiants à l'UQAM, Guillaume Meyzonnat, Alexandra Mattei, Rachid Barry, Djak Aimé Djongon, avec qui j'ai partagé les réunion biblio hebdomadaires pendant plusieurs années et à l'occasion desquelles j'ai pu élargir mes horizons grâce à chacune de vos revues critiques d'articles scientifiques portant sur divers sujets reliés à l'hydrogéologie. Un merci spécial à Karine Lefebvre, Laurence Labelle et Coralie Pontoreau qui ont partagé avec moi et contribué à motiver plus de 150 sessions de « co-working » sur zoom en cette période de télétravail.

Merci à Jérôme Leroy, Manon Leduc, Gabriel St-Jean à Polytechnique pour votre précieux soutien dans la préparation des campagnes de terrain, l'assistance dans les commandes de matériel et la réalisation des analyses géochimiques. Merci aussi pour vos généreux conseils et toutes les discussions concernant les bonnes pratiques au laboratoire et sur le terrain. Merci à Marina Tcaci et Jean-François Hélie à l'UQAM pour votre aide avec la réalisation des analyses isotopiques.

Merci à Dominique Claveau-Mallet pour tes précieux conseils et suggestions pour la préparation de mes dossiers de candidature à diverses bourses. Ta rigueur et discipline m'inspirent énormément!

Merci au CRSNG et à la Ville de Sainte-Marthe-sur-le-Lac pour avoir co-financé ce projet. Je remercie sincèrement les employés de la Ville et à l'usine de traitement pour avoir facilité l'accès au site d'étude et à la base de données.

Merci à mes colocs, Arielle, Mick, Jade, Coralie et Jean-Simon, pour avoir apporté autant de gaieté au quotidien. Préparer à souper, faire la vaisselle, le déneigement des voitures l'hiver ne seront jamais aussi drôle qu'avec vous! Merci aussi pour votre aide avec le transport des bouteilles de

soda pour mes campagnes de terrain et les interminables fous rires lors de ces soirées! Merci à tous mes amis, Jean-Simon, Camille, Jean-François, Émilie, qui m'ont généreusement accompagnée sur le terrain, même l'hiver sous un vent glacial!

Déjà remercié en tant que coloc et ami, merci une dernière fois à Jean-Simon, mon amoureux, mon complice. Merci pour m'avoir appuyée dans mon choix de passer au doctorat. Merci de pour tous les lifts et les bons soupers tous prêts après les grosses journées de terrain et de laboratoire. Merci pour ton calme et tout le réconfort que tu m'as apporté lors des moments de doute. Merci pour avoir fait passer mon bonheur en premier si souvent!

Le dernier mot va à ma grande famille. Un chaleureux merci à ma famille Dufresne pour s'être improvisée comme audience lors d'un beau dimanche après-midi pour pratiquer mon examen de synthèse. Merci à ma famille Masse pour m'avoir encouragé depuis les débuts de mon long parcours académique (et lors de mon arrivée dans *La Grande Ville*!). Merci à tous pour votre curiosité envers les sciences. C'est toujours un plaisir de discuter avec vous de mes passions! Merci à mes parents, Dominique et Pierre, qui m'ont grandement inspirée et encouragée à suivre mes passions depuis aussi longtemps que je puisse m'en souvenir! Maman, merci pour toute la confiance et la fierté (souvent exagérée!) que tu as envers moi. Papa, je suis persuadée que tu aurais partagé les mêmes sentiments et que tu aurais aimé lire cette thèse. C'est un honneur pour moi de constater que j'œuvre maintenant dans le même domaine que celui où tu as fait carrière. Tu m'accompagneras toujours! Bisous!

RÉSUMÉ

La filtration sur berge (FSB) est une méthode de prétraitement pour la production d'eau potable qui s'appuie sur la capacité naturelle des sédiments à atténuer les contaminants. Étant donné que les systèmes de FSB fonctionnent dans des conditions transitoires, il est difficile de prédire leur efficacité, tout particulièrement lors d'inondations. Toutefois, le fonctionnement de ces systèmes dans les régions où le cycle hydrologique est fortement marqué par la fonte des neiges (impliquant des crues printanières et des inondations fréquentes) reste encore peu étudié et méconnu.

L'objectif de cette thèse était de révéler la dynamique de l'écoulement des eaux souterraines sur un site de FSB affecté par des inondations printanières induites par la fonte des neiges. Les objectifs spécifiques étaient : (1) de distinguer le rôle des contrôles anthropiques et météorologiques sur l'origine et la qualité physico-chimique de l'eau brute pompée, (2) de développer une stratégie de surveillance à courte échelle de temps pour révéler la dynamique spatio-temporelle des schémas d'écoulement lors de crues extrêmes, et (3) de différencier le rôle des apports directs d'eau de crue et du stockage souterrain temporaire des eaux de crue dans le bilan hydrique d'un lac alimentant le site de FSB.

Premièrement, un modèle de mélange binaire transitoire a été développé pour étudier la compétition entre les forçages anthropiques et météorologiques sur l'origine de l'eau pompée à une échelle mensuelle. Sachant que les sites de FSB sont opérés sous des conditions hautement transitoires, il apparaissait crucial de déterminer la variabilité spatiotemporelle de l'origine de l'eau pompée induite par le pompage (forçage anthropique) et les variations des niveaux d'eau (forçage météorologique). Il a été démontré que les schémas de pompage peuvent être utilisés pour contrôler l'origine et la qualité de l'eau pompée. L'opération des puits de pompage sur une base continue a permis de moduler l'origine de l'eau pompée en contrant l'effet des variations des niveaux d'eau, sauf pendant une période de crue. Une telle opération à un débit de pompage élevé a contribué à maintenir la contribution du Lac A à ~62% (le reste correspondant au Lac B) et à limiter les concentrations totales de fer (Fe) et de manganèse (Mn) dans l'eau pompée. À l'inverse, l'opération des puits de pompage sur une base intermittente ou occasionnelle a entraîné de plus importantes variations de l'origine de l'eau à l'échelle annuelle et a détérioré la qualité physico-chimique de l'eau pompée.

Deuxièmement, la combinaison de traceurs environnementaux, incluant la conductivité électrique (CE), les isotopes stables de la molécule d'eau ($\delta^{18}O$- $\delta^{2}H$) et la température, accompagnée par la mise en place d'un programme de suivi à court terme, a permis de mieux comprendre la dynamique des schémas d'écoulement des eaux souterraines de l'échelle quotidienne à mensuelle, pendant et après un événement de crue extrême. Il est reconnu que les crues représentent un enjeu pour l'opération des systèmes de FSB. En effet, la qualité des eaux de surface est typiquement détériorée et des temps de séjours courts sont souvent observés aux systèmes de FSB pendant des crues. Par conséquent, les systèmes de FSB sont potentiellement plus vulnérables à différentes contaminations pendant les inondations. Les différents traceurs se sont avérés complémentaires, fournissant des informations pouvant aider à anticiper les changements de la qualité microbienne de l'eau et à guider le moment et la fréquence des échantillonnages et analyses garantissant la qualité microbiologique de l'eau distribuée. Alors que l'évolution de la CE et de $\delta^{18}O$ aux puits de pompage et au mélange pompée ont révélé une évolution progressive de l'origine de l'eau sur une période d'un mois, les mesures automatiques de la température et de la CE au niveau des puits d'observation ont permis de détecter des perturbations au niveau des schémas d'écoulement à une échelle de temps quotidienne. Le suivi des traceurs environnementaux a également permis de suivre l'impact de la rupture d'une digue sur l'origine de l'eau dans la berge. Un suivi en continu de la CE et de la température a permis de constater une réorganisation rapide (c.-à-d. sub-journalière) des schémas d'écoulements souterrains, menant à une inversion temporaire des gradients hydrauliques à proximité des puits et un changement de l'origine de l'eau pompée. Enfin, le suivi de $\delta^{18}O$ dans les puits de pompage a permis de décrire l'évolution du système suite à l'événement de crue. Tel qu'anticipé, l'opération des puits à des débits de pompage élevés (c.-à-d. ≥ 1000 m^3/jour) a accéléré le retour aux conditions observées avant la crue.

Troisièmement, un bilan de masse isotopique transitoire a été développé pour estimer les apports en eau souterraine et en eau de crue au Lac A (c.-à-d., principale source d'eau de surface aux puits de pompage), en vue de comprendre la résilience de l'hydrosystème aux changements. Le modèle a révélé que les apports en eau souterraine dominaient le bilan hydrique annuel, les eaux souterraines représentant 60 à 72 % des apports totaux sur l'échelle de temps annuelle. Cependant, si l'on tient compte du potentiel stockage souterrain temporaire (et de la décharge) des eaux de crue, la répartition entre les apports en eau souterraine et en eau de surface tend à s'égaliser. Ceci

implique que les apports et le stockage des eaux de crue contribuent à augmenter la résilience du lac face à des changements de quantité et de qualité des apports en eau souterraine. Ainsi, les inondations récurrentes semblent contribuer positivement à l'hydrosystème et permettent d'assurer la production d'eau potable au site de FSB.

En considérant l'ensemble, cette thèse fournit à la fois des approches méthodologiques et des résultats concrets pour améliorer la connaissance du fonctionnement des systèmes de FSB soumis à des crues printanières récurrentes. Cette recherche a exploré la dynamique des schémas d'écoulements souterrains et du stockage des eaux de crue, du pas de temps journalier à annuel, à la fois à l'échelle du site de BF et de l'hydrosystème. Des stratégies d'opération et de suivi ont été appliquées et testées. Elles contribuent maintenant aux solutions dont disposent les opérateurs et les chercheurs pour gérer la qualité de l'eau. Ce travail profite donc aux gestionnaires de l'eau et aux scientifiques, car il peut contribuer à améliorer l'opération des sites de FSB existants et à la planification de futurs projets de FSB, en particulier dans les régions où le cycle hydrologique est affecté par la fonte des neiges.

ABSTRACT

Bank filtration (BF) is a pre-treatment technology to produce drinking water that benefits from the natural capacity of the sediments to attenuate contaminants. As BF systems operate in transient conditions, predicting their efficiency is difficult, especially under flood conditions. Meanwhile, little has been done to understand how these systems function in snowmelt-dominated basins, where the hydrological cycle is shaped by springtime freshets and frequent flood events.

The objective of this thesis was to reveal the dynamics of groundwater flow patterns at a BF site affected by recurring springtime flood events. The specific objectives were: (1) to distinguish the role between anthropic and meteorological controls on the mixing ratios and on the physico-chemical quality of the raw water, (2) to develop a short time-step monitoring strategy to reveal the spatiotemporal dynamics of the groundwater flow patterns under extreme flood events, and (3) to differentiate the respective role of direct floodwater inputs and temporary subsurface storage of floodwater on the water balance of a lake used as source water for the BF site.

First, a time-varying binary mixing model was developed to investigate the competition between anthropic and meteorological forcings on the origin of pumped water at a monthly timescale. Given that the BF sites are operated under highly transient conditions, it appeared crucial to determine the spatiotemporal variability of the origin of raw water due to pumping (anthropic forcing) and water level variations (meteorological forcing). It was shown that pumping schemes can be used to control the origin and quality of the pumped water. The operation of the pumping wells on a continuous basis allowed to outweigh the meteorological control (i.e., water levels), except during flood event. Such pumping scheme at high pumping helped at maintaining the mixing ratios at ~62% of Lake A water and at limiting the total iron (Fe) and total manganese (Mn(concentrations in the pumped water. Conversely, the operation of wells on an intermittent or occasional basis resulted in large variations in mixing ratios (i.e., from 0% to 100%) on the annual timescale and was found to deteriorate the physcio-chemical quality of the pumped water.

Second, an optimized combination of environmental tracers, including electrical conductivity (EC), stable isotopes of the water molecule ($\delta^{18}O$- $\delta^{2}H$) and temperature, and a short time-step monitoring, allowed to better understand the daily to monthly dynamics of groundwater flow patterns reorganization during and after an extreme flood event. It is recognized that floods

represent a challenge for the operation of BF systems. In fact, the quality of surface water is typically deteriorated, and short travel times are often observed at BF systems during floods. Thereby, BF systems are vulnerable to various contaminations during inundation. The different tracers were found to be complementary and to provide information that can help at anticipating microbial water quality changes and guide the timing and the frequency of more expensive and time-consuming monitoring analyses (e.g., bacteriological indicators) to secure the production of high-quality drinking water. While the evolution of EC and $\delta^{18}O$ in the pumped mixed water and at the pumping wells revealed a gradual evolution of the origin of water over a 1-month period, automated measurements of temperature and EC at observation wells allowed to detect changes in the groundwater flow patterns at a daily timescale. Monitoring for environmental tracers additionally allowed to track the impact of a dyke failure on the origin of the bank filtrate. A continuous monitoring of CE and temperature revealed a rapid reorganization of the groundwater flow patterns, leading to a temporary inversion of the hydraulic gradients in the vicinity of the pumping wells and a change in the origin of the pumped water. Lastly, the monitoring of $\delta^{18}O$ at the pumping wells helped at depicting the recovery dynamics to normal conditions. As expected, the operation of wells at high rates (i.e., $\geq 1000\ m^3$/day) accelerated the recovery to pre-flood mixing ratios.

Third, a volume-dependent stable isotope mass balance was developed to estimate the partitioning between groundwater and floodwater to Lake A (i.e., principal source water to the pumping wells), in order to depict the resilience of the hydrosystem to changes. The model revealed that groundwater inputs dominated the annual water budget, with groundwater representing 60%-72% of the total inputs on the annual timescale. However, when considering the potential temporary subsurface storage (and discharge) of floodwater, the partitioning between groundwater and surface water inputs tends to equalize. This implies that floodwater inputs and storage contribute to increase the resilience of the lake to groundwater quantity and quality changes. Thereby, the recurring floods appear to contribute positively to the hydrosystem and help at securing the sustainability of drinking water production at the BF site.

Considering all parts, this thesis provides methodological approaches to enhance knowledge on the functioning of BF systems affected by recurring springtime freshets. This research explored the dynamics of groundwater flows and floodwater storage from the daily to annual timescales at both

the BF site scale and hydrosystem scale. Monitoring and operational strategies were applied and tested. They now contribute to the solutions that operators and scientists dispose to manage water quality. This work thus benefits to the water managers and scientists, as it can help at operating existing BF sites and planning future BF projects in snowmelt-dominated basins.

TABLE OF CONTENTS

DEDICATION III

ACKNOWLEDGEMENTS IV

RÉSUMÉ X

ABSTRACT XIII

TABLE OF CONTENTS XVI

LIST OF TABLES XXI

LIST OF FIGURES XXII

LIST OF SYMBOLS AND ABBREVIATIONS XXX

LIST OF APPENDICES XXXIV

CHAPTER 1 INTRODUCTION 1

1.1 Water Resources and Drinking Water Production in a Changing World 1

1.2 Bank Filtration: A Resilient Solution to Produce Drinking Water 1

1.3 Thesis Outline 4

CHAPTER 2 LITTERATURE REVIEW 5

2.1 Challenges Relative to the Use of Bank Filtration 5

2.1.1 Efficiency of BF systems 5

2.1.2 Evolution of operational conditions 5

2.1.3 Impact of floods on bank filtration 6

2.1.4 Bank filtration in snowmelt-dominated basins 6

2.2 Study site 8

2.2.1 Geological and hydrological setup 8

2.2.2 Climate 10

2.2.3 Topography 12

2.2.4 Description of the BF system 13

2.3 Environmental tracers 14

2.3.1 Electrical conductivity 15

2.3.2 Stable isotopes of the water molecule 15

2.3.3 Temperature 16

CHAPTER 3 RESEARCH OBJECTIVES, HYPOTHESES AND METHODOLOGY 18

3.1 Objectives of the thesis 18

3.2 Hypotheses 19

3.3 Research strategy 19

3.4 Monitoring and water sampling program 20

CHAPTER 4 ARTICLE 1: ANTHROPIC AND METEOROLOGICAL CONTROLS ON THE ORIGIN AND QUALITY OF WATER AT A BANK FILTRATION SITE IN CANADA 23

4.1 Introduction 23

4.2 Site Description 25

4.2.1 Hydrogeological Context 25

4.2.2 Hydraulics of the Two-Lake BF System 27

4.3 Materials and Methods 30

4.3.1 Surface and Groundwater Sampling 30

4.3.2 Analytical Techniques 31

4.3.3 Estimating Mixing Ratios 31

4.4 Results and Discussion 32

4.4.1 Highly Transient Pumping Schemes 32

4.4.2 Geochemistry as a Proxy of the Hydrosystem Dynamics 35

4.4.3 EC Time-Varying Mixing Model 39

4.4.4 Dominant Controls on the Origin of the Bank Filtrate 45

4.4.5 Implications for the Quality of the Bank Filtrate 48

4.5 Conclusions 50

CHAPTER 5 ARTICLE 2: OPTIMIZING MONITORING AND MANAGEMENT STRATEGIES AT FLOOD-AFFECTED BANK FILTRATION SITES 53

5.1 Introduction 54

5.2 Study Site Description 56

5.2.1 Hydrological and Geological Contexts 56

5.2.2 Flood-proof Measures 59

5.2.3 Operation of the BF System 59

5.3 Materials and Methods 60

5.3.1 Instrumentation 60

5.3.2 Water Sampling and Analytical Procedures 61

5.4 Results and Discussion 62

5.4.1 Long-lasting Hydraulic Control by Floods 62

5.4.2 Water Quality Risk Assessment 64

5.4.3 Groundwater Flow Dynamics: from Normal to Flood Conditions 66

5.4.4 Temperature as a Proxy of Transient Groundwater Flow Patterns During Flood Events 70

5.4.5 Water Quality Management Implications 75

5.5 Conclusions 79

CHAPTER 6 ARTICLE 3: QUANTIFYING FLOOD-WATER IMPACTS ON A LAKE WATER BUDGET VIA VOLUME-DEPENDENT TRANSIENT STABLE ISOTOPE MASS BALANCE 81

6.1 Introduction 82

6.2 Study site 84
6.2.1 Geological and hydrological setting 84
6.2.2 Hydrodynamics of the major flood event 87
6.2.3 Conceptual model of Lake A water balance 88
6.3 Methods 90
6.3.1 Field measurements 90
6.3.2 Water sampling and analytical techniques 91
6.3.3 Stable isotope mass balance 92
6.3.4 Daily volume changes at Lake A and water fluxes 94
6.4 Results 96
6.4.1 Isotopic and geochemical framework 97
6.4.2 Evaluation of the water budget 100
6.4.3 Importance of temporary floodwater storage on the water balance partition 105
6.4.4 Temporal variability in the water balance partition 106
6.5 Discussion 108
6.5.1 Resilience of lakes to surface water and groundwater changes 108
6.5.2 Implications for water management 110
6.6 Conclusions 111
CHAPTER 7 GENERAL DISCUSSION 113
7.1 Transience of the pumping schemes 113
7.2 Control of the pumping schemes on Fe and Mn concentrations 116
7.3 Design of the observation wells 118
7.4 Stratification of lakes in cold climate 119
7.5 Anticipating breakthrough of microorganisms 120

CHAPTER 8 CONCLUSION AND PERSPECTIVES 122

REFERENCES 125

APPENDICES 143

LIST OF TABLES

Table 1-1 List of the existing bank filtration (BF) sites as reported in the global inventory of managed aquifer recharge sites (IGRAC, 2021). Underlined countries correspond to regions where BF sites are presumably in snowmelt-dominated basins (Barnett et al., 2005). 3

Table 2-1 Mean, minimum and maximum pumping rates and total pumped volume from 2013 to 2019. Estimates calculated from the daily pumped volume at each well. 14

Table 3-1 Conceptualization of the physico-chemical, geochemical and isotopic sampling program. The frequency of the water sampling was monthly (M), quarterly (3M) or occasionally (O). 21

Table 6-1 Observed depth-averaged (or mean) and standard deviation (std) of isotopic composition of Lake A for the sampling campaigns in February 2017, August 2017 and January 2018 and all samples. The isotopic composition of the samples collected at the surface of Lake A on May 9-10, 2017 and April 27th, 2017 are also listed. The asterisks (*) indicate that a mean value was calculated (instead of a depth-averaged value). 100

Table 6-2 Water mass balance of Lake A for scenarios A and B. The difference between the total inputs and total outputs corresponds to the lake volume difference over the study period. The total inputs (I) correspond to the sum of precipitations (P), surface water inflow (I_S) and groundwater inflow (I_G). The total outputs (Q) correspond to the sum of evaporation (E) and surface water and groundwater outflow (Q). The mean flushing time (t_f) is the ratio of the lake volume to the mean groundwater inputs (I_G). 103

LIST OF FIGURES

Figure 1-1 Schematic representation bank filtration 2

Figure 2-1 Location of (a) the site and Ottawa River watershed, (b) Lake A, Lake B and Lake DM, and (c) pumping wells and observation wells. Approximate limits and extent of the paleo-channel are depicted in (b). 9

Figure 2-2 Geological cross-section of the study site (adapted from Ageos, 2010) 10

Figure 2-3 Daily average precipitation (left axis) and daily average temperature (right axis) from 1981 to 2010 at Montreal-Mirabel International Airport meteorological station (based on Environment and Climate Change Canada data). The dashed lines correspond to the monthly mean of the daily minimum and the daily maximum temperatures. 11

Figure 2-4 View on well field on (a) May 16, 2017 and (b) January 24, 2019, and view on Lake A on (c) August 28, 2018 and (d) February 27, 2018. The location and orientation of the pictures are illustrated in Figure A-2 in Appendix A. 12

Figure 2-5 Topography of the study site. Data correspond to the digital elevation model produced from Lidar data (Ministère des Forêts, 2020). 13

Figure 4-1 Study site location maps (a–c) and schematic lithological cut along pumping wells (d) (adapted with permission from Ageos, 2010) 26

Figure 4-2 Schematic representation of the flow patterns and directions at the study site when (a) elevation of Lake B > elevation of Lake A, (b) elevation of Lake A > elevation of Lake B, and (c) the pumping wells are in operation. Black, blue, and red arrows refer to regional groundwater and water originating from Lake A and Lake B, respectively. Theoretical elevation difference between Lake A and Lake B in (d). Numbers 1 to 3 correspond to different hydraulic conditions, namely high, moderate, and low hydraulic gradients between Lake A and Lake B. 29

Figure 4-3 Pumping rates for wells (a) P1, (b) P3, (c) P5, and (d) P6 during a typical one-week period (from 16 January 2017 to 23 January 2016). Monitoring and water sampling were conducted on 17 January 2017 at all the pumping wells. 33

Figure 4-4 Monthly mean total pumping rate from March 2016 to March 2017. Above each bar are the proportions of the total pumped volume supplied by the continuously (in black) and intermittently (in grey) pumping wells. The occasionally pumping wells supply only <1–2% of the total pumped volume.....34

Figure 4-5 Boxplots of (a) temperature, (b) electrical conductivity (EC), (c) pH, and (d) redox potential (Eh) at the lakes, pumping wells (PW), and observation wells (OW). Blue and red boxes are associated with Lake A (<1 m depth) and Lake B (<1 m depth), whereas dark, medium, and light grey boxes correspond to continuously, intermittently, and occasionally pumping wells, respectively. Numeric values above each box correspond to the median. ...36

Figure 4-6 Boxplots of (a) total Fe, and (b) total Mn concentrations at the lakes, pumping wells, and observation wells. Blue and red boxes are associated with Lake A (<1 m depth) and Lake B (<1 m depth), whereas dark, medium, and light grey boxes correspond to continuously, intermittently, and occasionally pumping wells, respectively. Numeric values above each box correspond to the median. Red circle represents the maximal observed total Mn in Lake B (at 6 m depth).....37

Figure 4-7 Comparison of the geochemical facies of Lake A, Lake B, pumping wells, and the regional groundwater (GW). The solid black line represents the mixing line between Lake A and Lake B mean values.....39

Figure 4-8 Time series of electrical conductivity (EC) at (a) Lake A (<1 m depth), and (b) Lake B (<1 m depth) and Z12. The grey shaded area represents the timing for hydraulic connection between Lake A and Lake C. Error bars (±20 µS/cm) represent the maximal expected measurement error on EC. The yellow dashed line corresponds to the mean EC value at Z12. 40

Figure 4-9 Electrical conductivity (EC) measurements against depth at Lake A and Lake B in winter and summer. Solid lines represent depth-average value at the lakes, while the yellow dashed line is associated with mean EC values at observation well Z12. Blue and red shaded areas illustrate the variability in EC at the surface (<1 m depth) of Lake A and Lake B, respectively.....42

Figure 4-10 Estimated contribution from Lake A to the pumping wells according to the reference scenario. Lake A end-member is defined as a time-varying electrical conductivity (EC) signal, which was derived from the observed EC values at <1 m depth. Lake B end-member is a fixed EC value which corresponds to the mean of the wintertime and summertime depth-average value. 44

Figure 4-11 Relationship between electrical conductivity (EC) and the one-month average pumping rate prior to the sampling date, according to (a) the pumping regime and (b) the hydraulic gradient between Lake A and Lake B. A schematic representation of the dominant forcing is illustrated in (c), where solid and dashed lines represent the range of observed values and the delimitation between regimes where meteorological and anthropic forcings are dominant, respectively.....47

Figure 4-12 Relationship between (a) total Fe and (b) total Mn concentrations and the 1-month average pumping rate prior to the sampling date. 50

Figure 5-1 (a) Location of the study site and Ottawa River watershed, (b) schematic representation of the hydrogeological context and location of Lake A, Lake B and Lake DM, and (c) location of monitoring and sampling points and geological cross-section A-A'. The maps were created based on open access Geographic Information System (GIS) data. Canada's provinces boundary files were obtained from Statistics Canada © and USA Cartographic Boundary Files were retrieved from the United States Census Bureau ©. Hydrological data (lakes, streams and watershed) was sourced from the Nation Hydro Network – NHN – GeoBase Series and provided by the Strategic Policy and Results Sector of Natural Resources Canada ©. The flood extent products are derived from RADARSAT-2 images with a system developed and operated by the Strategic Policy and Results Sector of Natural Resources Canada ©. 58

Figure 5-2 Hydrogeological cross-section A-A' and location of the pumping wells and PZ-6. The screened sections of the pumping wells are located at the bottom of the aquifer. The blue and the red dashed lines represent the pre-flood and flood peak water levels at Lake A, respectively. Direct infiltration of floodwater did not occur during the intense flood events. 59

Figure 5-3 Schematic illustration of the BF system and treatment plant. The pumping wells are equipped with submersible pumps, which enable control on the active pumping wells. The pumped water flows either towards a purging system or towards the treatment plant, accordingly to the needs of the waterworks. Hand valves are open (in green) or closed (in red) to allow water to flow towards the desired direction. Sampling of the raw water can be performed at the individual pumping wells, if they are actively pumping (in blue). Typically, three pumping wells are active and contribute to the pumped mix (e.g., P6-P1-P3), which can also be sampled. The wells can also be sampled when operated in purging mode (e.g., P4 and P5). An advanced treatment and chlorination are performed on the raw pumped mix prior to its distribution to the drinking water supply system. The advanced treatment consists of biological filtration (Mangazur®) and nanofiltration (NF90 Filmtec™). 60

Figure 5-4 Temporal evolution of water levels at (a) Lake DM from 2014 to 2020, (b) Lake DM, Lake A, Lake B and PZ-4 during springtime 2017, (c) Lake DM and PZ-4 during springtime 2018 and (d) Lake DM, Lake A, Lake B and PZ-4 during springtime 2019. The black dashed line corresponds to the topographic threshold at 22.12 m.a.s.l., above which a hydraulic connection is established between Lake DM and Lake A (Ageos, 2010). On April 27, 2019, failure of a dyke (at 1 km SE to the study area) caused the flooding of a residential area, including Lake B, and resulted in rapid water level rise at Lake B (and PZ-4). 64

Figure 5-5 Spatiotemporal evolution of total bacterial counts on m-Endo media (i.e., sum of total coliform and atypical bacteria) at the pumping wells (P6, P1, P8, P2, P7, P3, P4 and P5) from January 2014 to June 2019. The data was provided by the municipal authorities. The gray shaded area represents the springtime flood events. 66

Figure 5-6 (a) Temporal evolution of electrical conductivity (EC) and $\delta^{18}O$ at the pumped mix from April to August 2019. (b) Zoom on the period between mid-April and mid-May, emphasizing the timing of the dyke failure (on April 27) and the deviation of EC and $\delta^{18}O$ from the expected curve (in red). The pumped mix was composed of groundwater abstracted at P1, P3 and P6 until April 29, after which P7 (or occasionally P8) was contributing to the pumped mix as P3 was non-operational. 68

Figure 5-7 Temporal evolution of (a) electrical conductivity (EC) and (b) $\delta^{18}O$ at the pumping wells (gray boxplots) from March 2016 to June 2019. Sample size (n) for each boxplot is normally 8 (i.e., all the pumping wells). Note that on occasional circumstances, some wells were not sampled (due to pump failure) and the boxplot were generated with $n \geq 3$ to $n \leq 7$. The gray shaded area represents the 2016, 2017, 2018 and 2019 flood events. The blue and red dashed lines correspond to the mean EC values at Lake A and Lake B (≥2 m depth), respectively, while the black dashed line represents the mean $\delta^{18}O$ value for floodwater. Note that the EC values at the pumping wells from March 2016 and February 2017 and the mean floodwater $\delta^{18}O$ values are retrieved from previously published work (Masse-Dufresne et al., 2020; Masse-Dufresne et al., 2019).....70

Figure 5-8 (a) Temporal evolution of the temperature at the surface of Lake A (in blue) and at PZ-6 (in black), which is an observation distant from the BF system and thus not influenced by pumping. Vertical temperature profiles on March 19, 2019 and April 25, 2019 at (b) PZ-2 and (c) PZ-5. The observation well PZ-2 is located between Lake B and the pumping well P1 (continuously pumping), while PZ-5 is near P5 (occasionally pumping).....72

Figure 5-9 (a) Daily evolution of the temperature and electrical conductivity (EC) at observation well PZ-2. The temperature measurements were performed at 11 m and 20 m depth (below ground level), while the EC measurements were only carried at 20 m depth. The frequency of bacterial analyses sampling at the pumped mix and the pumping wells is marked with black asterisks and the corresponding maximum analytical delays (i.e., 8 days) are identified with the yellow shaded areas. (b) Zoom on the period between mid-April and early May 2019, which is denoting the important transience of the temperature at 11 m and 20 m depth. Additionally, the hydraulic gradient between Lake B and PZ-2 (in red) is illustrated. 74

Figure 5-10 Evolution of $\delta^{18}O$ at the pumping wells during the recovery period in 2017. The black circles mark the wells that are contributing to the pumping mix and, therefore operating at a daily pumping rate $Q \geq 1000$ m^3/day, while the gray circles correspond to the wells that operate at $Q < 1000$ m^3/day. From mid-May to early August, pumping well P3 (in red) was not pumping (out of operation). 79

Figure 6-1 (a-c) Location of the study site, relative to the Ottawa River watershed, Lake Deux-Montagnes (DM) and the area of Greater Montreal, (d) location of Lake A and Lake B relative to Lake DM and schematic representation of the hydrogeological context. The grey dashed lines illustrate the approximative extent of the paleo valley. LA-S1 and LB-S1 are surface water sampling points at Lake A and Lake B, respectively. LA-P1 to LA-P4 correspond to vertical profile sampling locations at Lake A. The maps were created from openly available data and used in accordance with the Open Government Licence – Canada or the Open Data Policy, M-13-13 of the United States Census Bureau. Detailed source information is provided in Appendix C. 86

Figure 6-2 Daily mean water levels at Lake A, Lake DM and observation well VP from February 9th, 2017 to January 25th, 2018. The grey shaded area corresponds to the floodwater control period. Q_{max} and Q_{min} indicate the timing of the adjusted maximum and minimum output from the lake. 88

Figure 6-3 Schematic representation of the hydrological processes at Lake A during (a) groundwater control, and (b) floodwater control periods. Inputs include precipitation (P), surface water (I_S) and groundwater (I_G) while outputs include evaporation (E), surface water outflow (Q_S) and groundwater outflow (Q_G). The area between Lake DM and Lake A is flooded in (b) and I_S from Lake DM contribute to the water balance of Lake A.....89

Figure 6-4 Isotopic composition of precipitation, Lake A water, and floodwater from March 2017 to January 2018. Hollow and solid blue circles correspond to samples collected at ≤2 m and >2 m depth, respectively. Analytical precision is 0.15‰ and 1‰ at 1σ for $\delta^{18}O$ and $\delta^{2}H$. Precipitation data are retrieved from the research infrastructure on groundwater recharge database (Barbecot et al., 2019). 98

Figure 6-5 Geochemical facies of Lake A (n = 23) and floodwater (n = 1). Mean values for Lake B (n = 42) and regional groundwater (GW) (n = 11) geochemical facies are also plotted. Lake A and floodwater are characterized by Ca-HCO_3 water types, while Lake B and regional GW correspond to Na-Cl water types. Note that regional GW was sampled upstream of Lake B. 99

Figure 6-6 Observed and modelled depth-average isotopic composition of the lake (δ_L) for $\delta^{18}O$ (a-b) and δ^2H (c-d) from February 9th, 2017 to January 25th, 2018 for scenarios A and B. The hollow and solid blue circles correspond to Lake A water samples collected at ≤2 m and >2 m, respectively. The modelled δ_L is fitted against the three depth-averaged δ_L and an additional sample collected at ≤2 m depth on May 9-10, 2017 (scenario A) and April 27th, 2017 (scenario B). These samples are marked by the hollow red squares. The grey shaded area corresponds to the floodwater control period. The error bars correspond to the standard error on the samples for each campaign. The dashed lines represent the modelled δ_L when considering that 25% to 100% of the outputs from the lake during the floodwater control period were temporally stored in the aquifer and discharged to the lake as floodwater-like inputs (δ_{Is}). 102

Figure 6-7 Temporal evolution of the G-Index from February 9th, 2017 to January 25th, 2018 for scenario A and the associated scenarios considered in the sensitivity analysis (i.e., A1 to A22). The grey shaded area corresponds to the floodwater control period. A hypothetical scenario is also depicted to decipher the impact of potential surface water bank storage on the evolution of the G-Index. Indeed, during the floodwater control period, the outputs (Q) from the lake can be stored in the aquifer and gradually discharge back to the lake. Conceptually, this contribution to the lake can be considered as surface water inputs (I_s), rather than groundwater inputs (I_G). Hence, G-Index is corrected for surface water bank storage considering that 50%, 75% or 100% of the Q during the floodwater control period returns to the lake as I_S (dashed lines). 107

Figure 6-8 Resilience of lakes to groundwater quantity and quality changes for Lake A (this study) and kettle lakes (Arnoux et al., 2017b) in southern Quebec (Canada). G-Index is the ratio of groundwater inputs to total inputs and t_f is the mean flushing time by groundwater. This representation is adapted from Arnoux et al. (2017b). 109

Figure 7-1 Schematic representation of the effects of pumping on groundwater flow patterns (adapted from Barlow & Leake, 2012) 114

Figure 7-2 Pumping rates at the wells P1 to P8 from January 2015 to December 2019 inclusively. The grey dots are the daily mean pumping rates and the black lines are the 30-day moving average of the pumping rates for each well. The grey shaded area represents the period

assessed in the Article #1, while the vertical dashed line represents the onset of the advanced water treatment system. 115

Figure 7-3 Total Fe and total Mn concentrations at the wells P1 to P8 from January 2015 to December 2019 inclusively. The grey shaded area represents the period assessed in the Article #1, while the vertical dashed line represents the onset of the advanced water treatment system. 117

Figure 7-4 Relationship between the pumping rate and (a) the total Fe concentration and (b) the total Mn concentration 118

LIST OF SYMBOLS AND ABBREVIATIONS

‰	Per mill
A	Cross-sectional area through which the water flows
BF	Bank filtration
CFU	Colony forming unit
C_K	Ratio of molecular diffusivities of the heavy and light molecules
D	Vapor pressure deficit
DOC	Dissolved organic carbon
E	Evaporation
EC	Electrical conductivity
f	remaining fraction of lake water at the end of the time-step
$f(u)$	Wind function
f_A	fraction of Lake A water
f_B	fraction of Lake B water
G-Index	Ratio of cumulative groundwater inputs to the cumulative total inputs
h	Relative humidity normalized to water surface temperature (in decimal fraction)
i	Hydraulic gradient
I	Instantaneous inflow
I_G	Groundwater inflow
I_S	Surface water inflow
k	Seasonality factor
K	Hydraulic conductivity
LEL	Local Evaporation Line
LMWL	Local Meteoric Water Line

m	Temporal enrichment slope
m.a.s.l.	Meters above seal level
MAR	Managed aquifer recharge
NTU	Nephelometric Turbidity Unit
OLSR	Ordinary least square regression
P	Precipitation
PWLSR	Precipitation amount weighted least square regression
Q	Instantaneous outflow
Q_G	Groundwater outflow
Q_{max}	Maximum outflow
Q_{min}	Minimum outflow
Q_S	Surface water outflow
RH	Relative humidity
R_n	Net solar radiation
R_S	Solar radiation
T	Water surface temperature
t	Time
T_{air}	Air temperature
t_f	flushing time by groundwater
U	Wind speed at 2m above ground
V	Lake volume
V	Residual volume at the end of the time step
V_0	Original volume at the beginning of the time step
X	Fraction of lake water lost by evaporation

X_A	Concentration (or value) of tracer for end-member A
X_B	Concentration (or value) of tracer for end-member B
X_w	Concentration (or value) of tracer at the pumping well
Y	Fraction of lake water lost to liquid outflows
α^+	Equilibrium isotopic fractionation
γ	Psychrometric coefficient
Δ	Slope of the saturation vapor pressure curve
δ^*	Limiting isotopic composition that the lake would approach as $V \rightarrow 0$
δ_0	Isotopic composition of the lake at the beginning of the time-step
$\delta^{18}O$	Ratio of stable isotopes ^{18}O and ^{16}O
δ^2H	Ratio of stable isotopes ^2H and ^1H
δ_A	Isotopic signature of atmospheric moisture
δ_E	Isotopic signature of evaporating moisture
δ_G	Isotopic signature of groundwater inflow
δ_I	Isotopic signature of I
δ_{Is}	Isotopic signature of surface water inflow
δ_L	Isotopic signature of the lake
δ_P	Isotopic signature of precipitation
δ_Q	Isotopic signature of Q
δ_{Qg}	Isotopic signature of groundwater outflow
δ_{Qs}	Isotopic signature of surface water outflow
δ_S	Steady-state isotopic composition the lake would attain if f tends to 0
ε^+	Equilibrium isotopic separation
ε_K	Kinetic isotopic separation, with $\varepsilon^+=(\alpha^+-1)10^3$ and $\varepsilon_K=\theta*C_K(1-h)$

θ	Transport resistance parameter
λ	Latent heat of vaporization

LIST OF APPENDICES

Appendix A Complementary hydrogeological data 143

Appendix B Supplementary material – Article #2 147

Appendix C Complementary information to Figure 6-1 149

Appendix D Computation of isotope mass balance parameters 151

Appendix E Comparison of the evaporative fluxes (E) estimations 153

Appendix F Estimation of the water surface temperature based on the equilibrium method (de Bruin, 1982) 154

Appendix G Isotopic composition along vertical profiles in Lake A 156

Appendix H Results of the sensitivity analysis for reference scenarios A and B 157

Appendix I ARTICLE 4: Bank filtration from flood-affected quarry lakes: issues and solutions in a cold climate (Canada) 159

CHAPTER 1 INTRODUCTION

1.1 Water Resources and Drinking Water Production in a Changing World

Water resources are under increasing pressure due to population growth, anthropogenic pollution and land-use changes. Population growth results in increased water demand, not only due to drinking water consumption (Arbués et al., 2003), but also indirectly via irrigation and process water needs for the agricultural and industrial spheres (Maggioni, 2014; Wang et al., 2018). Groundwater overexploitation (i.e., abstraction rate exceeds, or is close to the renewal rate) can lead to adverse effects, such as water table depression, water quality changes, increase of abstraction cost, perturbation of ecosystems, subsidence, and saltwater intrusion (Custodio, 2002; Ferguson & Gleeson, 2012; Molle et al., 2018). Anthropogenic activities may generate polluted waters (e.g., urban and agricultural run-offs, domestic and industrial wastewaters) loaded with nutrients, organic, inorganic and microbial contaminants, which contaminates surface water and, eventually groundwater (Masoner et al., 2019; Schwarzenbach et al., 2010). Land-use changes can also impact the quantity and quality of surface water and groundwater by modifying run-off and infiltration patterns (Fiener et al., 2011).

In this context, securing the production of high-quality drinking water from either surface water or groundwater is becoming challenging. There is thus a need to consider and to promote the use of more resilient methods to produce drinking water. Bank filtration (BF) is an opportune technology to jointly enhance water supplies and improve surface water quality.

1.2 Bank Filtration: A Resilient Solution to Produce Drinking Water

Induced Bank filtration consists in abstracting groundwater in the vicinity of a lake or river. It controls the hydraulic gradient at the groundwater/surface water interface and induces surface water to infiltrate the sediments (Sprenger et al., 2017). In this document, the term “bank filtration” (or BF) is used to ease the reading, although it refers to the intentional use of pumping wells to benefit from the infiltration of surface water in the aquifer.

The pumped water at BF systems is a mixture of 1) ambient groundwater and 2) recently infiltrated surface water, referred to as "bank filtrate". In addition to reducing the risk of overexploiting groundwater resources, this water supply method provides a pre-treatment for surface water (Ray et al., 2003). In the aquifer, a series of physical, chemical and biological processes enhance the quality of the surface water during its subsurface passage (Figure 1-1) (Hiscock & Grischek, 2002). Given sufficiently long travel times, BF was demonstrated to attenuate turbidity and particles (Sahu et al., 2019), organic chemicals (Dragon et al., 2018), nutrients (Regnery et al., 2015), and pathogens (Ren et al., 2019; Weiss, 2004). The mixing ratio between "source water" (i.e., typically river or lake water) and ambient groundwater can additionally help attenuating contaminants due to dilution (Tufenkji et al., 2002).

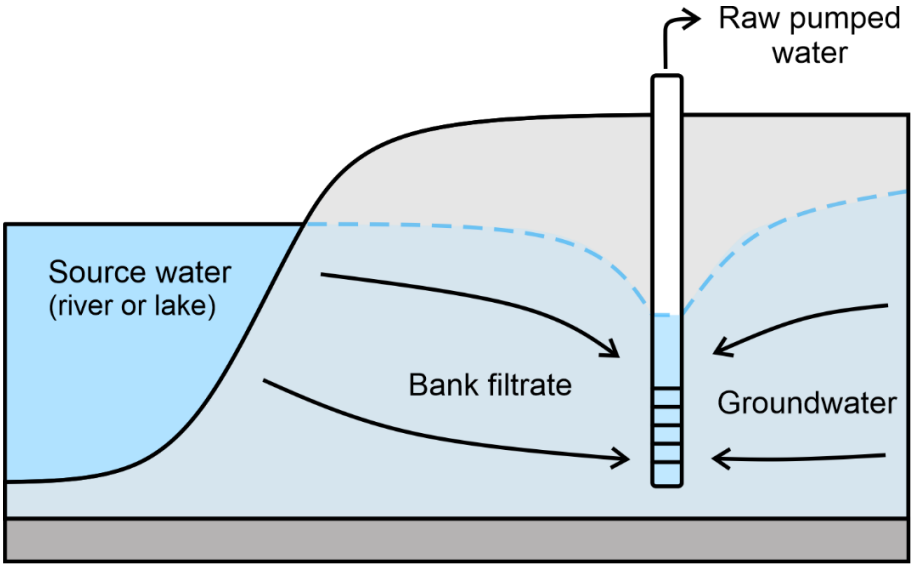

Figure 1-1 Schematic representation bank filtration

BF has been used as a (pre-)treatment method for over 200 years. The first known BF site was in Glasgow (UK) in 1810. The method rapidly gained in popularity across Europe to cope with deteriorated quality of rivers and growing water demand due to the Industrial Revolution (Sprenger et al., 2017). As of today, BF is widely used in some European countries, such as Slovakia and Hungary, where it accounts for 55% and 50% of the total public water supply, respectively (Sprenger et al., 2017).

Table 1-1 List of the existing bank filtration (BF) sites as reported in the global inventory of managed aquifer recharge sites (IGRAC, 2021). Underlined countries correspond to regions where BF sites are presumably in snowmelt-dominated basins (Barnett et al., 2005).

			Source water			Main objective		
Continent	**country**	***n***	**River water**	**Lake water**	**No data**	**Water Quality Management**	**Maximize Natural Storage**	**Other[1]**
Africa	Egypt	1	1			1		
Total Africa		*1*	*1*			1		
Asia	India	3	2	1		3		
	Malaysia	1	1			1		
	Vietnam	1		1				1
Total Asia		*5*	*3*	*2*		4		1
Europe	Austria	7	6		1	5		2
	Czech Republic	2	2			1		1
	Finland	7	4	3		4	1	2
	France	7	7			6	1	
	Germany	47	43	4		40		7
	Hungary	5	5			5		
	Italy	1	1					1
	Latvia	1	1				1	
	Netherlands	39	36	3		32	5	2
	Norway	2	1	1				2
	Poland	5	4	1		5		
	Romania	3	3			3		
	Russia	1	1					1
	Serbia and Montenegro	2	2			1	1	
	Slovakia	4	4			1	3	
	Slovenia	1	1				1	
	Spain	1	1				1	
	Switzerland	4	4			2		2
	United Kingdom	5	5			4		1
Total Europe		*144*	*131*	*12*	*1*	109	14	21
North America	USA	9	9					9
Total North America		*9*	*9*					9
South America	Brazil	5	2	3		5		
	Costa Rica	2	2					2
Total South America		*7*	*4*	*3*		5		2
Total		***166***	***148***	***17***	***1***	***119***	***14***	***33***
			(89%)	***(10%)***	***(1%)***	***(72%)***	***(8%)***	***(20%)***

[1]Includes management of water distribution systems, physical aquifer management, other benefits and no data.

Recently, an extensive effort has been made to collect data on existing managed aquifer recharge (MAR) sites (Stefan & Ansems, 2018). This global inventory lists a total of 1130 MAR sites worldwide, among which 166 are BF sites, located in 26 countries (Table 1-1). The majority of the listed BF sites are in Europe ($n = 144$), 33% and 27% of them being in Germany ($n = 47$) and Netherlands ($n = 39$) respectively. Other BF sites ($n = 22$) are found in countries of the Global South (Egypt, India, Malaysia, Vietnam, Brazil, and Costa Rica) and USA. River water is used as source water for 89% of the BF sites globally, while only 10% of the reported sites rely on lake water. Water quality management represents the main objective for 72% of the listed BF sites (IGRAC, 2021). While informative, this global inventory represents a lower limit estimation of the existing MAR sites as it is based on self-reported information.

1.3 Thesis Outline

This thesis is organized in 8 sections. Chapter 2 presents a critical literature review concerning the challenges relative to the use of BF systems. It also includes a description of the study site and the selected environmental tracers that are used in this work. Chapter 3 introduces the research objectives, hypotheses, and describes the monitoring and sampling program. Chapters 4 to 6 form a paper-based core, which includes three published manuscripts. A fourth paper, submitted to the journal Groundwater and available in appendix, was elaborated with the aim of sharing knowledge with the community of regulatory authorities and water professionals. It highlights the noteworthy aspects of the study site, i.e., a flood-affected quarry lake BF site in Quebec (Canada), and summarizes the challenges and lessons learnt from one decade of operation and research projects, including this work. A general discussion on methodological aspects is presented in Chapter 7. Overall conclusions and research perspectives are provided in Chapter 8.

CHAPTER 2 LITTERATURE REVIEW

2.1 Challenges Relative to the Use of Bank Filtration

2.1.1 Efficiency of BF systems

The quality of the pumped water at BF sites is difficult to anticipate, as it depends on the quality of both source water and ambient groundwater, and the flow and transport parameters of the aquifer (Hiscock & Grischek, 2002). To optimize the quality of the pumped water, some design parameters can help control the travel times and mixing ratios. These include distance from surface water to wells and spacing between wells (Dillon et al., 2002; Mustafa et al., 2016; Zhu et al., 2019). However, travel times and mixing ratios are also influenced by site-specific environmental parameters, such as the hydraulic conductivity and porosity of the aquifer materials. As BF sites are typically found in alluvial aquifers along rivers (Sprenger et al., 2017), these two last parameters are often heterogenous at the scale of a BF site, which adds to the inherent complexity of BF systems. Consequently, there is greater uncertainty regarding the quality of the pumped water at the planning phase of BF systems than for conventional water production plants (Jasperse, 2011).

2.1.2 Evolution of operational conditions

The quality of the pumped water may also evolve during the operational phase of BF systems. Below are examples of BF sites where modifications to the initial concept or management strategies were required to cope with changing conditions.

The water quality of the Lower Rhine was seriously deteriorated from 1950 to 1975 due to contamination with organic pollutants. This caused a shift in reduction-oxidation (redox) conditions (from oxic to reduced) at BF sites along this river (e.g., Düsseldorf waterworks, Germany) and resulted in the need to treat the raw pumped water for iron, manganese and ammonium (Schubert, 2002).

In the 1990s, there was a decrease in water demand in Saxony and, consequently, a lowering of the abstraction rates. This situation resulted in an increase of the share of the nitrate- and sulfate-containing groundwaters in the raw pumped mix at BF sites and a difficulty to meet the drinking-water quality standards (Grischek et al., 2010). To cope with this issue, many management

measures can be adopted. According to Grischek et al. (2010), these include strategies at i) the BF site scale (e.g., preferential operation of wells where the share of river water is the highest, construction of new wells with optimized mixing ratios, removal of low-permeability sediments in the river bed) and at ii) the regional scale (e.g., land-use management to limit contamination of groundwater).

Successful modifications to initial design or management strategies are often the result of long-lasting trial-and-error experiments and/or years of accumulated empirical knowledge of the functioning of a BF system (Nagy-Kovács et al., 2018). Indeed, to implement management and operational strategies, water managers need to have a clear picture of groundwater flow patterns at the BF scale, i.e., spatiotemporal variability of mixing ratios, travel times, and a comprehension of the variability of the quality of the source water.

2.1.3 Impact of floods on bank filtration

Flooding also adds to the challenges of using BF. During flood events, the transience of BF sites is exacerbated, and groundwater flow patterns are expected to evolve at short (e.g., daily) timescales (Wett et al., 2002). High stream flow often results in rapid travel times (Eckert & Irmscher, 2006; Hunt et al., 2005; Wett et al., 2002) and deteriorates source water quality (Whitehead et al., 2009). These conditions affect the capacity of BF systems to attenuate contaminants and may lead to the breakthrough of pathogens, metals, suspended solids, dissolved organic carbon and organic micropollutants (Sprenger et al., 2011).

Common measures to mitigate the risk of contamination thus include the construction of watertight well head and well casing to prevent short-circuiting of floodwater (Musche et al., 2018). However, infiltration of floodwater in the aquifer and its rapid movement to the wells cannot be prevented by any man-made measure or construction. Understanding of BF systems resilience to hydrological condition changes and water quality changes is essential to ensure proper management (Ascott et al., 2016).

2.1.4 Bank filtration in snowmelt-dominated basins

At latitudes higher than 45° and in mountainous regions, the hydrological cycle mainly depends on snow precipitations and snowmelt water (Barnett et al., 2005). Snowmelt waters are not only

important to recharge aquifers and maintain streamflow (Flerchinger et al., 1992), but also for the renewal of lakes in floodplains during springtime freshets[1] (Falcone, 2007). In fact, in snowmelt-dominated basins, floodplain inundation is not uncommon during springtime, as melting of snowpack results in peak discharge in late spring and early summer (Miller et al., 2014).

The springtime freshets represent an additional challenge to the use of BF, as they can lead to floods which magnitude and timing are difficult to predict (Agnihotri & Coulibaly, 2020; Ahmed et al., 2015). This concern is exacerbated in the actual context of climate change. With warmer temperatures, a shift from snow- to rain-dominated winter precipitations is expected (Kapnick & Hall, 2012). This change will likely result in earlier onset of snowpack melting and advanced timing of peak streamflow (Barnett et al., 2005; Leveque et al., 2021), and lead to a decrease of the mean annual streamflow (Berghuijs et al., 2014). Under projected climate conditions, it is also expected that snowmelt-dominated regions will experience an increase in extreme flooding events during springtime (Rouhani & Leconte, 2018).

On the other hand, springtime freshets and floodplain inundation may represent an opportunity to use BF in snowmelt-dominated basins. The use of BF in the vicinity of small rivers or small lakes is not common, as the pumped volumes could exceed the renewal of water resources. Preferred sites to implement BF systems are usually along large rivers or lakes (Gillefalk et al., 2018). However, in snowmelt-dominated basins, the yearly contribution of floodwater aquifers and lakes offers the potential to implement pumping wells in the vicinity of smaller scale rivers and lakes.

According to the global managed aquifer inventory (IGRAC, 2021), there is a fair number of BF systems applications (n = 30) in these regions (Table 1-1). This estimate represents a lower limit, as it is very likely that many systems are not reported. For instance, in Quebec (Canada), municipal wells are often located at < 500 m from a surface water body and are potentially benefiting from BF (Patenaude et al., 2019). In sum, the BF sites in snowmelt-dominated regions are operating in highly transient hydrological conditions and are presumably numerous.

---

[1] Freshets are defined as snowmelt-induced floods.

Yet, it appears that no studies have assessed the functioning of BF sites affected by recurring springtime freshets. This knowledge gap leaves the water managers with a lack of examples and experience to base monitoring and operational strategies on. There is, thus, a need to better understand the dynamics of groundwater flow and storage at BF sites affected by recurring springtime freshets.

2.2 Study site

The selected BF site is located in the greater metropolitan region of Montreal, Quebec (Canada). The following sub-sections provide an overview of the hydrogeological and climate contexts in addition to providing a description of the studied BF system.

2.2.1 Geological and hydrological setup

The BF system is located on a small alluvial sandy bank (500 m x 100 m) separating two artificial lakes, namely Lake A and Lake B (Figure 2-1). The sandy bank is part of a paleochannel aquifer extending in the North-East South-West (NE-SW) direction and carved within the Champlain Sea clays. The maximum depth of the aquifer is ~26 m (Figure 2-2). In the area between the wellfield area and Lake DM, there is a thin layer (few centimeters to ~ 2 m) of alluvial sands atop the clayey sediments (Figure 2-2; Appendix A).

Lake A (2.8×10^5 m^2) and Lake B (7.6×10^4 m^2) were both excavated within the aforementioned paleochannel and have maximal depth of ~ 20 m (see bathymetry of the lakes; Figure A3 and Figure A4, Appendix A). While the sand dredging activities are still on-going at Lake A, they stopped at Lake B decades ago. A residential area and a public beach border Lake B on the NW, NE and SE shores. Before the onset of the BF system, the water levels at Lake A and Lake B were fluctuating between ~22 m.a.s.l and ~23 m.a.s.l (Ageos, 2010).

Lake A receives surface water inflow from a small stream (S1) and has an intermittent hydraulic connection with Lake DM via two channelized streams (S2 and S3). The direction of the surface water fluxes at S2 and S3 depends on 1) the water levels of both lakes and 2) the exceedance of the topographic threshold at 22.12 m.a.s.l. (observed along the streambed of S2) (Ageos, 2010). All three streams (S1, S2 and S3) are currently ungauged. It was estimated that the annual flow rate at S1 is ~ 0.32 m^3/d (Ageos, 2010). The location of groundwater inflows at Lake A are unclear

because there are no observation wells in the vicinity of Lake A. Nevertheless, groundwater outflows undoubtedly occur at the NE shore of Lake A due to the pumping at the BF site.

Lake B receives no surface water inputs. According to Ageos (2010), the regional groundwater flow direction is from NE to SW and contributes to the groundwater inputs of Lake B. Similarly to Lake A, pumping at the BF site forces water to exist Lake B as groundwater outflows along the SW shore. Water can also exit Lake B through an artificial ungauged outlet (at an elevation of ~21.8 m.a.s.l.) connected to the Town's stormwater collection system and located on the South shore of the lake.

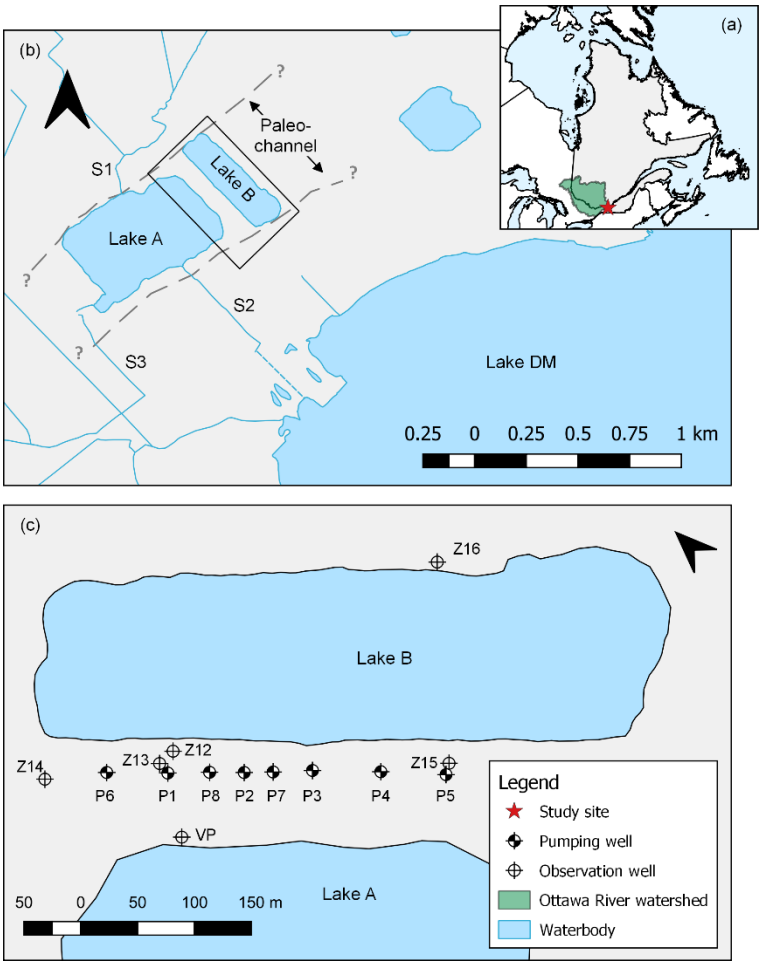

Figure 2-1 Location of (a) the site and Ottawa River watershed, (b) Lake A, Lake B and Lake DM, and (c) pumping wells and observation wells. Approximate limits and extent of the paleo-channel are depicted in (b).

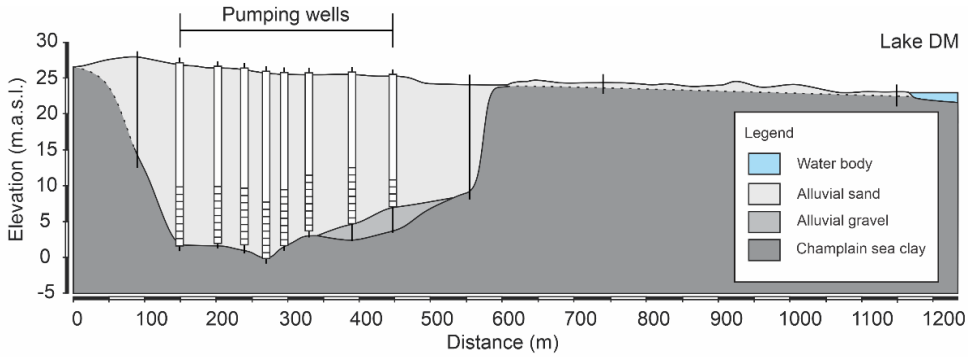

Figure 2-2 Geological cross-section of the study site (adapted from Ageos, 2010)

Lake DM corresponds to a widening of the Ottawa River at the confluence with St Lawrence River. The Ottawa River is the second largest river in eastern Canada, draining a watershed of approximately 150,000 km^2 (MDDELCC, 2015). The water level of Lake DM is partly controlled by dams upstream on Ottawa River. According to the Centre d'Expertise Hydrique du Québec (2020), long-term median water level of Lake DM ranges between ~21.6 m.a.s.l.(early August to early October) and ~22.9 m.a.s.l. (late April to early May). High water levels typically occur during springtime due to precipitations and melting of the snowpack over the Ottawa River watershed.

In sum, the BF site is located within a highly anthropized hydrosystem – the lakes being man-made and the water level being partly controlled by human activities or infrastructures (pumping, artificial outlet at Lake B, dammed-controlled water level of Lake DM). While the hydrogeological setting is well described, a detailed understanding of the inter- and intra-annual dynamics of groundwater flow at the BF system and the role of flood events on water availability could benefit the short-term and long-term management of the BF system.

2.2.2 Climate

Figure 2-3 illustrates the average precipitation and temperature from 1981 to 2010 at Montréal-Trudeau International Airport meteorological station located at an 18 km distance from the study site (available from weatherstats.ca and based on Environment and Climate Change Canada data).

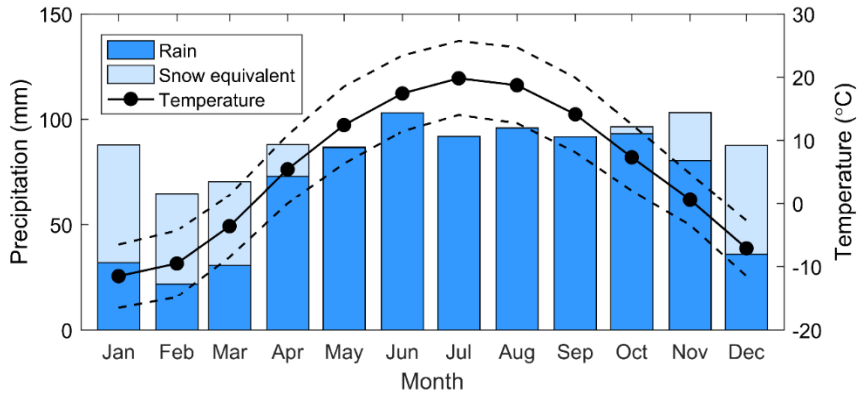

Figure 2-3 Daily average precipitation (left axis) and daily average temperature (right axis) from 1981 to 2010 at Montreal-Mirabel International Airport meteorological station (based on Environment and Climate Change Canada data). The dashed lines correspond to the monthly mean of the daily minimum and the daily maximum temperatures.

On average, the monthly precipitation ranges between 65 mm (in February) and 103 mm (in November), and the annual precipitation is 1068 mm (Figure 2-3; left axis). Precipitation mainly falls as snow from December to March. Snowpack melting occurs from the end of winter to early spring (i.e., late March to early May). Figure 2-4 (a-b) compares a view on the well field during springtime and wintertime. A few centimeter-thick snowpack is observable on Figure 2-4 (b).

Average temperatures range from -11.5°C (in January) to 19.8°C (in July), and mean annual temperature is 5.3°C (Figure 2-3; right axis). Extreme minimum and maximum temperatures are -37°C (January) and 36.1 °C (August). Temperatures are below 0°C from December to March. During this period, the surface of Lake A and Lake B freezes, as shown on Figure 2-4 (d).

Figure 2-4 View on well field on (a) May 16, 2017 and (b) January 24, 2019, and view on Lake A on (c) August 28, 2018 and (d) February 27, 2018. The location and orientation of the pictures are illustrated in Figure A-2 in Appendix A.

2.2.3 Topography

Figure 2-5 illustrates the topography of the study site. Overall, the elevation increases from SE to NW and ranges from ~22 m.a.s.l. to ~30 m.a.s.l. Pumping wells P5 (the lowest) and P6 (the highest) are at an elevation of ~24.5 m.a.s.l. and ~26.7 m.a.s.l., respectively. In the area between Lake A and Lake DM, the topography is nearly flat and ranges mainly from ~22 m.a.s.l. to ~24 m.a.s.l. It is worth noting that the mounds on the SE side of Lake A are man-made sand piles resulting from the on-going sand dredging activities.

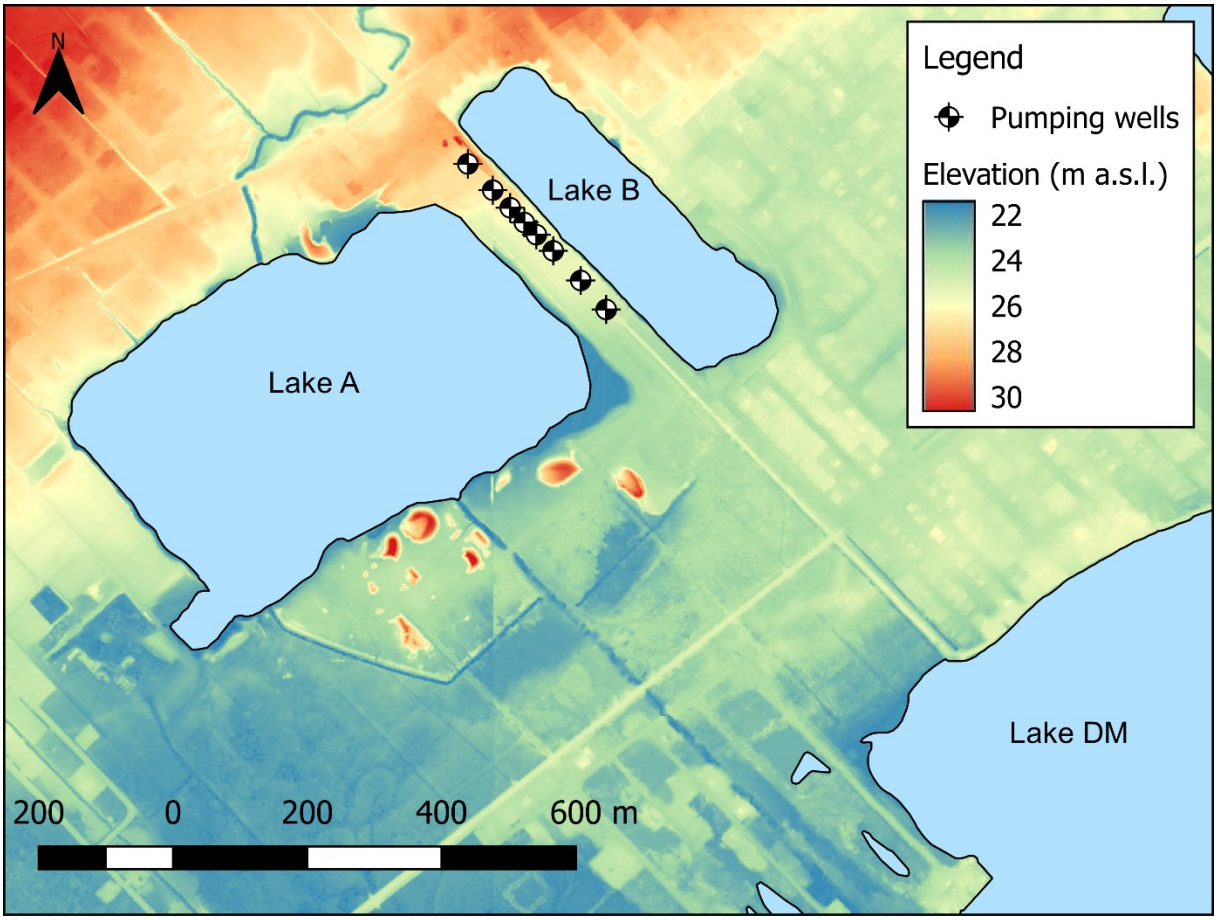

Figure 2-5 Topography of the study site. Data correspond to the digital elevation model produced from Lidar data (Ministère des Forêts, 2020).

2.2.4 Description of the BF system

The BF system has been operating since October 2012. It is composed of eight pumping wells (P1 to P8). Each well is equipped with a variable flow rate pump, except for P5 which has a fixed flow rate pump (3600 m^3/d). This setup allows the water managers to operate the wells independently and to adjust the pumping rates according to the real-time water demand and adapt the pumping strategy to optimise the quality of the pumped water. Precisely, the wells are operated according to a priority order (i.e., P6, P3, P1, P8, P2, P7, P4 and P5) aiming at lowering iron and manganese concentrations in the raw pumped water. During this research project, P6 and P3 were the most solicited, while P4 and P5 were rarely in operation. P1, P8, P2 and P7 were mainly used to fulfill the daily or seasonal peak water demand. Table 2-1 lists the mean, minimum and maximum

pumping rates from 2013 to 2018. The pumping wells are typically operating at rates between ~4600 m^3/d and ~7500 m^3/d (all wells combined).

Table 2-1 Mean, minimum and maximum pumping rates and total pumped volume from 2013 to 2019. Estimates calculated from the daily pumped volume at each well.

			Year							Mean
			2013	2014	2015	2016	2017	2018	2019	
Rate	mean	(m^3/d)	5 643	5 539	4 935	5 263	4 872	5 572	5 428	5 322
	min	(m^3/d)	4 382	3 975	3 912	3 979	3 680	4 075	4 637	4 091
	max	(m^3/d)	6 969	6 820	6 957	7 425	6 982	7 909	6 883	7 135
Volume	total	(x 10^6 m^3)	2.172	2.098	1.804	1.944	1.803	2.037	1.801	1.951

2.3 Environmental tracers

Over the last few decades, environmental tracers have been applied to a variety of hydrogeological contexts to depict the origin and evolution of water masses. As water is a good solvent, its 'history' is encoded at each step of the hydrological cycle through dissolution, transport, and precipitation of solutes. Environmental tracers are particularly interesting to depict the functioning of complex hydrosystems, as they allow to reconstruct flow patterns of water masses by information in time and space. Environmental tracers are thus complementary to the hydrodynamic measurements, which can be affected by local heterogeneities and transience of complex hydrosystems.

Tracers can be categorized into two groups: artificial and environmental. Artificial tracers are tracers that are deliberately introduced into an hydrosystem, whereas environmental tracers are naturally present in the water cycle. Environmental tracers are advantageous compared to artificial tracer tests from a logistical and legislative point of view (preparation and authorizations). They are also widely used in studies of surface and groundwater interactions, as they encode information about the origin of the water, its age and the processes it has undergone.

Sprenger (2016) argues that there are three types of environmental tracers, dissolved tracers (e.g., Cl^-, Br) or a measure of the sum of dissolved ions (EC), stable isotopes (e.g., $\delta^{18}O$, δ^2H, $\delta^{11}B$, ^{87}Sr, δ^7Li) and temperature. Another category that can be added to this classification is radioactive tracers (e.g., ^{222}Rn, ^{226}Ra). There is no ideal tracer, but rather an optimal combination of tracers for a specific context. By combining their use, it is possible to achieve an improved understanding of

a hydrogeochemical system. They highlight a range of residence times and the presence of a variety of processes occurring in the subsurface. As a result, environmental tracers are robust tools for monitoring BF systems and understanding the evolution of water quality over long periods (Kloppmann et al., 2009).

In the context of this thesis, electrical conductivity (EC), stable isotopes of the water molecule ($\delta^{18}O$, $\delta^{2}H$) and temperature were used as tracers to identify different water masses, including floodwater. For each of these selected tracers, a brief description and example of application at BF sites are provided below.

2.3.1 Electrical conductivity

Electrical conductivity (EC) is representative of the water's mineralization, i.e., it is roughly proportional to the concentration of dissolved ions in the water. Although major cations (Ca^{2+}, Mg^{2+}, Na^{+} and K^{+}) contributing to the EC can interact with the aquifer matrix, EC can be considered as a quasi-conservative tracer in some contexts. Specifically, during BF, the source water travels rapidly in the aquifer towards a pumping well, and advective transport is typically dominant (over water-matrix interactions) (Sprenger, 2016). From a practical point of view, the use of EC is convenient as it is a robust and low-cost measure (Sheets et al., 2002).

In the context of BF systems, the natural EC contrast between source water (i.e., river or lake) and groundwater is typically significative, and EC can be used to assess mixing ratios (Bertin & Bourg, 1994). Given a temporal variability of EC signal in the source water, it can also be used to estimated travel times of the bank filtrate (Cirpka et al., 2007; Sheets et al., 2002; Vogt et al., 2010).

2.3.2 Stable isotopes of the water molecule

Water is composed of two hydrogen and one oxygen atoms, and both atoms have more than one stable isotopes[2]. The most abundant hydrogen and oxygen isotopes are ^{1}H and ^{16}O. Deuterium (^{2}H or D), ^{17}O and ^{18}O also exist naturally, but in small proportions. Hence, most water molecules

[2] Isotopes are atoms with different number of neutrons and thus different mass.

weight 18 amu (^{1}H, ^{1}H, ^{16}O), but some molecules can weight from 19 amu (^{2}H, ^{1}H, ^{16}O or ^{1}H, ^{1}H, ^{17}O) to 22 amu (^{2}H, ^{2}H, ^{18}O).

The distribution of the isotopologues[3] of water molecules in the environment is heterogenous as they partition during the hydrological cycle due to mass differences. For instance, light water molecules (^{1}H, ^{1}H, ^{16}O) will preferentially evaporate from a water body, while the heavier molecules will preferentially remain in the liquid phase. As a result, the isotopic composition of surface waters present a seasonal cyclicity, which is convenient for tracking the infiltration of surface water (Rozanski et al., 2013). In the context of BF systems, the seasonal cyclicity of ^{18}O and ^{2}H in surface waters has been used to assess the travel time of bank filtrate (Maloszewski, 2000; Massmann et al., 2008).

The concentration in stable isotopes is expressed as the difference between the isotope ratio (rare to abundant isotope) of the sample and a reference:

$$\delta^{18}O_{sample} = \left(\frac{(^{18}O/^{16}O)_{sample} - (^{18}O/^{16}O)_{reference}}{(^{18}O/^{16}O)_{reference}}\right) \times 1000\ ‰$$

$$\delta^{2}H_{sample} = \left(\frac{(\ ^{2}H/\ ^{1}H)_{sample} - (\ ^{2}H/\ ^{1}H)_{reference}}{(\ ^{2}H/\ ^{1}H)_{reference}}\right) \times 1000\ ‰$$

Positive δ-values are enriched in ^{18}O (or ^{2}H), while negative δ-values are depleted in ^{18}O (or ^{2}H) relative to the reference. The standard reference for water molecule is the Vienna Standard Mean Ocean Water (VSMOW) (Clark, 2015).

2.3.3 Temperature

In aquifers, heat is transported via groundwater (advective heat transfer) and porous matrix (conductive heat transfer). Temperature can be used qualitatively to identify surface water/groundwater interactions. In BF context, temperature is used as a tracer to estimate travel time of the bank filtrate (Bekele et al., 2014; Hoehn & Cirpka, 2006; Sheets et al., 2002). Similarly to EC, the use of heat as a tracer is interesting as temperature measurements are robust and low-

[3] Isotopologues are molecules which have different isotopic composition.

cost (Conant et al., 2004; Johnson et al., 2005). However, its quantitative interpretation requires computational work and skills, as temperature is a non-conservative parameter.

CHAPTER 3 RESEARCH OBJECTIVES, HYPOTHESES AND METHODOLOGY

3.1 Objectives of the thesis

The main research goal of this thesis is **to reveal the dynamics of groundwater flow patterns at a BF site affected by recurring springtime flood events**. To meet this goal, an investigation method is developed and applied to a selected BF site in Quebec (Canada).

As demonstrated above, BF systems are not operated under steady-state pumping regimes (i.e., anthropic control) and/or hydrological conditions (i.e., meteorological control). Yet, the spatio-temporal variability of mixing ratios is rarely assessed, although crucial to anticipate water quality changes at BF systems. The dynamics of groundwater flows at the selected BF site are first assessed at the monthly timescale with the specific objective **to distinguish the role between anthropic and meteorological controls on the mixing ratios and on the physico-chemical quality of the raw water**.

To anticipate changes in water quality during flood events, water managers would benefit from understanding the dynamics of groundwater flow patterns at a shorter timestep. With an optimized monitoring strategy, water managers could adapt the timing for the time-consuming and costly routine monitoring of microbial water quality. The second specific objective of this thesis is **to develop a short time-step monitoring strategy to reveal the spatiotemporal dynamics of groundwater flow patterns under major flood events.**

At flood-affected lakes, direct measurements of surface water fluxes are difficult to perform. Nonetheless, such fluxes impact the resilience of a lake to groundwater quantity and quality changes. Long-term management of flood-affected BF systems would benefit from a quantification of these fluxes. The third specific objective is **to differentiate the respective role of direct floodwater inputs and temporary subsurface storage of floodwater on the water balance of a lake used as source water for the BF site.**

3.2 Hypotheses

The specific objectives relate to the following hypotheses:

- Surface water level changes and pumping rate changes affect the groundwater flow patterns at BF sites and result in spatiotemporal variability of mixing ratio and physico-chemical quality of the pumped water ;
- Combining different environmental tracers, timestep monitoring and spatial resolutions allows to critically depict groundwater flow pattern changes during and after a major flood event, and can help at planning the sampling for pathogen indicators ;
- In ungauged floodplains, identification and quantification of floodwater fluxes can be obtained indirectly by measurements of isotopic signature of water masses and transient modelling of lake water budget, and help at predicting the resilience of a lake to perturbations.

3.3 Research strategy

The results of this research project are included in three published articles presented in Chapter 4, Chapter 5 and Chapter 6, respectively. This section outlines the general results of each article and their coherence with the research objectives.

Article #1 (Chapter 4), published in the journal *Water* (2019), addresses the first specific objective of the research project. It investigates the monthly evolution of the mixing ratios at pumping wells and examines the control of pumping rates and hydraulic conditions. To do so, an EC-based and time-varying binary mixing model of the contributing source waters to the pumping wells is developed. The results of the model are then used to discuss the implications for the water quality (i.e., Fe and Mn concentrations) of the bank filtrate over a 1-year period, which spans a springtime flood event.

Article #2 (Chapter 5), published in the journal *Science of the Total Environment* (2021), aims at fulfilling the specific objective 2. The impacts of annually recurring and major flood events on the dynamics of groundwater flow patterns during bank filtration are further investigated. A multi-tracer monitoring framework is performed to qualitatively depict i) the sub-daily evolution of

groundwater flow patterns during a flood event and ii) the infiltration and storage of floodwater at a monthly timescale. The frequency of typical water quality routine analysis (i.e., total coliforms and *E. coli*) is linked to the timescale of observable changes in the tracers' signals (i.e., electrical conductivity, temperature and stable isotopes of the water molecule). An optimized tracer-based monitoring framework was revealed to be useful to anticipate water quality changes and to help adapting the timing of the routine sampling for water quality in real time.

Article #3 (Chapter 6), published in the journal *Hydrology and Earth System Sciences* (2021), focuses on the specific objective 3. It explores the water balance of a lake which constitutes a source water for the studied BF system and receives floodwater inputs during springtime freshets. A volume-dependent isotopic mass balance model was developed and used to predict the implications of temporary subsurface floodwater storage and discharge on the water balance partition and resilience to changes in groundwater quantity and quality.

Collectively, the papers address the research objectives. They explore the transience of a flood-affected BF site and link groundwater flow pattern changes to water quality changes. The papers also allow identifying the role of the recurring springtime freshets in supporting the sustainability of the studied BF system. A fourth paper, submitted to the journal *Groundwater*, is included in the Appendix. As mentioned above, it aims at highlighting the main characteristics of this BF facility, at emphasizing on its unique and noteworthy aspects and illustrating the lessons learnt from one decade of operation and research projects.

3.4 Monitoring and water sampling program

Hydrological and geochemical data was collected within the scope of this thesis at the study site during a 3-year period (from May 2016 to June 2019) and spanned two historical springtime flood events. Unprecedented water levels (≥ 24.77 m.a.s.l.) were reached at Lake DM on May 8th, 2017 and April 29th, 2019. This data complements the data obtained from monitoring campaigns by the municipality since the beginning of the BF system operation.

The pumping wells are equipped with automatic loggers and the mean daily pumping rates at P1 to P8 were obtained from the Town. In addition, pressure-temperature loggers were installed at

selected observation wells (Z12, Z13, Z14, Z15, Z16, Z22 and/or VP) and at Lake A and Lake B during specific periods.

Table 3-1 details the conceptualization of the physico-chemical, geochemical and isotopic sampling program. Water sampling was performed monthly and occurred on the same day as the Town's regulatory surveillance program. Aliquots were systematically collected at pumping wells (P1 to P8), selected observation wells (Z12, Z13, Z14 Z15, Z16, Z22 and/or VP) and at Lake A and Lake B (at the surface and along depth-resolved profiles). Additional sampling campaigns were conducted to perform depth-resolved profiles at the lakes. Physico-chemical parameters, including temperature, EC, pH and redox potential, were measured on-site. Aliquots were collected for the analysis of major ions (including Na^+, Ca^{2+}, Mg^{2+}, Cl^-, NO_3^-, SO_4^{2-}), alkalinity, metals (Fe and Mn) and stable isotopes of the water molecule ($\delta^{18}O$ and δ^2H).

Table 3-1 Conceptualization of the physico-chemical, geochemical and isotopic sampling program. The frequency of the water sampling was monthly (M), quarterly (3M) or occasionally (O).

	Pumping wells	Selected observation wells	Lake A		Lake B	
			Surface	Depth	Surface	Depth
Physico-chemical parameters[1]	M	M	M	3M	M	M to 3M
Major ions[2]	M[5]	M	M	M	M	M
Alkalinity	M	M	M	M	M	M
Metals[3]	M[6]	O	O	O	O	O
Isotopes[4]	M	M	M	3M	M	M to 3M

[1]Physico-chemical parameters include the temperature, electrical conductivity (EC), pH and redox potential.
[2]Major ions include Na^+, Ca^{2+}, Mg^{2+}, Cl^-, NO_3^-, SO_4^{2-}.
[3]Dissolved Fe and dissolved Mn concentrations.
[4]Stable isotopes of the water molecule ($\delta^{18}O$-H_2O and δ^2H-H_2O).
[5]Water sampling was performed by the Town's water managers. Aliquots were not analyzed for NO_3^-.
[6]Water sampling was performed by the Town's water managers. Aliquots were analyzed for both total and dissolved metal (Fe and Mn) concentrations.

Described above is the baseline monitoring and sampling program. Complementary measurements were performed to supplement the data when necessary. Details are provided in the methodology section of each article (Chapter 4 to Chapter 6) when applicable.

CHAPTER 4 ARTICLE 1: ANTHROPIC AND METEOROLOGICAL CONTROLS ON THE ORIGIN AND QUALITY OF WATER AT A BANK FILTRATION SITE IN CANADA

This chapter was published as a research paper in the journal *Water* (Special Issue *Managed Aquifer Recharge for Water Resilience*) in 2019.

Masse-Dufresne, J., Baudron, P., Barbecot, F., Patenaude, M., Pontoreau, C., Proteau-Bedard, F., Menou, M., Pasquier, P., Veuille, S. & Barbeau, B. (2019). Anthropic and Meteorological Controls on the Origin and Quality of Water at a Bank Filtration Site in Canada. Water, 11(12), 2510. doi:10.3390/w11122510

ABSTRACT

At many bank filtration (BF) sites, mixing ratios between the contributing sources of water are typically regarded as values with no temporal variation, even though hydraulic conditions and pumping regimes can be transient. This study illustrates how anthropic and meteorological forcings influence the origin of the water of a BF system that interacts with two lakes (named A and B). The development of a time-varying binary mixing model based on electrical conductivity (EC) allowed the estimation of mixing ratios over a year. A sensitivity analysis quantified the importance of considering the temporal variability of the end-members for reliable results. The model revealed that the contribution from Lake A may vary from 0% to 100%. At the wells that were operated continuously at >1000 m^3/day, the contribution from Lake A stabilized between 54% and 78%. On the other hand, intermittent and occasional pumping regimes caused the mixing ratios to be controlled by indirect anthropic and/or meteorological forcing. The flow conditions have implications for the quality of the bank filtrate, as highlighted via the spatiotemporal variability of total Fe and Mn concentrations. We therefore propose guidelines for rapid decision-making regarding the origin and quality of the pumped drinking water.

4.1 Introduction

Bank filtration (BF) is known as a cost-effective treatment step to produce drinking water (Haas et al., 2018; Ross & Hasnain, 2018). This natural or artificially induced process occurs as surface water infiltrates into the aquifer from the banks and/or bed of a lake or a river and is subsequently

intercepted by a pumping well (Gillefalk et al., 2018). During subsurface passage, water is exposed to physical, chemical, and biological processes, which may attenuate contaminants initially present in the surface water but also release unwanted minerals (Gunkel & Hoffmann, 2009; Hiscock & Grischek, 2002). BF systems have proven to be efficient for the removal of turbidity (Dash et al., 2010; Ronghang et al., 2019; Sahu et al., 2019), pathogens (Harvey et al., 2015; Otter et al., 2019; Romero et al., 2014), and organic compounds (Grunheid et al., 2005; Hamann et al., 2016; Massmann et al., 2006; Nagy-Kovacs et al., 2018). The efficiency of BF systems to attenuate contaminants is strongly controlled by travel times (Dragon et al., 2018; Hamann et al., 2016) and redox conditions (Burke et al., 2014; Greskowiak et al., 2006; Munz et al., 2019), which in turn depend on numerous site-specific natural and engineered parameters. Natural parameters include the hydrological and hydrogeological conditions, surface and groundwater quality, and prevailing physico–chemical conditions (Groeschke et al., 2017). Engineered parameters refer to the number of wells, the distance between wells and surface water, well spacing, the well type, depth, radius, location, and screen length (Ahmed & Marhaba, 2017; Jiang et al., 2019).

Most BF systems are in the vicinity of rivers, where the bank filtrate is a mixture of surface water and ambient groundwater (Dillon et al., 2019; Hiscock & Grischek, 2002). Numerous studies have shown that the dilution of contaminants by high-quality groundwater can also help to attenuate contaminants, enhancing the efficiency of a BF system. For instance, Kvitsand et al. (2017) reported that dilution with ambient groundwater was significant enough to lower concentrations of natural organic matter. Derx et al. (2013) numerically studied the effects of flooding on virus removal by bank filtration. They reported that a rapid decrease in river water level can lead to a hydraulic gradient towards the river and a dilution of virus concentrations by regional groundwater. In addition, some BF systems are placed in hydrogeological contexts with low-quality groundwater but can still achieve high-quality raw water with adequate regulation of mixing ratios (Dillon et al., 2002; Gupta et al., 2015; Shamrukh & Abdel-Wahab, 2008; Zhu et al., 2019). Hence, when assessing the performance of a BF system, estimating mixing ratios is crucial to: (1) correctly differentiate between dilution and removal mechanisms and (2) control the occurrence of groundwater-borne contaminants (Hu et al., 2016). BF systems typically show spatial variability of mixing ratios at the pumping wells, since they are affected by the distance to the surface water body (Jiang et al., 2019). Another factor governing the mixing ratios is the drawdown at the

pumping wells (Zhu et al., 2019). The latter is subject to spatial and temporal variations, since BF systems are rarely operated under steady-state hydraulic conditions (e.g., river stage) and/or pumping regimes. However, when calculating mixing ratios, authors rarely discuss the temporal variations and the factors controlling this variability, even though erroneous estimation of the mixing ratios can lead to misinterpretation of the performance of the BF system.

This study aims to provide a better understanding of the relationship between anthropic (i.e., pumping regimes) and meteorological (i.e., hydraulic gradients) effects on the origin of bank filtrate. To this end, we investigated the spatiotemporal variability of flow patterns and mixing ratios at a two-lake BF site, where two surface water types (Lake A and Lake B) contribute to eight pumping wells. A time-varying mixing model based on electrical conductivity (EC) was developed in order to quantify the contributions of Lake A and Lake B (i.e., two water sources and further referred to as end-members) over a one-year period. A sensitivity analysis was conducted in order to test the assumptions concerning the definition of the end-members.

4.2 Site Description

4.2.1 Hydrogeological Context

4.2.1.1 Description of the Bank Filtration and Aquifer System

The studied BF system supplies drinking water to more than 18,000 people in a town near Montreal, Canada (Figure 4-1a). A total of eight pumping wells are located between two artificial lakes (Figure 4-1a,b), which were created by sand dredging activities. The exploitation stopped a few decades ago at Lake B, while Lake A is still in operation. As described by Ageos (2010), the aquifer is a buried valley embedded in the Champlain Sea clays (Figure 4-1b,d). The aquifer is mainly composed of alluvial fine to medium sands. A small lens (≤3.45 m thick) of alluvial gravel (with a sandy matrix in places) lies between the Champlain Sea clays and the alluvial sands near pumping wells P4 and P5 (see Figure 4-1d). The aquifer is fully unconfined. Hydraulic conductivity was estimated as 2.7×10^{-3} m/s (Ageos, 2010).

The maximum thickness of the aquifer is 26 m and the static water level is about 4 m below the ground surface. The sandy bank is 100 m to 120 m wide and approximately 500 m long. All the

pumping wells are screened at the base of the aquifer over an 8 m long section, except for pumping well P5, which only has a 4 m long screen due the shallower depth of the aquifer at this location. The distance between Lake A and the well cluster is 70 m to 80 m, whereas a distance of 30–35 m separates the wells from Lake B. Finally, the wells are spaced 30–60 m from one another.

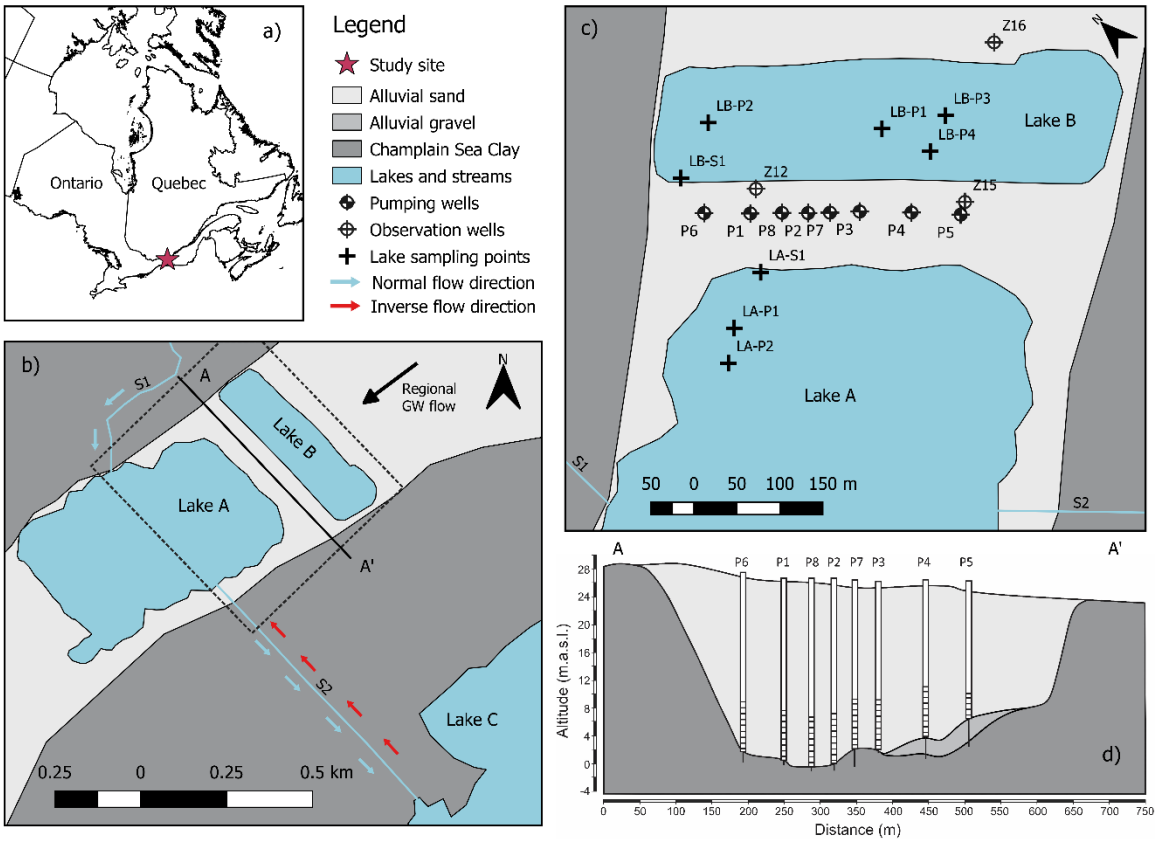

Figure 4-1 Study site location maps (a–c) and schematic lithological cut along pumping wells (d) (adapted with permission from Ageos, 2010)

4.2.1.2 Lake A and Lake B

Lake A (2.8×10^5 m^2) is fed by a stream named S1, which discharges from the North with a mean annual rate of 0.32 m^3/s (Ageos, 2010). It drains a small watershed (14.4 km^2), where land use is mostly industrial and agricultural. A 1 km long channeled stream named S2, located at the southeastern bank, allows water to exit Lake A and flow towards Lake C. The flow direction between Lake A and Lake C can be temporally reversed (Figure 4-1b) when the surface water level of Lake C exceeds both the elevation of Lake A and a topographic threshold at 22.12 m.a.s.l. (Ageos, 2010). Under these hydraulic conditions, Lake A receives surface water inputs from Lake

C. This process typically occurs during spring (from April to May) and more occasionally during autumn (from October to December) due to snowpack melting and/or abundant precipitations. Ageos (2010) reported that surface water input into Lake A seems to control its geochemistry, as it features a Ca-HCO_3 water type.

Lake B (7.6×10^4 m^2) is a groundwater-fed lake without any inlet stream. An artificial outlet channel can drain Lake B water towards the town's stormwater collection system (when Lake B elevation is above approximately 21.8 m.a.s.l.). A NaCl water type is found in Lake B (Ageos, 2010). Pazouki et al. (2016) stated that the salinity of Lake B originates from de-icing road salts that are applied during wintertime. This is supported by the fact that a regional and widely used road is located less than 100 m from the study site. Precipitations are approximately 1000 mm/year and contribute to the water mass balance of both lakes. Runoff is likely a negligible contribution to the water mass balances of the lakes, considering the nearly flat topography. The maximum observed depths at Lake A and Lake B are 20 m and 19 m, respectively (at LA-P2 and LB-P2). Based on the lithological cross sections at the pumping wells and observation wells (Ageos, 2010), it is believed that lake bottoms roughly correspond to the elevation of the marine clay sediments. In this geological context, no or only minor groundwater flow could occur beneath the lake bottom. The sediments at the bottom of the lakes were not sampled and no quantitative information concerning clogging is available. However, while sampling for surface water, relatively high turbidity (denoted by the color and the milky appearance of water) was observed at Lake A, which indicates that the sediments at the lake–aquifer interface are susceptible to clogging (Grischek & Bartak, 2016; Pholkern et al., 2015). Sampling of the sediments would be needed to confirm this hypothesis.

4.2.2 Hydraulics of the Two-Lake BF System

A water table monitoring program was performed by Ageos (2016) from 2012 to 2015. This study reported that, prior to the activation of the BF system in October 2012, surface water levels of Lake B were higher than in Lake A. Such conditions forced surface water to infiltrate and flow naturally through the sandy bank from Lake B to Lake A (Figure 4-2a). For instance, during summer 2012, the water level difference was about 0.1 m, which created a natural hydraulic

gradient of approximately 0.001 between the lakes. Based on Darcy's law, the mean residence time of the water in the bank was approximately one month.

The above-mentioned water table monitoring program also demonstrated that the water level in Lake A was significantly higher than in Lake B during springtime from 2012 to 2016 (i.e., up to 1 m water level difference). This is due to the intermittent hydraulic connection between Lake C and Lake A and supporting surface water inputs into Lake A (see Section 4.2.1). Under such hydraulic conditions, the direction of groundwater flow into the bank is reversed, i.e., from Lake A to Lake B (Figure 4-2b).

Since the implementation of the BF system (on 3 October 2012), the relative surface water elevations of Lake A and Lake B have not been the only controlling factors on the direction and intensity of groundwater flow through the sandy bank. Drawdown of the water table in the vicinity of the active pumping wells induces an artificial hydraulic gradient, forcing surface water from both lakes (A and B) to infiltrate into the sandy bank and travel toward the pumping wells (Figure 4-2c). A schematic representation of the theoretical elevation difference between Lake A and Lake B is shown in Figure 4-2d. When analyzing the data from the monitoring program conducted by Ageos (2016), we depicted three typical hydraulic conditions recurring each year. First, a high hydraulic gradient between Lake A and Lake B develops in response to the hydraulic connection between Lake A and Lake C (as explained above). Second, in summertime, the hydraulic connection between Lake A and Lake C stops and water demand increases. This leads to a moderate hydraulic gradient between the lakes. Finally, in wintertime, a low hydraulic gradient is expected, as surface water inputs into Lake A are very limited and municipal water demands are reduced. In sum, the lake dynamics and the pumping regimes both influence the relative surface water elevations of Lake A and Lake B and allow for a gradual transition from high (during springtime) to low (during wintertime) hydraulic gradient between the lakes.

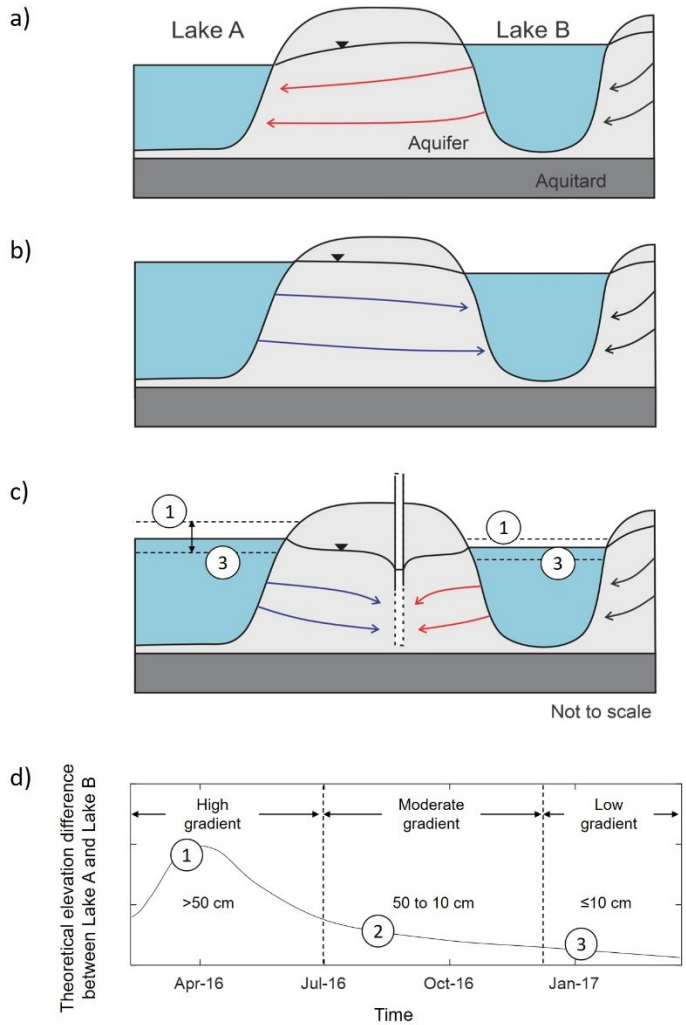

Figure 4-2 Schematic representation of the flow patterns and directions at the study site when (a) elevation of Lake B > elevation of Lake A, (b) elevation of Lake A > elevation of Lake B, and (c) the pumping wells are in operation. Black, blue, and red arrows refer to regional groundwater and water originating from Lake A and Lake B, respectively. Theoretical elevation difference between Lake A and Lake B in (d). Numbers 1 to 3 correspond to different hydraulic conditions, namely high, moderate, and low hydraulic gradients between Lake A and Lake B.

4.3 Materials and Methods

4.3.1 Surface and Groundwater Sampling

Monitoring of surface water and groundwater was conducted on a monthly basis and included measurements of physico–chemical parameters and water sampling for geochemical analyses. Surface water sampling was performed near the shore (see location of lake sampling points LA-S and LB-S in Figure 4-1c). Additional sampling campaigns were conducted at Lake A (on 15 February 2017 at LA-P1 and LA-P2) and Lake B (on 9 September 2016 at LB-P1 and LB-P2 and on 3 March 2017 at LB-P3 and LB-P4) to assess for vertical heterogeneity. Physico–chemical parameters were measured along vertical profiles at 1 to 2 m intervals and water was sampled at multiple depths (e.g., 3 m, 7 m, and 12 m) with a submersible pump. Groundwater sampling was conducted at the pumping wells via a bypass faucet, as submersible pumps permanently regulate flow rate at each well. Water sampling was conducted at least 30 min after pumping started, allowing the stagnant water to be purged. In the case of observation wells, a submersible pump (WSP-12V-5 Tornado, Proactive Environmental Products, Bradenton, Florida, United-States) with a 30 m long polyvinyl chloride (PVC) tube was used and sampling was conducted after purging at least three well volumes and stabilizing the physico–chemical parameters.

Measurements of temperature, pH, electrical conductivity (EC), and redox potential (Eh) were performed with a multiparameter probe (YSI Pro Plus 6051030 and Pro Series pH/ORP/ISE and Conductivity Field Cable 6051030-1, YSI Incorporated, Yellow Springs, Ohio, United-States) installed in an airtight cell connected to the pump. Samples for major ions and alkalinity were collected in 50 mL low-density polyethylene (LDPE) containers and were filtered through a 0.45 µm hydrophilic polyvinylidene fluoride (PVDF) membrane (Millex-HV, Millipore, Burlington, Massachusetts, United-States) prior to analysis. Water samples were transported and stored at 4 °C. The same sampling and transport procedures were applied for total and dissolved metals analysis (Fe and Mn). Following on-site filtration, acidification with HNO_3 (in order to lower pH < 2) was performed in the laboratory within a 24 h delay.

4.3.2 Analytical Techniques

Major ion quantification was performed via either atomic absorption (Aanalyst 200 Atomic Absorption Spectrometer, Perkin Elmer, Waltham, Massachusetts, United-States) or ion chromatography (ICS 5000 AS-DP DIONEX Thermo Fisher Scientific, Saint-Laurent, Quebec, Canada) for all surface water samples and groundwater samples collected at observation wells, depending on the availability of the equipment. Total Fe and Mn concentrations were measured via atomic absorption for all surface water and observation wells samples. Inductively coupled plasma mass spectrometry was used for the quantification of major ions and total and dissolved Fe and Mn concentrations for the water samples collected at the pumping wells. The limit of detection (LOD) was 0.2 mg/L for all major ions and 0.01 mg/L or 0.05 mg/L for total and dissolved Fe and Mn, depending on the quantification method. For subsequent calculations and interpretations, all results ≤ LOD will be considered equal to LOD/2. Duplicates were analyzed to confirm the repeatability of the quantification methods. Bicarbonate concentrations were derived from alkalinity, which was measured manually in the laboratory according to the Gran method (Gran, 1952). On samples with measured alkalinity (n = 98), the ionic balance errors were all below 10%. The mean and median ionic balance errors were 1% and the standard deviation was 3%.

4.3.3 Estimating Mixing Ratios

The mixing between two end-members can be quantified via a binary mixing model which can be described by the following equations:

$$f_A + f_B = 1, \tag{1}$$

$$X_A f_A + X_B f_B = X_W, \tag{2}$$

where f represents the fraction of the different sources and X the concentration (or value) of the tracer. A and B correspond to the two water sources, whereas W represents the water sampled at the well.

Tracer-based approaches can be used to estimate mixing ratios and travel times, as long as the tracer presents conservative or predictable behavior (Baudron et al., 2013; Sprenger, 2016). Various natural tracers, such as chloride (Cl^-), electrical conductivity (EC), and stable isotopes of

waters ($\delta^{18}O$-$\delta^{2}H$), have been applied in numerous BF or alluvial aquifer contexts (Baudron et al., 2016; Boving et al., 2014; Buzek et al., 2012; Glorian et al., 2018; Lorenzen et al., 2012; Wett et al., 2002). In this paper, we used EC values as a quantitative mass balance tracer for the application of the mixing model, with the assumption that it behaves conservatively. Violation of this assumption was unlikely at the study site, considering that the aquifer matrix is alluvial sands (mainly siliceous with no calcite). Good correlation (R^2 = 0.95) between EC values and Cl^- (a conservative tracer) was also observed. The advantages of using EC instead of Cl^- are that measurements can be done at a low-cost, as well as remotely and continuously.

4.4 Results and Discussion

4.4.1 Highly Transient Pumping Schemes

In this section, we (1) identify typical pumping schemes and (2) depict the seasonal variability of the total pumped volume.

Figure 4-3a–d shows the pumping rates for P1, P3, P5, and P6 over a typical one-week period (from 16 January 2017 to 23 January 2017). P1 was mainly active during daytime for 1–12 h (Figure 4-3a). A similar pumping scheme was applied to P2, P7, and P8 during summertime (data not shown). P3 and P6 were operated at rates ranging from 1000 m^3/day to 3000 m^3/day. Both were typically active on a daily basis, although P3 was turned off during night time (for less than 6 h) as water demand diminished (Figure 4-3b,d). P5 and P4 were typically activated on a monthly basis for monitoring and sampling procedures (Figure 3c). Three general pumping schemes emerged from this analysis of pumping rates and made it possible to distinguish three groups: (1) wells operated at nearly continuous rates (P3 and P6); (2) wells operated intermittently (P1, P2, P7 and P8); and (3) wells operated occasionally (P4 and P5).

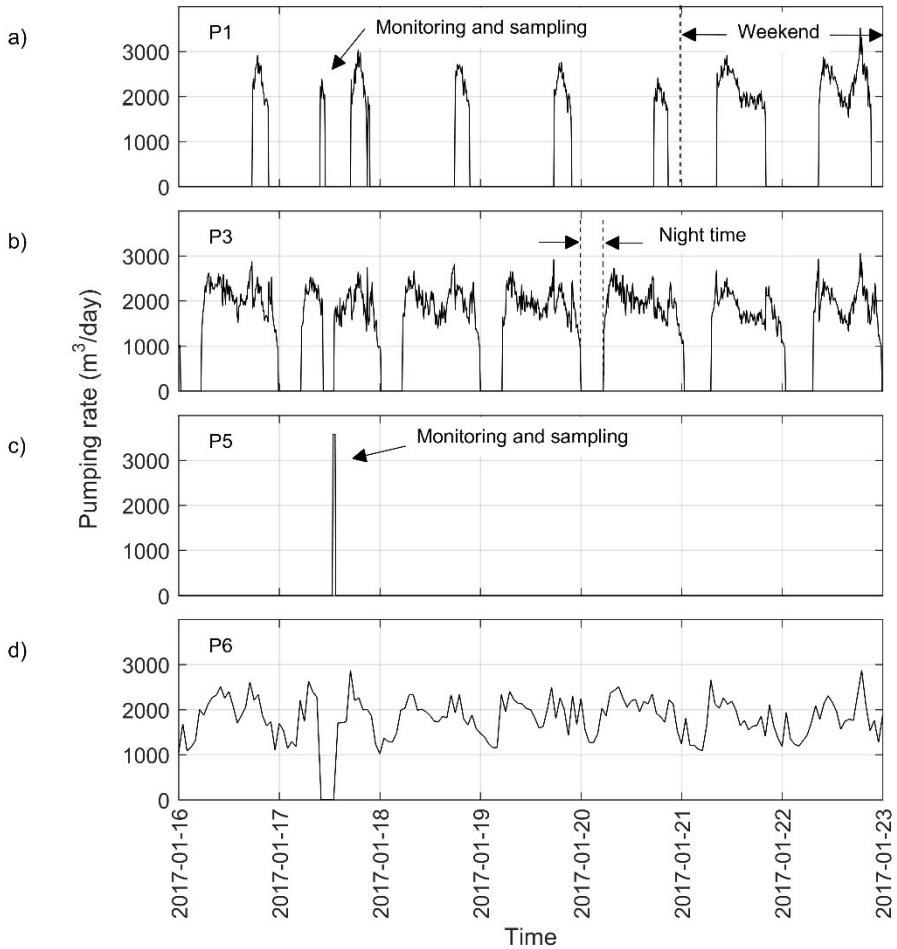

Figure 4-3 Pumping rates for wells (a) P1, (b) P3, (c) P5, and (d) P6 during a typical one-week period (from 16 January 2017 to 23 January 2016). Monitoring and water sampling were conducted on 17 January 2017 at all the pumping wells.

Figure 4-4 illustrates the monthly mean total pumping rate for all wells from March 2016 to March 2017. The mean pumping rate was about 4400 m^3/day, excluding summertime (May 2016 to September 2016), during which it was approximately 7000 m^3/day. Throughout most of the year, with the exception of summer months, 71% to 83% of the total daily pumped volume was provided by the continuously pumping wells. The intermittently pumping wells provided 16% to 29% of the pumped volume. The remaining volume (<1%) was supplied by the occasionally pumping wells. In summertime, pumping rates increased at all wells, except for P5. Continuously pumping wells were operated at mean rates of approximately 2000 m^3/day, representing from 52% to 63% of the

total pumping rate. The intermittently pumping wells together supported 36% to 46% of the total pumped rate and the occasionally pumping wells supplied together the remaining 3%.

Over the study period, the total pumped volume fluctuated daily and seasonally to accommodate the municipal water demand. Indeed, higher pumping rates prevailed during (1) mornings and evenings, (2) weekends, and (3) summertime. This well field is typically operated with a hierarchical system, giving priority to the continuously pumping wells. If the water demand increases, intermittently pumping wells are subsequently activated. Lastly, the occasionally pumping wells can be solicited. This implies that anywhere from one to eight pumping wells were solicited to fulfill the water demand and accommodate for the daily and seasonal water demand fluctuations.

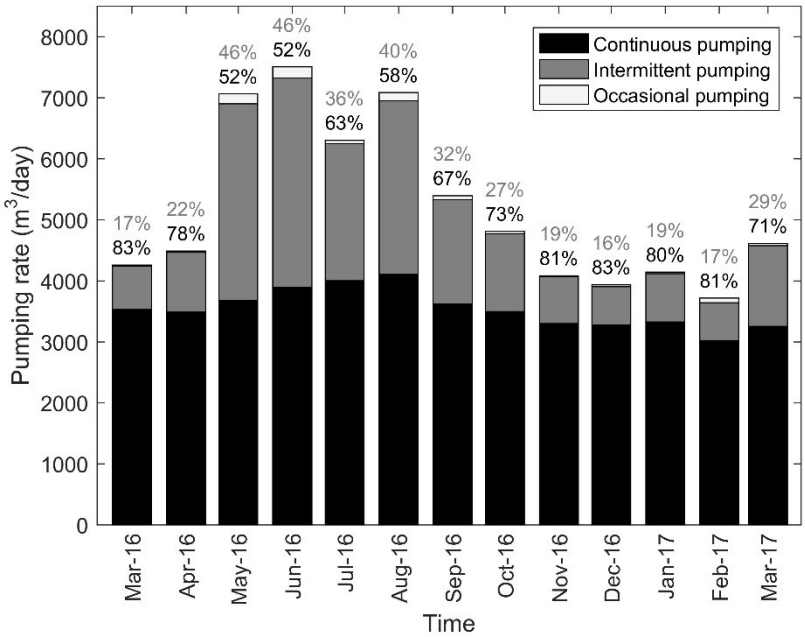

Figure 4-4 Monthly mean total pumping rate from March 2016 to March 2017. Above each bar are the proportions of the total pumped volume supplied by the continuously (in black) and intermittently (in grey) pumping wells. The occasionally pumping wells supply only <1–2% of the total pumped volume.

4.4.2 Geochemistry as a Proxy of the Hydrosystem Dynamics

The objective of this section was to examine the geochemistry of Lake A, Lake B, regional groundwater, and the bank filtrate in order to identify the contributing water sources to the pumping wells.

Box plots of the temperature, EC, pH, and Eh at Lake A (<1 m depth), Lake B (<1 m depth), the pumping wells, and the observation wells Z12, Z15, and Z16 are illustrated in Figure 4-5. Concerning Lake A and Lake B, note that the presented data correspond to measurements at the surface of the lakes (i.e., <1 m depth). Hence, the medians and the 25th and 75th quartiles values may not be representative of the entire water column. Observed temperatures at Lake A and Lake B ranged from 1.3 °C to 27.5 °C and from 3.9 °C to 27.5 °C, respectively. For the pumping wells, box plots are spatially sorted (P6; P1; P8; P2; P7; P3; P4; P5) from the northwest to the southeast ends of the well field (see location of the pumping wells in Figure 4-1c). Temperatures ranged from 3.4 °C to 16.2 °C, with minimum and maximum values being observed in occasionally and continuously pumping wells, respectively. EC values at the pumping wells ranged from 491 µS/cm (at P5) to 895 µS/cm (at P8), which is in between observed EC values in Lake A and Lake B. Note that the EC values for Lake A and Lake B in Figure 4-5 are associated with water sampled at <1 m depth. Higher EC values were measured in situ in Lake B at >12 m deep (further details in Section 4.4.3). Observed EC values at Z12 were similar to those in Lake B, whereas Z15 showed lower values, similar to Lake A. The highest EC values were observed at Z16, which is representative of regional groundwater. Measured pH values at the pumping wells tended to increase spatially from NW to SE (P6 to P5). Redox conditions also varied spatially and decreased from NW to SE. A H_2S odor was noticed when sampling at P4, P5, Z15, and Z16, which is consistent with Eh measurements that indicate more reduced conditions.

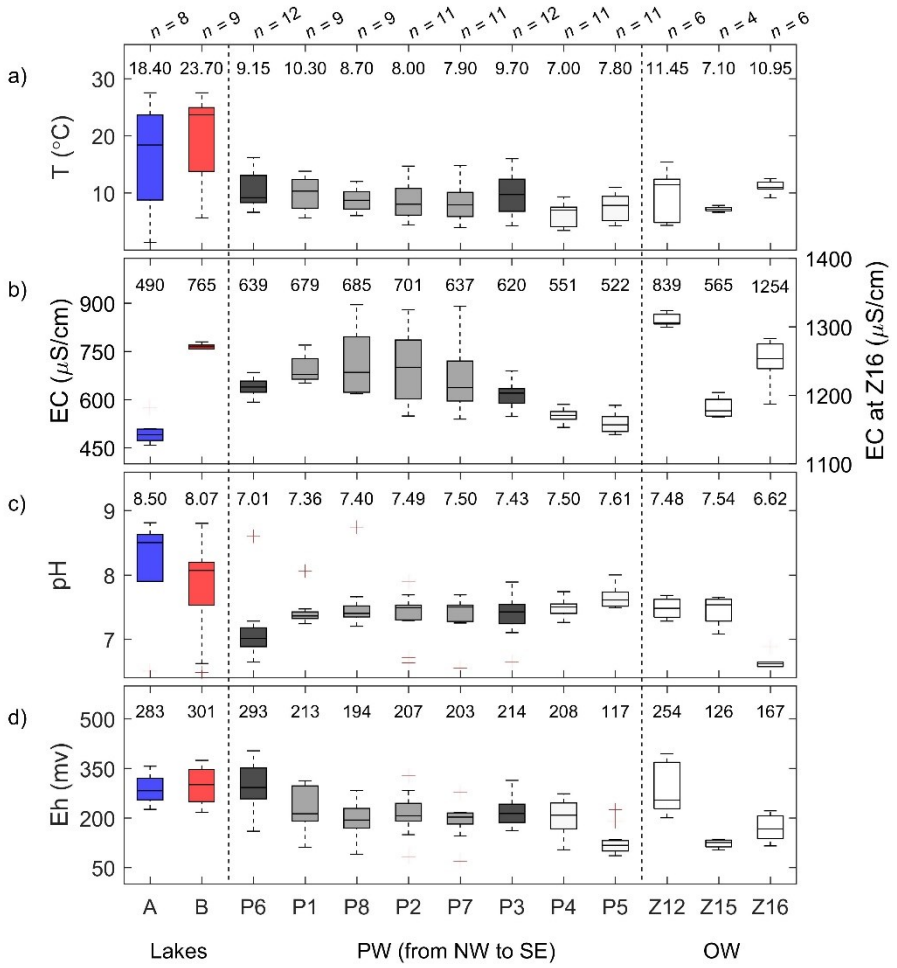

Figure 4-5 Boxplots of (a) temperature, (b) electrical conductivity (EC), (c) pH, and (d) redox potential (Eh) at the lakes, pumping wells (PW), and observation wells (OW). Blue and red boxes are associated with Lake A (<1 m depth) and Lake B (<1 m depth), whereas dark, medium, and light grey boxes correspond to continuously, intermittently, and occasionally pumping wells, respectively. Numeric values above each box correspond to the median.

Figure 4-6 shows the spatial variability of total Fe and Mn concentrations at Lake A (<1 m depth), Lake B (<1 m depth), the pumping wells, and the observation wells Z12, Z15, and Z16. Concentrations in total Fe ranged from <0.01 mg/L to 1.28 mg/L at the pumping wells, with median concentrations increasing from NW to SE. Median total Fe concentrations at P4 and P5 were high relative to Canada's aesthetic objective for total Fe in drinking water (i.e., 0.3 mg/L) (Government of Canada, 2009). Analyses also reported high concentrations (from 0.05 mg/L to 2.12 mg/L) at Z15 (near P5). The highest total Fe concentrations were observed at Z16. Total Mn

concentrations ranged from 0.1 mg/L to 1.3 mg/L at the pumping wells, which exceeded the aesthetic objective for total Mn in drinking water in Canada (i.e., 0.02 mg/L) (Government of Canada, 2019). The highest concentrations were measured at the intermittently pumping wells. Total Mn concentrations at the surface of Lake A and Lake B were relatively low (i.e., typically ≤0.03 mg/L). However, it is important to note that 1.06 mg/L was observed at 6 m depth in Lake B (see red circle in Figure 4-6b). This result highlights that total Mn concentrations may be more important at greater depths in Lake B. Release of Fe and Mn to the water column in Lake A may potentially occur from sand dredging activities, as this lake is still actively mined for sand. However, no data are available to discuss the evolution of Fe and Mn concentrations in relation to these anthropic activities. Dissolved Fe concentrations were all <0.05 mg/L, while dissolved Mn concentrations were similar to the total ones.

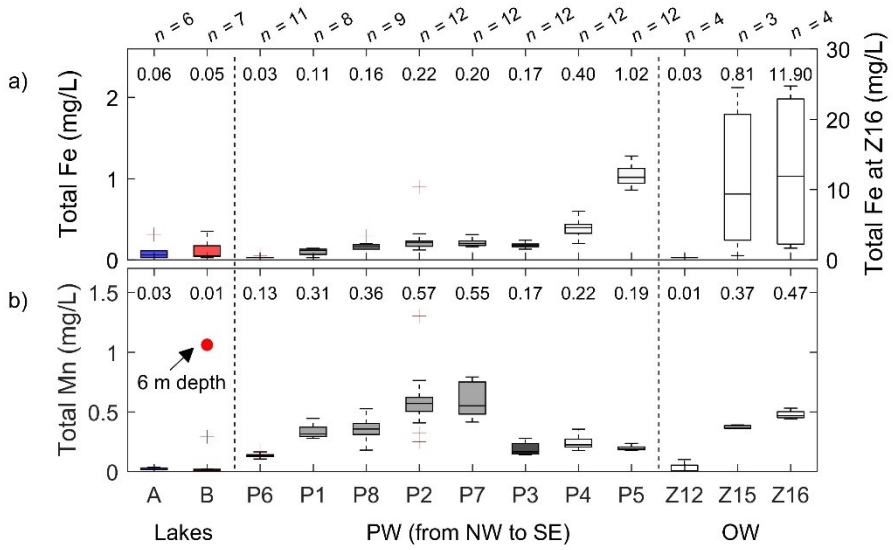

Figure 4-6 Boxplots of (a) total Fe, and (b) total Mn concentrations at the lakes, pumping wells, and observation wells. Blue and red boxes are associated with Lake A (<1 m depth) and Lake B (<1 m depth), whereas dark, medium, and light grey boxes correspond to continuously, intermittently, and occasionally pumping wells, respectively. Numeric values above each box correspond to the median. Red circle represents the maximal observed total Mn in Lake B (at 6 m depth).

Figure 4-7 shows the relationship between $(Ca^{2+} + Mg^{2+})/Na^{+}$ and cationic content (i.e., sum of major cations) for Lake A, Lake B, pumping wells, and regional groundwater. Potassium (K^{+}) was excluded from these calculations since only a few samples were analysed for K^{+} and concentrations

in K^+ only represent a small fraction of the total cation content (i.e., approximately 1.5%). Lake A and Lake B samples are plotted in opposing regions of the graph, Lake A having a high (Ca^{2+} + Mg^{2+})/Na^+ ratio and low cationic content and Lake B having a low (Ca^{2+} + Mg^{2+})/Na^+ ratio and high cationic content. Concerning the samples from the pumping wells, they are mostly plotted in the area extending from the Lake A to Lake B regions. Occasionally pumping wells had a geochemical signature similar to Lake A, whereas continuously and intermittently pumping wells spread between both lake signatures. Regional groundwater samples were sampled from one observation well, namely Z16, located on the NE side of Lake B (see Figure 4-1c). These samples were characterized by the lowest (Ca^{2+} + Mg^{2+})/Na^+ ratios and highest cationic content. It is believed that direct contribution to the pumping wells from regional groundwater is not likely at this site, due to the hydrogeological context (see Section 4.2.1). Hence, we hypothesize that the spreading of pumping well samples relative to the Lake A–Lake B mixing line is potentially due to an indirect contribution from regional groundwater, which discharged into Lake B. Only three wells (i.e., P2, P7, and P8) were affected from November 2016 to February 2017. During this period, the three wells together supplied <10% of the total pumped volume. Based on these observations, we propose that the mixing between Lake A and Lake B is the dominant process governing the geochemical facies of the pumping wells.

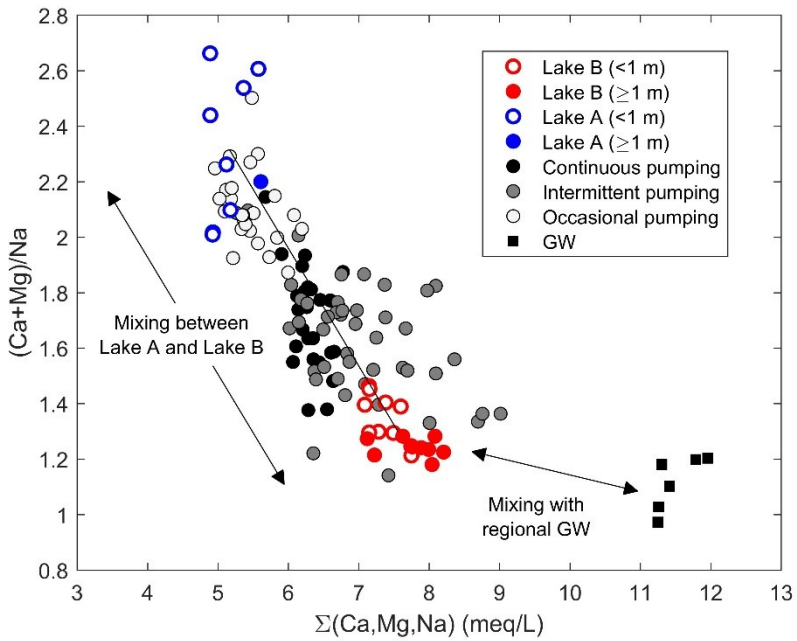

Figure 4-7 Comparison of the geochemical facies of Lake A, Lake B, pumping wells, and the regional groundwater (GW). The solid black line represents the mixing line between Lake A and Lake B mean values.

4.4.3 EC Time-Varying Mixing Model

It was discussed in Section 4.4.2 that the geochemical facies at the pumping wells are controlled by mixing between Lake A and Lake B. Hence, we used the binary mixing model of Equations (1) and (2) to estimate the relative contributions of each lake to the pumping wells. In this section, we first present the temporal and vertical variability of EC at Lake A and Lake B in order to define the end-member values. Then, estimations of the mixing ratios are evaluated with respect to a reference scenario, and spatiotemporal evolution is discussed. We also provide a sensitivity analysis, which helps strengthen the conclusions of the model.

4.4.3.1 Temporal and Vertical EC Variability at Lake A and Lake B

Temporal variability in EC values at the surface (<1 m depth) of Lake A and Lake B are illustrated in Figure 4-8a,b. At the surface of Lake A, minimal and maximal EC values were observed in springtime and wintertime, respectively. Low EC values were expected for springtime, since it corresponds to the period of hydraulic connection between Lake A and Lake C. During this period,

surface water with low EC is discharged into Lake A from streams S1 and S2 with inverted flow direction (see Figure 4-1b). In Lake B, EC values at the surface (<1 m depth) were also found to be variable over time. During springtime and summertime, EC values were relatively constant. A significant increase in EC values was observed in autumn–winter. Figure 4-8b also depicts the EC time series at an observation well (namely Z12) which was located between pumping well P1 and Lake B. It is screened at the bottom of the aquifer over a 9.14 m long section. EC measurements at Z12 are thus representative of the mixing between multiple flow lines originating from various depths in Lake B. The mean EC value at Z12 was 848 µS/cm and values were typically higher than at the surface of Lake B. These results reveal that (1) the EC measurements at the surface of Lake B are not representative of the infiltrating water and (2) considering the vertical variability in EC in Lake B is important.

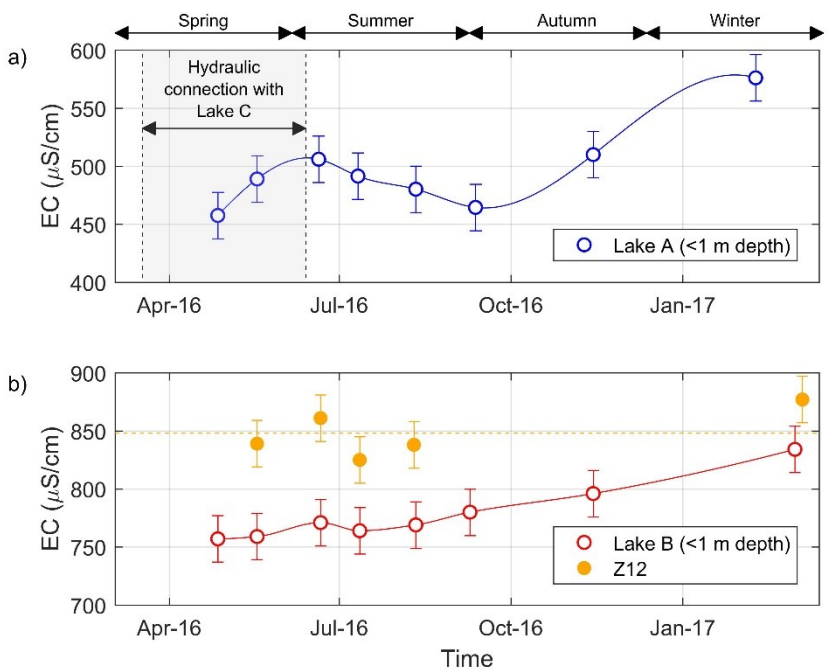

Figure 4-8 Time series of electrical conductivity (EC) at (a) Lake A (<1 m depth), and (b) Lake B (<1 m depth) and Z12. The grey shaded area represents the timing for hydraulic connection between Lake A and Lake C. Error bars (±20 µS/cm) represent the maximal expected measurement error on EC. The yellow dashed line corresponds to the mean EC value at Z12.

Figure 4-9 shows vertical EC profiles for Lake A and Lake B. EC was measured at depth in winter (on 15 February 2017) at Lake A and in summer and winter (on 9 September 2016 and 2 March

2017) at Lake B. For each campaign, at least two vertical profiles were conducted in order to assess the horizontal variability (see Figure 4-1c for location of the vertical profiles). Maximal EC differences (at the same depth) were 6 µS/cm and 25 µS/cm for Lake A and Lake B, respectively, suggesting no significant horizontal variability at both lakes.

Concerning Lake A, no significant vertical variability in EC values was observed. This suggests that Lake A was vertically well mixed in wintertime. Given that Lake A receives surface water from a stream and that some industrial activity (i.e., sand dredging) takes place in the lake during the ice-free period (typically form early May to late October), it is likely that some currents in Lake A are stimulating mixing of the water column. Hence, we assumed that Lake A is fully mixed and does not develop any significant vertical EC stratification over a hydrological year. Temporal variability in EC at the surface of Lake A (at <1 m depth) is presumably representative of the evolution of the entire water body.

At Lake B, observed EC values increased with depth for all vertical profiles. Higher EC at greater depth could be induced by regional groundwater inputs into Lake B. In Canada, groundwater inputs are typically found at the bottom of lakes, due to thermal (and density) contrast (Arnoux et al., 2017c). Smaller vertical variability was observed in wintertime (in comparison to summertime). However, both summertime and wintertime depth-averaged values were similar (861 µS/cm and 884 µS/cm; a difference of 23 µS/cm being barely significant). It is important to note that the wintertime vertical profiles were conducted in a shallower zone of the lake and could explain the discrepancy between the depth-averaged values. Additionally, it is interesting to note that the depth-averaged EC values were similar to the Z12 mean EC value. This suggests that the depth-averaged EC value was adequate to depict the EC signal originating from Lake B.

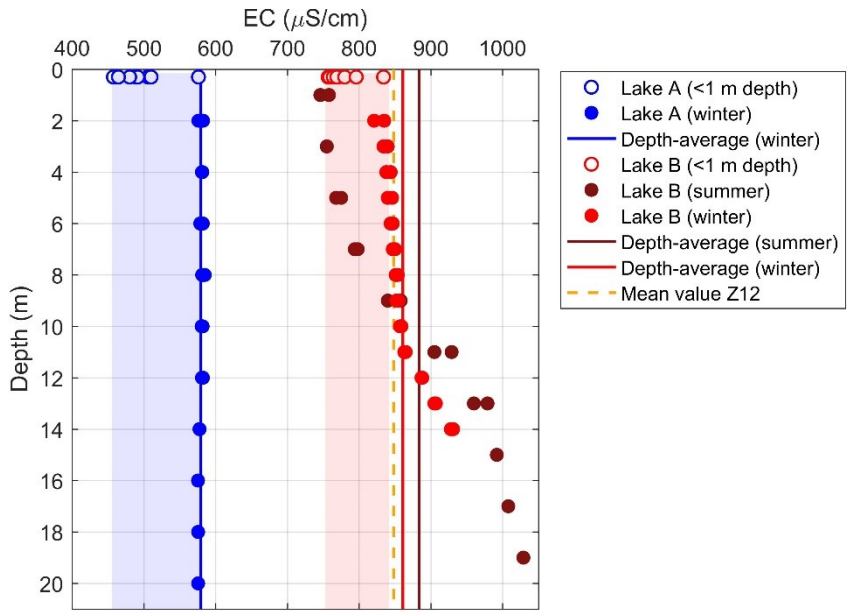

Figure 4-9 Electrical conductivity (EC) measurements against depth at Lake A and Lake B in winter and summer. Solid lines represent depth-average value at the lakes, while the yellow dashed line is associated with mean EC values at observation well Z12. Blue and red shaded areas illustrate the variability in EC at the surface (<1 m depth) of Lake A and Lake B, respectively.

4.4.3.2 Reference Scenario

Based on the assumption that Lake A is well mixed, we considered that EC measurements at <1 m depth were representative of the Lake A end-member. Hence, the Lake A end-member is a time-varying EC signal. Temporal interpolation between discrete measurements was done with the cubic spline method (using the *spline* function in MATLAB). The result of this calculation is represented in Figure 4-8a by the solid blue line and gives the best available estimate of the Lake A end-member from 27 April 2016 to 9 February 2017. No temporal shifting was considered, since travel times were expected to be much smaller than the observed changes in EC in Lake A. Concerning Lake B, a constant value of 873 µS/cm (i.e., mean of the wintertime and summertime depth-average values) was considered to correctly represent this second end-member. There was no need to consider temporal variation for Lake B end-member as both depth-averaged values were found to be similar.

The results of the mixing model are shown in Figure 4-10. By considering the relative pumping rates and the estimated contributions from Lake A at each well, we calculated that 62% of the annual pumped volume originated from Lake A. The continuously pumping wells are characterized by 54% to 78% of water originating from Lake A, with the highest contributions from Lake A occurring from April to July, i.e., during the highest hydraulic gradient period. The lowest contributions from Lake A were observed from July to September, i.e., during the moderate hydraulic gradient period. This is likely related to an increase in the total pumped volume during summertime (see Section 4.4.1).

The intermittently pumping wells showed the widest distribution in mixing ratios, with contributions from Lake A ranging from 0% to 87%. Similar to the continuously pumping wells, the highest contributions from Lake A were observed during the high hydraulic gradient period, while its contribution decreased as the hydraulic forcing became less important. It was estimated that during the low hydraulic gradient period, the fraction of Lake B can reach up to 100% for the intermittently pumping wells. In fact, the mixing model yields such mixing ratios when the measured EC at the pumping wells is greater or equal to the Lake B end-member (i.e., 873 µS/cm). This condition was observed four times and EC measurements at the concerned pumping wells ranged from 879 µS/cm to 895 µS/cm. However, expectations were that Lake A and Lake B would always contribute to the pumping wells, since a radial depression cone normally develops in the vicinity of an active pumping well, forcing water to infiltrate from both sides of the sandy bank. Hence, we considered that a calculated contribution of 100% of Lake B depicts a limit of the developed mixing model. In reality, this result could be an indication that, during winter, water preferentially infiltrates from the bottommost zone (≥12 m) of Lake B (where EC >873 µS/cm), leading to higher EC values at the intermittently pumping wells. Controls on the development of such preferential flow paths are not within the scope of this paper and, thus, will not be further discussed. Future work concerning the spatiotemporal variability of the hydraulic conductivity is still needed to draw any conclusions on this topic. The combination of various environmental tracers would help to differentiate between contributions from the surface and bottommost zones of the lakes.

Contribution from Lake A at the occasionally pumping wells is typically >90%. However, in April and May, it was estimated that the former wells were receiving a relatively smaller contribution

from Lake A (from 74% to 86%). This result possibly reflects that pore water with EC >500 µS/cm and originating from Lake A could have been stored during winter within the sandy bank and pumped only in April and May. Hence, mean residence time of the water in the sandy bank could reach months when the pumping wells are not active. Greater attenuation of the surface water temperature signal, at the occasionally pumping wells, also testifies to longer residence times. We thus highlighted the need for considering the variability of the residence time of water into the sediments when applying a time-variant mixing model.

In sum, contribution from Lake A is typically greater than Lake B throughout the year. However, the mixing ratios are temporally and spatially variable. Strong variability was found especially during the period of low hydraulic gradient at the intermittently and occasionally pumping wells. In such a context, the pumping regime seems to have a decisive impact on the mixing ratios and, ultimately, on water quality of the bank filtrate. Under high hydraulic gradient the mixing ratios tend to be more similar, regardless of the pumping regimes.

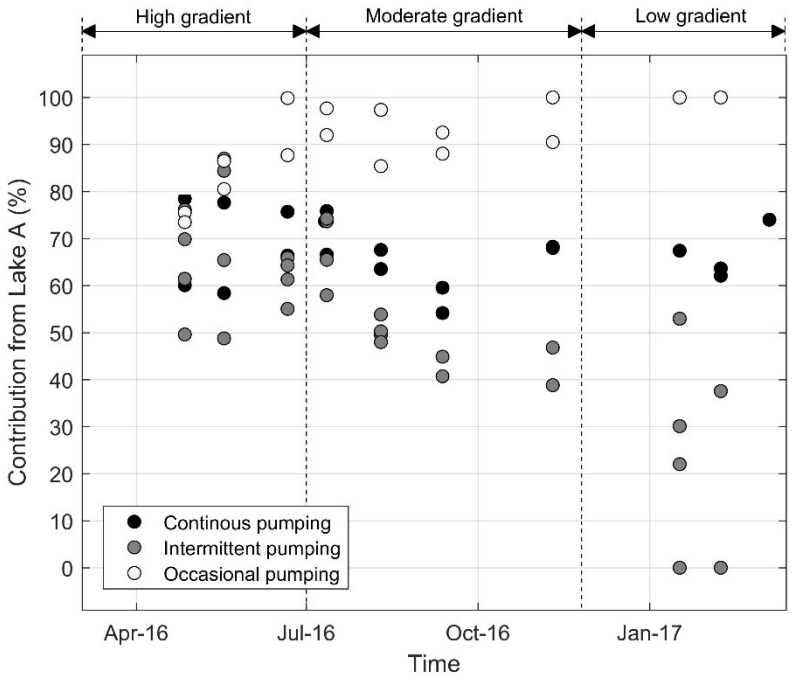

Figure 4-10 Estimated contribution from Lake A to the pumping wells according to the reference scenario. Lake A end-member is defined as a time-varying electrical conductivity (EC) signal, which was derived from the observed EC values at <1 m depth. Lake B end-member is a fixed EC value which corresponds to the mean of the wintertime and summertime depth-average value.

4.4.3.3 Sensitivity Analysis

A sensitivity analysis was conducted in order to investigate (1) the representativity of EC end-members values and (2) the uncertainties related to the EC measurements. Mixing ratios were therefore recalculated according to various scenarios where Lake A and Lake B end-member values varied from 458 µS/cm (i.e., minimal observed value) to 576 µS/cm (i.e., maximal observed value) and from 824 µS/cm to 924 µS/cm (i.e., reference scenario ±50 µS/cm), respectively. Also, a variation of ±40 µS/cm was applied to all the EC measurements at the pumping wells. Differences between the results of the scenarios were typically <10%, except for the ones concerning the Lake A end-member. When considering fixed EC values for the Lake A end-member, the estimation of the mixing ratios diverged up to 30% compared to the reference scenario. This result helped to quantify the importance of considering the temporal variability of the end-members to obtain reliable results when estimating mixing ratios. Despite the sensitivity of the model to Lake A end-member variability, general trends for mixing ratios were conserved for all the scenarios. This result was expected, as the mixing model was linear. Overall, the sensitivity analysis revealed that the relative estimations of mixing ratios were acceptable and that measurement errors were not likely to influence our conclusions.

The temporal resolution of the applied monitoring program did not allow for discussion of the short-term (i.e., hourly to daily) EC variability. Hence, it is not clear whether hourly variations in pumping rates could influence the observed EC values at the pumping wells.

4.4.4 Dominant Controls on the Origin of the Bank Filtrate

The time-variant binary mixing model highlights that the contribution of Lake A to the bank filtrate can vary from 0% to 100%. This section aims to understand the competing roles of anthropic and meteorological forcings on the origin of the bank filtrate. We define anthropic forcing as a process via which the origin of the bank filtrate at a given well is affected by its own pumping scheme and/or rate. Anthropic forcing can also occur indirectly, as drawdown of the water table in the vicinity of a given pumping well can influence the origin of water at less active adjacent pumping wells. Meteorological forcing is considered a natural process. Concerning our study site, the surface elevations of Lake A and Lake B showed seasonal variations, which are mainly controlled by meteorological conditions allowing or limiting surface water inputs into Lake A. Hence, we

considered that the hydraulic gradient between Lake A and Lake B is meteorological forcing acting on the BF system.

Figure 4-11a,b shows EC against the one-month average pumping rate prior to the sampling date. Distinction between the pumping regimes (i.e., continuous, intermittent and occasional) is illustrated in a, while hydraulic gradients between Lake A and Lake B (i.e., high, moderate, low) are represented in b. Figure 4-11c is a schematic representation of the dominant forcing in relation to the different hydraulic contexts. First, in Figure 4-11a,b, we observed little variability in EC measurements if the pumping rate was >1000 m^3/day. In fact, most samples associated with high pumping rates (Figure 4-11a) showed EC values ranging from 583 µS/cm to 689 µS/cm, despite the variability of the hydraulic gradient (Figure 4-11b). Hence, for high pumping rates (i.e., >1000 m^3/day), it appears that anthropic forcing is dominant over the meteorological forcing (Figure 4-11c). However, two samples (see downward arrow in Figure 4-11c) showed lower EC while being operated at >1500 m^3/day. These exceptions were observed exclusively when the hydraulic gradient between Lake A and Lake B was maximal (i.e., in May and June). Under such hydraulic conditions, the anthropic forcing cannot counteract the meteorological forcing, resulting in an increase in the contribution from Lake A during springtime. Second, higher EC values (>750 µS/cm) are associated with the intermittent pumping regime, while low EC values (<600 µS/cm) are mostly related to the occasionally pumping regime (Figure 4-11a). For these two pumping regimes, meteorological forcing was clearly dominant over the anthropic one (Figure 4-11c). In fact, high EC values were strictly observed during the low hydraulic gradient period (Figure 4-11b). In short, this revealed that when a pumping rate of approximately 1000 m^3/day is applied continuously, the mixing ratios are less variable due to direct anthropic forcing. When wells are operated only intermittently or occasionally, indirect anthropic and/or meteorological forcings control the mixing between Lake A and Lake B waters.

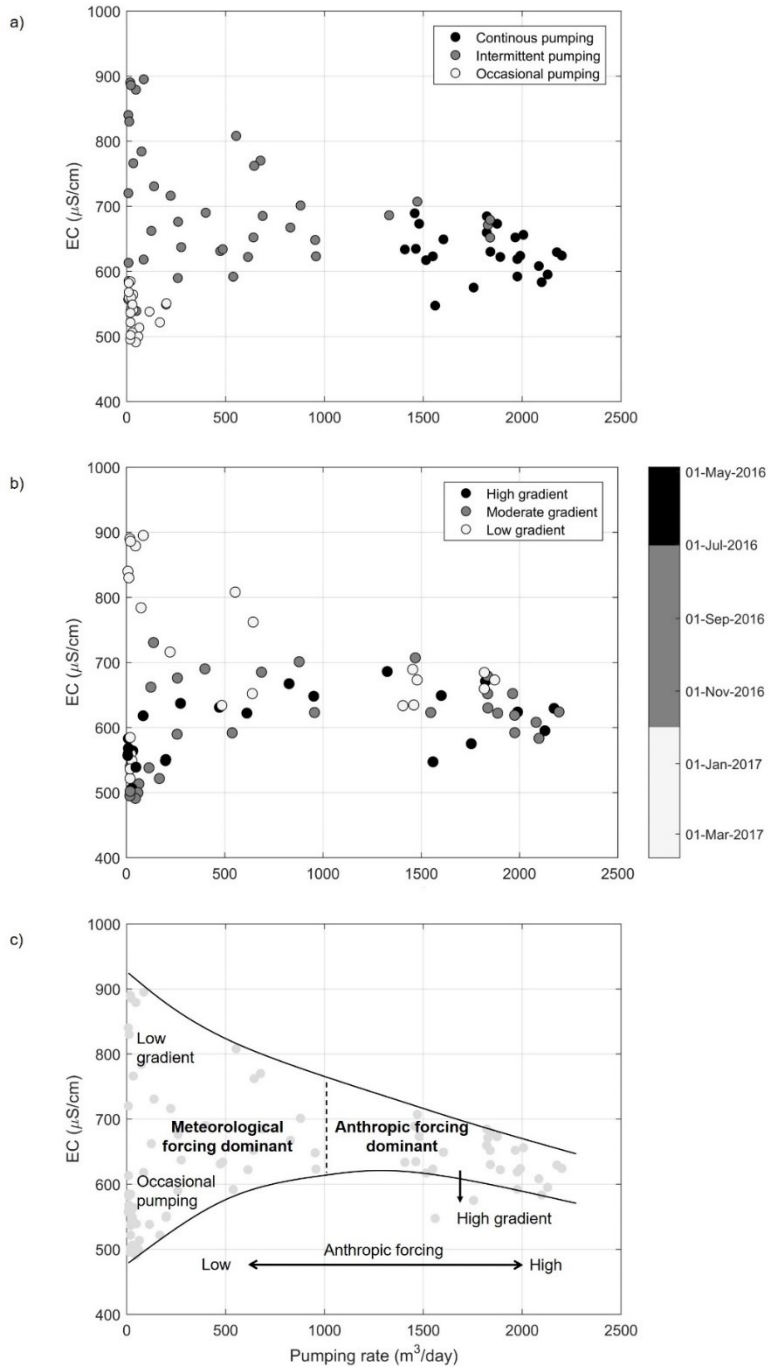

Figure 4-11 Relationship between electrical conductivity (EC) and the one-month average pumping rate prior to the sampling date, according to (a) the pumping regime and (b) the hydraulic gradient between Lake A and Lake B. A schematic representation of the dominant forcing is illustrated in (c), where solid and dashed lines represent the range of observed values and the delimitation between regimes where meteorological and anthropic forcings are dominant, respectively.

4.4.5 Implications for the Quality of the Bank Filtrate

In Section 4.4.2, we highlighted that geochemical analyses showed spatial variability in both total Fe and Mn concentrations at the pumping wells. This section aims to discuss the relationship between total Fe and Mn concentrations and the origin of water.

High total Fe concentrations were found at the occasionally pumping wells (i.e., at P5 and, to a lesser extent, at P4) and were associated with the highest contributions from Lake A (see Figure 4-10) and more reduced conditions (see Figure 4-5d). In comparison to the more anthropized section of the BF system, the residence times of the infiltrating water in the vicinity of the occasionally pumping wells are likely to be longer, because meteorological forcing alone is controlling groundwater flows (see Section 4.4.4). Since relatively low temperatures were observed at P4 and P5, it is also likely that higher viscosity, resulting in lower hydraulic conductivity, was responsible for longer residence times of the bank filtrate in the vicinity of these wells (des Tombe et al., 2018; Glass et al., 2019; Liu et al., 2019). The longer residence times are potentially responsible for the high total Fe concentrations at P4 and P5. Evolution of redox conditions (from oxic to anoxic) is typically observed at BF systems (Henzler et al., 2016) and can result in the dissolution of iron and/or manganese along flow paths (Grischek & Paufler, 2017). However, as dissolved Fe concentrations are very low (i.e., generally <LOD), total Fe is controlled predominantly by the particulate fraction. Hence, it is more likely that the high rate and/or occasional pumping are causing the mobilization and resuspension of particulate Fe at P4 and P5. In fact, when activated for monthly sampling and monitoring, P4 and P5 typically operate at 150 m^3/h, while the other wells operate at lower rates (i.e., from 40 m^3/h to 125 m^3/h). Moreover, P5 was the only pumping well equipped with a 4 m long screened section (i.e., half of those of the other wells). The mean effective velocity of water entering P4 and P5 screens was from 2 to 4 times greater than at the other wells. The total Fe concentration at P4 and P5 could thus potentially be reduced by lowering the hourly mean pumping rates and operating on a daily basis. However, such engineered operational strategy would not help to lower the total Fe concentration to <0.2 mg/L (see Figure 4-12a).

The highest total Mn concentrations were concomitant with the highest fraction of Lake B water at the intermittently pumping wells. The presence of total Mn in the raw water could also be explained

by the evolution of redox conditions along the flow path. Besides this, an elevated concentration in total Mn (1.06 mg/L) was measured at a 6 m depth in Lake B. As the latter was found to be geochemically stratified, relatively reduced conditions can develop in the epilimnion and promote the solubilization of Mn. Hence, it is also likely that Mn reaches the pumping wells by advective transport with water originating from the deeper zones of Lake B. Further investigation is needed to better understand the site-specific drivers of the Mn occurrence in the bank filtrate, since its mobility is controlled by numerous factors, such as travel times, temperature, pH, microbial activity, the extent of a clogging layer, and the degree of oxygen consumption (Grischek & Paufler, 2017). Figure 4-12b illustrates the relationship between total Mn concentrations and the one-month average pumping rate prior to the sampling date. Total Mn concentrations decrease with higher pumping rates (for intermittently and continuously pumping wells). This suggests that pumping rate can be used as an operational tool to control the total Mn concentration in the pumped water.

In sum, high total Fe and Mn concentrations in the pumped water are governed by two distinct processes. Total Fe seems to originate from particulate iron mobilization and resuspension when effective velocities of water entering the screens of the pumping wells are high, whereas high total Mn concentrations seem to be associated with an increase in the contribution from the bottom of Lake B. Total Fe and Mn concentrations could potentially be regulated by lowering the mean effective velocity of water entering the screens and adjusting mixing ratios (i.e., by operating at adequate pumping rates).

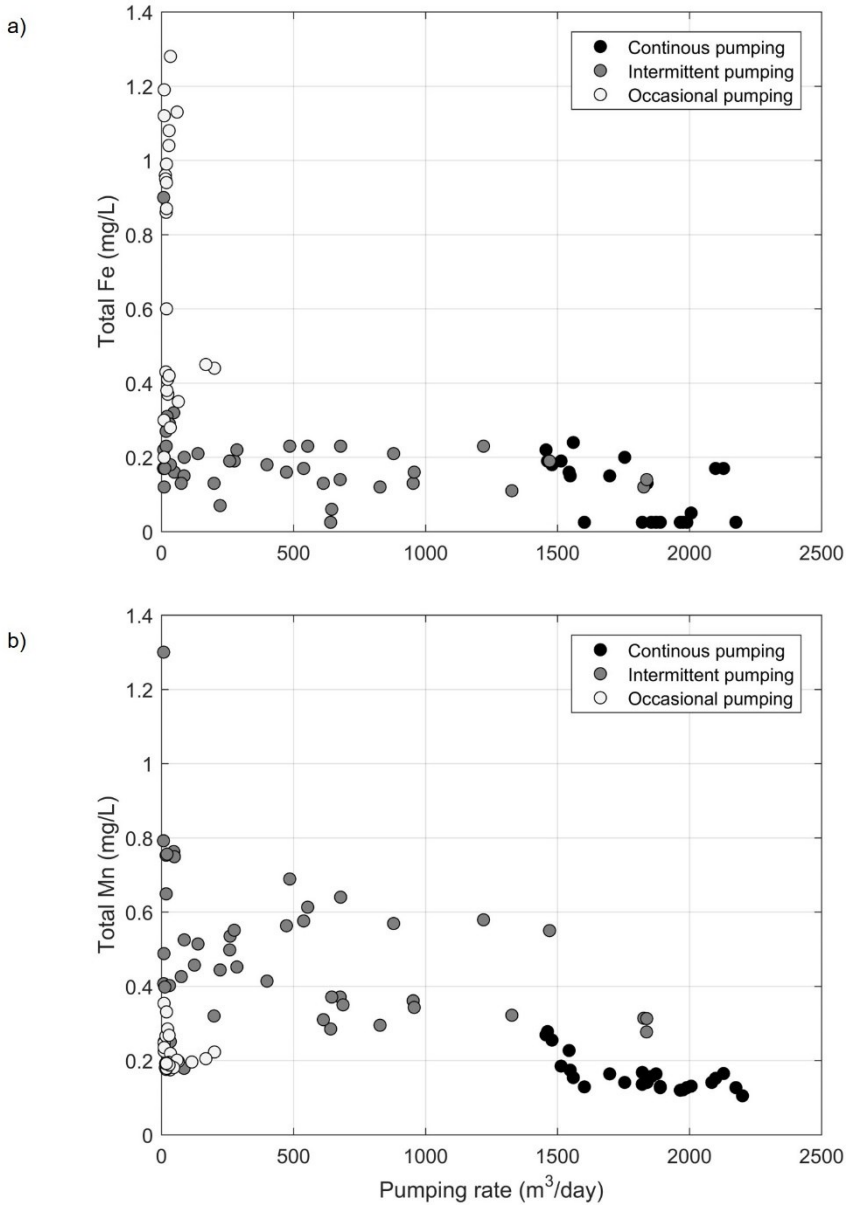

Figure 4-12 Relationship between (a) total Fe and (b) total Mn concentrations and the 1-month average pumping rate prior to the sampling date.

4.5 Conclusions

In this study, we demonstrated the controls of variable meteorological conditions and pumping schemes on the origin and quality of bank filtrate. Through a pumping rate analysis, the pumping schemes could be separated into three categories, namely the continuously, intermittently, and

occasionally pumping wells. The continuously pumping wells (i.e., P3 and P6) supported 71% to 83% of the total pumping rate, except in summertime, when they contributed from 52% to 63%, of the total pumping rate as it increased from approximately 4000 m^3/day to 7500 m^3/day. An investigation of the geochemical facies of Lake A, Lake B, regional groundwater, and the bank filtrate revealed that the geochemistry of the pumped water is governed by mixing of Lake A and Lake B. Therefore, a two end-member mixing model was developed to estimate the contribution from both lakes to the pumping wells over a one-year period. To this end, EC measurements were used as a quantitative environmental tracer. A time-varying EC signal was considered for the Lake A end-member, whereas a fixed EC value was used to depict the Lake B end-member. This simple mixing model revealed the following:

- By considering the relative pumping rates and the estimated contributions from Lake A at each well, it was estimated that 62% of the annual pumped volume originates from Lake A;
- All the pumping wells typically receive >50% of water from Lake A, but the competition between anthropic (i.e., pumping regime) and meteorological forcings (i.e., relative water level of both lakes) leads to a large variability of the mixing ratios (i.e., from 0% to 100% of water originating from Lake A);
- When the meteorological forcing is high, the pumping regime has little influence over the origin of water and the mixing ratios are similar at all the pumping wells. When the meteorological forcing is low, the pumping regime is a decisive factor on the fraction of the contributing sources to the pumping wells;
- When a pumping rate of >1000 m^3/day is applied continuously, the mixing ratios are less variable due to direct anthropic forcing. When wells are operated only intermittently or occasionally and at a rate of <1000 m^3/day, indirect anthropic and/or meteorological forcings govern the mixing ratio between Lake A and Lake B waters;
- A sensitivity analysis revealed that the relative estimation of the mixing ratios was acceptable and that measurement errors were not likely to influence our calculations. It also helped to quantify the importance of considering the temporal variability of the lakes' end-members to obtain reliable results when estimating mixing ratios;

- The pumping regime influences total metals (i.e., Fe and Mn) concentrations in the raw abstracted waters. High Fe concentrations originate from particulate iron mobilization and resuspension when effective velocities of water entering the screens of the pumping wells are high, whereas high Mn concentrations are associated with an increase in the contribution from Lake B.

This study highlights how understanding the competition between anthropic and meteorological forcings can help to recommend guidelines for rapid decision-making regarding the quality of the pumped water. For instance, by identifying contexts for which the anthropic forcing is dominant, one can control the origin of the bank filtrate. Moreover, predicting periods under which the meteorological forcing is governing the flow patterns can help to adjust post-BF treatment in order to secure high quality of the distributed drinking water.

CHAPTER 5 ARTICLE 2: OPTIMIZING MONITORING AND MANAGEMENT STRATEGIES AT FLOOD-AFFECTED BANK FILTRATION SITES

This chapter was published as a research paper in the journal *Science of The Total Environment* in 2021. Supplementary materials are presented in Appendix B.

Masse-Dufresne, J., Baudron, P., Barbecot, F., Pasquier, P., & Barbeau, B. (2021). Optimizing short time-step monitoring and management strategies using environmental tracers at flood-affected bank filtration sites. Science of The Total Environment, 750, 141429. doi:10.1016/j.scitotenv.2020.141429

ABSTRACT

Isotope mass balance models have undergone significant developments in the last decade, demonstrating their utility for assessing the spatial and temporal variability in hydrological processes and revealing significant value for baseline assessment in remote and/or flood-affected settings where direct measurement of surface water fluxes to lakes (i.e. stream gauging) are difficult to perform. In this study, we demonstrate that isotopic mass balance modelling can be used to provide evidence of the relative importance of direct floodwater inputs and temporary subsurface storage of floodwater at ungauged lake systems. A volume-dependent transient isotopic mass balance model was developed for an artificial lake (named lake A) in southern Quebec (Canada). This lake typically receives substantial floodwater inputs during the spring freshet period as an ephemeral hydraulic connection with a 150 000 km^2 large watershed is established. First-order water flux estimates to lake A allow for impacts of floodwater inputs to be highlighted within the annual water budget. The isotopic mass balance model has revealed that groundwater and surface water inputs account for 60 %–71% and 39 %–28% of the total annual water inputs to lake A, respectively, which demonstrates an inherent dependence of the lake on groundwater. However, when considering the potential temporary subsurface storage of floodwater, the partitioning between groundwater and surface water inputs tends to equalize, and the lake A water budget is found to be more resilient to groundwater quantity and quality changes. Our findings suggest not only that floodwater fluxes to lake A have an impact on its dynamics during springtime but also significantly influence its long-term water balance and help to inform, understand, and predict

future water quality variations. From a global perspective, this knowledge is useful for establishing regional-scale management strategies for maintaining water quality at flood-affected lakes, for predicting the response of artificial recharge systems in such settings, and for mitigating impacts due to land use and climate changes.

5.1 Introduction

Contamination of surface water resources is a worldwide concern (Lopez-Pacheco et al., 2019; Nannou et al., 2020). Many anthropogenic contaminants are routinely detected in rivers and lakes (de Sousa et al., 2014; Glassmeyer et al., 2005; Sjerps et al., 2016; Snyder & Benotti, 2010) and enter watercourses via many diffuse and point sources of contamination (Masoner et al., 2019; Schwarzenbach et al., 2010). For instance, wastewater treatment plants discharge can severely impact the quality of surface waters during droughts (Karakurt et al., 2019). In northern climates, snowmelt periods are particularly critical for combined sewer overflows (Madoux-Humery et al., 2013) and their cumulative effect can rapidly deteriorate the quality of receiving waters from upstream to downstream (Jalliffier-Verne et al., 2016).

Over the last decades, the use of bank filtration (BF) has gained in popularity as a pre-treatment method in regions where surface water resources are threatened by contamination and/or where groundwater resources are scarce (Ahmed & Marhaba, 2017; Tufenkji et al., 2002). BF consists in pumping groundwater from an aquifer which is hydraulically connected to a surface water body. An induced (or natural) hydraulic gradient forces the surface water to infiltrate the banks or bed of a surface water body and eventually reach the pumping well(s). As opposed to direct surface water abstraction, BF systems benefit from the natural capacity of the sediments to attenuate/remove contaminants (Hiscock & Grischek, 2002), including wastewater-derived pathogens (Derx et al., 2013; Lorenzen et al., 2010; Weiss et al., 2005), natural organic matter and xenobiotic organic micropollutants (Bertelkamp et al., 2016; Burke et al., 2014; Dragon et al., 2018; Hamann et al., 2016). However, the efficiency of a BF system to attenuate contaminants depends on numerous parameters, including quality of the surface water (Groeschke et al., 2017) and its travel time in the aquifer (Dragon et al., 2018; Hamann et al., 2016).

Under flood conditions, surface water quality is often deteriorated (Whitehead et al., 2009) and short travel times are typically observed at BF systems (Eckert & Irmscher, 2006; Hunt et al., 2005;

Wett et al., 2002). As a result, BF systems are vulnerable to pathogens, heavy metal, dissolved organic carbon and organic micropollutant contamination during flood events (Sprenger et al., 2011). Ray et al. (2002) pointed out that small capacity collector wells are less at risk of flood-induced contamination than medium to large capacity collector wells. Ascott et al. (2016) reported high turbidity, organic contaminants, microbial detects, dissolved oxygen and dissolved organic carbon, and low electrical conductivity (EC) during an extreme flood event at a shallow granular aquifer in England. Rose et al. (2018) observed cyanobacterial contamination due to direct infiltration and damage (i.e., erosion) of the bank during and after a flood event at a river BF site in Australia. BF systems under oxic conditions close to a highly dynamic river were reported to be particularly at risk of contamination under flood conditions, because normally degraded compounds (e.g., diclofenac and bezafibrate) during BF and a significant increase in large cells concentrations were observed in the bank filtrate (van Driezum et al., 2018; van Driezum et al., 2019). BF systems in hilly terrains were also reported to be vulnerable to contamination during flood events (Sandhu et al., 2013). In the province of Quebec (Canada), it is not rare to observe pathogen indicators (such as total coliforms) in municipal pumping wells during springtime freshets, which is perhaps linked to the fact that bank filtration is likely performed unintentionally due to the large density of lakes and rivers, and the close proximity of municipal wells to those waterbodies (Patenaude et al., 2020).

At BF sites, it can be expected that changes of flow patterns and travel times occur at short (e.g., daily) timescales, as demonstrated by Wett et al. (2002). In fact, time-consuming and labor-intensive traditional cultivation-based methods for pathogens analysis are still advocated for routine monitoring of drinking water treatment plants performance (World Health Organization, 2017). As a result, water quality management decisions for the operation of BF systems and post-treatment are typically based on weekly to monthly time-step assays. In addition, Adomat et al. (2020) recently evidenced short timescale bacterial fluctuations during a high temporal resolution monitoring at an ultrafiltration pilot plant and hypothesized a control by rainfall events and/or potential changes in surface water origin. To correctly interpret these variations, the authors highlighted the need to assess for “abiotic” parameters (i.e., EC, pH, dissolved oxygen) which can help to identify the processes controlling microbiological water quality. A promising avenue for providing management strategies would be to anticipate changes in the capacity of bank filtration

to attenuate contaminants, driven by the evolution of the origin and travel time of the bank filtrate. Since environmental tracers (i.e., temperature, EC and δ18O) have been shown to be good proxies for these two parameters (Baudron et al., 2016; des Tombe et al., 2018; Massmann et al., 2008; Vogt et al., 2010), the analysis of their evolution could provide an improved understanding for the management of bank filtration sites.

The aim of this study is to illustrate how monitoring strategies of environmental tracers at flood-affected sites can be optimized and to demonstrate how tracer-based evidence can help to define adequate pumping strategies. We performed a tracer monitoring which covered two intense flood events at a two-lake bank filtration site. It was conducted at various sampling locations (i.e., pumped mix, pumping wells and observation wells) and time-steps (i.e., from sub-daily to monthly), while bacterial sampling was conducted at a monthly time-step. By doing so, it was possible to better understand the timescales of changes in the groundwater flow patterns and, thus, anticipate the water quality dynamics. The comparison of the information provided by the different sampling locations allows discussing the representativity and relevance of environmental tracers and standard bacteriological analysis. Their contribution to the pumping strategies for real-time water quality management is then depicted.

5.2 Study Site Description

5.2.1 Hydrological and Geological Contexts

The studied lake-BF system is located in a peri-urban region in the south of the province of Quebec, Canada (Figure 5-1a). A total of 8 pumping wells were installed in a small fully unconfined aquifer of approximately 500 m wide and 120 m long and with a maximum thickness of 26 m. Ageos (2010) described this aquifer as a buried valley carved into the Champlain Sea clays (Figure 5-2). The aquifer is mainly composed of alluvial fine to medium sands and has a hydraulic conductivity of 2.7 x 10-3 m/s (Ageos, 2010). A small lens of alluvial gravel is also found at the bottommost part of the aquifer in the vicinity of P4 and P5. The topography of the study area is nearly flat, with minimum and maximum observed surface elevations of 23.76 m.a.s.l. and 27.91 m.a.s.l. (Ageos, 2010). On the North-East and South-West limits of the aquifer are two artificial lakes, namely Lake A and Lake B which were created from sand dredging activities.

The pumping wells are all screened at the base of the aquifer over 8 m long sections, except for P5 which has a 4 m long section. The screened sections of the observation wells PZ-2, PZ-5 and PZ-6 are also located at the bottom of the aquifer and over 9 m, 3 m and 6 m, respectively. No information is available concerning the design of the observation well PZ-4. The pumping wells receive water from Lake A and Lake B and no contribution from regional groundwater was identified. The mixing ratio between Lake A and Lake B waters range from 0% to 100% and is influenced by the pumping rate and the water level difference between the lakes. During springtime, the contribution from Lake A tends to be > 50% at all pumping wells (Masse-Dufresne et al., 2019b). A numerical groundwater flow model was previously developed by Ageos (2010) and the mean travel times were estimated as 2 days from Lake B and 10 days from Lake A.

Lake A is an exploited and flooded sandy pit of approximately 2.8 x 10^5 m^2 and has a maximal observed depth of 20 m. It receives surficial inflow from a small stream (S1) with an annual mean discharge of 0.32 m^3/s (Ageos, 2010). Surficial outflow fluxes via a 1 km long channeled stream (S2) can only occur given a sufficiently high water level, due to a topographic threshold at 22.12 m.a.s.l. (Ageos, 2010). The direction of water fluxes at S2 can be reversed when the water level of Lake DM is exceeding both the topographic threshold and the one of Lake A (see arrows on Figure 5-1b). Such conditions lead to surficial inputs from Lake DM, resulting in a hydraulic connection with a large watershed as the latter corresponds to a widening of the Ottawa river (Figure 5-1a). Subsurface water fluxes between Lake DM and Lake A are not likely, since impervious sediments (i.e., Champlain Marine Clays) are underlying the thin layer of alluvial sands (i.e., only few metres) between Lake A and Lake DM (Ageos, 2010). Lake B is a former sandy pit of approximately 7.6 x 10^4 m^2 with maximum observed depth of 19 m. It is nowadays surrounded by residential area and a public recreational beach. It has no surficial inlet and is thus mainly fed by precipitations and groundwater. An artificial surficial outlet (at approximately 21.8 m.a.s.l.) can drain Lake B water towards the town's stormwater collection system.

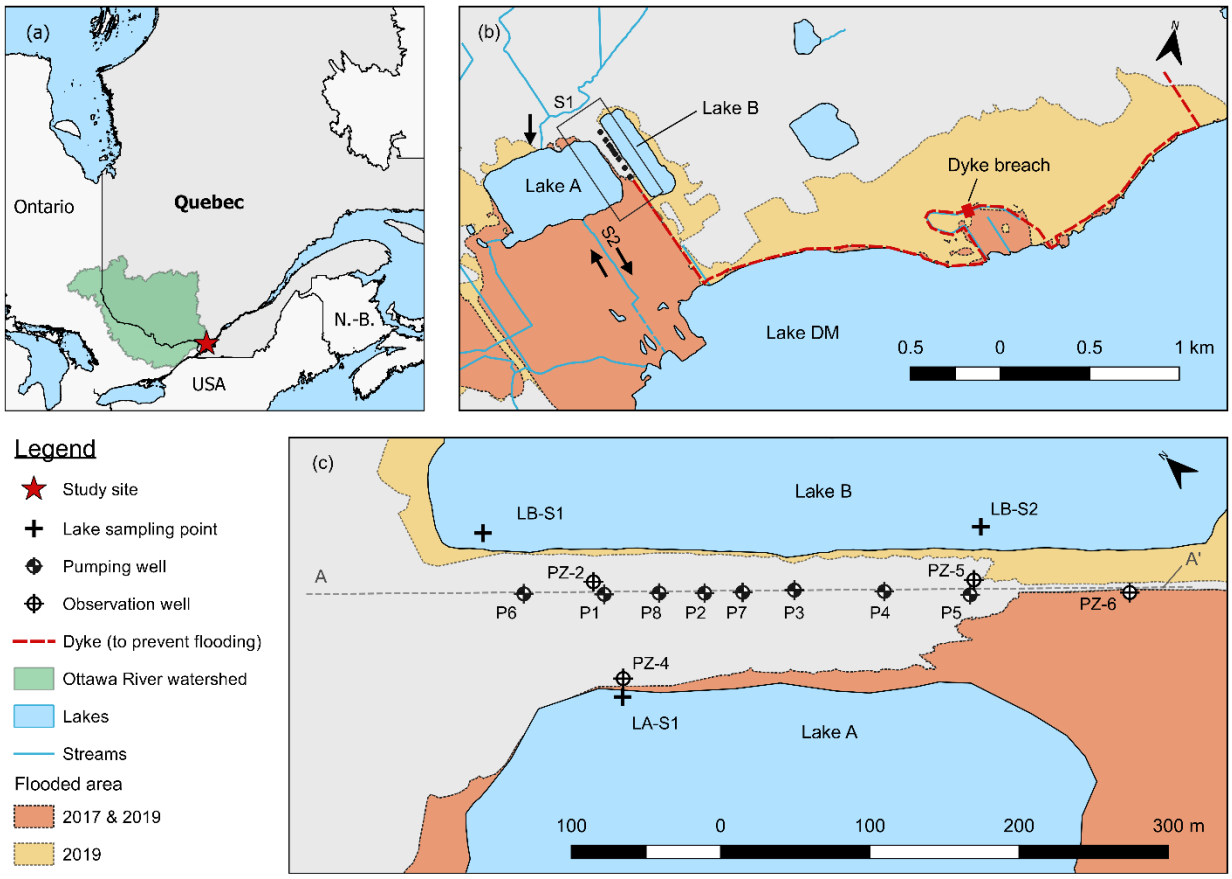

Figure 5-1 (a) Location of the study site and Ottawa River watershed, (b) schematic representation of the hydrogeological context and location of Lake A, Lake B and Lake DM, and (c) location of monitoring and sampling points and geological cross-section A-A'. The maps were created based on open access Geographic Information System (GIS) data. Canada's provinces boundary files were obtained from Statistics Canada © and USA Cartographic Boundary Files were retrieved from the United States Census Bureau ©. Hydrological data (lakes, streams and watershed) was sourced from the Nation Hydro Network – NHN – GeoBase Series and provided by the Strategic Policy and Results Sector of Natural Resources Canada ©. The flood extent products are derived from RADARSAT-2 images with a system developed and operated by the Strategic Policy and Results Sector of Natural Resources Canada ©.

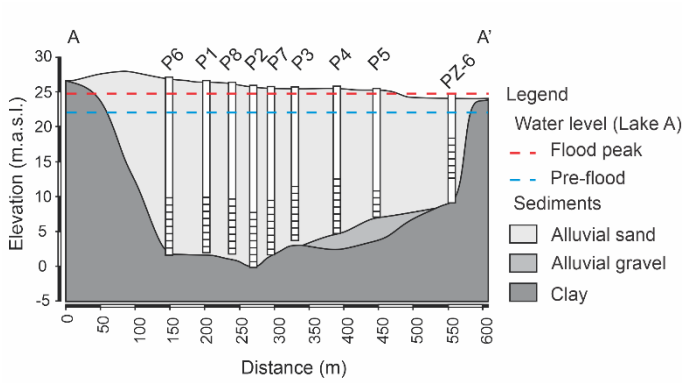

Figure 5-2 Hydrogeological cross-section A-A' and location of the pumping wells and PZ-6. The screened sections of the pumping wells are located at the bottom of the aquifer. The blue and the red dashed lines represent the pre-flood and flood peak water levels at Lake A, respectively. Direct infiltration of floodwater did not occur during the intense flood events.

5.2.2 Flood-proof Measures

All the pumping wells are equipped with a subsurface well chamber (in concrete) in which automatic pumps drain water that can infiltrate due to precipitations, snowpack melting and/or rising of the water table. Note that during normal hydrological conditions, the water table is below the well chambers. During intense flood events, temporary headworks are erected around the pumping wells to prevent infiltration of floodwater into the well chamber from the surface. Concerning the observation wells, steel casings prevent direct infiltration of floodwater.

5.2.3 Operation of the BF System

A schematic illustration of the BF system and treatment plant is shown in Figure 5-3. All the pumping wells are equipped with a variable flow submersible pump, except for P5 which has a fixed flow pump. When a well is abstracting water, the raw water can flow either towards a purging system or towards the treatment plant, accordingly to the position of the valves and the needs of the waterworks. All the active pumping wells contribute to the pumped mix, which is further treated and chlorinated before its distribution to the drinking water supply system.

The total pumping rate ranges between 4000 m^3/day and 7500 m^3/day. The pumping wells P3 and P6 are typically contributing the most to the pumped mix and are continuously operated at $\geq$ 1000 m^3/day. During the daily peak demand and/or the summertime, P1, P2, P7 and P8 are

operated intermittently (i.e., few hours per day). Lastly, P4 and P5 are only occasionally in operation (i.e., few minutes to hours per month). Further details concerning the pumping schemes are available in a previously published work (Masse-Dufresne et al., 2019b).

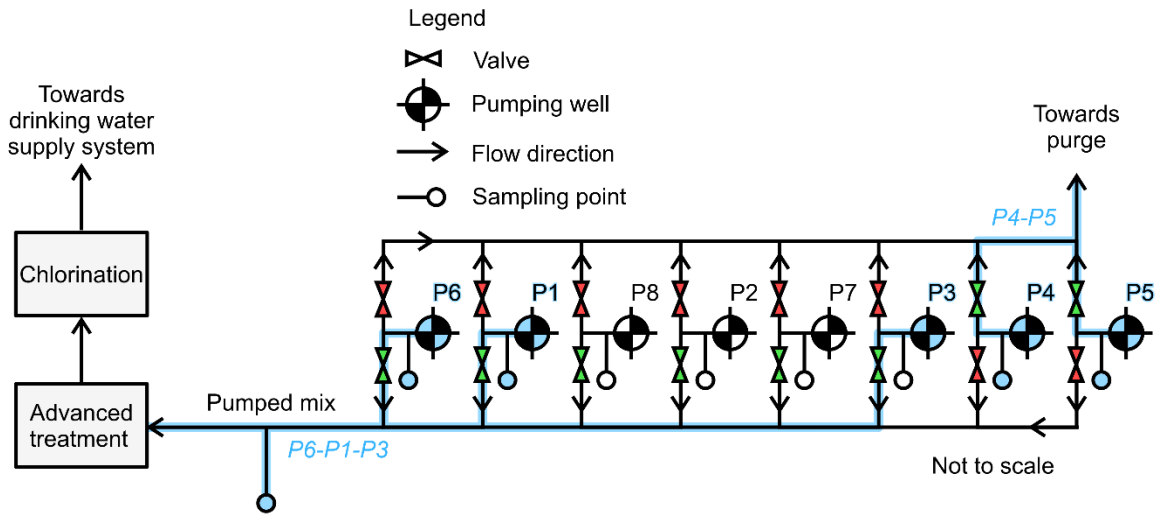

Figure 5-3 Schematic illustration of the BF system and treatment plant. The pumping wells are equipped with submersible pumps, which enable control on the active pumping wells. The pumped water flows either towards a purging system or towards the treatment plant, accordingly to the needs of the waterworks. Hand valves are open (in green) or closed (in red) to allow water to flow towards the desired direction. Sampling of the raw water can be performed at the individual pumping wells, if they are actively pumping (in blue). Typically, three pumping wells are active and contribute to the pumped mix (e.g., P6-P1-P3), which can also be sampled. The wells can also be sampled when operated in purging mode (e.g., P4 and P5). An advanced treatment and chlorination are performed on the raw pumped mix prior to its distribution to the drinking water supply system. The advanced treatment consists of biological filtration (Mangazur®) and nanofiltration (NF90 Filmtec™).

5.3 Materials and Methods

5.3.1 Instrumentation

Lake A, Lake B and observation wells (i.e., PZ-2, PZ-4 and PZ-6) were equipped with pressure-temperature data loggers (Divers®, micro-Diver, Van Essen Instruments, Delft, Netherland). The loggers were installed at roughly 10 m to 12 m depth below the ground level in all three observation wells. PZ-2 was additionally equipped with a pressure-temperature-EC data logger (Divers®,

CTD-Diver, Van Essen Instruments, Delft, Netherland) which was installed at 20 m depth below the ground level and in front of the screened section of the observation well. All measurements were done on at a 15 min to 30 min time-step. A barometer (Divers®, micro-Diver, Van Essen Instruments, Delft, Netherland) was also installed on-site to perform the barometric compensation (for the calculation of water level from pressure measurements). Accuracy for pressure, temperature and EC measurements were ± 1 cmH_2O, ± 0.1°C and ± 10 µS/cm, respectively. It is assumed that the EC measurements at PZ-2 (at 20 m depth) are representative of groundwater in its vicinity, since the level logger was placed in front of the screen, where water enters and exits the observation well according to the existing groundwater flow. It is also assumed that temperature measurements at the observation wells (at 10-12 m and 20 m) are representative of the adjacent groundwater conditions.

Mean daily water levels at Lake DM were obtained with permission from the Centre d'Expertise Hydrique du Quebec database (Centre d'Expertise Hydrique du Québec, 2020). Daily means (for water levels, temperature and EC measurements) were calculated in order to produce consistent time series. Precipitations from Mirabel International Airport, i.e., the closest meteorological station (18 km from the study site), were retrieved from Environment and Climate Change Canada database (available online at weatherstats.ca).

5.3.2 Water Sampling and Analytical Procedures

Water sampling was performed on a weekly to monthly basis at the surface of Lake A, Lake B and at the pumping wells (P1 to P8) following the procedure described in Masse-Dufresne et al. (2019b). During the 2017 and 2019 springtime flood events, additional sampling campaigns were conducted. In 2017, additional measurements and water samplings were performed at observation wells (i.e., PZ-2, PZ-4 and PZ-5) at a weekly to monthly timestep. In 2019, the raw pumped mix was sampled by the operators of the drinking water facility on a daily basis at a by-pass faucet, prior to treatment for potabilization, in order to perform measurements of EC and analyses of $\delta^{18}O$ and $\delta^{2}H$. Note that access to the pumping wells and the pumped mix sampling point was not restricted during the flood events. As stated in section 5.2, automatic pumps drain water that can infiltrate in each well chamber, which enables sampling of the pumping wells year-round. Also,

the sampling point for the pumped mix is in the water treatment plant building and is therefore easily accessible, even during flood events.

High-density polyethylene (HDPE) 60 mL bottles (Thermo Scientific™ Nalgene™ Narrow-Mouth HDPE Economy Botttles, Rochester, New York, United States) were used to collect samples for $\delta^{18}O$ and $\delta^{2}H$ analysis, which were stored at room temperature. Filtration through a 0.45 µm hydrophilic polyvinylidene fluoride (PVDF) membrane (Millex-HV, Millipore, Burlington, MA, USA) was performed in the laboratory when needed. Analyses for stable isotopes of water were performed with a Water Isotope Analyzer with off-axis integrated cavity output spectroscopy (LGR-T-LWIA-45-EP, Los Gatos Research, San Jose, CA, USA) at Geotop-UQAM laboratory (Montreal, Quebec). Three internal reference standards ($\delta^{18}O$ = -6.71 ‰, -4.31 ‰ and -20.31 ‰; $\delta^{17}0$ = -7.23 ‰, -2.31 ‰ and -19.96 ‰; $\delta^{2}H$ = -51.0 ‰, -25.19 ‰ and -155.40 ‰) calibrated on the VSMOW-SLAP scale were used to correct the data. The analytical uncertainty (1σ) is 0.15 ‰ and 1 ‰ for $\delta^{18}O$ and $\delta^{2}H$, respectively.

5.4 Results and Discussion

5.4.1 Long-lasting Hydraulic Control by Floods

5.4.1.1 Recurrent and Extreme Events

During springtime and autumn, water level at Lake DM normally rises due to snowpack melting and/or precipitations over the watershed. From 1987 to 2016, mean water levels of Lake DM in April and May are 22.82 m.a.s.l. and 22.51 m.a.s.l., respectively (Centre d'Expertise Hydrique du Québec, 2020), which is higher than the topographic threshold (at 22.12 m.a.s.l.). In fact, water level rise at Lake DM induces a yearly recurrent hydraulic connection with Lake A and allows for floodwater inputs (from Lake DM) to Lake A, typically from April to May (Ageos, 2016).

The evolution of water levels at Lake DM from 2014 to 2020 is represented in Figure 5-4a. For normal hydraulic conditions, the total duration of the flood events is typically between 80 and 95 days and the maximum water level rise above the threshold is 1.5 m. In 2017 and 2019, springtime water level rise at Lake DM was particularly important (i.e. > 2.6 m above the topographic

threshold) and the flood events lasted 150 days and 106 days, respectively. Unprecedented historical water levels (i.e., 24.77 m.a.s.l. and 24.75 m.a.s.l.) were reached on May 8, 2017 (Figure 5-4b) and April 29, 2019 (Figure 5-4d). Note that there was no risk of direct infiltration of floodwater into the pumping wells and the observation wells (see section 5.2.2) in 2017 and 2019, except for PZ-6 (in 2017 only) where the elevation of the steel casing is at 24.78 m.a.s.l., which is similar to the maximal water level at Lake DM (i.e., 24.77 m.a.s.l.). On the other hand, the area in the vicinity of PZ-6 was inundated in 2017 and 2019 (see Figure 5-1c) and short-circuiting of floodwater along the steel casing could have potentially occurred at PZ-6.

In 2017 and in 2019, the temporal evolution of water levels at Lake A, Lake B and PZ-4 are mainly showing similar trends as Lake DM, indicating a control of Lake DM over the water levels of the whole hydrosystem during the springtime flooding (Figure 5-4b and d). In 2018, the water level at PZ-4 is also governed by the fluctuation of Lake DM when the latter exceeds the topographic threshold (Figure 5-4c). These results suggest that Lake A receives floodwater inputs from Lake DM during both recurrent and extreme flood events.

5.4.1.2 Dyke Failure

To prevent inundation of inhabited areas, numerous municipalities surrounding Lake DM have built dykes. However, in April 2019, the important water level rise at Lake DM caused a dyke to fail at approximately 1 km eastwards from the study site, resulting in the flooding of a residential area (including Lake B) and forcing the evacuation of 6,000 people. Comparison between the extent of the flooded areas in 2017 and 2019 (Figure 5-1b) suggest that the dyke failure imposed different hydraulic conditions to the BF system. In fact, it caused an important water level rise at Lake B and PZ-4 (Figure 5-4d). The town authorities rapidly proceeded to (i) the construction of temporary dykes to constrain the flooded area and (ii) the installation of a pumping station at Lake B, which allowed to artificially lower the water levels at Lake B and PZ-4.

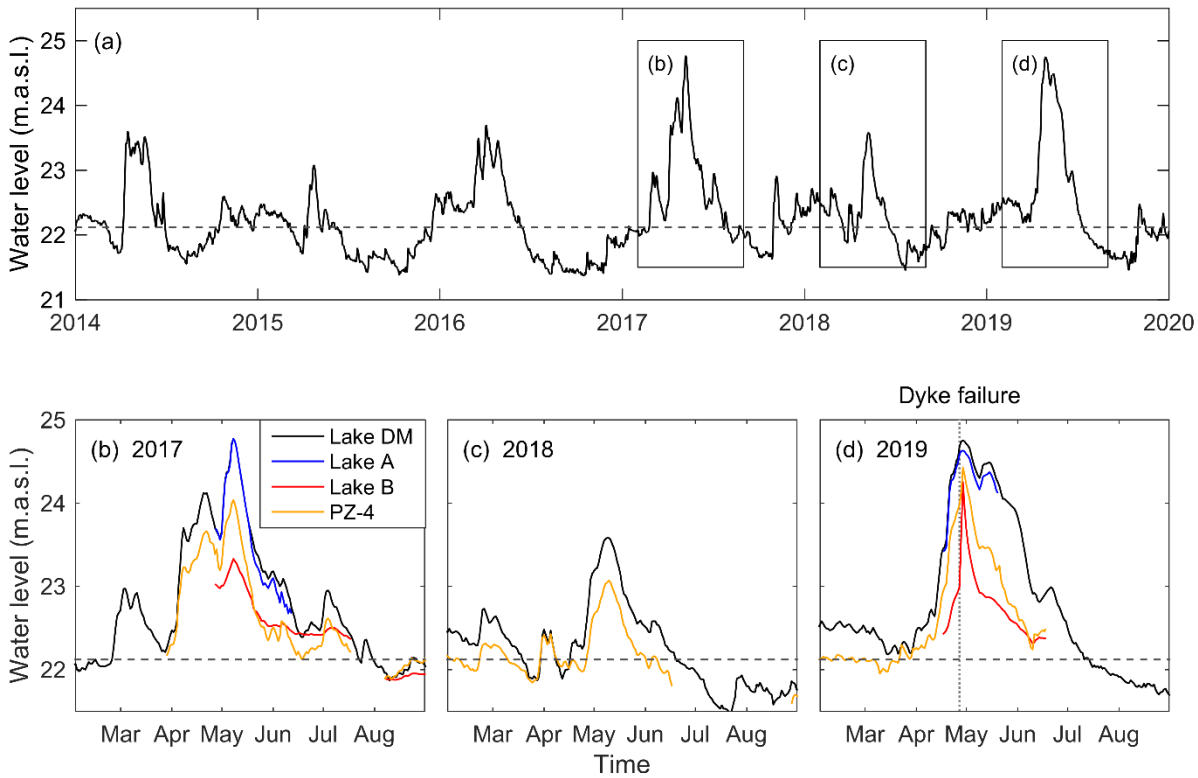

Figure 5-4 Temporal evolution of water levels at (a) Lake DM from 2014 to 2020, (b) Lake DM, Lake A, Lake B and PZ-4 during springtime 2017, (c) Lake DM and PZ-4 during springtime 2018 and (d) Lake DM, Lake A, Lake B and PZ-4 during springtime 2019. The black dashed line corresponds to the topographic threshold at 22.12 m.a.s.l., above which a hydraulic connection is established between Lake DM and Lake A (Ageos, 2010). On April 27, 2019, failure of a dyke (at 1 km SE to the study area) caused the flooding of a residential area, including Lake B, and resulted in rapid water level rise at Lake B (and PZ-4).

5.4.2 Water Quality Risk Assessment

5.4.2.1 Spatiotemporal Variability of Coliform Counts at the Pumping Wells

A regulatory microbiological water quality monitoring is performed monthly at all the pumping wells. Included in this routine monitoring are the standard culture-based analysis for total coliforms, which also includes the atypical counts (i.e., the colonies which do not produce a green shine on the m-Endo media), and for E. coli.

Figure 5-5 illustrates the spatiotemporal evolution of total counts on m-Endo media (sum of atypical and typical colonies) at the pumping wells from 2014 to 2019. Note that all analyses for E. coli were negative during the same period. Total counts at all the pumping wells are typically < 1 CFU/100 ml and, occasionally, ≥ 1 CFU/100 ml and < 10 CFU/100 ml. Bacterial detects are rarely summing > 10 CFU/100 ml, and if so, it is only occurring at one single pumping well, except during the extreme flood events. In May 2017, the bacterial detects were positive at all the pumping wells and > 60% (5/8) of the pumping wells showed ≥ 10 CFU/100 ml and < 100 CFU/100 ml. A similar pattern, but with less important bacterial detects, was observed during the 2019 flood event. Considering the above, the bank filtration system appears to be resilient to the yearly recurring flood events but more vulnerable to contamination during the intense flood events (such as 2017 and 2019).

5.4.2.2 Tracking the Origins of Coliform Bacteria

The quality of the Ottawa River (i.e., the discharging waters to Lake DM) is known to be altered by the contamination from combined sewage overflows (Jalliffier-Verne et al., 2016) and was particularly affected during the studied flood events (CBC News, 2017). Water quality of Lake DM was thus very likely to be affected by combined sewage overflows occurring at the watershed scale, which can be a source of wastewater-derive pathogens, including total coliforms. As Lake A receives floodwater inputs from Lake DM during springtime, wastewater-derived contamination is a potential threat to the BF system.

However, total coliforms are ubiquitous in the environment and are thus not only sourced from fecal origin (Glassmeyer et al., 2005; Martin et al., 2010). Rainfall events can lead to the transport of pathogens initially present in soils, resulting in the pollution of receiving waters (Frey et al., 2015). Precipitations were particularly important in 2017 and 2019, as the cumulated precipitation (as rain and/or snow equivalent) from January to May summed at 578 mm and 498 mm, while it was ranging from 330 mm to 418 mm for the other years (Appendix B; Figure B1). Moreover, the 2017 and 2019 springs are characterized by more heavy and consecutive rainfalls. Given the intensity of rainfalls along with the snowpack melting during springtime in 2017 and 2019, it is also likely that endogenous bacteria to the sediments were detected at the pumping wells due to water level rise and evolution of the prevailing groundwater flow patterns. Although the presence

of total coliforms is not strictly indicative of fecal contamination, the increase in bacterial counts during the two intense flood events (i.e., 2017 and 2019) are still indicative of a change in the hydrological process and/or flow patterns which affects the origin of the pumped water.

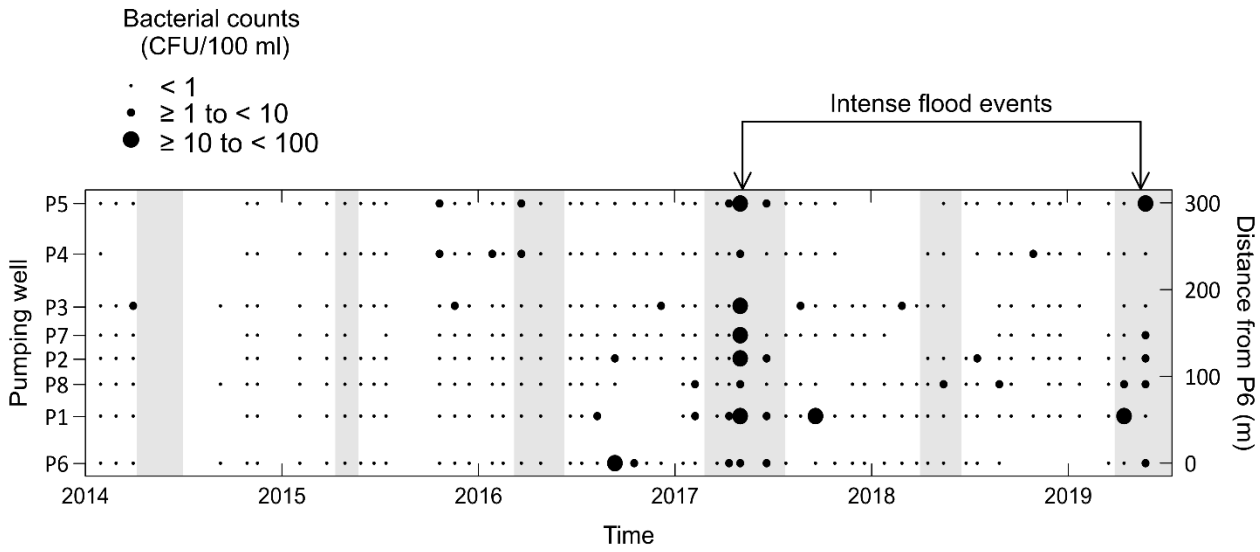

Figure 5-5 Spatiotemporal evolution of total bacterial counts on m-Endo media (i.e., sum of total coliform and atypical bacteria) at the pumping wells (P6, P1, P8, P2, P7, P3, P4 and P5) from January 2014 to June 2019. The data was provided by the municipal authorities. The gray shaded area represents the springtime flood events.

5.4.3 Groundwater Flow Dynamics: from Normal to Flood Conditions

This section aims at studying the evolution of the origin of the bank filtrate due to the 2019 intense flood event, in order to better understand the groundwater flow dynamics. To do so, the evolution of EC and $\delta^{18}O$ at short timescale (daily) at the pumped mix is examined. Then, the origin of the bank filtrate at the pumping wells and at a monthly time-step from January 2017 to June 2019 is assessed in order to discuss the representativity of the interpretations derived from monitoring at the pumped mix.

5.4.3.1 Temporal Evolution of EC and $\delta^{18}O$ at the Pumped Mix

The pumped mix corresponds to the raw pumped water from multiple wells, which is further treated and chlorinated before its distribution to the drinking water network (see Figure 5-3). Sampling of

the pumped mix was efficiently performed daily by the plant operators during springtime and summer 2019 to cover the flood event and the recovery to normal conditions.

Figure 5-6 depicts the temporal evolution of EC and $\delta^{18}O$ at the pumped mix, which is discretized in three periods. The evolution of $\delta^{2}H$ (data not shown) was found to be very similar to $\delta^{18}O$, which suggests that both stable isotopes of water ($\delta^{18}O$ and $\delta^{2}H$) are illustrating the same processes. Therefore, no discussion concerning $\delta^{2}H$ is provided. First, normal hydraulic conditions were prevailing in early April. The observed EC was 685 µS/cm at the pumped mix. In comparison, mean Lake A and Lake B EC values are 500 µS/cm and 800 µS/cm, respectively. As it was demonstrated in previous work, this indicates that the pumped water was a mixture between Lake A and Lake B waters (Masse-Dufresne et al., 2019b). Then, under flood conditions, a decreasing trend for both tracers was observed over a 1-month period (from April 15 to mid-May) as shown in Figure 5-6. The EC evolution indicates that the pumped water transitioned from a mix between Lake A and Lake B to exclusively Lake A water during the flood event. Considering that floodwater is characterized by a depleted signature in heavy isotopes (mean value of -11.7 ‰), it appears as a good proxy to denote the presence of floodwater. Depleted signatures (i.e. < -12 ‰) were observed at the pumped mix during a two-week period around mid-May, suggesting that the bank filtrate was particularly influenced by the flood-marked water. Finally, in late May, EC and $\delta^{18}O$ recovered towards initial values over a two-month period. This result suggests that when the water level at Lake DM exceeds the topographic threshold (at 22.12 m.a.s.l.), the latter has a decisive impact on the origin of the pumped water.

In early May, the observed EC and $\delta^{18}O$ values tended to slightly deviate from the expected curve (Figure 5-6b). This is very likely due to the above-mentioned failure of the dyke (see section 5.4.1.2; Figure 5-4d), which resulted in a rapid evolution of the water level difference between Lake DM (and Lake A) and Lake B. Another potential controlling factor is a change in the pumping scheme, as P3 was out of operation from April 29 and P7 (or occasionally P8) was activated to maintain the needed daily pumped volume. In either case, this result denotes the important reactivity of the BF system to changes in hydraulic conditions, and thus suggests that the travel times of water to the pumping wells are short. However, monitoring for environmental tracers at the pumped mix has limitations. In fact, no precise estimation of travel times can be done with this dataset since it is composed of abstracted water from different wells.

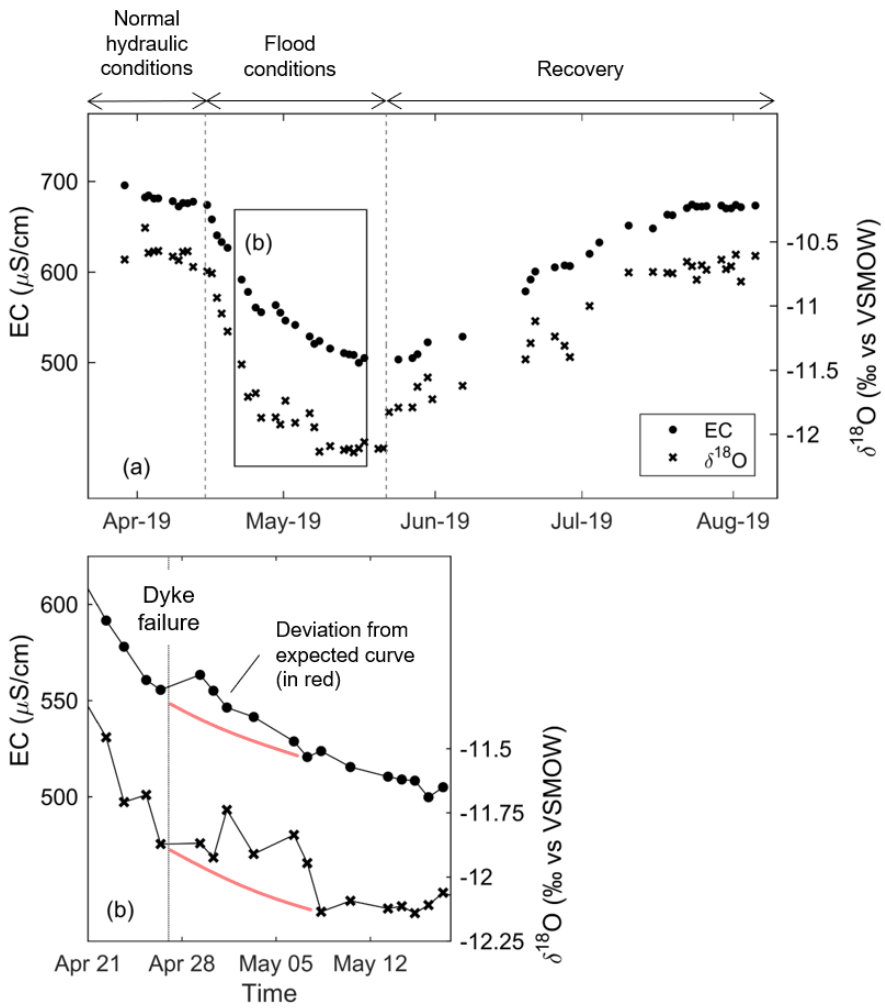

Figure 5-6 (a) Temporal evolution of electrical conductivity (EC) and $\delta^{18}O$ at the pumped mix from April to August 2019. (b) Zoom on the period between mid-April and mid-May, emphasizing the timing of the dyke failure (on April 27) and the deviation of EC and $\delta^{18}O$ from the expected curve (in red). The pumped mix was composed of groundwater abstracted at P1, P3 and P6 until April 29, after which P7 (or occasionally P8) was contributing to the pumped mix as P3 was non-operational.

5.4.3.2 Spatiotemporal Variability of EC and $\delta^{18}O$ at the Pumping Wells

Given the potential spatial heterogeneity of the hydrogeological parameters and the variability of the pumping rate at each well, it is expected that there is a spatial variability in the evolution of the flow patterns along the BF system. This raises questions concerning the representativity of the evolution of the origin of water in the pumped mix. This subsection aims at exploring such question

by confronting the interpretations derived from monitoring at the pumped mix (last subsection) to interpretations derived at a higher spatial resolution, i.e., at each pumping well.

Figure 5-7 depicts the monthly evolution of EC and $\delta^{18}O$ at the pumping wells from March 2016 to June 2019. For each sampling campaign, a boxplot illustrates the distribution of the environmental tracers at the sampled pumping wells (i.e., up to 8). For comparison purposes, representative values for Lake A and Lake B or for floodwater are also illustrated.

Under normal hydraulic conditions, there is typically a large variability of the two tracers at each pumping well. For instance, the EC can range between mean Lake A (i.e., 506 µS/cm) and mean Lake B (i.e., 802 µS/cm) values for a single sampling campaign. This observation demonstrates that the groundwater flow patterns are normally heterogenous along the BF system. In contrast, all the pumping wells tend to converge towards floodwater and Lake A water types during the flood events, suggesting a common forcing on the origin of the bank filtrate. Since the same trends were observed at all the pumping wells during the flood events, interpretations derived from monitoring at the pumped mix can be extrapolated to the whole BF system. More precisely, the dynamics of the origin of water to the pumping wells contributing to the pumped mix also apply to the less active pumping wells under flooding conditions. However, the transition to a homogeneous behavior was not detected as it occurred between two sampling campaigns, i.e., within a one-month period. Hence, based only on the EC and $\delta^{18}O$ variations we infer that the travel time of the bank filtrate during the flood events is < 1 month.

Additionally, it appears that the intensity of the flood event drives the amplitude of the EC and $\delta^{18}O$ shifts. In fact, for the 2016 and 2018 flood events, EC values remained higher than the mean Lake A value at the pumping wells. Concerning the isotopic composition, depleted values (< -11.5 ‰, i.e., mean floodwater value) were only observed during the more intense flood events (2017 and 2019). Hence, the isotopic composition is proven to be useful due to its specificity to depict significant floodwater contribution and, consequently, differentiate between the recurrent yearly floods and the extreme events at this study site. Also, a tardy recovery to initial values is observed at some wells for the 2017 intense flood event, suggesting potential flood water storage which is likely influenced by the pumping rates. Further discussion on this topic is provided in section 5.4.5.2.

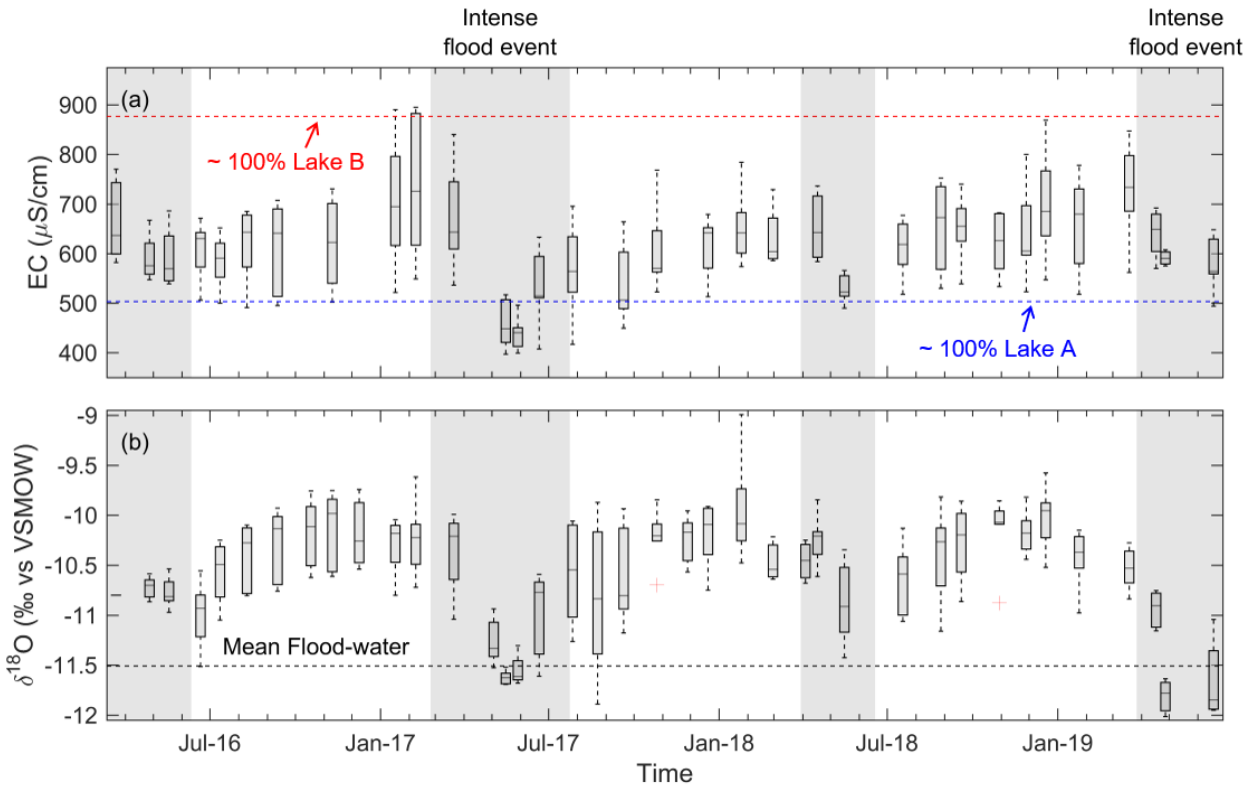

Figure 5-7 Temporal evolution of (a) electrical conductivity (EC) and (b) $\delta^{18}O$ at the pumping wells (gray boxplots) from March 2016 to June 2019. Sample size (n) for each boxplot is normally 8 (i.e., all the pumping wells). Note that on occasional circumstances, some wells were not sampled (due to pump failure) and the boxplot were generated with $n \geq 3$ to $n \leq 7$. The gray shaded area represents the 2016, 2017, 2018 and 2019 flood events. The blue and red dashed lines correspond to the mean EC values at Lake A and Lake B (≥2 m depth), respectively, while the black dashed line represents the mean $\delta^{18}O$ value for floodwater. Note that the EC values at the pumping wells from March 2016 and February 2017 and the mean floodwater $\delta^{18}O$ values are retrieved from previously published work (Masse-Dufresne et al., 2020; Masse-Dufresne et al., 2019).

5.4.4 Temperature as a Proxy of Transient Groundwater Flow Patterns During Flood Events

The combined use of EC and $\delta^{18}O$ was proven to be adequate to track the origin of the pumped water. When such monitoring is applied to the pumped mix or the pumping wells, it is, however, not possible to gain insights into the travel times of the bank filtrate which is of utmost importance for water quality risk management. In this section, we develop an interpretative framework of the

behavior of temperature which helps at understanding timescales and the timing of the impacts of flood events on the groundwater flow pattern.

Figure 5-8 illustrates the temporal evolution of temperature at PZ-6 (distant from the BF system) and vertical temperature profiles at two observation wells (PZ-2 and PZ-5) along the BF system during normal hydraulic conditions (March 19, 2019) and flood conditions (April 25, 2019). Observation well PZ-6 is located southeastwards from the BF system (see Figure 5-1). In that area, the groundwater flow pattern is believed not to be influenced by the pumping. Surface water from Lake A infiltrates the bank and flows towards Lake B, as the water level of Lake A is higher than Lake B. Electrical conductivity at PZ-6 (476 µS/cm; in September 2018) also supports this interpretation. A similar flow pattern is expected at PZ-5, as the latter is located near pumping well P5, which is only rarely abstracting water (i.e., 1-2 hours for the regulatory monthly monitoring). On the other hand, observation well PZ-2 is located between Lake B and the pumping well P1 (continuously pumping). Under normal hydraulic conditions, surface water from Lake B infiltrates the sandy bank and eventually reaches pumping well P1. Thus, the groundwater in the vicinity of PZ-2 is normally originating from Lake B and physicochemical parameters are governed by the conditions at Lake B. Hence, it can help at understanding the dynamics of temperature under the influence of pumping.

As shown in Figure 5-8a, from September 2018 to late February 2019, the temperature measured at PZ-6 increased gradually (up to 17°C), while it was decreasing (down to 4°C) at Lake A. Under flood conditions, temperature at PZ-6 decreased rapidly, and low temperatures (< 2°C) were observed in late April. Similarly, a decrease of the temperatures also occurred at PZ-5 (Figure 5-8c). At PZ-2, the temperature ranged from 1°C to 5°C on March 19, 2019 (Figure 5-8b). Such cold temperatures are resulting from the infiltration of cold water from Lake B during wintertime. Then, under flood conditions, a rapid warming of groundwater was observed at PZ-2 (Figure 5-8b).

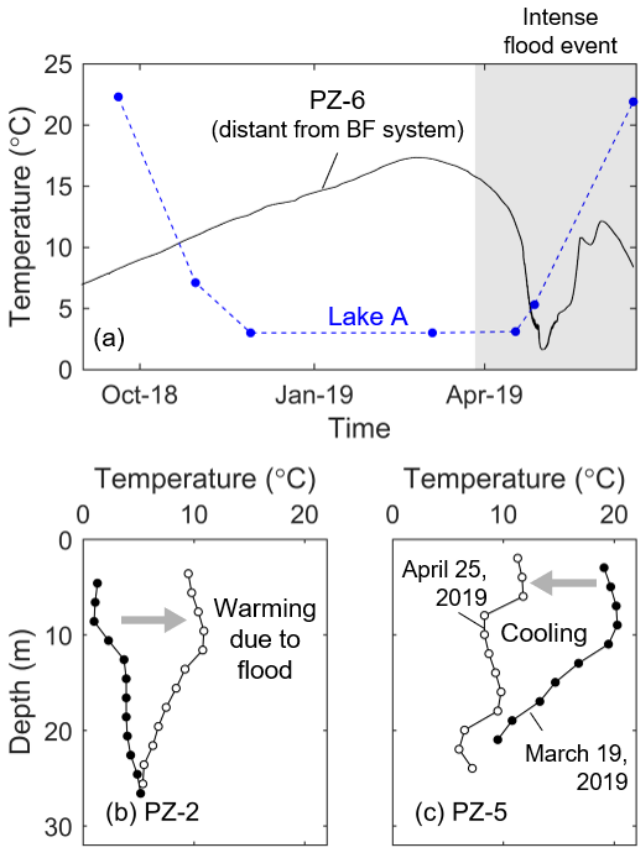

Figure 5-8 (a) Temporal evolution of the temperature at the surface of Lake A (in blue) and at PZ-6 (in black), which is an observation distant from the BF system and thus not influenced by pumping. Vertical temperature profiles on March 19, 2019 and April 25, 2019 at (b) PZ-2 and (c) PZ-5. The observation well PZ-2 is located between Lake B and the pumping well P1 (continuously pumping), while PZ-5 is near P5 (occasionally pumping).

To summarize, the flood event has significantly altered the temperature dynamics at the observation wells and the vertical temperature profiles (at PZ-2 and PZ-5) seem to converge towards 10°C. Based on the available data, it is not possible to conclude on the origin of this 10-degree water. It is potentially corresponding to the floodwater. However, as the mean air temperature was mainly < 10°C until early May (see Appendix B; Figure B2), we expected that the floodwater temperature would be lower than 10°C. Besides, the flood event modified the prevailing groundwater flow pattern and likely triggered the mobilization of a warm groundwater which could have mixed with cold and recently infiltrated water from Lake A. Such scenario would have resulted in the observed

10-degree water at both observation wells PZ-2 and PZ-5, but further research is still needed to test this hypothesis.

In addition, daily time-step measurements of temperature and EC were performed at PZ-2 (Figure 5-9), in order to gain further insights into the timescales and the timing of the flood event impacts on the groundwater flow in the vicinity of the pumping wells. Only continuous measurements of water levels, temperature and EC were performed, due to robustness and practicality of those measurements.

From late March to mid-April, normal hydraulic conditions were prevailing, and the observed temperatures and EC were nearly constant (Figure 5-9a). In mid-April, temperature at 11 m depth, and to a lesser extent at 20 m, started to decrease (Figure 5-9b). This temperature change coincides with the timing of the EC decrease and $\delta^{18}O$ depletion at the pumped mix (see Figure 5-6). On April 23, a rapid increase of temperature was observed at both depths. In the meantime, EC values rapidly decreased and plateaued at 500 µS/cm in late April (Figure 5-9a), suggesting that the origin of the water at PZ-2 transitioned from Lake B to Lake A water within a 1-week period. The hydraulic gradient between Lake B and PZ-2 is coherent with this interpretation (Figure 5-9b). Then, a rapid decrease of the temperature at 11 m and 20 m was observed (starting on April 25, 2019) and temperatures < 5°C were reached within a 2-day to 3-day period. As EC remained approximately 500 µS/cm, this is evidencing the existence of short travel times between Lake A and PZ-2, which are of major concern for the evolution of water quality at bank filtration sites (Sandhu et al., 2018).

A repetition of this pattern (i.e., temperature increase-decrease) was observed immediately following the dyke failure (Figure 5-9b). This possibly led to the remobilization and “back-flow” of the warmer groundwater, as an inversion of the hydraulic gradient was observed (Figure 5-9b). Again, constant EC values (at 500 µS/cm) suggest that this remobilized warm water originated from Lake A. As mentioned in the section 5.4.3.1, a change in the pumping scheme also occurred shortly after the dyke failure, and the activation of pumping well P8 (next to P1) could also have influenced the groundwater patterns in the vicinity of PZ-2.

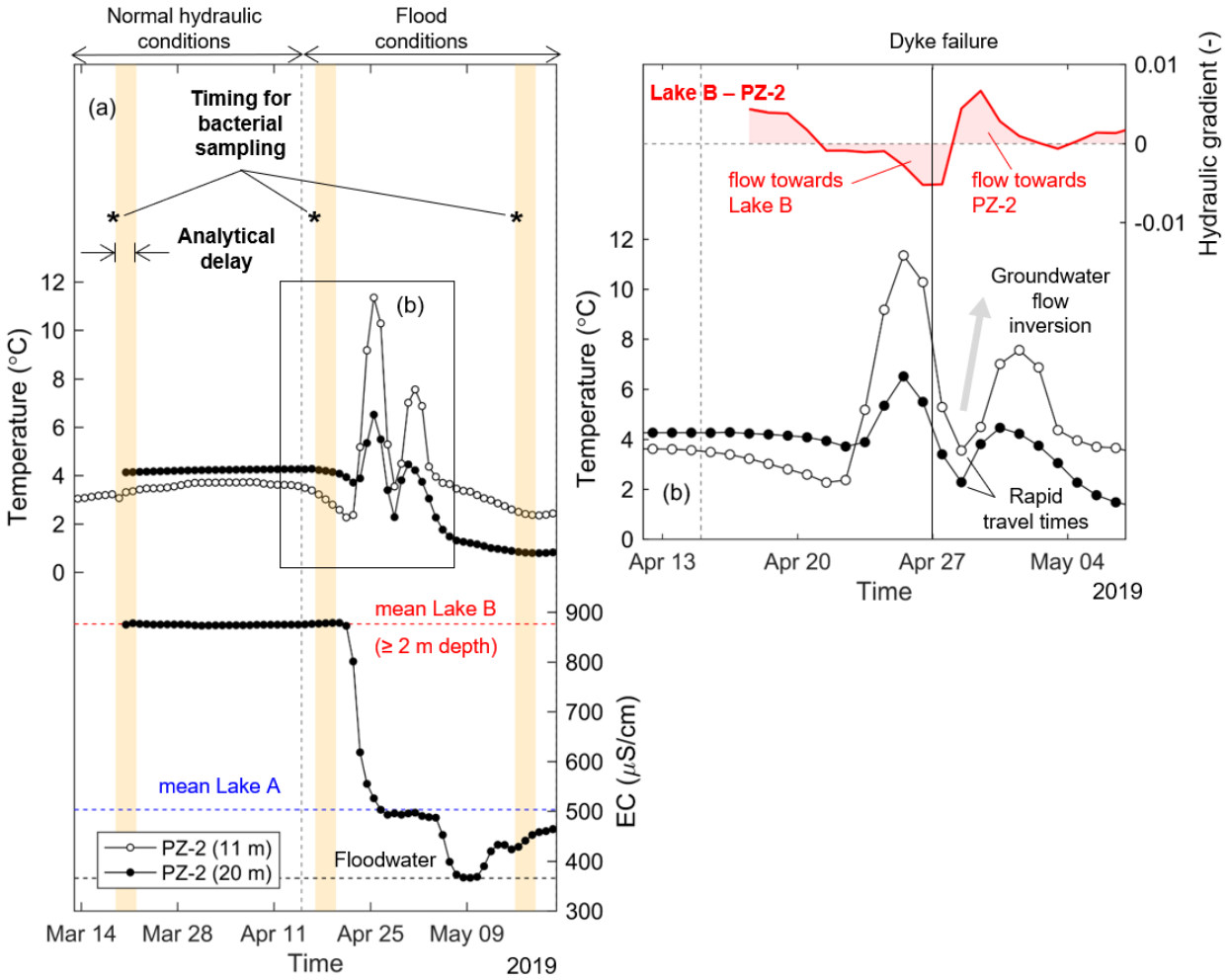

Figure 5-9 (a) Daily evolution of the temperature and electrical conductivity (EC) at observation well PZ-2. The temperature measurements were performed at 11 m and 20 m depth (below ground level), while the EC measurements were only carried at 20 m depth. The frequency of bacterial analyses sampling at the pumped mix and the pumping wells is marked with black asterisks and the corresponding maximum analytical delays (i.e., 8 days) are identified with the yellow shaded areas. (b) Zoom on the period between mid-April and early May 2019, which is denoting the important transience of the temperature at 11 m and 20 m depth. Additionally, the hydraulic gradient between Lake B and PZ-2 (in red) is illustrated.

The observed dynamics of the temperature at PZ-2, PZ-5 and PZ-6 indicate that the flood event led to a reorganization of the groundwater flow patterns between Lake A and Lake B. Indeed, the flood event could have forced the vertical infiltration of cold water and/or a horizontal mobilization of

cold water from Lake A due to increased hydraulic gradients across the sandy bank. It is, however, not possible to differentiate between the two processes and thermo-hydrodynamic modeling would be needed to conclude on the origin of the cold water. Yet, it was demonstrated that a descriptive interpretation of temperature, combined with the evolution of water levels and EC, can depict the timescales and timing of the impact of flood events on the groundwater flow pattern.

5.4.5 Water Quality Management Implications

5.4.5.1 Optimizing Monitoring Strategies with Low-cost Precursors of Water Quality Changes

When comparing the timescales of groundwater flow dynamics to the frequency of bacterial analyses sampling (see black asterisks in Figure 5-9a), it becomes clear that contamination events may occur between the monthly regulatory monitoring. The current strategy is therefore not adequate for the surveillance of microbiological water quality at this BF system under flood conditions. Moreover, the analytical delay for standard cultured-based analysis is typically 24 h to 48 h, to which is to be added the transport of the samples to the laboratory. In total, it can take up to three days from sample collection to delivery of the analytical result (see gray shaded areas in Figure 5-9a). Under flood conditions, the origin and travel times of the water at BF sites are subject to evolve at a much shorter timescale (i.e., within a 1-day period), as evidenced by the evolution of temperature and EC in Figure 5-9a. In summary, discrete sampling for microbiological assays at the pumping wells and/or the pumped mix is only representative of a “snapshot” in time and most probably in space, and water quality management decisions based on a monitoring at a monthly time-step may not represent the full picture and may lead to misinformation.

High frequency monitoring of microbiological water quality is not yet common practice. Near real-time monitoring technologies for the detection of microbial indicators via fluorescence-based methods, such as flow cytometry (Clausen et al., 2018) or enzymatic activity (Burnet et al., 2019), are in development and might in the future provide additional information at a proper timescale. Adomat et al. (2020) assessed the biomass dynamics at high resolution at three BF sites via flow cytometry and enzymatic detection methods. While such monitoring was shown to enhance the understanding of microbiological dynamics of the treated water at BF sites, they reported some

divergence between the results due to methodological limitations. Some practical disadvantages (e.g., cost, maintenance, no species differentiation) are also presently limiting the widespread implementation of high frequency monitoring technologies of biomass (Zamyadi et al., 2016).

Despite the worldwide application of managed aquifer recharge techniques, which include BF systems, management guidelines are limited to few examples, and field-scale studies are still needed to improve design, operation and maintenance of existing and future sites (Dillon et al., 2019). Indeed, the operation and management of most BF systems are based on practical knowledge derived from past applications (Ahmed & Marhaba, 2017). Hydrogeochemical conceptual models are developed according to site-specific hydrogeological (e.g., water levels, porosity, hydraulic conductivity) and geochemical data (e.g., quality of surface water and groundwater, redox conditions) in order to characterize the general performance of a BF system and to determine the operational pumping rates. Depending on the spatio-temporal resolution of the assessments, the representativity of hydrogeochemical models may be limited and only informative of the baseline trends. Sprenger et al. (2011) highlighted that prediction tools to assess the risk of contamination under extreme hydraulic conditions (i.e., floods and droughts) are particularly needed. Measurement of robust and low-cost parameters, such as EC and temperature, are part of the routine monitoring strategy at a number of existing BF systems and it is worth using these parameters as management tools. Monitoring of turbidity is also common at many BF sites. For instance, Ascott et al. (2016) studied the evolution of the turbidity over a 6-month period, which spanned over an extreme flood event, at a river-BF site along the Thames (England). While the turbidity of the river fluctuated between roughly 5 NTU and 50 NTU, the turbidity of the pumped water remained < 0.5 NTU for all the study period, except during the flooding of the ground surface. During this period, the turbidity of the pumped water reached up to 1.5 NTU. Ascott et al. (2016) suggested that the increase of the turbidity indicated a rapid vertical infiltration of floodwater, while the reduction in turbidity (river vs. bank filtrate) testified that the attenuation processes were still occurring and help at maintaining the quality of the bank filtrate. Hence, turbidity monitoring is valuable as it can serve as a dual indicator for (1) the development of rapid flow paths and (2) the resilience of the BF system to flood events.

In the previous sections, it was demonstrated that monitoring for environmental tracers at a short time-step fully captures the transience of groundwater flow paths at the BF system, as it allowed

to track the evolution of the origin and residence time of the bank filtrate in near real-time. Hence, monitoring for environmental tracers can help at better understanding the vulnerability to microbiological contamination. For instance, in the studied case, monitoring for EC was shown to be useful to detect changes in mixing ratios (between Lake A and Lake B), while $\delta^{18}O$ helped to decipher the contribution of floodwater to the bank filtrate. By combining high frequency monitoring for EC and $\delta^{18}O$, changes of the origin of the bank filtrate were detected in real-time. Assuming that the quality of the water sources to the pumping wells are different, knowledge of the origin of water is crucial to anticipate water quality changes of the bank filtrate.

Monitoring for temperature was shown to depict the local flow heterogeneity and can be used as an early warning tool for potential evolution of the travel times. Since shorten travel times (and/or shorten travel distances) may lower the performance of BF systems to attenuate pathogens (Sprenger et al., 2011), such information is of paramount importance for the understanding of the vulnerability to microbiological contamination. A comprehensive review of the use of temperature as a tracer is provided in Anderson (2005) and states that its applicability is limited to contexts where there is a marked contrast between surface water and groundwater. Other environmental tracers, such as radon (Gilfedder et al., 2019), would be suited to depict the transience of BF systems in other contexts, where temperature is less adequate.

Considering the above, monitoring for environmental tracers provides guidance for optimizing the timing and the frequency of more expensive and time-consuming monitoring analyses (e.g., pathogens or trace organic contaminants). Besides, monitoring for environmental tracers at the pumping wells and/or the pumped mix can provide crucial insights for the implementation of near real-time evidence-based preventive measures in order to secure the quality of the drinking water while regulatory water quality analyses are awaited.

5.4.5.2 Towards a Control of the Bank Filtrate Quality Through Modulated Pumping Schemes

Based on the data at the pumping wells, it was demonstrated that there is a spatial variability of the groundwater flow pattern under normal hydraulic conditions (section 5.4.3.2). Hence, it was suspected that the recovery at each single well could vary from the one of the pumped mix, due to the variability of the pumping rates. A selection of two to four wells are normally contributing to

the pumped mix on a daily basis and they operate at a daily pumping rate Q ≥ 1000 m^3/day, while the other three wells are rarely active. This selection is typically consistent on the long-term, but changes may occur if a well is out of operation due to a pump failure for instance.

Figure 5-10 shows the evolution of $\delta^{18}O$ at the pumping wells during the recovery period in 2017. It illustrates that the recovery at the wells contributing to the pumped mix (i.e., Q ≥ 1000 m^3/day; in black) is more rapid than for the other wells. The isotopic signature of the more active pumping wells plateaued at approximately -10.25 ‰ in late July, suggesting a complete recovery. Besides, from mid-May to early August 2017, pumping well P3 was out of operation. When it started pumping again in August, $\delta^{18}O$ was relatively depleted and similar to the observed isotopic signature during the flood event, suggesting a significant contribution from flood-marked water, which was likely stored in the bank in the vicinity of P3. These results suggest that high pumping rates (Q ≥ 1000 m^3/day) accelerated the recovery in comparison to lower pumping rates. Also, bank storage of flood-marked water was possible in the vicinity of the less active pumping wells. This water could have been pumped by the wells more than three months after the flooding.

These results establish new perspectives to control the origin of the bank filtrate and anticipate water quality changes through modulated pumping schemes. Monitoring and surveillance strategies will naturally depend on site-specific water quality issues. Hereafter are presented two examples of management strategies considering that wastewater-derived contamination were transported by floodwater. Firstly, one could attempt to increase the travel time in order to limit the development of rapid flow paths. This strategy would help maintain the efficiency of the BF system in attenuating the contaminants by simply distributing the total pumping rate over all the available pumping wells prior and during the flood events. Secondly, given that some wastewater derived contaminants are persistent in the water cycle (Reemtsma et al., 2016), bank storage of surface water could pose a threat for the quality of the bank filtrate during few months. In fact, if the surface water were hypothetically polluted with persistent contaminants (during a flood event or not), persistent contaminants could potentially be found in the bank filtrate event after the remediation of the surface water quality. Hence, when reactivating a pumping well, it would be possible to rapidly purge the stored water by pumping at high rates. Note that the purged water is not to be distributed in the drinking water supply system, but rather flushed to an adjacent urban runoff collector. Overall, the monitoring of environmental tracers at the pumping wells and pumped

mix would help at defining such pumping strategies and appreciate the impacts of a pumping scheme modification in real-time.

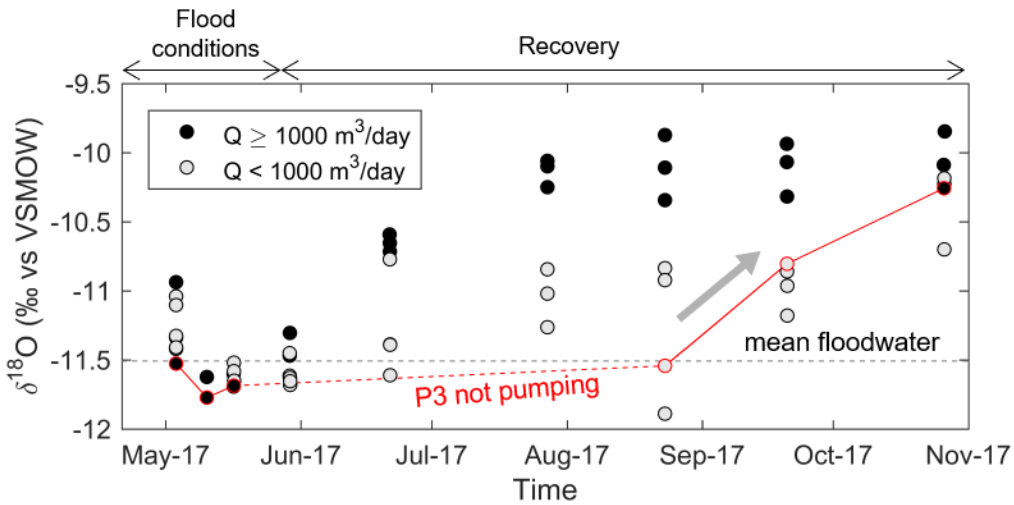

Figure 5-10 Evolution of $\delta^{18}O$ at the pumping wells during the recovery period in 2017. The black circles mark the wells that are contributing to the pumping mix and, therefore operating at a daily pumping rate $Q \geq 1000$ m^3/day, while the gray circles correspond to the wells that operate at $Q < 1000$ m^3/day. From mid-May to early August, pumping well P3 (in red) was not pumping (out of operation).

5.5 Conclusions

In this study, we illustrated how monitoring strategies of environmental tracers at a flood-impacted BF site can be optimized to better understand the timescales of changes in the groundwater flow patterns and anticipate the water quality evolution. This knowledge provides key information to improve existing operational strategies through modulated pumping sequences.

Based on bacteriological indicators (total coliforms), the BF system was shown to be resilient to the yearly recurring flood events but more vulnerable to contamination during the intense flood events (such as 2017 and 2019). The evolution of EC and $\delta^{18}O$ at the pumped mix and at the pumping wells revealed that the hydraulic connection with a large watershed has a decisive impact on the groundwater flow patterns at the BF system. Under flood conditions, the origin of the bank filtrate gradually evolved from a mixture between Lake A and Lake B waters towards a contribution from Lake A and Lake DM (i.e., floodwater) only. Additionally, monitoring for

environmental tracers allowed to track the impact of a dyke failure on the origin of the bank filtrate, and revealed the rapid reactivity of the BF system.

Automated measurements of temperature and EC at observation wells allowed to detect changes in the groundwater flow patterns at a daily timescale, while the regulatory monthly monitoring for microbiological water quality did not fully capture the potential short timescale variability of the water quality. Hence, real-time monitoring of environmental tracers at observation wells can be seen as early warning tools to anticipate potential changes in the water quality of the bank filtrate.

The recovery of the BF was accelerated for the wells operating at high rates (i.e., $\geq 1000\ m^3$/day) in comparison to the other wells, partly because of floodwater storage in the vicinity of the less active wells. These results establish new perspectives to control the origin of the bank filtrate and anticipate water quality changes through selected pumping schemes, which depend on and must be adapted to site-specific water quality issues.

In summary, the monitoring of environmental tracers at BF sites should be performed at different observation points in order to anticipate water quality changes and, thus, provide guidance for optimizing the timing and the frequency of more expensive and time-consuming monitoring analyses (e.g., pathogens or trace organic contaminants). Monitoring for environmental tracers can help to optimize and perform real-time surveillance of the pumping schemes strategies. However, field-scale experiments are still needed to test the application of such monitoring and pumping strategies and evaluate their effectiveness in controlling the quality of the pumped water.

CHAPTER 6 ARTICLE 3: QUANTIFYING FLOOD-WATER IMPACTS ON A LAKE WATER BUDGET VIA VOLUME-DEPENDENT TRANSIENT STABLE ISOTOPE MASS BALANCE

This chapter was published as a research paper in the journal *Hydrology and Earth System Sciences* in 2021. Appendices of this manuscript are presented in Appendix C to Appendix H.

Masse-Dufresne, J., Barbecot, F., Baudron, P., & Gibson, J. J. (2021). Quantifying floodwater impacts on a lake water budget via volume-dependent transient stable isotope mass balance. Hydrol. Earth Syst. Sci.(25), 3731–3757. doi:10.5194/hess-25-3731-2021

ABSTRACT

Isotope mass balance models have undergone significant developments in the last decade, demonstrating their utility for assessing the spatial and temporal variability of hydrological processes, and revealing significant value for baseline assessment in remote and/or flood-affected settings where direct measurement of surface water fluxes to lakes (i.e., stream gauging) are difficult to perform. In this study, we demonstrate that isotopic mass balance modelling can be used to provide evidence of the relative importance of direct floodwater inputs and temporary subsurface storage of floodwater at ungauged lake systems. A volume-dependent transient isotopic mass balance model was developed for an artificial lake (named Lake A) in southern Quebec (Canada). This lake typically receives substantial floodwater inputs during the spring freshet period, as an ephemeral hydraulic connection with a 150,000-km^2 large watershed is established. First-order water flux estimates to Lake A allow for impacts of floodwater inputs to be highlighted within the annual water budget. The isotopic mass balance model has revealed that groundwater and surface water inputs account for 60-71% and 39-28% of the total annual water inputs to Lake A respectively, which demonstrates an inherent dependence of the lake on groundwater. However, when considering the potential temporary subsurface storage of floodwater, the partitioning between groundwater and surface water inputs tends to equalize, and Lake A water budget is found to be more resilient to groundwater quantity and quality changes. Our findings suggest not only that floodwater fluxes to Lake A have an impact on its dynamics during springtime, but significantly influence its long-term water balance and help to inform, understand and predict future water quality variations. From a global perspective, this knowledge is useful for establishing

regional-scale management strategies for maintaining water quality at flood-affected lakes, for predicting the response of artificial recharge systems in such settings, and to mitigate impacts due to land-use and climate changes.

6.1 Introduction

Lakes are complex ecosystems which play a valuable economic, social and environmental role within watersheds (Kløve et al., 2011). In fact, lacustrine ecosystems can provide a number of ecosystem services, such as biodiversity, water supply, recreation and tourism, fisheries and sequestration of nutrients (Schallenberg et al., 2013). The actual benefits that can be provided by lakes depend on the water quality, and poor resilience to water quality changes can lead to benefit losses (Mueller et al., 2016). Globally, the quantity and quality of groundwater and surface water resources are known to be affected by land-use (Baudron et al., 2013; Cunha et al., 2016; Lerner & Harris, 2009; Scanlon et al., 2005) and climate changes (Delpla et al., 2009). As both surface water and groundwater contribute to lake water balances (Rosenberry et al., 2015), changes that affect the surface water/groundwater apportionment can potentially modify or threaten lake water quality (Jeppesen et al., 2014). Understanding hydrological processes in lakes can help to depict the vulnerability and/or resilience of a lake to pollution (Rosen, 2015) as well as to invasive species (Walsh et al., 2016) and thus secure water quantity and quality over time for drinking water production purposes (Herczeg et al., 2003). In Quebec (Canada), there are an important number of municipal wells that receive contributions from surface water resources (i.e., lakes or rivers) and are thus performing unintentional (Patenaude et al., 2020) or intentional (Masse-Dufresne et al., 2021b; Masse-Dufresne et al., 2019b) bank filtration.

Over the past few decades, significant developments have been made in the application of isotope mass balance models for assessing the spatial and temporal variability of hydrological processes in lakes; most notably, the quantification of groundwater and evaporative fluxes (Arnoux et al., 2017b; Bocanegra et al., 2013; Gibson et al., 2016; Herczeg et al., 2003). In remote environments, such as in northern Canada, application of isotopic methods is particularly convenient, as direct measurements of surface water and groundwater fluxes is time-consuming, expensive, and difficult (Welch et al., 2018). Isotopic mass balance models can notably be applied to ungauged lake systems to efficiently characterize the impacts of floods on water apportionment (Haig et al., 2020).

While isotopic frameworks were successfully used to assess the relative importance of floodwater inputs to lakes (Brock et al., 2007; Turner et al., 2010), no attempt was made at evaluating the timing of the floodwater inputs and to differentiating between the role of i) direct floodwater inputs and ii) temporary subsurface storage of floodwater on a lake's annual water budget. In this study, direct inputs refer to the floodwater that enters a lake via the surface (e.g., by inundating and/or flowing through a stream), while temporary subsurface storage of floodwater encompasses the floodwater-like inputs that reach the lake via subsurface (e.g., through floodplain recharge or bank storage).

To gain information on the timing of hydrological processes, one may use a transient and short time step isotopic mass balance. A previous study by Zimmermann (1979) used a transient isotope balance to estimate groundwater inflow and outflow, evaporation, and residence times for two young artificial groundwater lakes near Heidelberg, Germany, although these lakes had no surface water connections, and volumetric changes were considered negligible. Zimmermann (1979) showed that the lakes were actively exchanging with groundwater, which controlled the long-term rate of isotopic enrichment to isotopic steady state, but the lakes also responded to seasonal cycling in the magnitude of water balance processes. While informative, Zimmermann (1979) did not attempt to build a predictive isotope mass balance model, but rather used a best-fit approach to obtain a solitary long-term estimate of water balance partitioning for each lake. Petermann et al. (2018) also constrained groundwater connectivity for an artificial lake near Leipzig, Germany, with no surface inlet or outlet. By comparing groundwater inflow rates obtained via stable isotope and radon mass balances on a monthly time-step, Petermann et al. (2018) highlighted the need to consider seasonal variability when conducting lake water budget studies. Our approach builds on that of Zimmermann (1979) and Petermann et al. (2018), developing a predictive model of both atmospheric and water balance controls on isotopic enrichment, and accounting for volumetric changes on a daily time step.

The main objective of this study is to provide evidence of the relative importance of direct floodwater inputs and temporary subsurface storage of floodwater at ungauged lake systems using an isotopic mass balance model. To do so, we first aim to establish an isotopic framework based on the local water cycle, to verify the applicability of isotopic mass balance in the present setting, as contrasting isotopic signatures are required between various water reservoirs and fluxes,

including floodwater inputs. Secondly, we quantify the water budget according to two reference scenarios (A and B) to grasp the impact of site-specific uncertainties on the computed results. Then, we analyze the temporal variability of the groundwater inputs and the sensitivity of the lake to floodwater driven pollution. Finally, we demonstrate the implications of floodwater-like subsurface inputs on the water balance partition.

The water balance is computed via a volume-dependent transient isotopic mass balance model, which is applied to predict the daily isotopic response of an artificial lake in Canada that is ephemerally connected to a 150,000 km^2 watershed during spring freshet. During these flood events, the surficial water fluxes entering the study lake are not constrained in a gaugeable river or canal but occur over a 1-km wide surficial flood area. Our study period spans a flood with an average recurrence interval of 100 years, and is therefore an example of the response of the system to a major hydrological event.

6.2 Study site

6.2.1 Geological and hydrological setting

The study site is located in the area of Greater Montreal and is bordering the Lake Deux-Montagnes (further referred to as Lake DM), which corresponds to a widening of the Ottawa River at the confluence with the St-Lawrence River in Quebec (Canada) (Figure 6-1). The Ottawa River is the second largest river in eastern Canada, draining a watershed of approximately 150,000 km^2 (MDDELCC, 2015). The water level of Lake DM is partly controlled by flow regulation structures (e.g., hydroelectric dams) upstream on the Ottawa River. Lake DM water levels also show seasonal fluctuations in response to precipitation and snowpack melting over the Ottawa River watershed. High water levels at Lake DM are typically observed during springtime (April-May) and, less prominently, during autumn (November-December), while lowest water levels normally occur at the end of the summer (September) (Centre d'Expertise Hydrique du Québec, 2020).

Lake A (2.79×10^5 m^2) and Lake B (7.6×10^4 m^2) are two small artificial lakes created from sand-dredging activities and are located at approximately 1 km from the shore of Lake DM. The dredging is still on-going at Lake A, while it ceased a few decades ago at Lake B. Both lakes are approximately 20 m deep (Masse-Dufresne et al., 2019b) and were excavated within alluvial sands

which were deposited in a paleo valley extending in the NE-SW direction and carved into the Champlain Sea Clays (Ageos, 2010). Lithostratigraphic data (i.e., well logs) suggest that the paleo valley is approximately 600 m wide and has a maximum depth of 25 m. Between Lake DM and Lake A, a thin layer (few centimeters to roughly 2 meters) of alluvial sands are deposited on top the clayey sediments (Figure C1; Appendix C) (Ageos, 2010).

Lake A is connected to a small stream (S1) with a mean and maximum annual discharge of 0.32 $m^3 s^{-1}$ and 1.19 $m^3 s^{-1}$, respectively (Ageos, 2010). Maximum discharge typically occurs during the month of April as S1 drains snowmelt water from a small watershed (14.4 km^2) (Centre d'Expertise Hydrique du Québec, 2019), whereas low flow is recorded for the rest of the hydrological year. For the springtime 2017, the surface water flows from S1 are deemed negligible compared to the floodwater inputs and are thus not considered in this study.

Two channelized outlet streams (S2 and S3) allow water to exit Lake A and flow towards Lake DM. The direction of the surface water fluxes at S2 can be reversed if water level at Lake DM exceeds both a topographic threshold at 22.12 m.a.s.l. (determined from a topographic land survey along S2) and the water level at Lake A (Ageos, 2010). Flow reversal also occurs in S3, but the elevation of the topographic threshold is unknown.

Lake A and Lake B both contribute to the supply of a bank filtration system which is composed of eight wells and is designed to supply drinking water for up to 18000 people (Ageos, 2010). Typically, two to three wells are operated on a daily basis at a total pumping rate ranging from 4000 m^3/d (in wintertime) to 7500 m^3/d (in summertime) (Masse-Dufresne et al., 2019b). Although the operation of the bank filtration system does not form a complete hydraulic barrier between the two artificial lakes, it does lead to a lowering of Lake B water level below that of Lake A (Ageos, 2010).

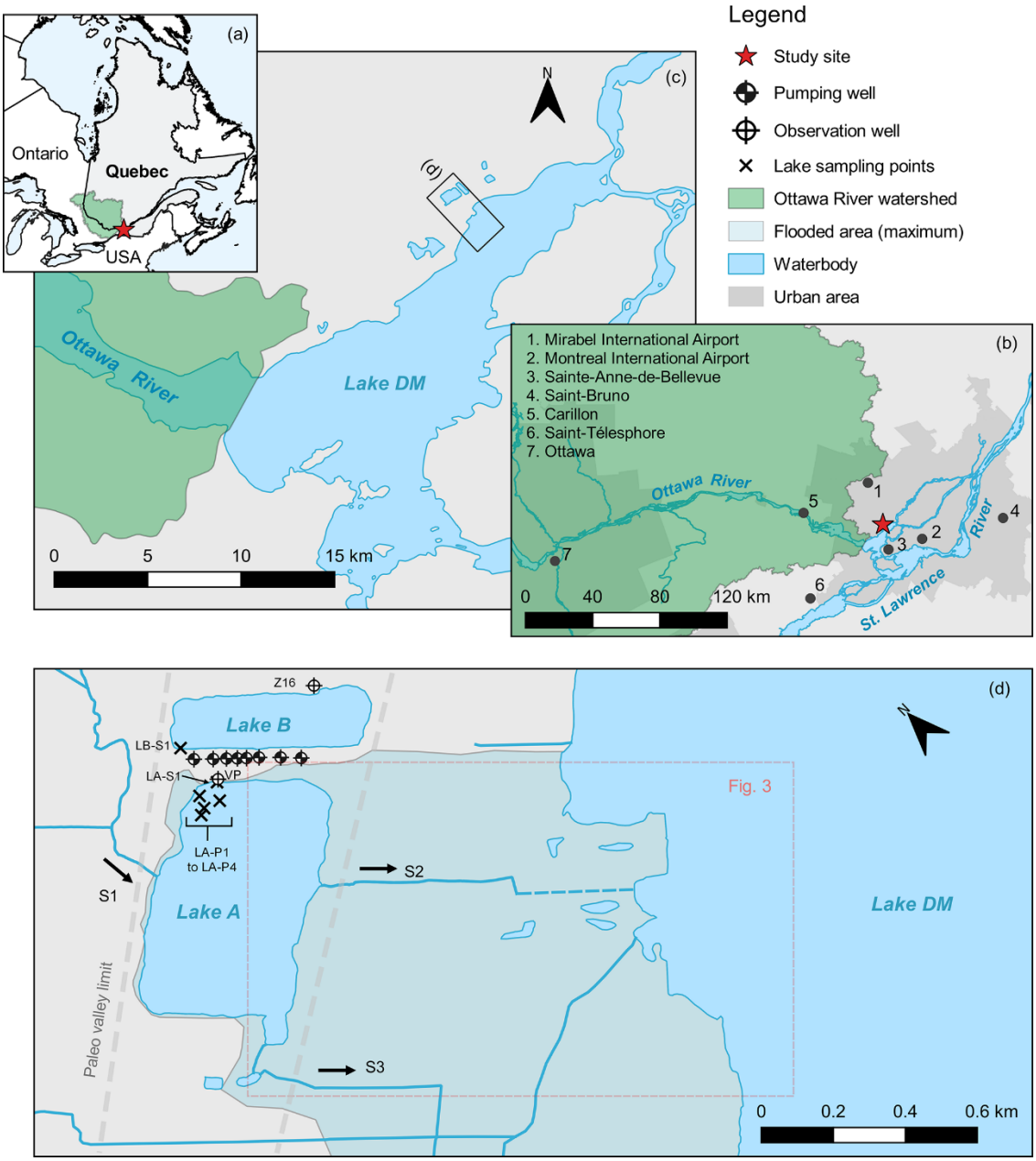

Figure 6-1 (a-c) Location of the study site, relative to the Ottawa River watershed, Lake Deux-Montagnes (DM) and the area of Greater Montreal, (d) location of Lake A and Lake B relative to Lake DM and schematic representation of the hydrogeological context. The grey dashed lines illustrate the approximative extent of the paleo valley. LA-S1 and LB-S1 are surface water sampling points at Lake A and Lake B, respectively. LA-P1 to LA-P4 correspond to vertical profile sampling locations at Lake A. The maps were created from openly available data and used in accordance with the Open Government Licence – Canada or the Open Data Policy, M-13-13 of the United States Census Bureau. Detailed source information is provided in Appendix C.

6.2.2 Hydrodynamics of the major flood event

In 2017, a major flood event occurred in the peri-urban region of Montreal and was caused by the combination of intense precipitations and snowpack melting over the Ottawa River watershed (Teufel et al., 2019). Rapid water level rise at Lake DM occurred in late February, early April and early May at rates of approximately 0.11 m d^{-1}, 0.19 m d^{-1} and 0.16 m d^{-1}, respectively. A historical maximum water level (i.e., 24.77 m.a.s.l.) was reached on May 8, 2017, corresponding to a net water level rise of >2.7 m compared to early February (Figure 6-2). High water levels at Lake DM resulted in the inundation of the area between Lake A and Lake DM (Figure 6-1d), and the surface water fluxes were not constrained in S2 and S3 but occurred over a 1 km wide area.

The water level in Lake A was equivalent to Lake DM during the flood peak (on May 8, 2017) and daily mean water levels at Lake A and Lake DM show good correlation ($R^2 = 0.98$, p-value < 0.01) for the observed period (April 27th, 2017 to May 17th, 2017). Daily mean water levels at observation well VP and Lake DM also follow a similar pattern from late February 2017 to late July 2017 ($R^2 = 0.93$, p-value < 0.01). Considering the above and a visible hydraulic connection between the Lake DM and Lake A, the data indicates that the daily water level variations at observation well VP were controlled by Lake DM from late February to late July 2017. Lake A water level was also presumably controlled by Lake DM until late July 2017, but technical issues prevented confirmation (i.e., logger in Lake A broke on May 17th, 2017).

Then, from August 2017 to late October 2017, the water level in Lake DM was below the topographical threshold, and there is no similarity between the evolution of the water level at Lake DM and observation well VP ($R^2 = 0.11$, p-value > 0.01). It is thus possible to infer that the Lake A water level was not controlled by Lake DM from August 2017 to late October 2017. This is also supported by the manual measurement of Lake A water level in September.

The water level of Lake DM exceeded the topographic threshold again from November 2017 to January 2018, but the daily mean water levels at Lake DM and observation well VP show a moderate correlation ($R^2 = 0.63$, p-value < 0.01). The manual measurements also indicate discrepancy between Lake DM and Lake A water levels in December 2017 and January 2018. The weaker correlation between the water level measurements suggest that Lake DM was not controlling the dynamics of Lake A water level. It is thus likely that Lake A received little to no

surface water inputs from Lake DM from November 2017 to January 2018. In this context, surface water inflows from Lake DM during autumn and winter are considered negligible in this study and not included in the developed stable isotope mass balance model (Sect. 6.4.2).

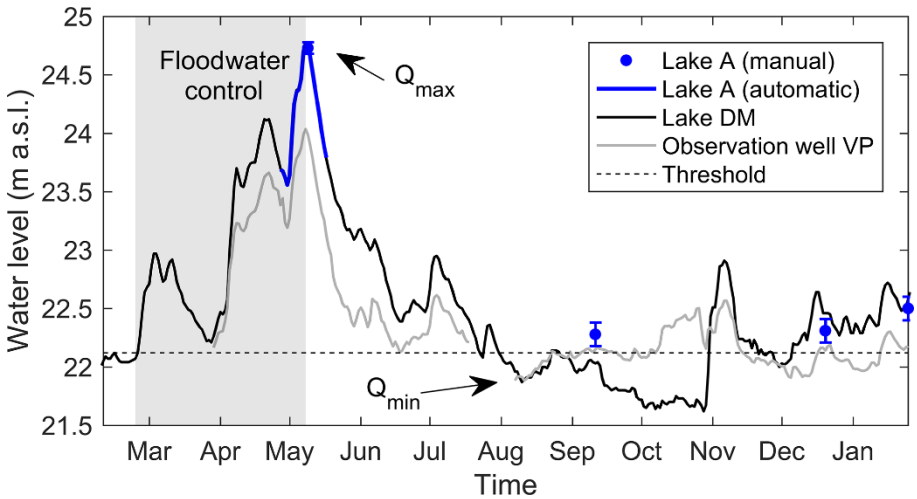

Figure 6-2 Daily mean water levels at Lake A, Lake DM and observation well VP from February 9th, 2017 to January 25th, 2018. The grey shaded area corresponds to the floodwater control period. Q_{max} and Q_{min} indicate the timing of the adjusted maximum and minimum output from the lake.

6.2.3 Conceptual model of Lake A water balance

Based on the geological and hydrological setting of the study site (Sect. 6.2.1) and flood-specific considerations (Sect. 6.2.2), we established a conceptual model of Lake A water balance, as described below.

Considering that Lake A is sitting in alluvial sands (i.e., a highly permeable material), it is assumed that groundwater inputs (I_G) and outputs (Q_G) contribute to the water budget. Although it is difficult to interpret the location of I_G, it appears evident that Q_G occur along the NE bank of Lake A. In fact, there are subsurface fluxes across the sandy bank that contribute to the bank filtration system or discharge into Lake B, as its water level is lower since the initiation of the bank filtration system (Masse-Dufresne et al., 2019b). Given the regional groundwater flow in the NE to SW, Q_G can also presumably occur along the SW bank of Lake A. Besides, it is likely that little to no subsurface fluxes exist in the area between Lake A and Lake DM, where clayey sediments are found.

For the study period, it is conceptualized that the direction of the surface water fluxes in S2 and S3 is from Lake A to Lake DM, except from February 27th, 2017, 2017 to May 8th, 2017. During this period (hereafter referred to as the floodwater control period), the water level of Lake DM exceeds the topographic threshold, and Lake A receives surface water inflow (I_S) from Lake DM. Also, it is likely that high water level in Lake A imposed a hydraulic gradient at the lake-aquifer interface, which allowed for Q_G from the lake and inhibited I_G. Then, as Lake A and Lake DM water levels started to decrease (from May 8th, 2017), it is assumed that water exits Lake A as surface water outputs (Q_S) towards Lake DM or as Q_G. Although Lake DM water level again exceeded the topographic threshold from November 2017 to January 2018, the weaker correlation between the water levels suggests that Lake A water level was not controlled by Lake DM. In this context, we conceptualized that Lake A water level variations are mainly controlled by groundwater flows (I_G and Q_G). Surface water inputs (I_S) are set to zero during this period (see Sect. 6.2.2).

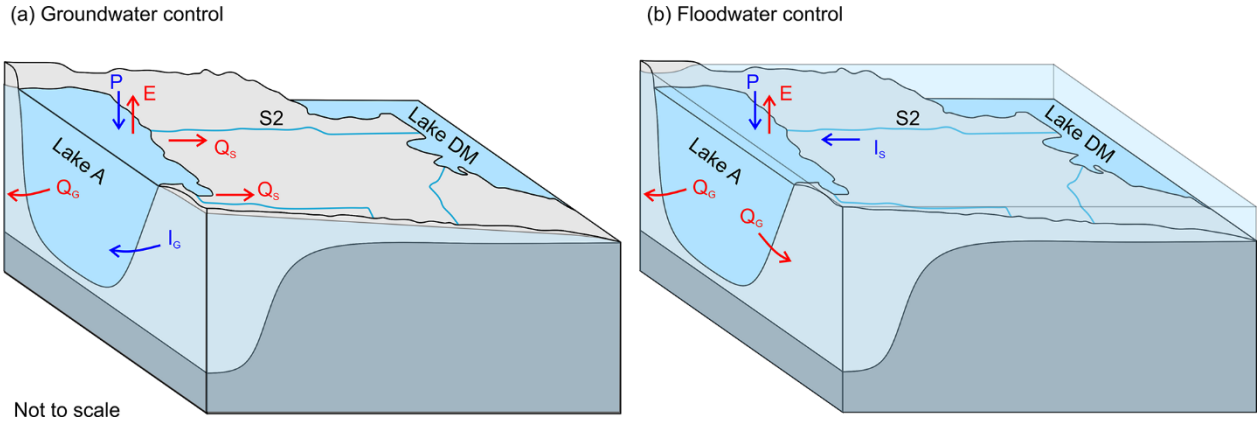

Figure 6-3 Schematic representation of the hydrological processes at Lake A during (a) groundwater control, and (b) floodwater control periods. Inputs include precipitation (P), surface water (I_S) and groundwater (I_G) while outputs include evaporation (E), surface water outflow (Q_S) and groundwater outflow (Q_G). The area between Lake DM and Lake A is flooded in (b) and I_S from Lake DM contribute to the water balance of Lake A.

To summarize, for the year 2017, Lake A water budget can be conceptualized with two distinct hydrological periods: (a) the groundwater control period and (b) the floodwater control period (Figure 6-3). While the groundwater control period concerns most of the hydrological year, the floodwater control period only applies from February 23rd, 2017 to May 8th, 2017. During the groundwater control period (Figure 6-3a), it is assumed that groundwater inflows (I_G) and

precipitations (P) constitute the total water inputs to Lake A, while surface water inflows (I_S) are negligible. During this period, the outputs are occurring through evaporative fluxes (E), surface water outflows (Q_S) and groundwater outflows (Q_G). In contrast, it is assumed that I_S and P represent the total water inputs to Lake A during the floodwater control period (Figure 6-3b). High-water levels at Lake A impose a hydraulic gradient at the lake-aquifer interface which allows for Q_G and inhibits I_G.

6.3 Methods

6.3.1 Field measurements

Pressure-temperature loggers (Divers®; TD-Diver and CTD-Diver, Van Essen Instruments, Delft, Netherland) were used to measure surface water levels at Lake A and groundwater levels at observation well VP on a 15-minute time step. Water levels were recorded from April 27th, 2017 (after the ice-cover melted) to May 17th, 2017 at Lake A and from March 29th, 2017 to January 25th, 2018 (except between July 19th, 2017 and August 6th, 2017) at observation well VP. All the level loggers' clocks were synchronized with the computer's clock when launching automatic measurements. This procedure was done via the Diver-Office 2018.2 software. Manual measurements of the water level were regularly performed to calibrate (relatively to a reference datum) and validate the automatic water level measurements. A level logger was also used to measure on-site atmospheric pressure and perform barometric compensation on water level measurements. Also, note that water levels in Lake A were not continuously recorded after May 17th, 2017 due to a logger failure, but manual water level measurements (in September 2017, December 2017 and January 2018) depict the general evolution of Lake A water level.

Mean daily water levels at Lake DM were retrieved with permission from the Centre d'Expertise Hydrique du Quebec database (Centre d'Expertise Hydrique du Québec, 2020). Meteorological data was measured at land-based meteorological stations near the study site and obtained from the Environment and Climate Change Canada database (available online at weatherstats.ca). Daily air temperature, relative humidity, wind speed, dew point and atmospheric pressure were measured at Mirabel International Airport station (45.68 °N, -74.04 °E; 18 km from the study site). Daily precipitation and solar radiation were measured at Sainte-Anne-de-Bellevue station

(45.43 °N, -73.93 °E; 10 km from the study site) and Montreal International Airport station (45.47 °N, -73.75 °E; 17 km from the study site), respectively.

6.3.2 Water sampling and analytical techniques

Physico-chemical parameter measurements and water sampling were performed at Lake A at approximately 0.3 m below the surface and 1 m from the lake shoreline (at LA-S1) on a weekly to monthly basis from February 9th, 2017 to January 25th, 2018. Physico-chemical parameters (including temperature, electrical conductivity, pH and redox potential) were measured using a multiparameter probe (YSI Pro Plus 6051030 and Pro Series pH/ORP/ISE and Conductivity Field Cable 6051030-1, YSI Incorporated, Yellow Springs, OH, USA). Additionally, vertical profile measurements and depth-resolved water sampling were conducted on February 9th, 2017, August 17th, 2017 and January 25th, 2018 (at LA-P1 to LA-P4). Lake A water sampling was performed in the northern part of the lake for logistical reasons and due to ease of accessibility. As horizontal homogeneity has been previously demonstrated by Pazouki et al. (2016), the water samples were deemed representative of the whole waterbody.

Flood water was sampled at two locations (near S2 and S3) on April 19th, 2017 and at Lake DM on May 10th, 2017. Water samples were also collected at the surface and at depth within Lake B and at observation well Z16, which is upstream of Lake B and, thus, representative of the regional groundwater contributing to the latter (Ageos, 2016).

Water samples were analyzed for major ions, alkalinity and stable isotopic compositions of water ($\delta^{18}O$ and $\delta^{2}H$). Water was filtered in the field using 0.45 µm hydrophilic polyvinylidene fluoride (PVDF) membranes (Millex-HV, Millipore, Burlington, MA, USA) prior to sampling for major ions and alkalinity. From December to March, cold weather prevented field filtration, so this procedure was performed in the laboratory on the same day. All samples were collected in 50-ml polypropylene containers and cooled during transport to the laboratory. The samples were then kept refrigerated at 4 °C until analysis, except for stable isotopes, which were stored at room temperature. Major ions were analyzed within 48 h via ionic chromatography (ICS 5000 AS-DP Dionex Thermo Fisher Scientific, Saint-Laurent, QC, Canada) at Polytechnique Montreal (Montreal, Quebec). The limit of detection was ≤0.2 mg/L for all major ions. Bicarbonate concentrations were derived from alkalinity, which was measured manually in the laboratory

according to the Gran method (Gran, 1952) at Polytechnique Montreal (Montreal, Quebec). On samples with measured alkalinity (n = 12), the ionic balance errors were all below 8%. The mean and median ionic balance errors were 1%. Stable isotopes of oxygen and hydrogen were measured with a Water Isotope Analyser with off-axis integrated cavity output spectroscopy (LGR-T-LWIA-45-EP, Los Gatos Research, San Jose, CA, USA) at Geotop-UQAM (Montreal, Quebec). 1 ml of water was pipetted in a 2 ml vial and closed with a septum cap. Each sample was injected (1 microliter) and measured 10 times. The first two injections of each sample were rejected to limit memory effects. Three internal reference waters ($\delta^{18}O$ = 0.23±0.06‰, -13.74±0.07‰ & -20.35±0.10‰; $\delta^{2}H$ = 1.28±0.27‰, -98.89±1.12‰ & -155.66±0.69) were used to normalize the results on the VSMOW-SLAP scale. A 4th reference water ($\delta^{18}O$ = -4.31±0.08‰; $\delta^{2}H$ = -25.19±0.83) was analyzed as an unknown to assess the exactness of the normalization. The overall analytical uncertainty (1 σ) is better than ±0.1‰ for $\delta^{18}O$ and ±1.0 ‰ for $\delta^{2}H$. This uncertainty is based on the long-term measurement of the 4th reference water and does not include the homogeneity nor the representativity of the sample.

6.3.3 Stable isotope mass balance

Stable isotope mass balances for lakes can either be performed based on (i) a well-mixed single layer model or (ii) a depth resolved multi-layered model. Arnoux et al. (2017c) performed a comparison of both methods and reported that well-mixed and depth resolved multi-layered models yielded similar results and showed that groundwater inputs and outputs play an important role on lake water budgets. Arnoux et al. (2017c) further highlighted that the multi-layer model additionally allowed for the determination of groundwater flow with depth, but required a temporally- and depth-resolved sampling in order to ensure a thorough understanding of the stability/mixing of the different layers. Such time-consuming sampling and monitoring efforts are however often unrealistic in remote and/or flood-affected contexts. Additionally, Gibson et al. (2017) showed that the timing of the lake water sampling may introduce greater bias in a well-mixed isotopic mass balance model than the uncertainty related to the lake stratification. For these reasons, we opted to develop a well-mixed model in the context of this study. Note that, despite the biases underlying well-mixed models, this approach remains adequate to characterize the

relative importance of hydrological processes and is particularly useful to give first-order estimates of water fluxes in ungauged basins.

The water and stable isotope mass balance of a well-mixed lake can be described, respectively as Eq. (1) and Eq. (2):

$$\frac{dV}{dt} = I - E - Q \quad (1)$$

$$V\frac{d\delta_L}{dt} + \delta_L\frac{dV}{dt} = I\delta_I - E\delta_E - Q\delta_Q \quad (2)$$

where V is the lake volume, t is time, I is the instantaneous inflow, E is evaporation, Q is the instantaneous outflow. I corresponds to the sum of surface water inflow (I_S), groundwater inflow (I_G) and precipitations (P). Similarly, Q is the sum of surface water outflow (Q_S) and groundwater outflow (Q_G). δ_L, δ_I, δ_E and δ_Q are the isotopic compositions of the lake, I, E and Q, respectively. In the context of this study, the balance equations can be simplified based on the conceptual model. During the groundwater control period, $I_S = 0$ and, thus, $I = I_G + P$ and $\delta_I = (\delta_G I_G + \delta_P I_P)/I$. In contrast, $I_G = 0$ during the floodwater control period, $I = I_S + P$ and $\delta_I = (\delta_{Is} I_S + \delta_P I_P)/I$. Note that δ_G and δ_{Is} are the isotopic signatures of groundwater and surface water inputs, respectively.

The application of Eq. (1) and Eq. (2) for both $\delta^{18}O$ and $\delta^{2}H$ is valid during the ice-free period and also assumes constant density of water (Gibson, 2002). In this study, the potential impacts of the ice-cover formation and melting are neglected, as the ice volume is likely to represent only a small fraction (<2%) of the entire water body. Moreover, considering the ice-water isotopic separation factor, i.e., 3.1 ‰ for $\delta^{18}O$ and 19.3 ‰ for $\delta^{2}H$ (O'Neil, 1968) and assuming well-mixed conditions, the lake water isotopic variation would be comprised within the analytical uncertainty. Also, floodwater inputs from Lake DM were expected to be much more important and occurring simultaneously with ice-melt during the freshet period.

Thus, a volume-dependent model is applied, as described in Gibson (2002). The change in the isotopic composition of the lake (δ_L) with f (i.e., the remaining fraction of lake water) can be expressed as Eq. (3):

$$\delta_L(f) = \delta_S - (\delta_S - \delta_0)f^{\left[\frac{-(1+mX)}{1-X-Y}\right]} \quad (3)$$

where X = E/I is the fraction of lake water lost by evaporation, Y=Q/I is the fraction of lake water lost to liquid outflows, m is the temporal enrichment slope (see Appendix B), δ_0 is the isotopic composition of the lake at the beginning of the time-step, and δ_S is the steady-state isotopic composition the lake would attain if f tends to 0 (see Appendix B).

A step-wise approach is used to solve Eq. 3 on a daily time-step. At each time step, recalculation of $f=V/V_0$ is needed, where V is the residual volume at the end of the time step and V_0 the original volume at the beginning of the time step (or V^{t-dt}). Hence, Eq. (3) is based on the water level difference between two days. The water flux parameters (E, I and Q) and isotopic signatures (δ_E, δ_A, δ_I and δ_Q) are thus evaluated on a daily time-step.

The flushing time (t_f) is defined as the ratio of the volume of water in a system to the rate of renewal (Monsen et al., 2002). In this study, t_f by groundwater inputs is considered and is expressed as:

$$t_f = V/I_G \quad (4)$$

6.3.4 Daily volume changes at Lake A and water fluxes

The initial lake volume (4.7×10^6 m^3) was estimated from the observed lake surface area (2.79×10^5 m^2) and the maximal depth (20 m) and assuming bank slopes of 25 degrees. Assuming bank slopes of 20 degrees or 30 degrees, a typical range for saturated sands (Holtz & Kovacs, 1981), would result in an estimated initial lake volume of 4.84×10^6 m^3 (+3%) and 4.32×10^6 m^3 (-8%). Lake A volume variations are estimated from daily water level changes and assuming a constant lake area. As water level measurements are only available for a short period at Lake A, water levels at Lake DM and observation well VP are used as proxies. Water levels at observation well VP were used as a proxy from August 24th, 2017 to October 30th, 2017, while water levels at Lake DM were assumed representative of Lake A for the rest of the study period (i.e., from February 9th, 2017 to August 23rd, 2017 and from October 31st, 2017 to January 25th, 2018). This approximation is deemed acceptable because the simulation of δ_L depends on the remaining fraction of lake water f (not the absolute water level), and daily variations of the water levels at Lake A, Lake DM and observation well VP were shown to be similar (see Sect. 6.2.2).

Evaporative fluxes (E) are calculated using the standardized Penman-48 evaporation equation, as described in Valiantzas (2006):

$$E_{Penman-48} = \frac{\Delta}{\Delta+\gamma} \cdot \frac{R_n}{\lambda} + \frac{\gamma}{\Delta+\gamma} \cdot \frac{6.43 f(u) D}{\lambda} \quad (5)$$

where R_n is the net solar radiation (MJ m^{-2} d^{-1}), Δ is the slope of the saturation vapor pressure curve (kPa °C^{-1}), γ is the psychrometric coefficient (kPa °C^{-1}), λ is the latent heat of vaporization (MJ kg^{-1}), $f(u)$ is the wind function (see Appendix D) and D is the vapor pressure deficit. For comparative purposes, estimation of the daily evaporative fluxes was also conducted with the Linacre-OW equation (Linacre, 1977) and the simplified - Penman-48 equation (Valiantzas, 2006).These methods yielded similar evaporation estimates from April to August but underestimated total evaporation by 24% to 33% compared to the standardized Penman-48 equation. The discrepancy between the models is restricted to late summer and autumn (see Appendix E, Figure E1) and is attributed to the difference between the air and water surface temperature, which was estimated based on the equilibrium method as described by de Bruin (1982) (see Appendix F). Note that E and P are set to zero during the ice-cover period (i.e. from January 1st to March 31st, based on meteorological data and field observations).

For well-mixed conditions, the δ_{Qs} and δ_{Qg} are assumed to be equal to δ_L. Hence, no separation of these two fluxes is attempted and they are merged into one variable, i.e., the outflow (Q). The direction and intensity of the water flux at the lake-aquifer interface can be conceptually described by Darcy's Law which states that Q = KAi, where K is the hydraulic conductivity, A is the cross-sectional area through which the water flows, and i is the hydraulic gradient. Given the significant depth of Lake A (i.e., 20 m) in comparison to the maximum water level change during the flooding event (i.e., 2.7 m), the variations of A and K are expected to have minor impact on Q. Hence, the change in outflows from the lake is expected to be mainly controlled by i changes and, consequently, to be roughly proportional to the change in lake water level. Considering the above, it was assumed that the daily outflow flux from Lake A varied linearly according to the lake water level; the minimum and maximum outflow (Q_{min} and Q_{max}) correspond to the minimum and maximum water level, respectively. The outflow range (i.e., minimum and maximum values) was adjusted to obtain the best fit between the calculated and observed δ_L.

Total daily inflow (sum of daily P, I_S and I_G) into Lake A compensates for the adjusted daily outflow and daily lake volume difference. The precipitations (P) are evaluated from the available meteorological data (see Sect. 6.3.1), while direct measurement of I_S and I_G was not possible in

this hydrogeological context (see Sect. 6.2.1). Consequently, further assumptions are needed to apportion these contributions. Considering the proposed conceptual model of the groundwater-surface water interactions (see Sect. 6.2.2), I_S is set to zero, while I_G is contributing to the lake during the groundwater control period. On the other hand, during the floodwater control period (i.e., from February 23rd, 2017 to May 8th, 2017), it is assumed that the rising water level at Lake A results in a hydraulic gradient forcing the lake water to infiltrate into the aquifer, inhibiting I_G.

6.4 Results

From February 23rd, 2017 to May 8th, 2017, the net water fluxes are mainly positive, and an overall volume increase is observed at Lake A. The maximum volume change of Lake A was 7.6 x 10^5 m^3, which represents 16 % of the lake's initial volume. The maximum net water flux was 1.2 x 10^5 m^3 d^{-1}, corresponding to a water level rise of 0.43 m (on April 5th, 2017 only). From May 9th, 2017 to mid-August 2017, Lake A volume was decreasing, and the daily net water fluxes were mainly negative. In early August 2017, Lake A regained its initial volume. Then, in autumn and winter, the volume of Lake A was oscillating, and the net water fluxes were ranging from -6.4 x 10^4 m^3 d^{-1} to 5.3 x 10^4 m^3 d^{-1}. At the end of the study period (i.e., on January 25th, 2018), a net volume difference of 1.5 x 10^5 m^3 remained at Lake A compared to February 9th, 2017.

However, the evolution of Lake A volume and the net water fluxes are not representative of the surface water/groundwater interactions. Indeed, gross water fluxes are likely to exceed net water fluxes at natural and dredged lakes sitting in permeable sediments (Arnoux et al., 2017a; Jones et al., 2016; Zimmermann, 1979). In the context of this study, we conceptualized two main hydrological periods, during which the lake water can either drain towards Lake DM or exit the lake as groundwater output. To balance out these outputs, the inflows to Lake A must therefore be greater than the net water fluxes.

For that reason, the development of a volume-dependent transient stable isotope mass balance was required to correctly depict the importance of the floodwater inputs on the water mass balance of the lake.

6.4.1 Isotopic and geochemical framework

The isotopic composition of precipitation (δ_P), Lake A and floodwater are depicted in Figure 6-4. The Local Meteoric Water Line (LMWL) was defined using an ordinary least squares regression (Hughes & Crawford, 2012) using isotope data in precipitation from Saint-Bruno station IRRES database (*n* = 27; from December 2015 to June 2017).

For the study period, the isotopic composition of bulk precipitation was available on a biweekly to monthly time-step (*n* = 15) and ranged from -19.19‰ to -6.85‰ for $\delta^{18}O$ and -144‰ to -38‰ for $\delta^{2}H$. Interpolation was used to simulate the δ_P on a daily-time step for the isotope mass balance model computation.

Isotopic compositions of Lake A water samples (*n* = 39) are linearly correlated (see solid blue line) and all plot below the Local Meteoric Water Line (LMWL), which confirms that Lake A is influenced by evaporation. Linear regression of Lake A water samples defines the Local Evaporation Line (LEL), which is $\delta^{2}H = 5.68\ (\pm 0.27) * \delta^{18}O - 12.80\ (\pm 2.83)$ ($R^2 = 0.92$). Some samples from the surface of Lake A plot below the LEL, likely indicating snowmelt water inputs as noted in previous studies of Canadian lakes (Wolfe et al., 2007).

The isotopic composition of the floodwater samples (*n* = 3) is indeed more depleted than Lake A waters (i.e. $\delta^{18}O$ from -11.85 ‰ to -11.18 ‰ and $\delta^{2}H$ from -81 ‰ to -78 ‰) and is most likely to reflect the significant contribution from heavy isotope depleted snowmelt waters. The floodwater samples are also linearly correlated and plot along a line ($\delta^{2}H = 5.33\ \delta^{18}O - 18.82$) which slope is similar to Lake A LEL, suggesting that the sampled floodwater evaporated under the same conditions as Lake A water samples. For simplification purposes, the isotopic composition of the surface water inflow (δ_{Is}) was set to the intersection between the floodwater LEL and the LMWL ($\delta^{18}O$ = -12.00 ‰ and $\delta^{2}H$ = -83 ‰). The long-term (1997-2008) average, minimum and maximum isotopic signature of Ottawa River water at Carillon (~34 km upstream from Lake DM; see Figure 6-1b) for the month of April are -11.19 ‰, -12.01 ‰ and -10.23 ‰ for $\delta^{18}O$ and -81 ‰, -85 ‰ and -77 ‰ for $\delta^{2}H$, respectively (Rosa et al., 2016). The mean and minimum values compare well with the observed isotopic signatures at Lake DM during springtime 2017.

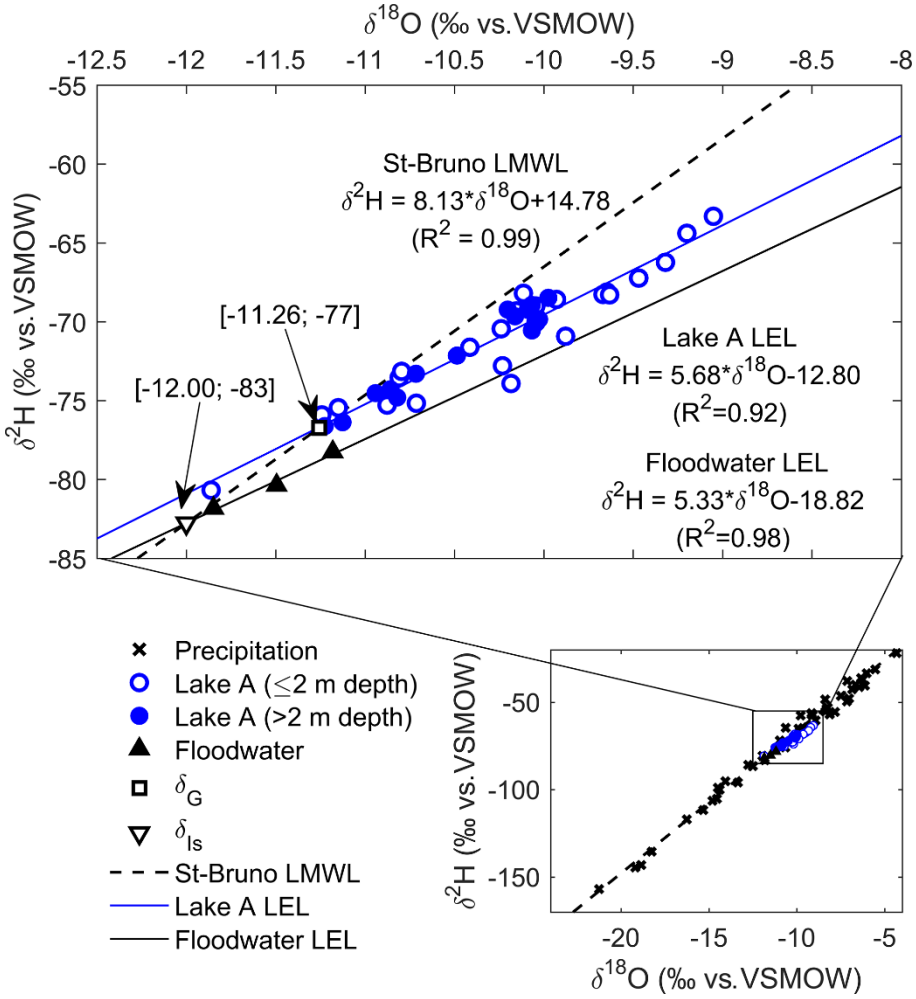

Figure 6-4 Isotopic composition of precipitation, Lake A water, and floodwater from March 2017 to January 2018. Hollow and solid blue circles correspond to samples collected at ≤2 m and >2 m depth, respectively. Analytical precision is 0.15‰ and 1‰ at 1σ for $\delta^{18}O$ and $\delta^{2}H$. Precipitation data are retrieved from the research infrastructure on groundwater recharge database (Barbecot et al., 2019).

The isotopic composition of groundwater (δ_G) can be determined from direct groundwater samples or indirectly from the amount-weighted mean δ_P. However, in highly seasonal climates, there is a widespread cold season bias to groundwater recharge (Jasechko et al., 2017), and estimating δ_G via groundwater samples or amount-weighted mean δ_P may be misleading. In fact, it has been argued that the LMWL-LEL intersection better represents the isotopic composition of the inflowing water to a lake and is thus commonly used to depict the δ_G in isotopic mass balance applications (Edwards et al., 2004; Gibson et al., 1993; Wolfe et al., 2007). Concerning the study site, the estimated δ_G is -11.26 ‰ for $\delta^{18}O$ and -77 ‰ for $\delta^{2}H$ (i.e., the Saint-Bruno LMWL and Lake A LEL intersection).

The latter compares well with the mean isotopic signature of groundwater at Saint-Télesphore station (-11.1‰ for $\delta^{18}O$ and -78.5‰ for $\delta^{2}H$) (Larocque et al., 2015) and is more depleted than the long-term amount-weighted mean δ_P at Ottawa (-10.9‰ for $\delta^{18}O$ and -75‰ for $\delta^{2}H$) (IAEA/WMO, 2018). Note that the locations of Saint-Télesphore station and Ottawa are depicted in Figure 6-1b.

The geochemical facies of Lake A and Lake DM samples are illustrated in Figure 6-5 by the means of a Piper diagram. Mean values for Lake B and regional groundwater (GW) geochemical facies are also plotted for comparison purposes. Both Lake A and floodwater were found to be Ca-HCO_3 types, which is typical for precipitation- and snowmelt-dominated waters (Clark, 2015). The geochemistry of Lake A is relatively constant throughout the year and reveals a depth-wise homogeneity. The geochemistry of Lake B is distinct from Lake A and appears to be influenced by regional groundwater characterized by a Na-Cl water type.

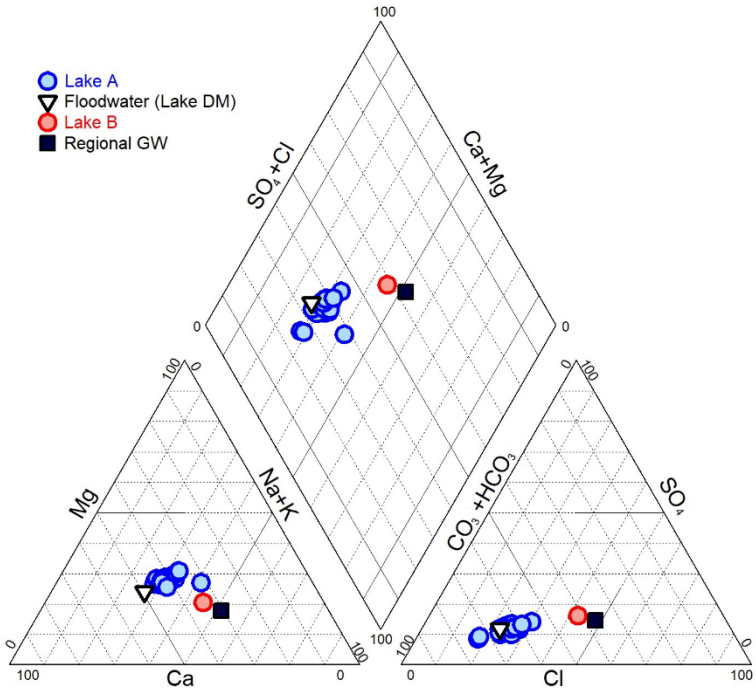

Figure 6-5 Geochemical facies of Lake A (n = 23) and floodwater (n = 1). Mean values for Lake B (n = 42) and regional groundwater (GW) (n = 11) geochemical facies are also plotted. Lake A and floodwater are characterized by Ca-HCO_3 water types, while Lake B and regional GW correspond to Na-Cl water types. Note that regional GW was sampled upstream of Lake B.

6.4.2 Evaluation of the water budget

6.4.2.1 Volume dependent isotopic mass balance model

As described in Sect. 6.3.3, the isotopic mass balance model was solved iteratively by recalculating δ_L on a daily time-step. This model was developed assuming (1) well-mixed conditions and (2) that the outflow flux changes are roughly proportional to the lake's water level changes. We adjusted minimum and maximum outflow fluxes (Q_{min} and Q_{max}) so that they corresponded to the minimum and maximum water levels (see Figure 6-3).

Three sampling campaigns (i.e., on February 9th, 2017, August 17th, 2017 and January 25th, 2018) were conducted at Lake A in order to collect water samples for isotopic analyses from the epilimnion, metalimnion and hypolimnion (Figure 6-6; Appendix G, Figure G1) to account for the vertical stratification of the isotopic signature (Gibson et al., 2017). The vertical isotopic profiles were volume-weighted according to the representative layer for each discrete measurement in order to obtain the observed δ_L for each campaign (Table 6-1). The depth-averaged isotopic composition of the lake on February 9th, 2017 (i.e., $\delta^{18}O$ = -10.15 ‰ and $\delta^{2}H$ = -70 ‰) was used as the initial modelled δ_L.

Table 6-1 Observed depth-averaged (or mean) and standard deviation (std) of isotopic composition of Lake A for the sampling campaigns in February 2017, August 2017 and January 2018 and all samples. The isotopic composition of the samples collected at the surface of Lake A on May 9-10, 2017 and April 27th, 2017 are also listed. The asterisks (*) indicate that a mean value was calculated (instead of a depth-averaged value).

Period	Date	*n*	$\delta^{18}O$ (‰)		$\delta^{2}H$ (‰)	
			depth-averaged	std	depth-averaged	std
Groundwater control	Feb 9th, 2017	9	-10.15	0.11	-69.92	0.41
Floodwater control	May 9-10, 2017 (Scenario A)	2	-11.20	0.05	-75.68	0.23
	April 27th, 2017 (Scenario B)	1	-11.86	-	-80.68	-
Groundwater control	Aug 17th, 2017	7	-10.61	0.82	-73.33	4.41
Groundwater control	Jan 25th, 2018	6	-10.70	0.26	-73.70	1.22
	All samples	34	-10.32*	0.62	-71.35*	3.69

While depth-averaged δ_L was not available during the floodwater control period (i.e., late February to early May), water samples from the surface of Lake A provide relevant evidence to better

constrain the model. It is likely that Lake A was fully mixed during the floodwater control period, and that the water samples collected at the surface of Lake A on April 27th, 2017 or May 9-10th, 2017 are representative of the whole water body. Indeed, the observed surface water temperature was < 5°C until early May (see Figure. E1) and suggests a limited density gradient along the water column which does not allow for the development of thermal stratification. In this context, we opted to simulate two scenarios (A and B), for which the isotopic mass balance model is either constrained at $\delta^{18}O$ = -11.20 ‰ and $\delta^{2}H$ = -76 ‰ on May 9-10, 2017 or at $\delta^{18}O$ = -11.86 ‰ and $\delta^{2}H$ = -80.68 ‰ on April 27th, 2017.

The results of the volume-dependent isotopic mass balance for $\delta^{18}O$ and $\delta^{2}H$ are illustrated in Figure 6-6. The fitted Q_{min} and Q_{max} from Lake A are 3.7 x 10^4 m^3 d^{-1} and 8.0 x 10^4 m^3 d^{-1} for scenario A and 1.0 x 10^3 m^3 d^{-1} and 2.8 x 10^5 m^3 d^{-1} for scenario B. These first-order water flux estimates represent equivalent water level variations ranging from 0.004 m d^{-1} and 1.0 m d^{-1}. From February 23rd, 2017 to May 8th, 2017 (see grey shaded area), hydraulic conditions allowed for surface inputs (I_s) from Lake DM to Lake A at a mean rate of 6.61 x 10^4 m^3 d^{-1} with a total floodwater volume of 4.82 x 10^6 m^3 for scenario A. The total floodwater volume was twice as important (9.96 x 10^6 m^3) for scenario B. Then, from May 9th, 2017, we considered that these floodwater inputs stopped, as the lake water level started to decrease. As a consequence, the model yielded a gradual enrichment of δ_L due to the combined contribution from I_G and E for both scenarios. From May 9th, 2017 to January 25th, 2018, the total I_G were 1.16 x 10^7 m^3 and 1.48 x 10^7 m^3 for scenario A and B respectively. Overall, the $\delta^{18}O$ and $\delta^{2}H$ models were better at reproducing the January 2018 and August 2017 observed δ_L, respectively. This is likely linked to the uncertainties and representativeness of the meteorological data, which is controlling the isotopic fractionation due to evaporation.

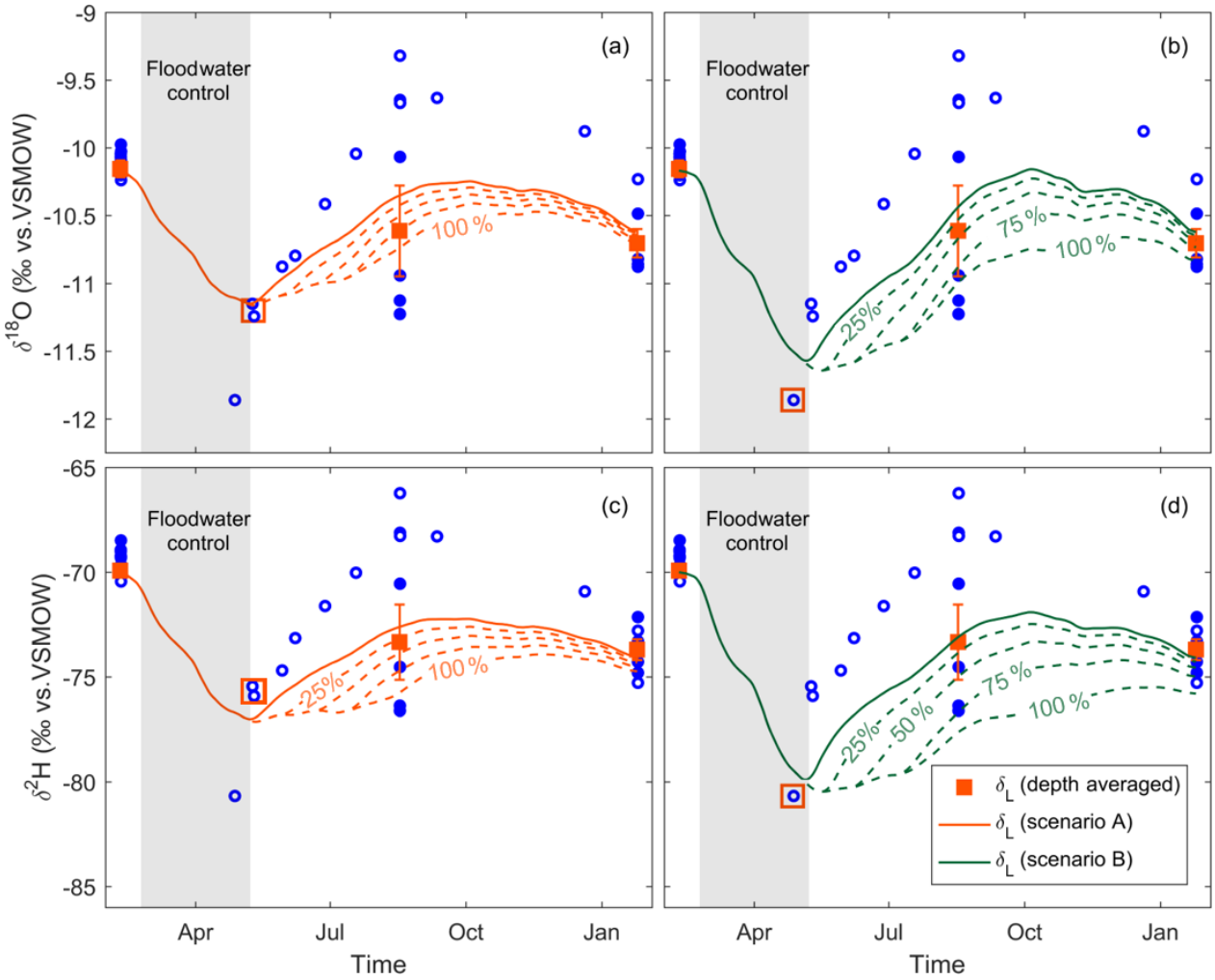

Figure 6-6 Observed and modelled depth-average isotopic composition of the lake (δ_L) for $\delta^{18}O$ (a-b) and δ^2H (c-d) from February 9th, 2017 to January 25th, 2018 for scenarios A and B. The hollow and solid blue circles correspond to Lake A water samples collected at ≤2 m and >2 m, respectively. The modelled δ_L is fitted against the three depth-averaged δ_L and an additional sample collected at ≤2 m depth on May 9-10, 2017 (scenario A) and April 27th, 2017 (scenario B). These samples are marked by the hollow red squares. The grey shaded area corresponds to the floodwater control period. The error bars correspond to the standard error on the samples for each campaign. The dashed lines represent the modelled δ_L when considering that 25% to 100% of the outputs from the lake during the floodwater control period were temporally stored in the aquifer and discharged to the lake as floodwater-like inputs (δ_{ls}).

While the computed flows for scenario A are within a plausible range for the combination of surface and groundwater outflow processes (i.e., minimum and maximum equivalent water level

variations of 0.13 m d^{-1} and 0.29 m d^{-1}), scenario B yielded less realistic results (i.e., minimum and maximum equivalent water level variations of 0.004 m d^{-1} and 1.0 m d^{-1}). As mentioned above, scenario B was constrained at $\delta^{18}O$ = -11.86 ‰ and $\delta^{2}H$ = -80.68 ‰ in late April (Figure 6-6), based on a surface water sample which was taken during a temporarily decreasing water level period (Figure 6-3) and is thus likely less representative of the overall lake's dynamics compared to scenario A. This is demonstrating the limit of the approach and that it is important to correctly constrain the model during flood events in order to perform precise estimations of the water balance.

Table 6-2 Water mass balance of Lake A for scenarios A and B. The difference between the total inputs and total outputs corresponds to the lake volume difference over the study period. The total inputs (I) correspond to the sum of precipitations (P), surface water inflow (I_S) and groundwater inflow (I_G). The total outputs (Q) correspond to the sum of evaporation (E) and surface water and groundwater outflow (Q). The mean flushing time (t_f) is the ratio of the lake volume to the mean groundwater inputs (I_G).

Scenario	Inputs (x 10^6 m^3)			Total I	Outputs (x 10^6 m^3)		Total Q	t_f
	P	I_S	I_G	(x 10^6 m^3)	E	Q	(x 10^6 m^3)	(days)
A	0.2	4.8	12.2	17.3	0.4	16.8	17.2	135
B	0.2	10.0	15.1	25.3	0.4	24.8	25.2	110
Difference	0.0	5.1	2.9	8.0	0.0	8.0	8.0	-25
	(0%)	(+107%)	(+24%)	(+46%)	(0%)	(+48%)	(+47%)	(-19%)

The water mass balance of Lake A from February 9th, 2017 to January 25th, 2018 is summarized in Table 6-2 for both scenarios. The difference between the total inputs and total outputs correspond to the lake volume difference (1.48 x 10^5 m^3) between the start and the end of the model run. Groundwater inputs (I_G) and surface water inputs (I_S) account for 71 % and 28 % of the total water inputs to the lake for scenario A. While I_S are twice as important for scenario B, they only account for 39% (+11%) of the total inputs and the I_G are 60% (-11%). It thus appears that the annual dynamic of Lake A is dominated by groundwater inputs for both scenarios, despite the intensity of the flood event. For scenarios A and B, t_f, as defined in Eq. 4,4, is similar (i.e., 135 days and 110 days). Precipitations are contributing 1% of the total annual inputs and evaporation only accounts for 2% of the total annual outputs. Although the establishment of a hydraulic connection between Lake DM and Lake A is a recurring yearly hydrological process, it is important to note that the

magnitude and duration of the flooding event of 2017 was particularly important and, thus, had a greater impact on the dynamic of Lake A in comparison to other years.

6.4.2.2 Sensitivity analysis

A one-at-a-time (OAT) sensitivity analysis was performed to grasp the relative impact of the input parameters' uncertainties on the model outputs. For each parameter, we tested two scenarios which delimit the uncertainty for each parameter. First, we tested the sensitivity of the model for V + 3 % and V – 8 % (i.e., estimated with slopes of 30° and 20°). Concerning δ_{Is} and δ_G, the model was tested for ± 0.5 ‰ for $\delta^{18}O$ and ± 4 ‰ for δ^2H, assuming they would both evolve along the LMWL (see Figure 6-4). Then, we assessed the sensitivity of the model to δ_A, by fixing the seasonality factor k at 0.5 and 0.9. Evaporation was computed with ± 20%, whereas the meteorological parameters (i.e., RH, T_{air}, U, P and Rs) were tested for ± 10%. As E and δ_A are dependent on the water surface temperature, we also tested the sensitivity of the model when considering that T is equal to the daily mean air temperature (T_{air}). Finally, we tested for the uncertainties concerning the definition of the LMWL. For the reference scenario, the LMWL ($\delta^2H = 8.13 * \delta^{18}O + 14.78$) was estimated using an ordinary least square regression (OLSR). For the sensitivity analysis, we estimated the LMWL via a precipitation amount weighted least square regression (PWLSR), which was developed by Hughes and Crawford (2012). Using the PWLSR method, the LMWL is defined as $\delta^2H = 8.28 * \delta^{18}O + 17.73$, and δ_{Is} and δ_G are estimated at -12.39 ‰ and -11.74 ‰ for $\delta^{18}O$ and at -85 ‰ and -79 ‰ for δ^2H, respectively. Recalculation of δ_{Is} and δ_G was needed, as they were both assumed to plot on the LMWL (see Sect. 6.4.1).

The results of this sensitivity analysis are listed in Table H1 and Table H2 (Appendix H) for scenarios A and B. Overall, the model was found to be highly sensitive to the uncertainties associated with δ_{Is}, δ_G and E, as the annual mean water fluxes (Q and I) varied up to -31% and +46% compared to the reference scenarios A and B. A negligible to slight change on the modelled δ_L was found when considering the uncertainties for V, δ_A, RH, T_{air}, U, P and Rs. For these variables, the mean flux estimate (Q and I) changes ranged from -8% to +4% compared to the reference scenarios A and B. As expected, the value of δ_{Is} affects the modelled δ_L exclusively during the floodwater control period. Similarly, the values of δ_G and E particularly influence the modelled δ_L from late summer to early winter. This is due to the fact that Q and E are the dominant

fluxes during this period. When considering that T is equal to T_{air}, despite the significantly different maximum and minimum values for Q, the mean Q was relatively similar to the reference scenarios and only a small change for t_f (+3% and +2% compared to reference scenarios A and B) was found. Finally, the model is highly sensitive to the uncertainties associated with the LMWL, as a translation of the LMWL implies an enrichment or depletion of both the δ_{Is}, δ_G at the same time. Such modifications result in mean flux estimate (Q and I) changes of up to -38% and -43% compared to reference scenarios A and B.

6.4.3 Importance of temporary floodwater storage on the water balance partition

The developed isotopic mass balance model yielded significant floodwater inputs during springtime to best-fit the observed δ_L. A first-order estimate of the total floodwater volume summed to 4.82 x 106 m^3 (for scenario A), which is nearly equal to the lake's initial volume (i.e., 4.70 x 10^6 m^3). Similar results were obtained by Falcone (2007) who studied the hydrological processes influencing the water balance of lakes in the Peace-Athabasca Delta, Alberta (Canada) using water isotope tracers. They reported that a springtime freshet (in 2003) did replenish the flooded lakes from 68% to >100% (88% in average).

As mentioned in Sect. 6.2.3, it was conceptualized that the high surface water elevation of Lake A during springtime resulted in hydraulic gradients that forced lake water to infiltrate into the aquifer and induce local recharge (see Figure 6-3). An important volume of flood-derived water could thus be stored during the increasing water level period and eventually discharged back to the lake as its water level decreased. Hence, the groundwater inputs to Lake A following the flooding event likely corresponded to flood-derived surface water originating from Lake DM. Considering that these fluxes are characterized by a floodwater-like isotopic signature (δ_{Is}), rather than the isotopic signature of groundwater (δ_G), the temporal evolution of the modelled δ_L would be modified. Such consideration is noteworthy to better depict the importance of floodwater inputs in the water balance partition.

Assuming that from 25% to 100% of the outputs (Q) from the lake during the floodwater control period were temporally stored in the aquifer and did eventually discharge back to the lake, the modelled δ_L diverges more or less from the reference scenarios A and B (Figure 6-6, see the dashed

lines). It is noteworthy that a better fit between the modelled δ_L and depth-averaged δ_L is obtained when considering that 25% to 50% of the outputs (Q) from the lake during the floodwater control period discharges back to the lake. In fact, it is likely that part of the potential stored floodwater could have effectively discharged back to the lake. For instance, part of the floodwater-like groundwater could have been abstracted by the pumping wells at the adjacent bank filtration site or discharged to Lake B. These results illustrate the importance of considering temporary subsurface floodwater storage when assessing water balances, especially as the magnitude and frequency of floods are likely to be more important in the future (Aissia et al., 2012).

6.4.4 Temporal variability in the water balance partition

The water balance presented in Table 6-2 provides an overview of the relative importance of the hydrological processes at Lake A for the study period (i.e., February 2017 to January 2018). As the surface water inputs (as floodwater) only occurred during springtime at Lake A, it is also important to decipher the temporal variability of the water fluxes. The dependence of a lake on groundwater can be quantified via the G-Index, which is the ratio of cumulative groundwater inputs to the cumulative total inputs (Isokangas et al., 2015). Figure 6-7 shows the temporal evolution of the G-Index from February 9th, 2017 to January 25th, 2018 for scenario A and the associated scenarios (A1 to A22) considered in the sensitivity analysis. Note that the G-Index is calculated at a daily time-step, based on the cumulative water fluxes. It is used to understand the relative importance of groundwater inputs over the studied period and does not consider the initial state of the lake. In early February, the G-Index is 100 %, because no surface water inputs (I_S) or precipitation (P) had yet contributed to the water balance. During the floodwater control period (see grey shaded area), the G-Index rapidly decreased and reached 12 % on May 8th, 2017 (for the reference scenario A). A gradual increase of the G-Index is then computed for the rest of the study period. On January 25th, 2018, the G-Index is 71 % and is likely more representative of annual conditions. Despite the sensitivity of the model to the input parameters, all scenarios yielded similar results. The G-Index ranged from 62 % to 75 % on an annual timescale for the different scenarios.

The impact of the potential temporary subsurface storage is also depicted in Figure 6-7 (see dashed lines). As highlighted in Sect. 6.4.3, part of the potentially stored floodwater in the aquifer could have discharged back to the lake as floodwater-like inputs (δ_{Is}) after the flooding event.

Considering these fluxes as surface water inputs (I_S), rather than groundwater inputs (I_G), would alter the temporal evolution of the G-Index. Assuming that 25% to 100% of the outputs from the lake during the floodwater control period did eventually discharge back to the lake, the floodwater inputs would contribute to the lake water balance until early June to early August (Figure 6-7). Lake A would thus be dependent on flood-derived water during a 1- to 3-month period after the flooding event. On an annual timescale, the temporary subsurface storage could lower the G-Index to a minimum value of 47%.

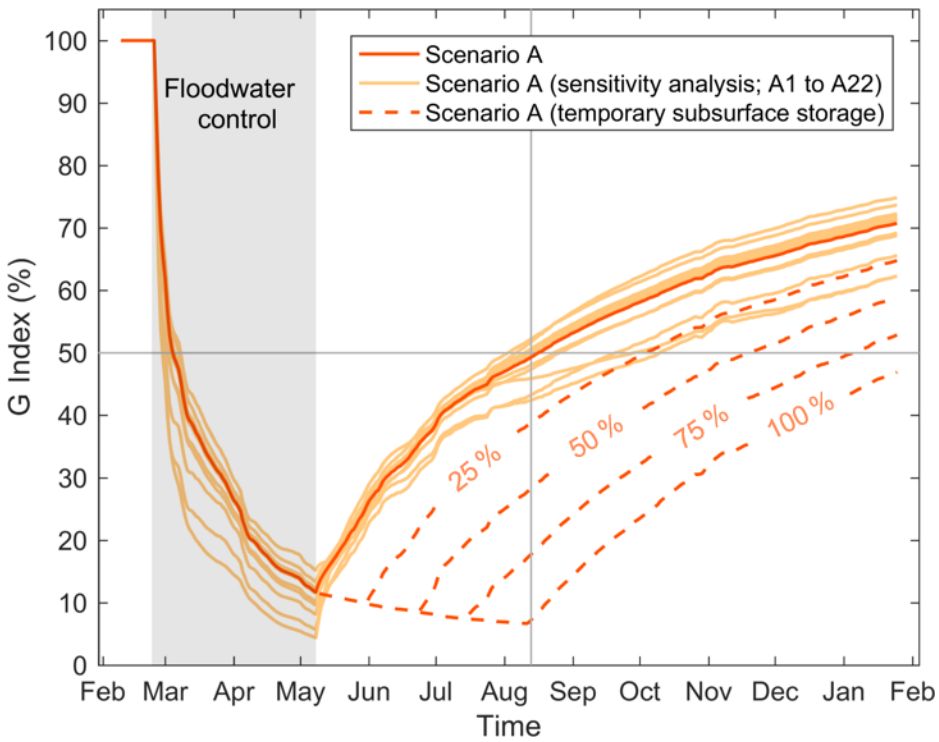

Figure 6-7 Temporal evolution of the G-Index from February 9th, 2017 to January 25th, 2018 for scenario A and the associated scenarios considered in the sensitivity analysis (i.e., A1 to A22). The grey shaded area corresponds to the floodwater control period. A hypothetical scenario is also depicted to decipher the impact of potential surface water bank storage on the evolution of the G-Index. Indeed, during the floodwater control period, the outputs (Q) from the lake can be stored in the aquifer and gradually discharge back to the lake. Conceptually, this contribution to the lake can be considered as surface water inputs (I_s), rather than groundwater inputs (I_G). Hence, G-Index is corrected for surface water bank storage considering that 50%, 75% or 100% of the Q during the floodwater control period returns to the lake as I_S (dashed lines).

6.5 Discussion

6.5.1 Resilience of lakes to surface water and groundwater changes

Resilience of a system has been defined as its capacity to cope with perturbations (i.e., internal and/or external changes) while maintaining its state (Cumming et al., 2005). In the case of a lake, perturbations can manifest as a change in the water quantity and quality contributing to the water balance. According to Arnoux et al. (2017b), the impact of a perturbation to a lake is not only dependent on the relative importance of water budget fluxes, but also on the residence time of water in the lake. Thus, they proposed an interpretation framework which relates the response time of a lake to changes in groundwater quantity and/or quality, thereby linking the G-Index with t_f, the mean flushing time by groundwater fluxes (Figure 6-8). They depict a general case, applicable to any pollution, regardless of reactivity or fate of contaminants. Hence, care should be taken when interpreting the sensitivity to specific contaminants which are subject to attenuation processes, such as degradation and sorption.

In their study, Arnoux et al. (2017b) assessed the resilience of kettle lakes ($n = 20$), located in southern Quebec (Canada), in similar morpho-climatic contexts to Lake A. The surveyed lakes were found to be characterized by a wide range of conditions; from resilient (i.e., G-Index <50% and t_f >5 years) to highly sensitive to groundwater changes (i.e., G-Index >50% and t_f <1 year). This is related to the variability of the hydrogeological contexts, resulting in variations in the importance of groundwater contributions and the range of mean flushing times of the lakes (see grey arrow in Figure 6-8). The majority of the lakes (i.e., 50%) were found to be characterized by intermediate conditions (G-Index >50% and 5< t_f <1 years) and, thus, were classified as being relatively resilient to both surface and groundwater changes.

Concerning Lake A, studied scenarios (i.e., reference scenario A and the sensitivity analysis) yielded values for G-Index >50% and t_f <1 year, i.e., indicating that Lake A is highly sensitive to groundwater changes, but resilient to surface pollution. Nevertheless, it was shown that temporary floodwater storage and discharge to lakes are crucial to correctly represent the G-Index by accounting for the origin of water fluxes (Figure 6-7; Sect. 6.4.4). While floodwater storage lowers the G-Index, the t_f slightly increases (see orange arrow in Figure 6-8). Therefore, the studied lake

receives a reduced groundwater contribution relative to the initial estimated apportionment when not accounting for floodwater storage, but is still characterized by a rapid flushing time. This implies that flood-affected lakes are more likely to be characterized by an intermediate condition, and thus are relatively resilient to groundwater quantity and quality changes. The geochemical data (Sect. 6.4.2) is in agreement with this interpretation. Indeed, a low-mineralization and Ca-HCO_3 water type at Lake A is consistent with the significant floodwater contributions (to the lake and aquifer). In comparison, the neighboring lake (i.e., Lake B) does not undergo yearly recurrent flooding and was shown to be more mineralized with a Na-Cl water type, likely originating from road-salt contamination of regional groundwater (Pazouki et al., 2016). Biehler et al. (2020) similarly reported hydrological controls on the geochemistry of a shallow aquifer in an hyporheic zone, where river stage influenced the mixing ratio between river water and the deeper aquifer.

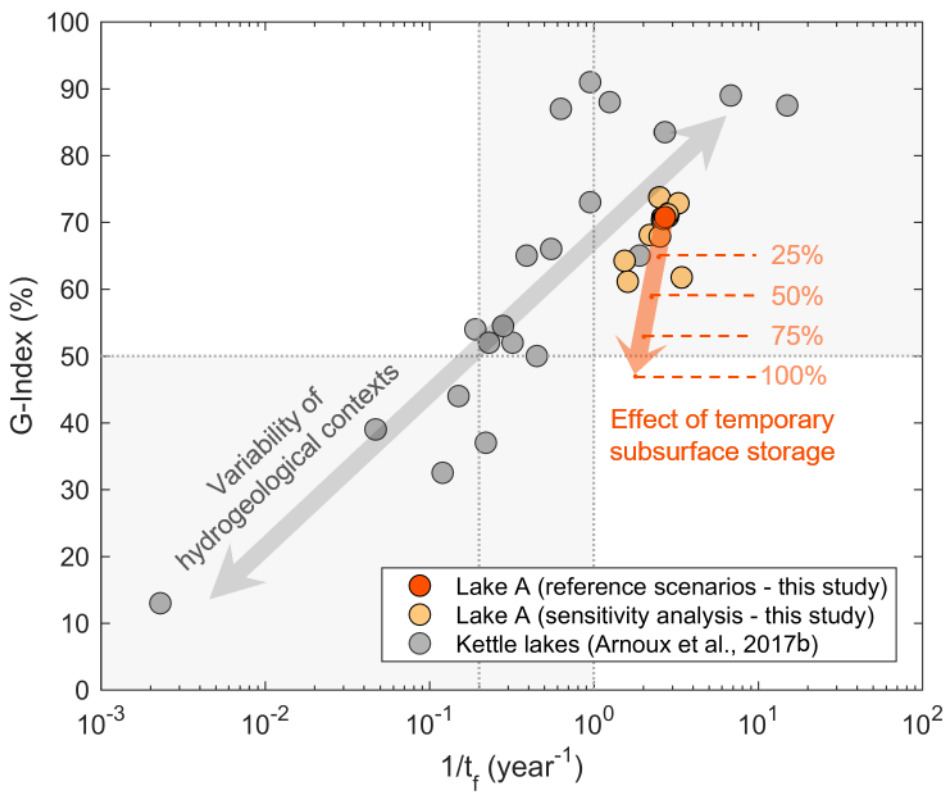

Figure 6-8 Resilience of lakes to groundwater quantity and quality changes for Lake A (this study) and kettle lakes (Arnoux et al., 2017b) in southern Quebec (Canada). G-Index is the ratio of groundwater inputs to total inputs and t_f is the mean flushing time by groundwater. This representation is adapted from Arnoux et al. (2017b).

Considering the above, it is possible to speculate about the potential future impacts of climate change on Lake A. Globally, future meteorological scenarios are predicting changes in precipitation and climate extremes, including floods and droughts (Salinger, 2005). In Quebec (Canada), river stages are expected to increase across various watersheds in response to future climate scenarios (Dibike & Coulibaly, 2005; Minville et al., 2008; Roy et al., 2001). These hydrological responses could result in floods of longer duration and higher intensity (Aissia et al., 2012) and more pronounced droughts (Wheaton et al., 2007). Such changes could directly affect the quality of Lake A. If flooding becomes more prevalent, enhanced floodwater input to Lake A would likely occur. In this case, the surface water inputs from floods would buffer the sensitivity of Lake A to groundwater quality changes originating from its watershed. On the other hand, if floods become less important and/or less frequent, we can expect that the water quality of Lake A would be more dependent on regional groundwater quality. In such a case, the geochemistry of Lake A could potentially shift towards that of Lake B, and an increase of the salinity and the concentration of Na^+, Ca^{2+}, SO_4^{2+} and Cl^- would be expected for Lake A.

6.5.2 Implications for water management

Water budget assessments at natural lakes can serve as a tool for quantifying local human impacts (i.e., land use changes and climate changes) on water resources (Arnoux et al., 2017b). Based on the results of this study, it becomes apparent that water budget assessments at artificial lakes (such as Lake A) can also be used to track human impacts on water resources. Recurring water budget assessments at a specific lake over time will serve to document changes in groundwater and surface water apportionment and can help to detect changes in local groundwater availability, and to anticipate impacts on local water supply utilities. As the response time of a lake to changes is controlled by its flushing time, the evolution of the G-Index will manifest at various rates. Indeed, lakes with different t_f would reflect changes at different timescales. For instance, lakes with $t_f > 5$ yr would be expected to respond to decadal changes, while lakes with $t_f < 5$ yr would track annual or interannual variability. By analogy, we might postulate that it would be informative to study lakes with rapid response times (i.e., $t_f < 1$ yr), as they will act as precursors of the evolution of nearby surface water bodies characterized by longer flushing times.

As demonstrated, isotopic approaches may be efficiently employed to solve water budget unknowns as the method can be performed at low-cost and requires limited sampling and monitoring efforts for flood-affected environments which may be difficult or dangerous to monitor using traditional approaches. To enhance the effectiveness of our approach, the sampling strategy may be improved. Firstly, surface water sampling for isotopic analyses is recommended during turnover periods (i.e., springtime and autumn) and should be combined with depth-resolved measurements of physico-chemical parameters to confirm the vertical homogeneity or stratification. Secondly, for long-duration flood events, monitoring of potential evolution in floodwater isotopic signatures could help to improve the accuracy and realism of the model. Groundwater level monitoring and groundwater sampling in the vicinity of the lake could also help to strengthen the conceptual model by providing data to interpret the direction of groundwater fluxes and the variability of isotopic composition through time.

6.6 Conclusions

In this study, a volume-dependent transient isotopic mass balance model was developed and applied to a flood-affected lake in an ungauged basin in southern Quebec (Canada). This allowed for better understanding of the resilience of a flood-affected lake to changes in the surface/groundwater water balance partition, to understand the role of floodwater, and to predict resilience to groundwater quantity and quality changes for a local water supply. Given the contrasting isotopic signature of the floodwater, the isotopic mass balance model was effectively applied at the study site. We anticipate that the isotopic framework is likely to be transferable to other lake systems subject to periodic flooding including lowland lakes fed by mountain floodwaters, river deltas, wadis, or nival (snowmelt-dominated) regimes, the latter of which dominates the high latitude and high altitude cold-regions including much of the Canadian landmass.

The isotopic mass balance model revealed that groundwater inputs dominated the annual water budget. To test the sensitivity, representativeness and resilience of the model, several model scenarios were evaluated to account for uncertainty in important input variables. Despite sensitivity to some variables, all model scenarios considered in the sensitivity analysis converged on the results that Lake A is mainly dependent on groundwater inputs and has a rapid (<1 year) flushing

time by groundwater, suggesting that Lake A would be highly sensitive to groundwater quantity and quality changes.

When taking into account potential subsurface storage, a better fit could be obtained between the modelled and depth-averaged isotopic signature of the lake, suggesting that the contribution of floodwater-like subsurface inputs is important to consider when assessing for water balance at flood-affected lakes. In fact, the increased contribution of surface water (from subsurface storage) resulted in a lower contribution from groundwater and, consequently, in an increased resilience to groundwater changes. This finding provides a basis for postulating the impact of climate change on the water quality of Lake A. If the importance of floods increases, more floodwater inputs to Lake A can be expected during springtime, causing increased recharge. In this case, the surface water inputs from floods would increase the resilience of flood-affected lakes to groundwater quantity and quality changes at the watershed scale. On the other hand, if floods become less severe and/or less frequent, we can expect that the water quality of flood-affected lakes become more dependent on regional groundwater quality. From a global perspective, performing water balance assessments at lakes with rapid flushing time (<1 year) can help to predict the evolution of other surface water bodies with longer flushing times in their vicinity and, therefore, is useful for establishing regional-scale management strategies for maintaining lake water quality.

CHAPTER 7 GENERAL DISCUSSION

This chapter presents a critical overview of some methodological aspects and results underpinning the paper-based core of this thesis. Challenges and opportunities regarding the spatial and temporal representativity of groundwater and surface water samples (or measurements) are discussed, with the objective of providing insights into the following questions:

1. Do pumping schemes (i.e., continuously, intermittently and occasionally) affect the representativity of the groundwater samples collected at the pumping wells?
2. What are the implications of transient pumping schemes regarding the applicability of the pumping strategies to control the total Fe and total Mn concentrations?
3. What is the representativity of the groundwater samples collected at the observation wells considering their screen length and location?
4. Does the thermal stratification (and turnover) of lakes in cold climate represent a challenge and/or an opportunity for the use of environmental tracers at BF sites?
5. Can environmental tracers provide significant inputs to anticipate breakthrough of microorganisms from stratified lakes to pumping wells?

7.1 Transience of the pumping schemes

The representativity of groundwater samples collected from pumping wells depends on whether a steady-state is achieved. When a pumping well is activated, groundwater flow patterns in the vicinity of the well are modified (Figure 7-1). In the early stage of pumping, a cone of depression starts to form in the aquifer around the well, and the abstracted groundwater is first obtained from the close proximity of the well (Figure 7-1b). As pumping continues, the groundwater flow reorganizes at a greater distance from the well and, given favorable hydraulic parameters and a sufficiently high pumping rate, a hydraulic connection with the surface water body eventually establishes as the drawdown cone develops (Figure 7-1c) (Barlow & Leake, 2012).

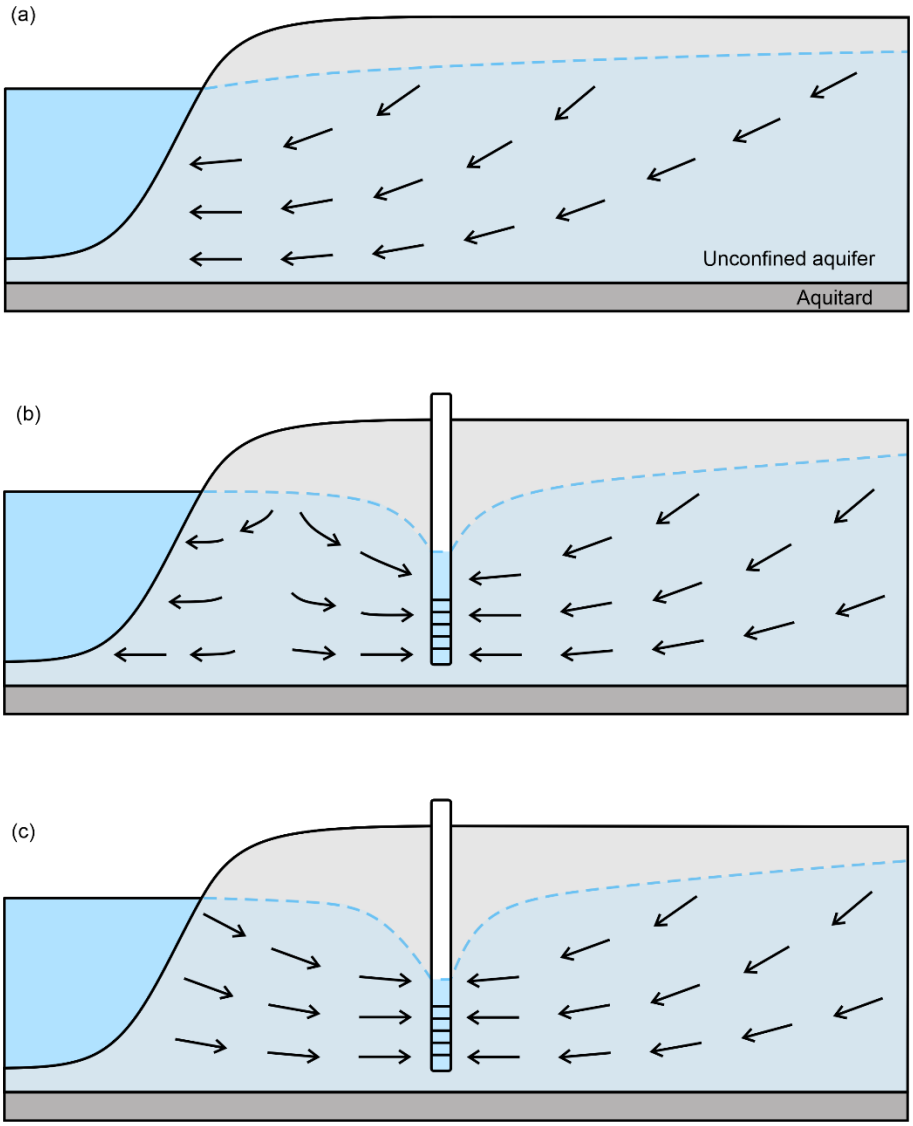

Figure 7-1 Schematic representation of the effects of pumping on groundwater flow patterns (adapted from Barlow & Leake, 2012)

In this research project, the pumping wells are not operated at steady state, but rather with fluctuating pumping rates to accommodate for the variations in the water demand. Additionally, an activation-shutdown procedure is applied to sample the pumping wells. That is, once a first well is sampled, its pump is shut down and the pump of another well is activated. This is repeated until all eight pumping wells are sampled. As two wells are typically active daily (i.e., continuously) and others are only activated for the monthly sampling program, the representativity of the water samples at each pumping well is likely different. The water samples collected at the continuously

pumping wells are likely representative of groundwater flow patterns in a relatively developed drawdown cone as in Figure 7-1(c), while the samples collected at the other wells could be representative of flow patterns in an earlier stage of pumping as in Figure 7-1(b).

In article #1, it is presumed that the representativity of groundwater samples at the pumping wells would individually compare from one campaign to the other. This is supported by the fact that the pumping strategy remains almost unchanged for the period assessed in article #1 (i.e., from late April 2016 to early February 2017). That is, the pumping wells were operated according to a priority order (P6, P3 P1, P8, P2, P7, P4 and P5), and the wells were sampled in the same (or similar) order (Figure 7-2). However, it is less clear how the samples from different wells compare with one another. To confirm whether the transience of the pumping schemes and the activation-shutdown procedure affects the representativity groundwater samples (or measurements) at the pumping wells, a time-resolved sampling could be performed at the pumping well upon activation of the pump and once a developed drawdown cone is formed.

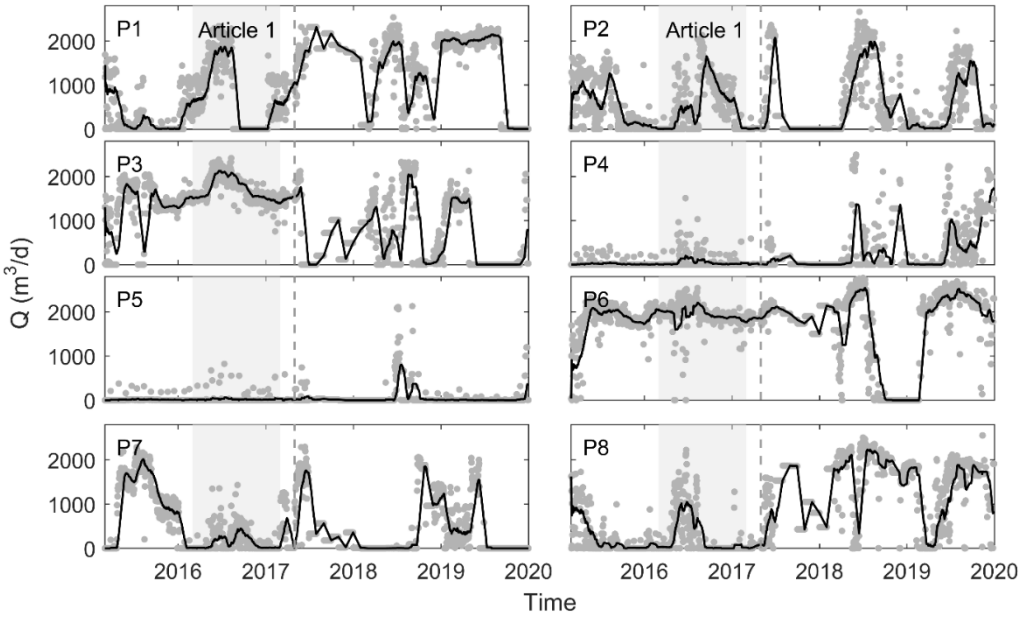

Figure 7-2 Pumping rates at the wells P1 to P8 from January 2015 to December 2019 inclusively. The grey dots are the daily mean pumping rates and the black lines are the 30-day moving average of the pumping rates for each well. The grey shaded area represents the period assessed in the Article #1, while the vertical dashed line represents the onset of the advanced water treatment system.

7.2 Control of the pumping schemes on Fe and Mn concentrations

In article #1, it was found that the pumping schemes have a control on the physico-chemical quality of the pumped water. The wells operating on an occasional basis have the highest total Fe concentration, and the operation of wells on an intermittent basis is associated with the highest total Mn concentration. These conclusions are obtained from the analysis of the pumping strategy from April 2016 to early February 2017, i.e., a period during which the pumping schemes remained unchanged (Figure 7-2).

From May 2017, the pumping schemes were gradually modified, as an advanced water treatment system was added to the drinking water production plant to better control the concentrations in Fe^{2+} and Mn^{2+} and lower the hardness in the distributed water. From the onset of this treatment system, most of the wells were operated on a more intermittent basis (Figure 7-2). Interestingly, this modification in the pumping strategy coincides with a deterioration of the water quality at the pumping wells. The total Mn concentrations gradually increased in 2019 for pumping wells that were operated on a more intermittent basis (P2, P7 and P8), as anticipated by the approach in Article #1. Also, the increased solicitation of P4 resulted in a gradual increase of the total Fe concentrations, which reached up to 3.45 mg/L (compared to less than 1 mg/L previously) (Figure 7-3). It is worth mentioning that Mn is mainly observed in the dissolved phase in the pumped water, while Fe is found in the particulate form. As explained in Article #1, Mn is likely transported by advection from Lake B as high total Mn concentrations were associated with important contribution from Lake B to the pumped water and similar total Mn concentrations were observed at depth (≥ 6 m). Additionally, it was hypothesized that occasional pumping at high pumping rates, causes the mobilization and transport of particulate Fe in the vicinity of the pumping wells.

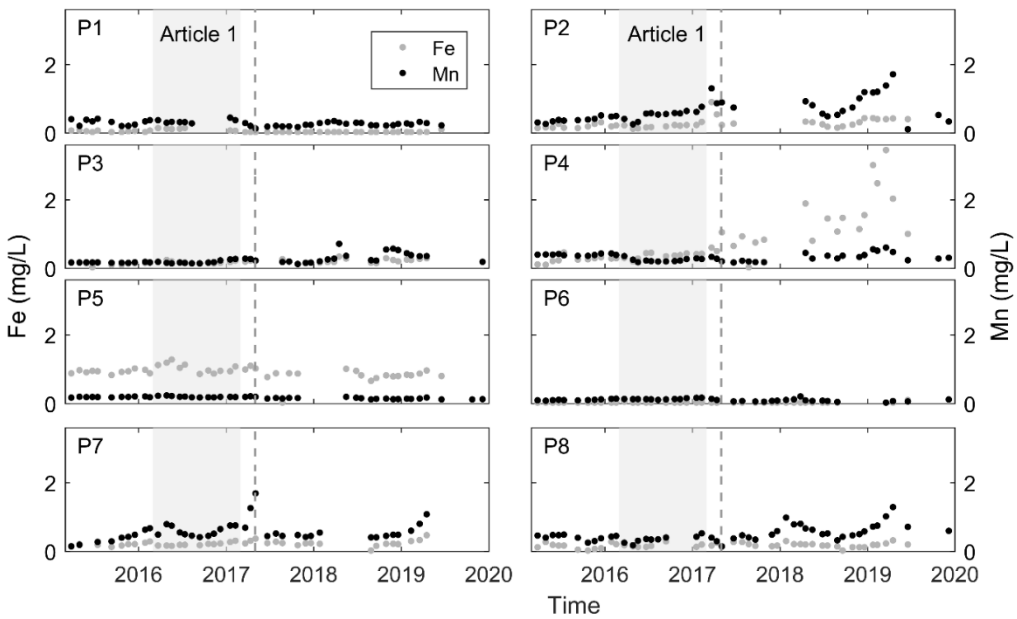

Figure 7-3 Total Fe and total Mn concentrations at the wells P1 to P8 from January 2015 to December 2019 inclusively. The grey shaded area represents the period assessed in the Article #1, while the vertical dashed line represents the onset of the advanced water treatment system.

To gain further insight on the control of pumping schemes on the quality of the pumped water on the long-term, i.e. to apply and extend the approach from article #1 to the entire dataset, a new definition of the proposed grouping from article #1 (i.e., continuously, intermittently and occasionally pumping) is needed. The modified grouping criteria, as listed below, allows pumping wells to shift between categories from one sampling campaign to the other, thus reflecting the transience of the pumping schemes:

- Occasionally pumping: contributes < 1% of the total monthly pumped volume
- Intermittently pumping: contributes from ≥1% to <20% of the total monthly pumped volume
- Continuously pumping: contributes ≥20% of the total monthly pumped volume

Updated relationships between the pumping rate and the total Fe and total Mn concentrations are illustrated in Figure 7-4. As previously predicted (article #1), the highest total Fe and Mn concentrations remain associated with low monthly averaged pumping rates. Also, these results confirm that the operation of the pumping wells on a more continuous basis allows to lower (at

best) the concentrations in total Fe and total Mn. This pumping strategy likely allowed to limit the mobilization of particulate Fe in the vicinity of the pumping wells and to benefit from the mixing between Lake A and Lake B to lower the dissolved Mn concentrations.

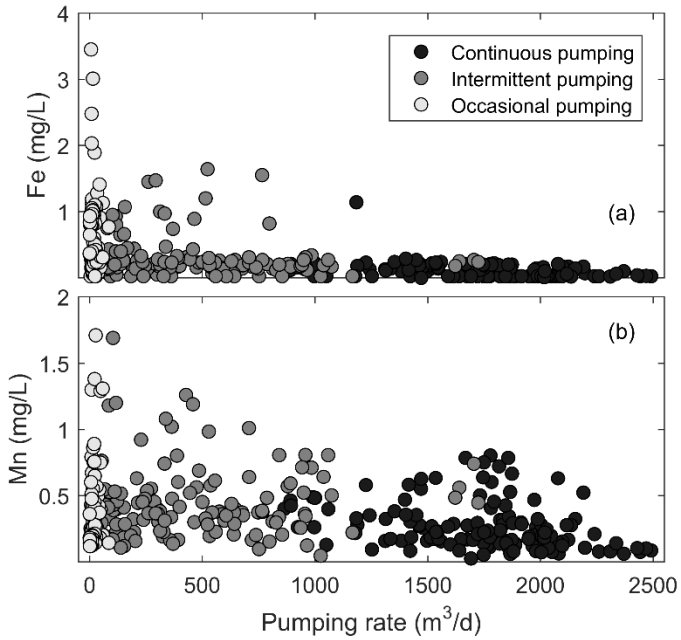

Figure 7-4 Relationship between the pumping rate and (a) the total Fe concentration and (b) the total Mn concentration

The operation of a well on an occasional or intermittent basis, however, does not appear to be as discriminant as in article #1 to predict total Fe and total Mn concentrations on the long term, and represents a limit of the approach. In fact, it is possible that the more transient pumping conditions from May 2017 induced a bias regarding the representativity of the groundwater samples.

7.3 Design of the observation wells

Also decisive for the representativity of the groundwater samples is the length and position of the well screen. It is recognized that short and long screen lengths provide different information. While a short screen length allows to intercept specific flow lines and inform on depth-specific processes, a long screen length provide a more comprehensive characterization as it integrates a greater vertical portion of the aquifer (Cook et al., 2017; Mayo, 2010). To depict the complexity of

groundwater flow patterns at BF sites, it is ideal to install multiple-depth observation well clusters with short screen length. However, single observation wells with relatively long screens may be preferentially installed due to practical considerations (e.g., cost) (Maliva, 2020).

At the studied BF site, the observation wells were equipped with screen lengths ranging from 3 m to 9 m (except for the observation well on the NE of Lake B which has a 1 m long screen). All the screens were positioned at the bottom of the aquifer (maximal depth is ~26 m). This setup implies that the collected groundwater samples at the selected observation wells provided data that characterizes flow lines in the lower part of the aquifer. In addition to the geochemical and isotopic approaches that relied on collected groundwater samples, depth-resolved temperature measurements were performed within the well's tubing (i.e., without the need for collecting groundwater sample), assuming that the water column was in thermal equilibrium with the ambient groundwater in the aquifer. As they were performed prior to sampling at observation wells, they helped at better understanding the groundwater flow paths, especially during a flood event (e.g., paper #2).

7.4 Stratification of lakes in cold climate

In cold climate regions, lakes are typically dimictic, i.e., their thermal stratification is interrupted twice a year as a complete (or partial) turnover of the water column occurs in autumn and spring (Pernica, 2014). The thermal stratification is composed of three layers: the epilimnion at the surface, the thermocline in the center and the hypolimnion at depth. As exchange between these layers is limited (due to density contrasts), thermal stratification typically leads to the development of a geochemical and isotopic stratification of the water column.

In the context of this thesis, depth-resolved measurements of temperature, EC and $\delta^{18}O$ and $\delta^{2}H$ confirmed the development of a thermal and isotopic stratification at both Lake A and Lake B during summertime, but geochemical stratification (i.e., EC) was only observed at Lake B. While evaporation mainly controls the development of the isotopic stratification, geochemical stratification is likely the result of vertically distributed groundwater inputs to lakes. In fact, during summertime, relatively cold and dense groundwater inputs may preferentially discharge and stagnate in the bottommost part of a lake (Arnoux et al., 2017c).

In article #1, EC was used to estimate the partitioning of water infiltrating from Lake A and Lake B and contributing to the pumping wells. To consider the geochemical stratification at Lake B, a depth-averaged EC value (~ 873 µS/cm) was used. This assumes that Lake B water infiltrates the aquifer homogeneously (i.e., the groundwater outflows from the lake are equal at all depths along the aquifer/surface water interface). This simplification is however disputable, as hydraulic conductivity is undoubtedly heterogenous along the aquifer/surface water interface, not only due to sediment characteristics, but also because of temperature contrasts along the water column. The temperature contrast between epilimnion and hypolimnion can reach up to 20°C which represents a two-fold change in hydraulic conductivity. Consequently, it is likely that there is a preferential infiltration of the water from the surface-most part of the lakes during summertime.

Considering the above, it appears that the lake stratification represents a challenge for the use of EC as a tracer to depict the groundwater/surface water interactions. To better represent the mixing ratios at a stratified-lake BF system, one would need to consider an amount-weighted EC value of the source water. Estimating the distribution of the intensity of groundwater flow rates at the aquifer/surface water interface is however not an easy task. An opportunity may lie in the coupling of geochemical and isotopic tracers. Similarly to the geochemical stratification, the isotopic stratification also helps at differentiating water from the epilimnion and hypolimnion of a lake. The two tracers could be used jointly to estimate the vertical distribution of the intensity of groundwater flow rates by fitting modeled EC and $\delta^{18}O$-$\delta^{2}H$ values to the observed values at the pumping wells.

7.5 Anticipating breakthrough of microorganisms

It is recognized that lake stratification limits the availability of dissolved oxygen and nutrients along the water column and that, by mixing, lake turnover can promote the development of cyanobacteria in the epilimnion in autumn (Diao et al., 2017). This process is likely to occur at the study site and may represent a threat to the water quality of the pumped water, as Pazouki et al. (2016) reported that insufficiently long travel times between Lake B and the pumping wells allows for cyanobacteria breakthrough.

As mentioned above, the tracer-based monitoring program that was applied for this research project may thus represent an opportunity to track the infiltration of surface water from the epilimnion

(prior to lake turnover) and could also allow to track the infiltration of the recently mixed surface water. The 3-year database that was acquired during this thesis could serve to test this hypothesis.

Given an adapted monitoring strategy that allows to detect the timing of the lake turnover in real time, it could be possible to anticipate the breakthrough of microorganisms and adapt the pumping strategy to manage the risk of microbial contamination. For instance, the operation of all available wells at moderate pumping rates could help at reducing the mean flow velocity of the bank filtrate and increase residence time of surface water in the aquifer (promoting natural die-off of microorganisms).

CHAPTER 8 CONCLUSION AND PERSPECTIVES

This research project sought to reveal the dynamics of groundwater flow patterns at a BF site affected by recurring springtime flood events. Using environmental tracers and a multi-scale approach, it has been possible to inspect the spatiotemporal variability of the pumped water origin under transient hydraulic conditions and to evaluate the role of the recurring floods in supporting the sustainability of a BF site.

First, the competition between anthropic and meteorological forcings on the origin of pumped water at a monthly timescale was elucidated. An EC-based and time-varying binary mixing model was developed, to establish that pumping schemes can be used to control the origin and quality of the pumped water. The operation of the pumping wells on a continuous basis allowed to outweigh the meteorological control (i.e., water levels), except during flood event. Furthermore, high pumping rates and a continuous operation of the pumping wells helped at limiting the total Fe and total Mn concentrations in the pumped water. Conversely, the operation of wells on an intermittent or occasional basis was found to deteriorate the physico-chemical quality of the pumped water.

Second, the daily dynamics of the water origin during a major flood event were investigated. An optimized combination of environmental tracers (i.e., EC, $\delta^{18}O$- $\delta^{2}H$ and temperature) at dedicated monitoring points allowed to better understand the timescales of groundwater flow patterns reorganization during and after an extreme flood event. The tracers were found to be complementary and to provide information that can help anticipating microbial water quality changes and guide the timing and the frequency of more expensive and time-consuming analyses (e.g., bacteriological indicators) to secure the production of high-quality drinking water.

Third, a volume-dependent stable isotope mass balance was developed to estimate the partitioning between groundwater and floodwater to Lake A, i.e., the principal source water to the studied BF site. The model revealed that considering the temporary subsurface floodwater storage (and discharge) was important to correctly depict the dependence of the flood-affected lake to groundwater. These results were then used to predict the resilience of the lake to perturbations. It was found that the lake is highly sensitive to groundwater quantity and quality changes, but that floodwater inputs and storage contribute to increase its resilience and to maintain the physico-chemical quality of the lake on the long term. Thereby, the recurring floods appear to contribute

positively to the hydrosystem and help at securing the sustainability of drinking water production at the BF site.

The results of this research have immediate application for water managers of the studied site and will benefit to the 18,000 inhabitants that are supplied with the drinking water produced at this site. Other drinking water production plants located in regions where the hydrological cycle is shaped by recurring springtime freshets could also benefit from this work. For instance, it could be applied at the watershed scale in the Province of Quebec, where many municipal wells are located in the vicinity of rivers, but BF is not specifically planned. By monitoring EC and $\delta^{18}O$-$\delta^{2}H$ in main rivers and at pumping wells, it would be possible to gain insights on the response of these systems to springtime freshest.

Directions for further research also include the investigation of the driving processes for Fe and Mn solubilization and transport. In this thesis, it was identified that the pumping schemes have a control on the Fe and Mn concentrations at the pumping wells, but the processes underlying the origin of these metals in the pumped water remained uncertain. It was hypothesized that high Fe concentrations were the result of the mobilization of iron-containing oxides or particulates due to rapid flow velocities in the vicinity of the pumping well upon sampling, while Mn was likely transported by advection with reduced water from depths in Lake B. It is also possible that the infiltration of organic matter-rich surface water promotes microbial activity in the subsurface and lead to a consumption of dissolved oxygen and solubilization of Fe and Mn as the bank filtrate is being reduced, as it was observed at many BF sites. Yet, it is unknown whether the solubilization and precipitation of Fe and Mn is mainly driven by abiotic reactions and/or is microbially mediated. Investigating the spatial distribution of metal-reducing and metal-oxidizing bacteria and redox conditions in the stratified lakes and the aquifer could help at better anticipating the evolution of Fe and Mn concentrations.

Overall, this work contributes to the scientific literature on BF systems in snowmelt-dominated basins. This research explored the dynamics of groundwater flows from the daily to annual timescales at both the BF site scale and hydrosystem scale. This thorough understanding of the response of a BF system to recurring springtime flood events allowed to envision and apply monitoring and operational strategies to improve raw water quality. This work benefits to the water

managers and scientists, as it can help at operating existing BF sites and planning future BF projects in snowmelt-dominated basins.

REFERENCES

Adomat, Y., Orzechowski, G. H., Pelger, M., Haas, R., Bartak, R., Nagy-Kovacs, Z. A., Appels, J., & Grischek, T. (2020). New Methods for Microbiological Monitoring at Riverbank Filtration Sites. *Water, 12*(2), 584. doi:10.3390/w12020584

Ageos. (2010). *Drinking water supply: Application for an authorization under Section 31 of Groundwater Catchment Regulation: Hydrogeological expert report* (2010-723, volume 1 de 2). Retrieved from Brossard, QC, Canada:

Ageos. (2016). *Drinking water supply: Monitoring of piezometric fluctuations in the water table and lake levels: Period from April 27, 2012 to December 17, 2015: Annual Report 2015*. Retrieved from Brossard, QC, Canada:

Agnihotri, J., & Coulibaly, P. (2020). Evaluation of Snowmelt Estimation Techniques for Enhanced Spring Peak Flow Prediction. *Water, 12*(5). doi:10.3390/w12051290

Ahmed, A. K. A., & Marhaba, T. F. (2017). Review on river bank filtration as an in situ water treatment process. *Clean Technologies and Environmental Policy, 19*(2), 349-359. doi:10.1007/s10098-016-1266-0

Ahmed, S., Coulibaly, P., & Tsanis, I. (2015). Improved Spring Peak-Flow Forecasting Using Ensemble Meteorological Predictions. *Journal of Hydrologic Engineering, 20*(2), 04014044. doi:10.1061/(ASCE)HE.1943-5584.0001014

Aissia, M. A. B., Chebana, F., Ouarda, T. B. M. J., Roy, L., Desrochers, G., Chartier, I., & Robichaud, É. (2012). Multivariate analysis of flood characteristics in a climate change context of the watershed of the Baskatong reservoir, Province of Québec, Canada. *Hydrological Processes, 26*(1), 130-142. doi:10.1002/hyp.8117

Anderson, M. P. (2005). Heat as a Ground Water Tracer. *Groundwater, 43*(6), 951-968. doi:10.1111/j.1745-6584.2005.00052.x

Arbués, F., García-Valiñas, M. a. Á., & Martínez-Espiñeira, R. (2003). Estimation of residential water demand: a state-of-the-art review. *The Journal of Socio-Economics, 32*(1), 81-102. doi:10.1016/S1053-5357(03)00005-2

Arnoux, M., Barbecot, F., Gibert-Brunet, E., Gibson, J., & Noret, A. (2017a). Impacts of changes in groundwater recharge on the isotopic composition and geochemistry of seasonally ice-covered lakes: insights for sustainable management. *Hydrology and Earth System Sciences, 21*(11), 5875-5889. doi:10.5194/hess-21-5875-2017

Arnoux, M., Barbecot, F., Gibert-Brunet, E., Gibson, J., Rosa, E., Noret, A., & Monvoisin, G. (2017b). Geochemical and isotopic mass balances of kettle lakes in southern Quebec (Canada) as tools to document variations in groundwater quantity and quality. *Environmental Earth Sciences, 76*(3), 106. doi:10.1007/s12665-017-6410-6

Arnoux, M., Gibert-Brunet, E., Barbecot, F., Guillon, S., Gibson, J., & Noret, A. (2017c). Interactions between groundwater and seasonally ice-covered lakes: Using water stable isotopes and radon-222 multilayer mass balance models. *Hydrological Processes, 31*(14), 2566-2581. doi:10.1002/hyp.11206

Ascott, M. J., Lapworth, D. J., Gooddy, D. C., Sage, R. C., & Karapanos, I. (2016). Impacts of extreme flooding on riverbank filtration water quality. *Sci Total Environ, 554-555*, 89-101. doi:10.1016/j.scitotenv.2016.02.169

Barbecot, F., Larocque, M., & Horoi, V. (2019). *Research infrastructure on groundwater recharge* [Isotopic composition of precipitation at Saint-Bruno, QC Canada].

Barlow, P. M., & Leake, S. A. (2012). *Streamflow depletion by wells - understanding and managing the effects of groundwater pumping on streamflow* (Circular 1376). Retrieved from http://pubs.usgs.gov/circ/1376/

Barnett, T. P., Adam, J. C., & Lettenmaier, D. P. (2005). Potential impacts of a warming climate on water availability in snow-dominated regions. *Nature, 438*(7066), 303-309. doi:10.1038/nature04141

Baudron, P., Barbecot, F., Gillon, M., Aróstegui, J. L. G., Travi, Y., Leduc, C., Castillo, F. G., & Martinez-Vicente, D. (2013). Assessing Groundwater Residence Time in a Highly Anthropized Unconfined Aquifer Using Bomb Peak 14C and Reconstructed Irrigation Water 3H. *Radiocarbon, 53*(2-3), 933-1006. doi:10.2458/azu_js_rc.55.16396

Baudron, P., Sprenger, C., Lorenzen, G., & Ronghang, M. (2016). Hydrogeochemical and isotopic insights into mineralization processes and groundwater recharge from an intermittent monsoon channel to an overexploited aquifer in eastern Haryana (India). *Environmental Earth Sciences, 75*(5), 434. doi:10.1007/s12665-015-4911-8

Bekele, E., Patterson, B., Toze, S., Furness, A., Higginson, S., & Shackleton, M. (2014). Aquifer residence times for recycled water estimated using chemical tracers and the propagation of temperature signals at a managed aquifer recharge site in Australia. *Hydrogeology Journal, 22*(6), 1383-1401. doi:10.1007/s10040-014-1142-0

Berghuijs, W. R., Woods, R. A., & Hrachowitz, M. (2014). A precipitation shift from snow towards rain leads to a decrease in streamflow. *Nature Climate Change, 4*(7), 583-586. doi:10.1038/nclimate2246

Bertelkamp, C., van der Hoek, J. P., Schoutteten, K., Hulpiau, L., Vanhaecke, L., Vanden Bussche, J., Cabo, A. J., Callewaert, C., Boon, N., Lowenberg, J., Singhal, N., & Verliefde, A. R. (2016). The effect of feed water dissolved organic carbon concentration and composition on organic micropollutant removal and microbial diversity in soil columns simulating river bank filtration. *Chemosphere, 144*, 932-939B. doi:10.1016/j.chemosphere.2015.09.017

Bertin, C., & Bourg, A. C. (1994). Radon-222 and chloride as natural tracers of the infiltration of river water into an alluvial aquifer in which there is significant river/groundwater mixing. *Environ Sci Technol, 28*(5), 794-798. doi:10.1021/es00054a008

Biehler, A., Chaillou, G., Buffin-Bélanger, T., & Baudron, P. (2020). Hydrological connectivity in the aquifer–river continuum: impact of river stages on the geochemistry of groundwater floodplains. *Journal of Hydrology, 590*, 125379. doi:10.1016/j.jhydrol.2020.125379

Bocanegra, E., Quiroz Londoño, O. M., Martínez, D. E., & Romanelli, A. (2013). Quantification of the water balance and hydrogeological processes of groundwater–lake interactions in the Pampa Plain, Argentina. *Environmental Earth Sciences, 68*(8), 2347-2357. doi:10.1007/s12665-012-1916-4

Boving, T. B., Choudri, B. S., Cady, P., Cording, A., Patil, K., & Reddy, V. (2014). Hydraulic and hydrogeochemical characteristics of a riverbank filtration site in rural India. *Water Environ Res, 86*(7), 636-648. doi:10.2175/106143013X13596524516428

Brock, B. E., Wolfe, B. B., & Edwards, T. W. D. (2007). Characterizing the Hydrology of Shallow Floodplain Lakes in the Slave River Delta, NWT, Canada, Using Water Isotope Tracers. *Arctic, Antarctic, and Alpine Research, 39*(3), 388-401. doi:10.1657/1523-0430(06-026)[BROCK]2.0.CO;2

Burke, V., Greskowiak, J., Asmuss, T., Bremermann, R., Taute, T., & Massmann, G. (2014). Temperature dependent redox zonation and attenuation of wastewater-derived organic micropollutants in the hyporheic zone. *Sci Total Environ, 482-483*, 53-61. doi:10.1016/j.scitotenv.2014.02.098

Burnet, J.-B., Dinh, Q. T., Imbeault, S., Servais, P., Dorner, S., & Prévost, M. (2019). Autonomous online measurement of β-D-glucuronidase activity in surface water: is it suitable for rapid E. coli monitoring? *Water Research, 152*, 241-250. doi:10.1016/j.watres.2018.12.060

Buzek, F., Kadlecova, R., Jackova, I., & Lnenickova, Z. (2012). Nitrate transport in the unsaturated zone: a case study of the riverbank filtration system Karany, Czech Republic. *Hydrological Processes, 26*(5), 640-651. doi:10.1002/hyp.8165

CBC News. (2017). Ottawa River full of untreated sewage during May flooding. Retrieved from https://www.cbc.ca/news/canada/ottawa/ottawa-river-full-of-untreated-sewage-1.4109239

Centre d'Expertise Hydrique du Québec. (2019). *Délimitation des bassins versants correspondant aux stations hydrométriques ouvertes et fermées*. Retrieved from: https://www.cehq.gouv.qc.ca/hydrometrie/index.htm

Centre d'Expertise Hydrique du Québec. (2020). *Niveau d'eau à la station 043108 (Lac des Deux Montagnes)*. Retrieved from: http://cehq.gouv.qc.ca/depot/historique_donnees_instantanees/043108_N_2017.txt

Cirpka, O. A., Fienen, M. N., Hofer, M., Hoehn, E., Tessarini, A., Kipfer, R., & Kitanidis, P. K. (2007). Analyzing bank filtration by deconvoluting time series of electric conductivity. *Ground water, 45*(3), 318-328. doi:10.1111/j.1745-6584.2006.00293.x

Clark, I. (2015). *Groundwater Geochemistry and Isotopes*. Boca Raton, FL: CRC Press Taylor & Francis Group.

Clausen, C. H., Dimaki, M., Bertelsen, C. V., Skands, G. E., Rodriguez-Trujillo, R., Thomsen, J. D., & Svendsen, W. E. (2018). Bacteria Detection and Differentiation Using Impedance Flow Cytometry. *Sensors (Basel), 18*(10), 3496. doi:10.3390/s18103496

Conant, B., Jr., Cherry, J. A., & Gillham, R. W. (2004). A PCE groundwater plume discharging to a river: influence of the streambed and near-river zone on contaminant distributions. *J Contam Hydrol, 73*(1-4), 249-279. doi:10.1016/j.jconhyd.2004.04.001

Cook, P., Dogramaci, S., McCallum, J., & Hedley, J. (2017). Groundwater age, mixing and flow rates in the vicinity of large open pit mines, Pilbara region, northwestern Australia. *Hydrogeology Journal, 25*(1), 39-53. doi:10.1007/s10040-016-1467-y

Craig, H., & Gordon, L. I. (1965). Deuterium and oxygen 18 variations in the ocean and the marine atmosphere. In E. Tongiorgi (Ed.), *Stable isotopes in oceanographic studies and paleotemperatures* (pp. 9-130). Lab. Geologia Nucleare, Pisa.

Cumming, G. S., Barnes, G., Perz, S., Schmink, M., Sieving, K. E., Southworth, J., Binford, M., Holt, R. D., Stickler, C., & Van Holt, T. (2005). An Exploratory Framework for the Empirical Measurement of Resilience. *Ecosystems, 8*(8), 975-987. doi:10.1007/s10021-005-0129-z

Cunha, D. G. F., Sabogal-Paz, L. P., & Dodds, W. K. (2016). Land use influence on raw surface water quality and treatment costs for drinking supply in São Paulo State (Brazil). *Ecological Engineering, 94*, 516-524. doi:10.1016/j.ecoleng.2016.06.063

Custodio, E. (2002). Aquifer overexploitation: what does it mean? *Hydrogeology Journal, 10*(2), 254-277. doi:10.1007/s10040-002-0188-6

Dash, R. R., Prakash, E. V. P. B., Kumar, P., Mehrotra, I., Sandhu, C., & Grischek, T. (2010). River bank filtration in Haridwar, India: removal of turbidity, organics and bacteria. *Hydrogeology Journal, 18*(4), 973-983. doi:10.1007/s10040-010-0574-4

de Bruin, H. A. R. (1982). Temperature and energy balance of a water reservoir determined from standard weather data of a land station. *Journal of Hydrology, 59*(3), 261-274. doi:10.1016/0022-1694(82)90091-9

de Sousa, D. N., Mozeto, A. A., Carneiro, R. L., & Fadini, P. S. (2014). Electrical conductivity and emerging contaminant as markers of surface freshwater contamination by wastewater. *Sci Total Environ, 484*, 19-26. doi:10.1016/j.scitotenv.2014.02.135

Delpla, I., Jung, A. V., Baures, E., Clement, M., & Thomas, O. (2009). Impacts of climate change on surface water quality in relation to drinking water production. *Environment International, 35*(8), 1225-1233. doi:10.1016/j.envint.2009.07.001

Derx, J., Blaschke, A. P., Farnleitner, A. H., Pang, L., Bloschl, G., & Schijven, J. F. (2013). Effects of fluctuations in river water level on virus removal by bank filtration and aquifer passage--a scenario analysis. *J Contam Hydrol, 147*, 34-44. doi:10.1016/j.jconhyd.2013.01.001

des Tombe, B. F., Bakker, M., Schaars, F., & van der Made, K. J. (2018). Estimating Travel Time in Bank Filtration Systems from a Numerical Model Based on DTS Measurements. *Ground water, 56*(2), 288-299. doi:10.1111/gwat.12581

Diao, M., Sinnige, R., Kalbitz, K., Huisman, J., & Muyzer, G. (2017). Succession of Bacterial Communities in a Seasonally Stratified Lake with an Anoxic and Sulfidic Hypolimnion. *Frontiers in Microbiology, 8*(2511). doi:10.3389/fmicb.2017.02511

Dibike, Y. B., & Coulibaly, P. (2005). Hydrologic impact of climate change in the Saguenay watershed: comparison of downscaling methods and hydrologic models. *Journal of Hydrology, 307*(1), 145-163. doi:10.1016/j.jhydrol.2004.10.012

Dillon, P., Stuyfzand, P., Grischek, T., Lluria, M., Pyne, R. D. G., Jain, R. C., Bear, J., Schwarz, J., Wang, W., Fernandez, E., Stefan, C., Pettenati, M., van der Gun, J., Sprenger, C., Massmann, G., Scanlon, B. R., Xanke, J., Jokela, P., Zheng, Y., Rossetto, R., Shamrukh, M., Pavelic, P., Murray, E., Ross, A., Valverde, J. P. B., Nava, A. P., Ansems, N., Posavec,

K., Ha, K., Martin, R., & Sapiano, M. (2019). Sixty years of global progress in managed aquifer recharge. *Hydrogeology Journal, 27*(1), 1-30. doi:10.1007/s10040-018-1841-z

Dillon, P. J., Miller, M., Fallowfield, H., & Hutson, J. (2002). The potential of riverbank filtration for drinking water supplies in relation to microsystin removal in brackish aquifers. *Journal of Hydrology, 266*(3), 209-221. doi:10.1016/S0022-1694(02)00166-X

Dragon, K., Gorski, J., Kruc, R., Drozdzynski, D., & Grischek, T. (2018). Removal of Natural Organic Matter and Organic Micropollutants during Riverbank Filtration in Krajkowo, Poland. *Water, 10*(10), 1457. doi:10.3390/w10101457

Eckert, P., & Irmscher, R. (2006). Over 130 years of experience with Riverbank Filtration in Düsseldorf, Germany. *Journal of Water Supply: Research and Technology - Aqua, 55*(4), 283-291. Retrieved from http://aqua.iwaponline.com/content/ppiwajwsrt/55/4/283.full.pdf

Edwards, T. W. D., Wolfe, B. B., Gibson, J. J., & Hammarlund, D. (2004). Use of water isotope tracers in high latitude hydrology and paleohydrology. In R. Pienitz, M. Douglas, & J. P. Smol (Eds.), *Long-term environmental change in Arctic and Antarctic Lakes, developments in paleoenvironmental research* (Vol. 7, pp. 187-207). Dordrecht, Netherlands: Springer.

Falcone, M. (2007). *Assessing hydrological processes controlling the water balance of lakes in the Peace-Athabasca Delta, Alberta, Canada using water isotope tracers.* University of Waterloo, Waterloo, Ontario, Canada. Retrieved from http://hdl.handle.net/10012/3081

Ferguson, G., & Gleeson, T. (2012). Vulnerability of coastal aquifers to groundwater use and climate change. *Nature Climate Change, 2*(5), 342-345. doi:10.1038/nclimate1413

Fiener, P., Auerswald, K., & Van Oost, K. (2011). Spatio-temporal patterns in land use and management affecting surface runoff response of agricultural catchments—A review. *Earth-Science Reviews, 106*(1), 92-104. doi:10.1016/j.earscirev.2011.01.004

Flerchinger, G. N., Cooley, K. R., & Ralston, D. R. (1992). Groundwater response to snowmelt in a mountainous watershed. *Journal of Hydrology, 133*(3), 293-311. doi:10.1016/0022-1694(92)90260-3

Frey, S. K., Gottschall, N., Wilkes, G., Gregoire, D. S., Topp, E., Pintar, K. D., Sunohara, M., Marti, R., & Lapen, D. R. (2015). Rainfall-induced runoff from exposed streambed sediments: an important source of water pollution. *J Environ Qual, 44*(1), 236-247. doi:10.2134/jeq2014.03.0122

Gibson, J. J. (2002). Short-term evaporation and water budget comparisons in shallow Arctic lakes using non-steady isotope mass balance. *Journal of Hydrology, 264*(1), 242-261. doi:10.1016/S0022-1694(02)00091-4

Gibson, J. J., Birks, S. J., Jeffries, D., & Yi, Y. (2017). Regional trends in evaporation loss and water yield based on stable isotope mass balance of lakes: The Ontario Precambrian Shield surveys. *Journal of Hydrology, 544*, 500-510. doi:10.1016/j.jhydrol.2016.11.016

Gibson, J. J., Birks, S. J., & Yi, Y. (2015). Stable isotope mass balance of lakes: a contemporary perspective. *Quaternary Science Reviews, 131*, 316-328. doi:10.1016/j.quascirev.2015.04.013

Gibson, J. J., Birks, S. J., Yi, Y., Moncur, M. C., & McEachern, P. M. (2016). Stable isotope mass balance of fifty lakes in central Alberta: Assessing the role of water balance parameters in determining trophic status and lake level. *Journal of Hydrology: Regional Studies, 6*, 13-25. doi:10.1016/j.ejrh.2016.01.034

Gibson, J. J., Edwards, T. W. D., Bursey, G. G., & Prowse, T. D. (1993). Estimating Evaporation Using Stable Isotopes: Quantitative Results and Sensitivity Analysis for Two Catchments in Northern Canada: Paper presented at the 9th Northern Res. Basin Symposium/Workshop (Whitehorse/Dawson/Inuvik, Canada - August 1992). *Hydrology Research, 24*(2-3), 79-94. doi:10.2166/nh.1993.0015

Gibson, J. J., Yi, Y., & Birks, S. J. (2019). Isotopic tracing of hydrologic drivers including permafrost thaw status for lakes across Northeastern Alberta, Canada: A 16-year, 50-lake assessment. *Journal of Hydrology: Regional Studies, 26*, 100643. doi:10.1016/j.ejrh.2019.100643

Gilfedder, B. S., Cartwright, I., Hofmann, H., & Frei, S. (2019). Explicit Modeling of Radon-222 in HydroGeoSphere During Steady State and Dynamic Transient Storage. *Ground water, 57*(1), 36-47. doi:10.1111/gwat.12847

Gillefalk, M., Massmann, G., Nutzmann, G., & Hilt, S. (2018). Potential Impacts of Induced Bank Filtration on Surface Water Quality: A Conceptual Framework for Future Research. *Water, 10*(9), 1240. doi:10.3390/w10091240

Glass, J., Li, T., Sprenger, C., & Stefan, C. (2019, 20-24 May 2019). *Investigation of viscosity effects caused by seasonal temperature fluctuations during MAR.* Paper presented at the International Symposium on Managed Aquifer, Madrid, Spain.

Glassmeyer, S. T., Furlong, E. T., Kolpin, D. W., Cahill, J. D., Zaugg, S. D., Werner, S. L., Meyer, M. T., & Kryak, D. D. (2005). Transport of chemical and microbial compounds from known wastewater discharges: potential for use as indicators of human fecal contamination. *Environ Sci Technol, 39*(14), 5157-5169. doi:10.1021/es048120k

Glorian, H., Bornick, H., Sandhu, C., & Grischek, T. (2018). Water Quality Monitoring in Northern India for an Evaluation of the Efficiency of Bank Filtration Sites. *Water, 10*(12), 1804. doi:10.3390/w10121804

Gonfiantini, R. (1986). Chapter 3 - ENVIRONMENTAL ISOTOPES IN LAKE STUDIES. In P. Fritz & J. C. Fontes (Eds.), *The Terrestrial Environment, B* (pp. 113-168). Amsterdam: Elsevier.

Government of Canada. (2009). Guidelines for Canadian Drinking Water Quality: Guideline Technical Document – Iron. Retrieved from https://www.canada.ca/en/health-canada/services/publications/healthy-living/guidelines-canadian-drinking-water-quality-guideline-technical-document-iron.html

Government of Canada. (2019). Guidelines for Canadian Drinking Water Quality: Guideline Technical Document – Manganese. Retrieved from https://www.canada.ca/en/health-canada/services/publications/healthy-living/guidelines-canadian-drinking-water-quality-guideline-technical-document-manganese.html

Gran, G. (1952). Determination of the equivalence point in potentiometric titrations. Part II. *Analyst, 77*(920), 661-671. doi:10.1039/AN9527700661

Greskowiak, J., Prommer, H., Massmann, G., & Nutzmann, G. (2006). Modeling seasonal redox dynamics and the corresponding fate of the pharmaceutical residue phenazone during artificial recharge of groundwater. *Environ Sci Technol, 40*(21), 6615-6621. doi:10.1021/es052506t

Grischek, T., & Bartak, R. (2016). Riverbed Clogging and Sustainability of Riverbank Filtration. *Water, 8*(12), 604. doi:10.3390/w8120604

Grischek, T., & Paufler, S. (2017). Prediction of Iron Release during Riverbank Filtration. *Water, 9*(5), 317. doi:10.3390/w9050317

Grischek, T., Schoenheinz, D., Syhre, C., & Saupe, K. (2010). Impact of decreasing water demand on bank filtration in Saxony, Germany. *Drinking Water Engineering and Science, 3*(1), 11-20. doi:10.5194/dwes-3-11-2010

Groeschke, M., Frommen, T., Winkler, A., & Schneider, M. (2017). Sewage-Borne Ammonium at a River Bank Filtration Site in Central Delhi, India: Simplified Flow and Reactive Transport Modeling to Support Decision-Making about Water Management Strategies. *Geosciences, 7*(3), 48. doi:10.3390/geosciences7030048

Grunheid, S., Amy, G., & Jekel, M. (2005). Removal of bulk dissolved organic carbon (DOC) and trace organic compounds by bank filtration and artificial recharge. *Water Res, 39*(14), 3219-3228. doi:10.1016/j.watres.2005.05.030

Gunkel, G., & Hoffmann, A. (2009). Bank filtration of rivers and lakes to improve the raw water quality for drinking water supply. In N. Gertsen & L. Sonderby (Eds.), *Water purification* (pp. 137-169). Hauppauge, NY: Nova Science Publishers, Inc.

Gupta, A., Singh, H., Ahmed, F., Mehrotra, I., Kumar, P., Kumar, S., Grischek, T., & Sandhu, C. (2015). Lake bank filtration in landslide debris: irregular hydrology with effective filtration. *Sustainable Water Resources Management, 1*(1), 15-26. doi:10.1007/s40899-015-0001-z

Haas, R., Opitz, R., Grischek, T., & Otter, P. (2018). The AquaNES Project: Coupling Riverbank Filtration and Ultrafiltration in Drinking Water Treatment. *Water, 11*(1), 18. doi:10.3390/w11010018

Haig, H. A., Hayes, N. M., Simpson, G. L., Yi, Y., Wissel, B., Hodder, K. R., & Leavitt, P. R. (2020). Comparison of isotopic mass balance and instrumental techniques as estimates of basin hydrology in seven connected lakes over 12 years. *Journal of Hydrology X, 6*, 100046. doi:10.1016/j.hydroa.2019.100046

Hamann, E., Stuyfzand, P. J., Greskowiak, J., Timmer, H., & Massmann, G. (2016). The fate of organic micropollutants during long-term/long-distance river bank filtration. *Sci Total Environ, 545-546*, 629-640. doi:10.1016/j.scitotenv.2015.12.057

Harvey, R. W., Metge, D. W., LeBlanc, D. R., Underwood, J., Aiken, G. R., Butler, K., McCobb, T. D., & Jasperse, J. (2015). Importance of the Colmation Layer in the Transport and Removal of Cyanobacteria, Viruses, and Dissolved Organic Carbon during Natural Lake-Bank Filtration. *J Environ Qual, 44*(5), 1413-1423. doi:10.2134/jeq2015.03.0151

Henzler, A. F., Greskowiak, J., & Massmann, G. (2016). Seasonality of temperatures and redox zonations during bank filtration – A modeling approach. *Journal of Hydrology, 535*, 282-292. doi:10.1016/j.jhydrol.2016.01.044

Herczeg, A. L., Leaney, F. W., Dighton, J. C., Lamontagne, S., Schiff, S. L., Telfer, A. L., & English, M. C. (2003). A modern isotope record of changes in water and carbon budgets in a groundwater-fed lake: Blue Lake, South Australia. *Limnology and Oceanography, 48*(6), 2093-2105. doi:10.4319/lo.2003.48.6.2093

Hiscock, K. M., & Grischek, T. (2002). Attenuation of groundwater pollution by bank filtration. *Journal of Hydrology, 266*(3-4), 139-144. doi:10.1016/S0022-1694(02)00158-0

Hoehn, E., & Cirpka, O. A. (2006). Assessing residence times of hyporheic ground water in two alluvial flood plains of the Southern Alps using water temperature and tracers. *Hydrology and Earth System Sciences, 10*(4), 553-563. doi:10.5194/hess-10-553-2006

Holtz, R. D., & Kovacs, W. D. (1981). *An Introduction to Geotechnical Engineering* (J. Lafleur, Trans. Presses internationales Polytechnique Ed.). Montreal, Canada.

Horita, J., Rozanski, K., & Cohen, S. (2008). Isotope effects in the evaporation of water: a status report of the Craig–Gordon model. *Isotopes in Environmental and Health Studies, 44*(1), 23-49. doi:10.1080/10256010801887174

Horita, J., & Wesolowski, D. J. (1994). Liquid-vapor fractionation of oxygen and hydrogen isotopes of water from the freezing to the critical temperature. *Geochimica Et Cosmochimica Acta, 58*(16), 3425-3437. doi:10.1016/0016-7037(94)90096-5

Hu, B., Teng, Y. G., Zhai, Y. Z., Zuo, R., Li, J., & Chen, H. Y. (2016). Riverbank filtration in China: A review and perspective. *Journal of Hydrology, 541*, 914-927. doi:10.1016/j.jhydrol.2016.08.004

Hughes, C. E., & Crawford, J. (2012). A new precipitation weighted method for determining the meteoric water line for hydrological applications demonstrated using Australian and global GNIP data. *Journal of Hydrology, 464-465*, 344-351. doi:10.1016/j.jhydrol.2012.07.029

Hunt, R. J., Coplen, T. B., Haas, N. L., Saad, D. A., & Borchardt, M. A. (2005). Investigating surface water-well interaction using stable isotope ratios of water. *Journal of Hydrology, 302*(1-4), 154-172. doi:10.1016/j.jhydrol.2004.07.010

IAEA/WMO. (2018). *Global Network of Isotopes in Precipitation. The GNIP Database.* Retrieved from: https://nucleus.iaea.org/wiser

IGRAC. (2021). Global Inventory of MAR Schemes - MAR Portal. Retrieved March 4th 2021, from https://www.un-igrac.org/ggis/mar-portal

Isokangas, E., Rozanski, K., Rossi, P. M., Ronkanen, A. K., & Kløve, B. (2015). Quantifying groundwater dependence of a sub-polar lake cluster in Finland using an isotope mass balance approach. *Hydrol. Earth Syst. Sci., 19*(3), 1247-1262. doi:10.5194/hess-19-1247-2015

Jalliffier-Verne, I., Heniche, M., Madoux-Humery, A. S., Galarneau, M., Servais, P., Prevost, M., & Dorner, S. (2016). Cumulative effects of fecal contamination from combined sewer

overflows: Management for source water protection. *J Environ Manage, 174*, 62-70. doi:10.1016/j.jenvman.2016.03.002

Jasechko, S., Wassenaar, L. I., & Mayer, B. (2017). Isotopic evidence for widespread cold-season-biased groundwater recharge and young streamflow across central Canada. *Hydrological Processes, 31*(12), 2196-2209. doi:10.1002/hyp.11175

Jasperse, J. (2011). Planning, Design and Operations of Collector 6, Sonoma County Water Agency. In C. Ray & M. Shamrukh (Eds.), *Riverbank Filtration for Water Security in Desert Countries. NATO Science for Peace and Security Series C: Environmental Security.* (pp. 169-202). Dordrecht: Springer.

Jeppesen, E., Meerhoff, M., Davidson, T. A., Trolle, D., SondergaarD, M., Lauridsen, T. L., Beklioglu, M., Brucet Balmaña, S., Volta, P., & González-Bergonzoni, I. (2014). Climate change impacts on lakes: an integrated ecological perspective based on a multi-faceted approach, with special focus on shallow lakes. *Journal of Limnology, 73*, 88-111. doi:10.4081/jlimnol.2014.844

Jiang, Y., Zhang, J. J., Zhu, Y. G., Du, Q. Q., Teng, Y. G., & Zhai, Y. Z. (2019). Design and Optimization of a Fully-Penetrating Riverbank Filtration Well Scheme at a Fully-Penetrating River Based on Analytical Methods. *Water, 11*(3), 418. doi:10.3390/w11030418

Johnson, A. N., Boer, B. R., Woessner, W. W., Stanford, J. A., Poole, G. C., Thomas, S. A., & O'Daniel, S. J. (2005). Evaluation of an Inexpensive Small-Diameter Temperature Logger for Documenting Ground Water-River Interactions. *Groundwater Monitoring & Remediation, 25*(4), 68-74. doi:10.1111/j.1745-6592.2005.00049.x

Jones, M. D., Cuthbert, M. O., Leng, M. J., McGowan, S., Mariethoz, G., Arrowsmith, C., Sloane, H. J., Humphrey, K. K., & Cross, I. (2016). Comparisons of observed and modelled lake $\delta^{18}O$ variability. *Quaternary Science Reviews, 131*, 329-340. doi:10.1016/j.quascirev.2015.09.012

Kapnick, S., & Hall, A. (2012). Causes of recent changes in western North American snowpack. *Climate Dynamics, 38*(9), 1885-1899. doi:10.1007/s00382-011-1089-y

Karakurt, S., Schmid, L., Hubner, U., & Drewes, J. E. (2019). Dynamics of Wastewater Effluent Contributions in Streams and Impacts on Drinking Water Supply via Riverbank Filtration in Germany-A National Reconnaissance. *Environ Sci Technol, 53*(11), 6154-6161. doi:10.1021/acs.est.8b07216

Kloppmann, W., Chikurel, H., Picot, G., Guttman, J., Pettenati, M., Aharoni, A., Guerrot, C., Millot, R., Gaus, I., & Wintgens, T. (2009). B and Li isotopes as intrinsic tracers for injection tests in aquifer storage and recovery systems. *Applied Geochemistry, 24*(7), p. 1214-1223. doi:10.1016/j.apgeochem.2009.03.006

Kløve, B., Ala-aho, P., Bertrand, G., Boukalova, Z., Ertürk, A., Goldscheider, N., Ilmonen, J., Karakaya, N., Kupfersberger, H., Kvœrner, J., Lundberg, A., Mileusnić, M., Moszczynska, A., Muotka, T., Preda, E., Rossi, P., Siergieiev, D., Šimek, J., Wachniew, P., Angheluta, V., & Widerlund, A. (2011). Groundwater dependent ecosystems. Part I: Hydroecological

status and trends. *Environmental Science & Policy, 14*(7), 770-781. doi:10.1016/j.envsci.2011.04.002

Kvitsand, H. M. L., Myrmel, M., Fiksdal, L., & Østerhus, S. W. (2017). Evaluation of bank filtration as a pretreatment method for the provision of hygienically safe drinking water in Norway: results from monitoring at two full-scale sites. *Hydrogeology Journal, 25*(5), 1257-1269. doi:10.1007/s10040-017-1576-2

Larocque, M., Meyzonnat, G., Ouellet, M. A., Graveline, M. H., Gagné, S., Barnetche, D., & Dorner, S. (2015). *Projet de connaissance des eaux souterraines de la zone de Vaudreuil-Soulanges - Rapport scientifique*. Retrieved from Quebec:

Lerner, D. N., & Harris, B. (2009). The relationship between land use and groundwater resources and quality. *Land Use Policy, 26*, S265-S273. doi:10.1016/j.landusepol.2009.09.005

Leveque, B., Burnet, J. B., Dorner, S., & Bichai, F. (2021). Impact of climate change on the vulnerability of drinking water intakes in a northern region. *Sustainable Cities and Society, 66*, 102656. doi:10.1016/j.scs.2020.102656

Linacre, E. T. (1977). A simple formula for estimating evaporation rates in various climates, using temperature data alone. *Agricultural Meteorology, 18*(6), 409-424. doi:10.1016/0002-1571(77)90007-3

Liu, S. D., Zhou, Y. X., Kamps, P., Smits, F., & Olsthoorn, T. (2019). Effect of temperature variations on the travel time of infiltrating water in the Amsterdam Water Supply Dunes (the Netherlands). *Hydrogeology Journal, 27*(6), 2199-2209. doi:10.1007/s10040-019-01976-3

Lopez-Pacheco, I. Y., Silva-Nunez, A., Salinas-Salazar, C., Arevalo-Gallegos, A., Lizarazo-Holguin, L. A., Barcelo, D., Iqbal, H. M. N., & Parra-Saldivar, R. (2019). Anthropogenic contaminants of high concern: Existence in water resources and their adverse effects. *Sci Total Environ, 690*, 1068-1088. doi:10.1016/j.scitotenv.2019.07.052

Lorenzen, G., Sprenger, C., Baudron, P., Gupta, D., & Pekdeger, A. (2012). Origin and dynamics of groundwater salinity in the alluvial plains of western Delhi and adjacent territories of Haryana State, India. *Hydrological Processes, 26*(15), 2333-2345. doi:10.1002/hyp.8311

Lorenzen, G., Sprenger, C., Taute, T., Pekdeger, A., Mittal, A., & Massmann, G. (2010). Assessment of the potential for bank filtration in a water-stressed megacity (Delhi, India). *Environmental Earth Sciences, 61*(7), 1419-1434. doi:10.1007/s12665-010-0458-x

Madoux-Humery, A. S., Dorner, S., Sauve, S., Aboulfadl, K., Galarneau, M., Servais, P., & Prevost, M. (2013). Temporal variability of combined sewer overflow contaminants: evaluation of wastewater micropollutants as tracers of fecal contamination. *Water Res, 47*(13), 4370-4382. doi:10.1016/j.watres.2013.04.030

Maggioni, E. (2014). Water demand management in times of drought: What matters for water conservation. *Water Resources Research, 51*(1), 125-139. doi:10.1002/2014WR016301

Maliva, R. G. (2020). *Anthropogenic Aquifer Recharge: WSP methods in water resources evaluation series no. 5*: Springer, Cham.

Maloszewski, P. (2000). *Lumped-parameter models as a tool for determining the hydrological parameters of some groundwater systems based on isotope data.* Paper presented at the TraM'2000: The International Conference on 'Tracers and Modelling in Hydrology', May 23, 2000 - May 26, 2000, Liege, Belgium.

Martin, A. R., Coombes, P. J., Harrison, T. L., & Hugh Dunstan, R. (2010). Changes in abundance of heterotrophic and coliform bacteria resident in stored water bodies in relation to incoming bacterial loads following rain events. *J Environ Monit, 12*(1), 255-260. doi:10.1039/b904042k

Masoner, J. R., Kolpin, D. W., Cozzarelli, I. M., Barber, L. B., Burden, D. S., Foreman, W. T., Forshay, K. J., Furlong, E. T., Groves, J. F., Hladik, M. L., Hopton, M. E., Jaeschke, J. B., Keefe, S. H., Krabbenhoft, D. P., Lowrance, R., Romanok, K. M., Rus, D. L., Selbig, W. R., Williams, B. H., & Bradley, P. M. (2019). Urban Stormwater: An Overlooked Pathway of Extensive Mixed Contaminants to Surface and Groundwaters in the United States. *Environ Sci Technol, 53*(17), 10070-10081. doi:10.1021/acs.est.9b02867

Masse-Dufresne, J., Barbecot, F., Baudron, P., & Gibson, J. (2021a). Quantifying floodwater impacts on a lake water budget via volume-dependent transient stable isotope mass balance. *Hydrol. Earth Syst. Sci.*(25), 3731–3757. doi:10.5194/hess-25-3731-2021

Masse-Dufresne, J., Baudron, P., Barbecot, F., Pasquier, P., & Barbeau, B. (2021b). Optimizing short time-step monitoring and management strategies using environmental tracers at flood-affected bank filtration sites. *Science of The Total Environment, 750*, 141429. doi:10.1016/j.scitotenv.2020.141429

Masse-Dufresne, J., Baudron, P., Barbecot, F., Pasquier, P., Barbeau, B., Patenaude, M., Pontoreau, C., & Proteau-Bédard, F. (2019a). Anticipating pathways and timing for cyanobacteria breakthrough at a 2-lake bank filtration site via environmental tracers. In Enrique Fernández E. Tragsa Group (Ed.), *Proceedings of the International Symposium on Managed Aquifer Recharge (ISMAR 10) - Managed Aquifer Recharge: Local solutions to the global water crisis* (pp. 657-659). Madrid, Spain.

Masse-Dufresne, J., Baudron, P., Barbecot, F., Patenaude, M., Pontoreau, C., Proteau-Bedard, F., Menou, M., Pasquier, P., Veuille, S., & Barbeau, B. (2019b). Anthropic and Meteorological Controls on the Origin and Quality of Water at a Bank Filtration Site in Canada. *Water, 11*(12), 2510. doi:10.3390/w11122510

Massmann, G., Greskowiak, J., Dunnbier, U., Zuehlke, S., Knappe, A., & Pekdeger, A. (2006). The impact of variable temperatures on the redox conditions and the behaviour of pharmaceutical residues during artificial recharge. *Journal of Hydrology, 328*(1-2), 141-156. doi:10.1016/j.jhydrol.2005.12.009

Massmann, G., Sultenfuss, J., Dunnbier, U., Knappe, A., Taute, T., & Pekdeger, A. (2008). Investigation of groundwater a residence times during bank filtration in Berlin: multi-tracer approach. *Hydrological Processes, 22*(6), 788-801. doi:10.1002/hyp.6649

Mayo, A. L. (2010). Ambient well-bore mixing, aquifer cross-contamination, pumping stress, and water quality from long-screened wells: What is sampled and what is not? *Hydrogeology Journal, 18*(4), 823-837. doi:10.1007/s10040-009-0568-2

McJannet, D. L., Webster, I. T., & Cook, F. J. (2012). An area-dependent wind function for estimating open water evaporation using land-based meteorological data. *Environmental Modelling & Software, 31*, 76-83. doi:10.1016/j.envsoft.2011.11.017

MDDELCC. (2015). *Portrait sommaire du bassin versant de la rivière des Outaouais*. Retrieved from http://www.environnement.gouv.qc.ca/eau/bassinversant/bassins/outaouais/portrait-sommaire.pdf

Miller, M. P., Susong, D. D., Shope, C. L., Heilweil, V. M., & Stolp, B. J. (2014). Continuous estimation of baseflow in snowmelt-dominated streams and rivers in the Upper Colorado River Basin: A chemical hydrograph separation approach. *Water Resources Research, 50*(8), 6986-6999. doi:https://doi.org/10.1002/2013WR014939

Ministère de l'Environnement du Québec (Cartographer). (1985). Relevés topographiques des lacs. Carte C-9809

Ministère de l'Énergie et des Ressources naturelles du Québec. (2018). Géologie du quaternaire - Jeux de données géographiques (Surface sediments polygons). Retrieved from http://gq.mines.gouv.qc.ca/documents/SIGEOM/TOUTQC/FRA/SHP/SIGEOM_QC_Geologie_du_Quaternaire_SHP.zip. from Données Québec http://gq.mines.gouv.qc.ca/documents/SIGEOM/TOUTQC/FRA/SHP/SIGEOM_QC_Geologie_du_Quaternaire_SHP.zip

Ministère des Forêts, de la Faune et des P. (2020). *LiDAR - Modèle numétique de terrain*.

Minville, M., Brissette, F., & Leconte, R. (2008). Uncertainty of the impact of climate change on the hydrology of a nordic watershed. *Journal of Hydrology, 358*(1), 70-83. doi:10.1016/j.jhydrol.2008.05.033

Molle, F., López-Gunn, E., & van Steenbergen, F. (2018). The local and national politics of groundwater overexploitation. *Water Alternatives, 11*(3), 445.

Monsen, N. E., Cloern, J. E., Lucas, L. V., & Monismith, S. G. (2002). A comment on the use of flushing time, residence time, and age as transport time scales. *Limnology and Oceanography, 47*(5), 1545-1553. doi:10.4319/lo.2002.47.5.1545

Mueller, H., Hamilton, D. P., & Doole, G. J. (2016). Evaluating services and damage costs of degradation of a major lake ecosystem. *Ecosystem Services, 22*, 370-380. doi:10.1016/j.ecoser.2016.02.037

Munz, M., Oswald, S. E., Schafferling, R., & Lensing, H. J. (2019). Temperature-dependent redox zonation, nitrate removal and attenuation of organic micropollutants during bank filtration. *Water Res, 162*, 225-235. doi:10.1016/j.watres.2019.06.041

Musche, F., Sandhu, C., Grischek, T., Patwal, P. S., Kimothi, P. C., & Heisler, A. (2018). A field study on the construction of a flood-proof riverbank filtration well in India – Challenges and opportunities. *International Journal of Disaster Risk Reduction, 31*, 489-497. doi:10.1016/j.ijdrr.2018.06.003

Mustafa, S., Bahar, A., Aziz, Z. A., & Suratman, S. (2016). Modelling contaminant transport for pumping wells in riverbank filtration systems. *Journal of Environmental Management, 165*, 159-166. doi:10.1016/j.jenvman.2015.09.026

Nagy-Kovacs, Z., Laszlo, B., Fleit, E., Czihat-Martonne, K., Till, G., Bornick, H., Adomat, Y., & Grischek, T. (2018). Behavior of Organic Micropollutants During River Bank Filtration in Budapest, Hungary. *Water, 10*(12), 1861. doi:10.3390/w10121861

Nagy-Kovács, Z., László, B., Simon, E., & Fleit, E. (2018). Operational Strategies and Adaptation of RBF Well Construction to Cope with Climate Change Effects at Budapest, Hungary. *Water, 10*(12), 1751.

Nannou, C., Ofrydopoulou, A., Evgenidou, E., Heath, D., Heath, E., & Lambropoulou, D. (2020). Antiviral drugs in aquatic environment and wastewater treatment plants: A review on occurrence, fate, removal and ecotoxicity. *Sci Total Environ, 699*, 134322. doi:10.1016/j.scitotenv.2019.134322

O'Neil, J. R. (1968). Hydrogen and oxygen isotope fractionation between ice and water. *The Journal of Physical Chemistry, 72*(10), 3683-3684. doi:10.1021/j100856a060

Otter, P., Malakar, P., Sandhu, C., Grischek, T., Sharma, S. K., Kimothi, P. C., Nuske, G., Wagner, M., Goldmaier, A., & Benz, F. (2019). Combination of River Bank Filtration and Solar-driven Electro-Chlorination Assuring Safe Drinking Water Supply for River Bound Communities in India. *Water, 11*(1), 122. doi:10.3390/w11010122

Patenaude, M., Baudron, P., Labelle, L., & Masse-Dufresne, J. (2020). Evaluating Bank-Filtration Occurrence in the Province of Quebec (Canada) with a GIS Approach. *Water, 12*(3), 662. doi:10.3390/w12030662

Patenaude, M., Baudron, P., Masse-Dufresne, J., Pontoreau, C., & Dion, G. (2019). A GIS approach to evaluating bank-filtration occurence and potential in the province of Quebec, Canada. In Enrique Fernández E. Tragsa Group (Ed.), *Proceedings of the International Symposium on Managed Aquifer Recharge (ISMAR 10) - Managed Aquifer Recharge: Local solutions to the global water crisis* (pp. 245-247). Madrid, Spain.

Pazouki, P., Prevost, M., McQuaid, N., Barbeau, B., de Boutray, M. L., Zamyadi, A., & Dorner, S. (2016). Breakthrough of cyanobacteria in bank filtration. *Water Res, 102*, 170-179. doi:10.1016/j.watres.2016.06.037

Pernica, P. M. (2014). *Implications of Periodic Weak Thermal Stratification in the Epilimnion of Lake Opeongo.* (Doctor of Philosophy). University of Toronto,

Petermann, E., Gibson, J. J., Knöller, K., Pannier, T., Weiß, H., & Schubert, M. (2018). Determination of groundwater discharge rates and water residence time of groundwater-fed lakes by stable isotopes of water (18O, 2H) and radon (222Rn) mass balances. *Hydrological Processes, 32*(6), 805-816. doi:10.1002/hyp.11456

Pholkern, K., Srisuk, K., Grischek, T., Soares, M., Schafer, S., Archwichai, L., Saraphirom, P., Pavelic, P., & Wirojanagud, W. (2015). Riverbed clogging experiments at potential river bank filtration sites along the Ping River, Chiang Mai, Thailand. *Environmental Earth Sciences, 73*(12), 7699-7709. doi:10.1007/s12665-015-4160-x

Ray, C., Melin, G., & Linsky, R. B. (2003). *Riverbank filtration: improving source-water quality* (Vol. 43): Springer Science & Business Media.

Ray, C., Soong, T. W., Lian, Y. Q., & Roadcap, G. S. (2002). Effect of flood-induced chemical load on filtrate quality at bank filtration sites. *Journal of Hydrology, 266*(3-4), 235-258. doi:10.1016/S0022-1694(02)00168-3

Reemtsma, T., Berger, U., Arp, H. P., Gallard, H., Knepper, T. P., Neumann, M., Quintana, J. B., & Voogt, P. (2016). Mind the Gap: Persistent and Mobile Organic Compounds-Water Contaminants That Slip Through. *Environ Sci Technol, 50*(19), 10308-10315. doi:10.1021/acs.est.6b03338

Regnery, J., Barringer, J., Wing, A. D., Hoppe-Jones, C., Teerlink, J., & Drewes, J. E. (2015). Start-up performance of a full-scale riverbank filtration site regarding removal of DOC, nutrients, and trace organic chemicals. *Chemosphere, 127*, 136-142. doi:10.1016/j.chemosphere.2014.12.076

Ren, W., Su, X., Zhang, X., Chen, Y., & Shi, Y. (2019). Influence of hydraulic gradient and temperature on the migration of E. coli in saturated porous media during bank filtration: a case study at the Second Songhua River, Songyuan, Northeastern China. *Environmental Geochemistry and Health*. doi:10.1007/s10653-019-00459-4

Romero, L. G., Mondardo, R. I., Sens, M. L., & Grischek, T. (2014). Removal of cyanobacteria and cyanotoxins during lake bank filtration at Lagoa do Peri, Brazil. *Clean Technologies and Environmental Policy, 16*(6), 1133-1143. doi:10.1007/s10098-014-0715-x

Ronghang, M., Gupta, A., Mehrotra, I., Kumar, P., Patwal, P., Kumar, S., Grischek, T., & Sandhu, C. (2019). Riverbank filtration: a case study of four sites in the hilly regions of Uttarakhand, India. *Sustainable Water Resources Management, 5*(2), 831-845. doi:10.1007/s40899-018-0255-3

Rosa, E., Hillaire-Marcel, C., Hélie, J.-F., & Myre, A. (2016). Processes governing the stable isotope composition of water in the St. Lawrence river system, Canada. *Isotopes in Environmental and Health Studies, 52*(4-5), 370-379. doi:10.1080/10256016.2015.1135138

Rose, A. K., Fabbro, L., & Kinnear, S. (2018). Cyanobacteria breakthrough: Effects of Limnothrix redekei contamination in an artificial bank filtration on a regional water supply. *Harmful Algae, 76*, 1-10. doi:10.1016/j.hal.2018.04.010

Rosen, M. R. (2015). The Influence of Hydrology on Lacustrine Sediment Contaminant Records. In J. M. Blais, M. R. Rosen, & J. P. Smol (Eds.), *Environmental Contaminants: Using natural archives to track sources and long-term trends of pollution* (pp. 5-33). Dordrecht: Springer Netherlands.

Rosenberry, D. O., Lewandowski, J., Meinikmann, K., & Nützmann, G. (2015). Groundwater - the disregarded component in lake water and nutrient budgets. Part 1: effects of groundwater on hydrology. *Hydrological Processes, 29*(13), 2895-2921. doi:10.1002/hyp.10403

Ross, A., & Hasnain, S. (2018). Factors affecting the cost of managed aquifer recharge (MAR) schemes. *Sustainable Water Resources Management, 4*(2), 179-190. doi:10.1007/s40899-017-0210-8

Rouhani, H., & Leconte, R. (2018). A methodological framework to assess PMP and PMF in snow-dominated watersheds under changing climate conditions – A case study of three

watersheds in Québec (Canada). *Journal of Hydrology, 561*, 796-809. doi:10.1016/j.jhydrol.2018.04.047

Roy, L., Leconte, R., Brissette, F. P., & Marche, C. (2001). The impact of climate change on seasonal floods of a southern Quebec River Basin. *Hydrological Processes, 15*(16), 3167-3179. doi:10.1002/hyp.323

Rozanski, K., Araguás-Araguás, L., & Gonfiantini, R. (2013). Isotopic Patterns in Modern Global Precipitation. In *Climate Change in Continental Isotopic Records* (pp. 1-36).

Sahu, R. L., Dash, R. R., Pradhan, P. K., & Das, P. (2019). Effect of hydrogeological factors on removal of turbidity during river bank filtration: Laboratory and field studies. *Groundwater for Sustainable Development, 9*, 100229. doi:10.1016/j.gsd.2019.100229

Salinger, M. J. (2005). Climate Variability and Change: Past, Present and Future – An Overview. *Climatic Change, 70*(1), 9-29. doi:10.1007/s10584-005-5936-x

Sandhu, C., Grischek, T., Kimothi, P. C., & Patwal, P. (2013). *Guidelines for flood-risk management of bank filtration schemes during monsoon in India*. Retrieved from http://www.saphpani.eu/fileadmin/uploads/Administrator/Deliverables/Saph_Pani_D1_2_Guidelines_for_flood-risk_managementof_bank_filtration_schemes_during_monsoon_in_India.pdf

Sandhu, C., Grischek, T., Musche, F., Macheleidt, W., Heisler, A., Handschak, J., Patwal, P. S., & Kimothi, P. C. (2018). Measures to mitigate direct flood risks at riverbank filtration sites with a focus on India. *Sustainable Water Resources Management, 4*(2), 237-249. doi:10.1007/s40899-017-0146-z

Scanlon, B. R., Reedy, R. C., Stonestrom, D. A., Prudic, D. E., & Dennehy, K. F. (2005). Impact of land use and land cover change on groundwater recharge and quality in the southwestern US. *Global Change Biology, 11*(10), 1577-1593. doi:10.1111/j.1365-2486.2005.01026.x

Schallenberg, M., de Winton, M. D., Verburg, P., Kelly, D. J., Hamill, K. D., & Hamilton, D. P. (2013). Ecosystem services of lakes. In J. R. Dymond (Ed.), *Ecosystem services in New Zealand: conditions and trends. Manaaki Whenua Press, Lincoln* (pp. 203-225). Lincoln, New Zealand: Manaaki Whenua Press.

Schubert, J. (2002). Hydraulic aspects of riverbank filtration—field studies. *Journal of Hydrology, 266*(3-4), 145-161. doi:10.1016/s0022-1694(02)00159-2

Schwarzenbach, R. P., Egli, T., Hofstetter, T. B., von Gunten, U., & Wehrli, B. (2010). Global Water Pollution and Human Health. *Annual Review of Environment and Resources, Vol 35, 35*(1), 109-136. doi:10.1146/annurev-environ-100809-125342

Shamrukh, M., & Abdel-Wahab, A. (2008). Riverbank filtration for sustainable water supply: application to a large-scale facility on the Nile River. *Clean Technologies and Environmental Policy, 10*(4), 351-358. doi:10.1007/s10098-007-0143-2

Sheets, R. A., Darner, R. A., & Whitteberry, B. L. (2002). Lag times of bank filtration at a well field, Cincinnati, Ohio, USA. *Journal of Hydrology, 266*(3), 162-174. doi:10.1016/S0022-1694(02)00164-6

Sjerps, R. M. A., Vughs, D., van Leerdam, J. A., Ter Laak, T. L., & van Wezel, A. P. (2016). Data-driven prioritization of chemicals for various water types using suspect screening LC-HRMS. *Water Res, 93*, 254-264. doi:10.1016/j.watres.2016.02.034

Snyder, S. A., & Benotti, M. J. (2010). Endocrine disruptors and pharmaceuticals: implications for water sustainability. *Water Sci Technol, 61*(1), 145-154. doi:10.2166/wst.2010.791

Sprenger, C. (2016). *Hydraulic characterisation of managed aquifer recharge sites by tracer techniques*. Retrieved from Berlin, Germany: https://pdfs.semanticscholar.org/4786/c43822f6d5a39b09c6f4496a977f7f156902.pdf

Sprenger, C., Hartog, N., Hernández, M., Vilanova, E., Grützmacher, G., Scheibler, F., & Hannappel, S. (2017). Inventory of managed aquifer recharge sites in Europe: historical development, current situation and perspectives. *Hydrogeology Journal, 25*(6), 1909-1922. doi:10.1007/s10040-017-1554-8

Sprenger, C., Lorenzen, G., Hulshoff, I., Grutzmacher, G., Ronghang, M., & Pekdeger, A. (2011). Vulnerability of bank filtration systems to climate change. *Sci Total Environ, 409*(4), 655-663. doi:10.1016/j.scitotenv.2010.11.002

Stefan, C., & Ansems, N. (2018). Web-based global inventory of managed aquifer recharge applications. *Sustainable Water Resources Management, 4*(2), 153-162. doi:10.1007/s40899-017-0212-6

Teufel, B., Sushama, L., Huziy, O., Diro, G. T., Jeong, D. I., Winger, K., Garnaud, C., de Elia, R., Zwiers, F. W., Matthews, H. D., & Nguyen, V. T. V. (2019). Investigation of the mechanisms leading to the 2017 Montreal flood. *Climate Dynamics, 52*(7), 4193-4206. doi:10.1007/s00382-018-4375-0

Tufenkji, N., Ryan, J. N., & Elimelech, M. (2002). The promise of bank filtration. *Environ Sci Technol, 36*(21), 422A-428A. doi:10.1021/es022441j

Turner, K. W., Wolfe, B. B., & Edwards, T. W. D. (2010). Characterizing the role of hydrological processes on lake water balances in the Old Crow Flats, Yukon Territory, Canada, using water isotope tracers. *Journal of Hydrology, 386*(1), 103-117. doi:10.1016/j.jhydrol.2010.03.012

Valiantzas, J. D. (2006). Simplified versions for the Penman evaporation equation using routine weather data. *Journal of Hydrology, 331*(3), 690-702. doi:10.1016/j.jhydrol.2006.06.012

van Driezum, I. H., Chik, A. H. S., Jakwerth, S., Lindner, G., Farnleitner, A. H., Sommer, R., Blaschke, A. P., & Kirschner, A. K. T. (2018). Spatiotemporal analysis of bacterial biomass and activity to understand surface and groundwater interactions in a highly dynamic riverbank filtration system. *Sci Total Environ, 627*, 450-461. doi:10.1016/j.scitotenv.2018.01.226

van Driezum, I. H., Derx, J., Oudega, T. J., Zessner, M., Naus, F. L., Saracevic, E., Kirschner, A. K. T., Sommer, R., Farnleitner, A. H., & Blaschke, A. P. (2019). Spatiotemporal resolved sampling for the interpretation of micropollutant removal during riverbank filtration. *Sci Total Environ, 649*, 212-223. doi:10.1016/j.scitotenv.2018.08.300

Vogt, T., Hoehn, E., Schneider, P., Freund, A., Schirmer, M., & Cirpka, O. A. (2010). Fluctuations of electrical conductivity as a natural tracer for bank filtration in a losing stream. *Advances in Water Resources, 33*(11), 1296-1308. doi:10.1016/j.advwatres.2010.02.007

Walsh, J. R., Carpenter, S. R., & Vander Zanden, M. J. (2016). Invasive species triggers a massive loss of ecosystem services through a trophic cascade. *Proceedings of the National Academy of Sciences, 113*(15), 4081. doi:10.1073/pnas.1600366113

Wang, X.-j., Zhang, J.-y., Gao, J., Shahid, S., Xia, X.-h., Geng, Z., & Tang, L. (2018). The new concept of water resources management in China: ensuring water security in changing environment. *Environment, Development and Sustainability, 20*(2), 897-909. doi:10.1007/s10668-017-9918-8

Weiss, W. J. (2004). Water quality improvements during riverbank filtration: Fate of disinfection by-product precursors, pathogens, and potential surrogates.

Weiss, W. J., Bouwer, E. J., Aboytes, R., LeChevallier, M. W., O'Melia, C. R., Le, B. T., & Schwab, K. J. (2005). Riverbank filtration for control of microorganisms: results from field monitoring. *Water Res, 39*(10), 1990-2001. doi:10.1016/j.watres.2005.03.018

Welch, C., Smith, A. A., & Stadnyk, T. A. (2018). Linking physiography and evaporation using the isotopic composition of river water in 16 Canadian boreal catchments. *Hydrological Processes, 32*(2), 170-184. doi:10.1002/hyp.11396

Wett, B., Jarosch, H., & Ingerle, K. (2002). Flood induced infiltration affecting a bank filtrate well at the River Enns, Austria. *Journal of Hydrology, 266*(3-4), 222-234. doi:10.1016/S0022-1694(02)00167-1

Wheaton, E., Koshida, G., Bonsal, B., Johnston, T., Richards, W., & Wittrock, V. (2007). *Agricultural Adaptation to Drought (ADA) in Canada: The Case of 2001 to 2002* (11927-1E07). Retrieved from Saskatoon, SK Canada:

Whitehead, P. G., Wilby, R. L., Battarbee, R. W., Kernan, M., & Wade, A. J. (2009). A review of the potential impacts of climate change on surface water quality. *Hydrological Sciences Journal-Journal Des Sciences Hydrologiques, 54*(1), 101-123. doi:10.1623/hysj.54.1.101

Wolfe, B. B., Karst-Riddoch, T. L., Hall, R. I., Edwards, T. W. D., English, M. C., Palmini, R., McGowan, S., Leavitt, P. R., & Vardy, S. R. (2007). Classification of hydrological regimes of northern floodplain basins (Peace–Athabasca Delta, Canada) from analysis of stable isotopes (δ18O, δ2H) and water chemistry. *Hydrological Processes, 21*(2), 151-168. doi:10.1002/hyp.6229

World Health Organization. (2017). *Guidelines for drinking-water quality: fourth edition incorporating first addendum* (4th ed + 1st add ed.). Geneva: World Health Organization.

Zamyadi, A., Choo, F., Newcombe, G., Stuetz, R., & Henderson, R. K. (2016). A review of monitoring technologies for real-time management of cyanobacteria: Recent advances and future direction. *Trac-Trends in Analytical Chemistry, 85*, 83-96. doi:10.1016/j.trac.2016.06.023

Zhu, Y. G., Zhai, Y. Z., Du, Q. Q., Teng, Y. G., Wang, J. S., & Yang, G. (2019). The impact of well drawdowns on the mixing process of river water and groundwater and water quality

in a riverside well field, Northeast China. *Hydrological Processes, 33*(6), 945-961. doi:10.1002/hyp.13376

Zimmermann, U. (1979). Determination by stable isotopes of underground inflow and outflow and evaporation of young artificial groundwater lakes. In *Isotopes in lakes studies* (pp. 87-94). Vienna, Austria: IAEA.

APPENDIX A COMPLEMENTARY HYDROGEOLOGICAL DATA

Figure A1 shows the quaternary sediments in the vicinity of the study site, according to the Ministère de l'Énergie et des Ressources naturelles du Québec (2018). Figure A1 also shows the presumed extent and limits of the paleo-channel, as interpreted by Ageos (2010)

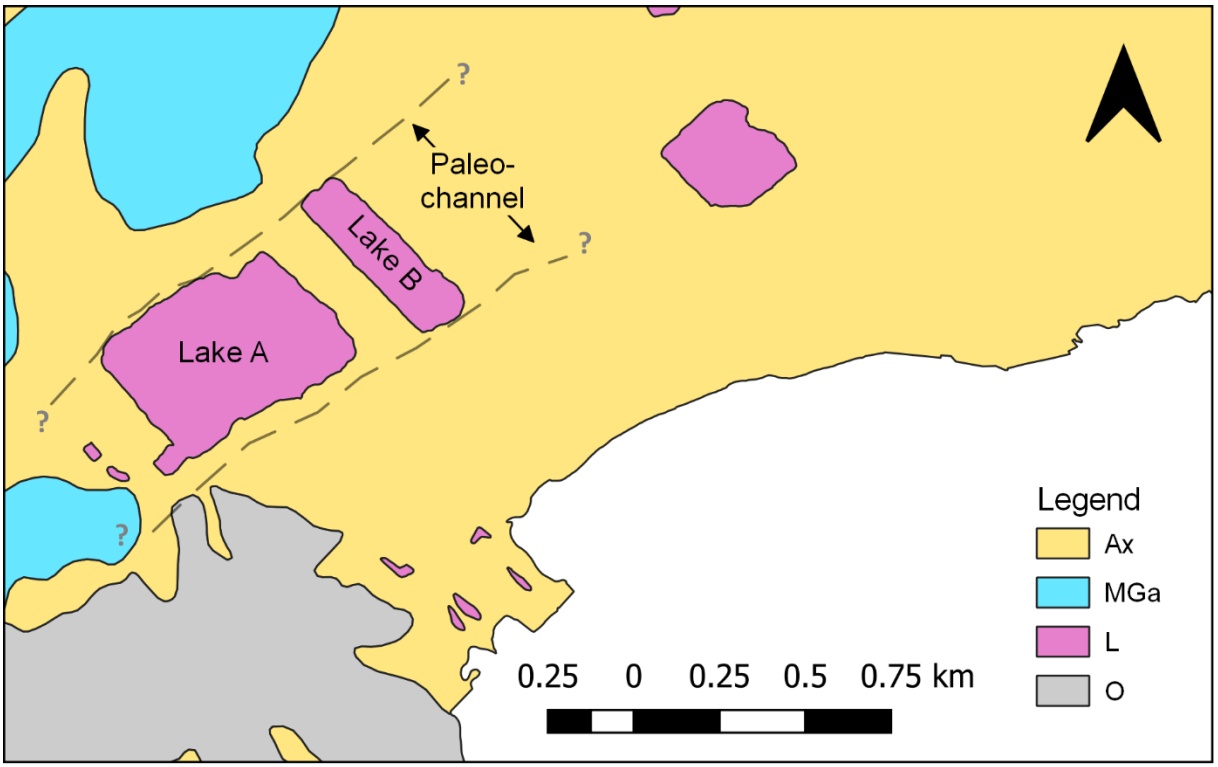

Ax: Ancient river terrace alluvial deposit
MGa: Deep-water fine-grained glaciomarine sediment
L: Lacustrine sediment (undifferentiated)
O: Undifferentiated organic sediment

Figure A1. Surface sediments at the study site and localisation of the paleo-channel (adapted from Ministère de l'Énergie et des Ressources naturelles du Québec, 2018).

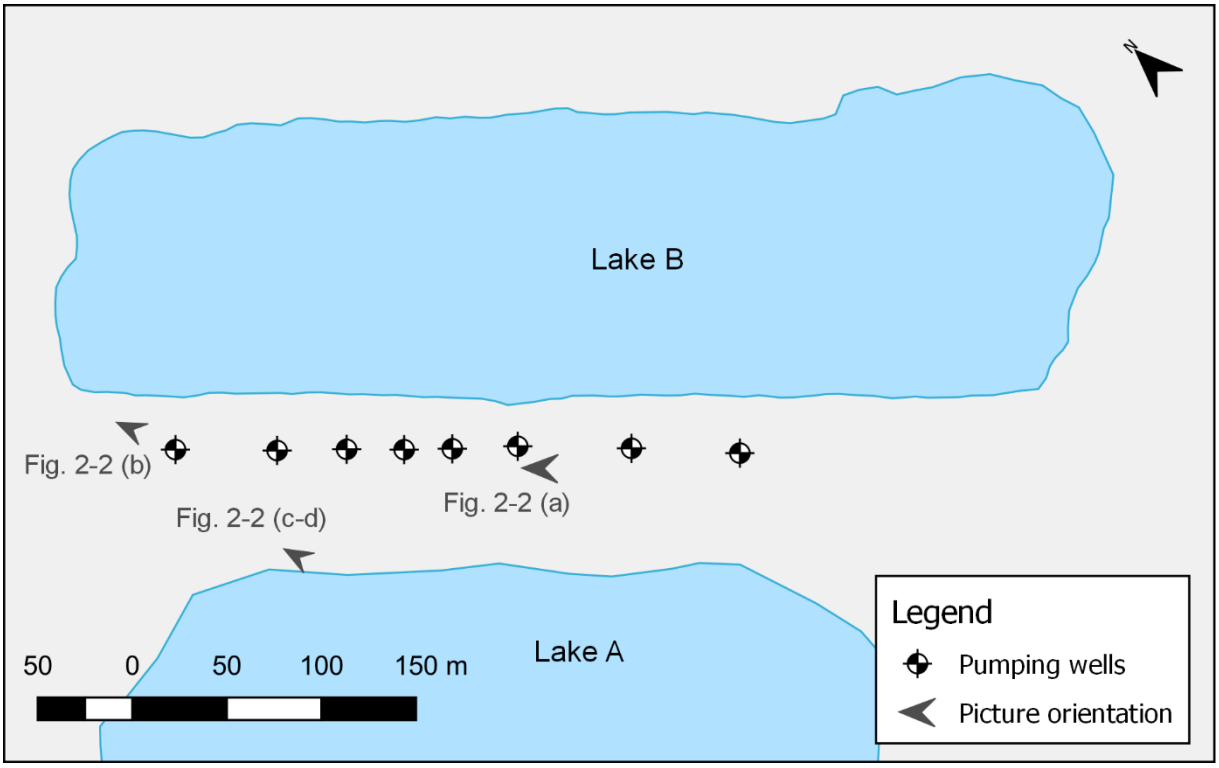

Figure A2. Location and orientation of pictures illustrated in Figure 2-4.

The bathymetry of Lake A and Lake B was performed by the Government of Quebec (Ministère de l'Environnement du Québec, 1985).

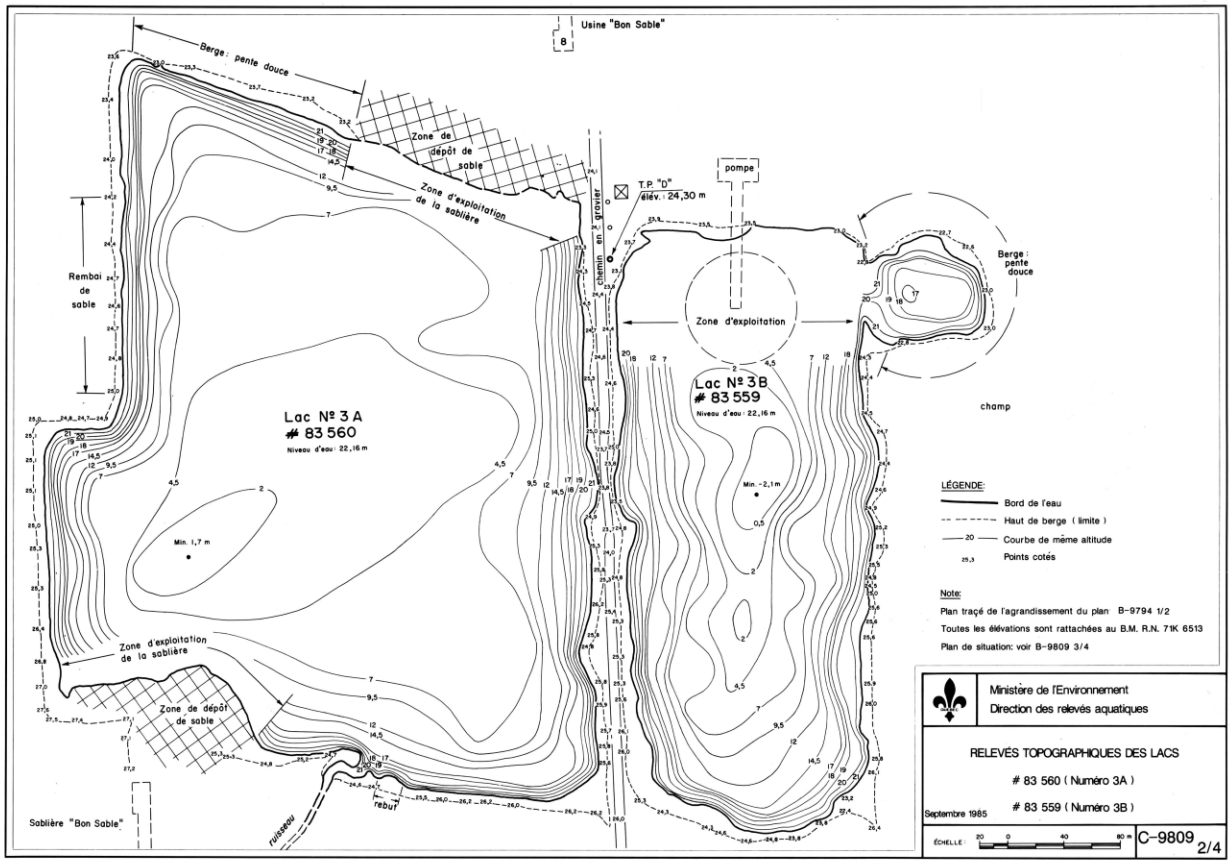

Figure A3. Bathymetry of Lake A (Ministère de l'Environnement du Québec, 1985).

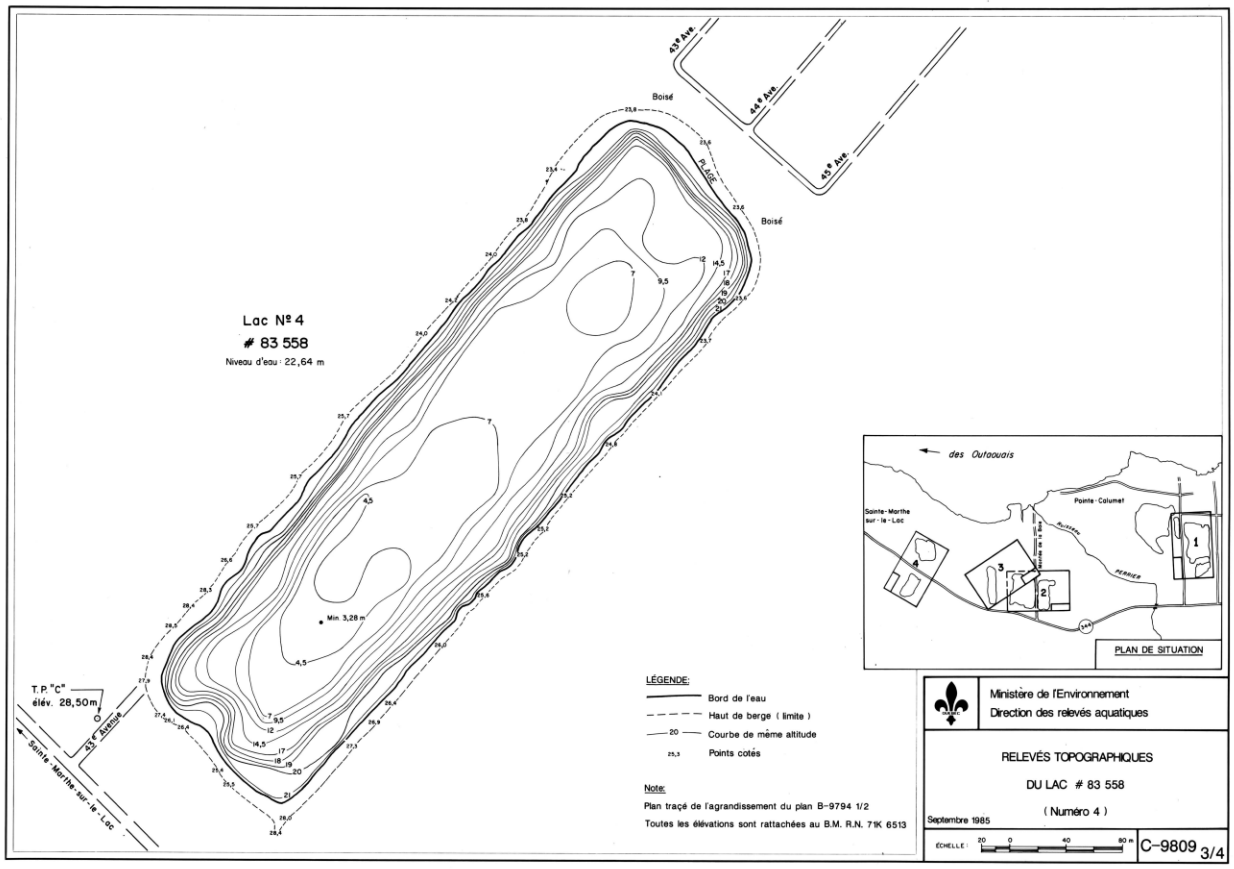

Figure A4. Bathymetry of Lake B (Ministère de l'Environnement du Québec, 1985).

APPENDIX B SUPPLEMENTARY MATERIAL – ARTICLE #2

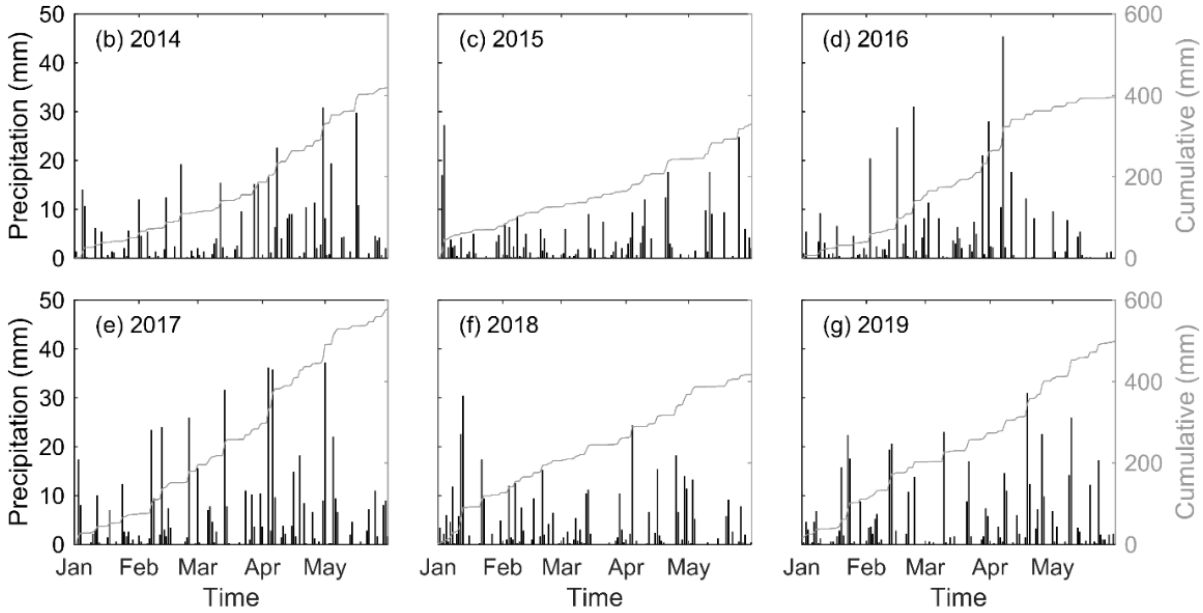

Figure B1. Daily precipitations (on left axis) and cumulative precipitations from January to May (on right axis) from 2014 to 2019. The data was obtained from Environment and Climate Change Canada database ©.

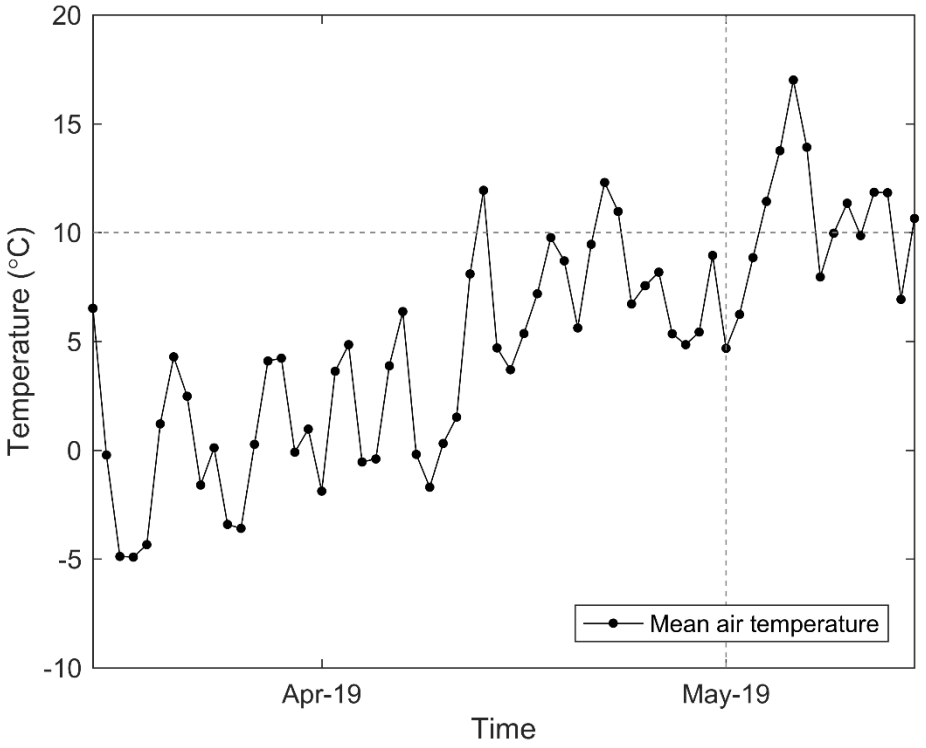

Figure B2. Daily mean air temperature from mid-March to mid-May 2019. The data was obtained from Environment and Climate Change Canada database ©.

APPENDIX C COMPLEMENTARY INFORMATION TO FIGURE 6-1

Table C1. Detailed source information and download links for the openly available geospatial data in Figure 6-1. All data are openly available and are used in accordance with the Open Government Licence – Canada or the Open Data Policy, M-13-13 of the United States Census Bureau.

Layer	Database description	Author	Year	Database website	Download link (if applicable)
Canada borders (contours)	Provinces and territories (cartographic boundary file)	Statistics Canada©	2016	https://www12.statcan.gc.ca/census-recensement/2011/geo/bound-limit/bound-limit-2016-eng.cfm	From database website
USA borders (contours)	Nation and states (cartographic boundary file)	United States Census Bureau©	2018	https://www.census.gov/geographies/mapping-files/time-series/geo/carto-boundary-file.2018.htmll	From database website
Ottawa River watershed	Ontario watershed boundaries	Provincial Mapping Unit, Government of Ontario©	2019	https://geohub.lio.gov.on.ca/datasets/53a1c537b320404087c54ef09700a7db?geometry=-108.934%2C40.791%2C-53.431%2C51.408	From database website
Urban area	Census metropolitan area (cartographic boundary file)	Statistics Canada©	2016	https://www12.statcan.gc.ca/census-recensement/2011/geo/bound-limit/bound-limit-2016-eng.cfm	From database website
Lakes and streams	National Hydrographic Network (NHN_0210001 and NHN_02OAA01)	Natural Resources Canada©	2017	https://www.nrcan.gc.ca/science-and-data/science-and-research/earth-sciences/geography/topographic-information/geobase-surface-water-program-geeau/national-hydrographic-network/21361	https://ftp.maps.canada.ca/pub/nrcan_rncan/vector/geobase_nhn_rhn/shp_en/02/
	CanVec Hydro (watercourse_1 and waterbody_2)	Natural Resources Canada©	2017	https://ftp.maps.canada.ca/pub/nrcan_rncan/vector/canvec/shp/	https://ftp.maps.canada.ca/pub/nrcan_rncan/vector/canvec/shp/Hydro/
Flooded area	Flood Extent Polygon (Lac des Deux Montagnes, Quebec - 2017-05-06 22:54:32)	Natural Resources Canada©	2017	https://open.canada.ca/data/en/dataset/34085f6d-106a-41af-a29b-53ed6947c249	ftp://data.eodms-sgdot.nrcan-rncan.gc.ca/EGS/2017/Flood_Products/QC/

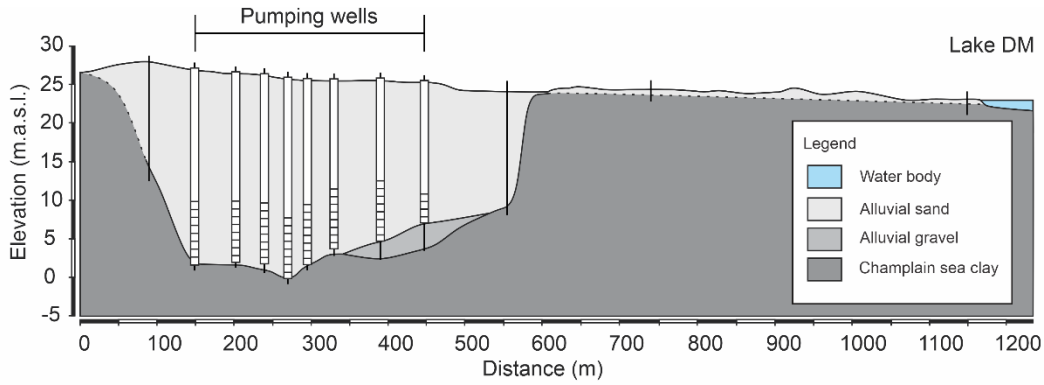

Figure C1. Geological cross-section along the pumping wells showing the buried valley carved into the Champlain Sea clays and filled with alluvial gravels and sands.

APPENDIX D COMPUTATION OF ISOTOPE MASS BALANCE PARAMETERS

The parameter $f(u)$, for the estimation of E (Eq. (5)), is calculated according to the area-dependent expression described by McJannet et al. (2012):

$$f(u) = (2.36 + 1.67u)A^{-0.05} \quad (6)$$

where u is the wind speed (m s^{-1}) measured at 2 m above the ground and A is the area (m^2) of the lake. Note that Eq. (6) was developed for land-based meteorological data.

The isotopic composition of the evaporating moisture (δ_E) is estimated based on the Craig and Gordon (1965) model and, as described by Gonfiantini (1986), is:

$$\delta_E = \frac{\frac{(\delta_L - \varepsilon^+)}{\alpha^+} - h\delta_A - \varepsilon_K}{1 - h + 10^{-3}\varepsilon_K} \ (‰) \quad (7)$$

where h is the relative humidity normalized to water surface temperature (in decimal fraction), δ_A is the isotopic composition of atmospheric moisture (described later on), ε^+ is the equilibrium isotopic separation and ε_K is the kinetic isotopic separation, with $\varepsilon^+=(\alpha^+-1)10^3$ and $\varepsilon_K=\theta*C_K(1-h)$. α^+ is the equilibrium isotopic fractionation, θ is a transport resistance parameter and C_K is the ratio of molecular diffusivities of the heavy and light molecules. θ is expected to be close to 1 for small lakes (Gibson et al., 2015) and C_K is typically fixed at 14.2 ‰ and 12.5 ‰ for $\delta^{18}O$ and δ^2H respectively in lake studies as these values represent fully turbulent wind conditions (Horita et al., 2008). Experimental values for α^+ were used (Horita & Wesolowski, 1994):

$$\alpha^+(^{18}O) = \exp\left[-\frac{7.685}{10^3} + \frac{6.7123}{(T+273.15)} - \frac{16666.4}{(T+273.15)^2} + \frac{350410}{(T+273.15)^3}\right] \quad (8a)$$

$$\alpha^+(^2H) = \exp\left[1158.8\left(\frac{(T+273.15)^3}{10^{12}}\right) + 1620.1\left(\frac{(T+273.15)^2}{10^9}\right) + 794.84\left(\frac{(T+273.15)}{10^6}\right) - \frac{161.04}{10^3} + \frac{2999200}{(T+273.15)^3}\right] \quad (8b)$$

where T is the water surface temperature (°C), which was estimated according to the equilibrium method as described by de Bruin (1982) (see Appendix D).

The parameters m and δ_s, for the computation of δ_L (Eq. (3)), are calculated as (Gibson, 2002):

$$m = \frac{\left(h - 10^{-3} \cdot \left(\varepsilon_K + \frac{\varepsilon^+}{\alpha^+}\right)\right)}{(1 - h + 10^{-3} \cdot \varepsilon_K)} \quad (9)$$

$$\delta_S = \frac{\delta_I + mX\delta^*}{1 + mX} \quad (10)$$

where, and δ^* is the limiting isotopic composition that the lake would approach as V → 0 and is calculated as:

$$\delta^* = \left(h\delta_A + \varepsilon_K + \frac{\varepsilon^+}{\alpha^+}\right) \Big/ \left(h - 10^{-3} \cdot \left(\varepsilon_K + \frac{\varepsilon^+}{\alpha^+}\right)\right) \quad (11)$$

The isotopic composition of atmospheric moisture (δ_A) is estimated using the partial equilibrium model of Gibson et al. (2015):

$$\delta_A = \frac{\delta_P - k\varepsilon^+}{1 + 10^{-3} \cdot k\varepsilon^+} \quad (12)$$

where δ_P is the isotopic composition of precipitation and k is a seasonality factor, fixed at 0.5 in this study. The k value (ranging from 0.5 to 1) is selected to provide a best-fit between the measured and modelled local evaporation line. In Eq. (12), δ_P and monthly exchange parameters (ε^+, α^+ and ε_K) are evaporation flux-weighted based on daily evaporation records.

APPENDIX E COMPARISON OF THE EVAPORATIVE FLUXES (E) ESTIMATIONS

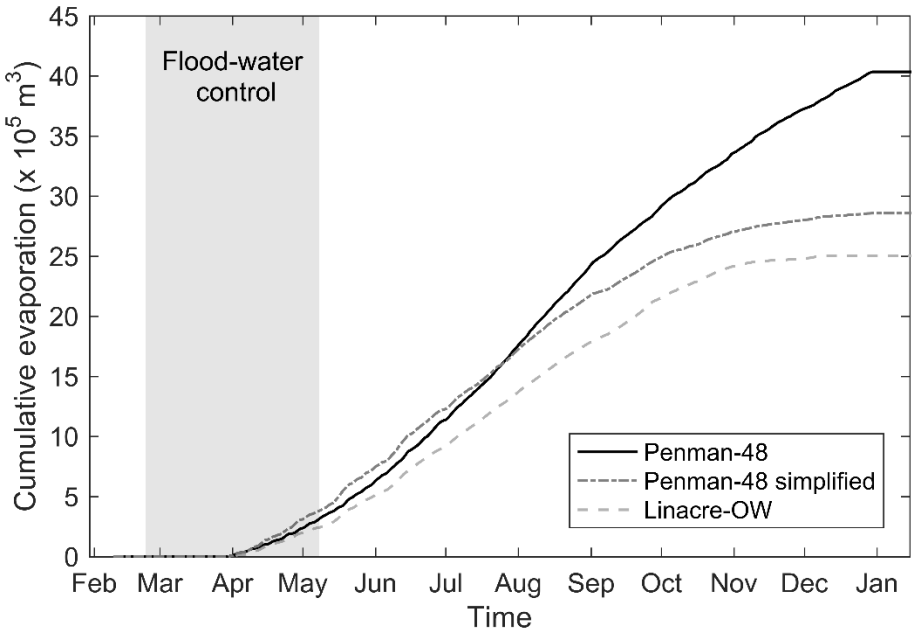

Figure E1. Cumulative evaporative fluxes from Lake A via the Penman-48, Penman-48 simplified method (Valiantzas, 2006) and Linacre-OW (Linacre, 1977) methods.

APPENDIX F ESTIMATION OF THE WATER SURFACE TEMPERATURE BASED ON THE EQUILIBRIUM METHOD (DE BRUIN, 1982)

The water surface temperature (T) was estimated via the equilibrium method presented by de Bruin (1982), because no continuous measurements were available. This model is based on the assumption of a well-mixed surface body and was developed from standard land-based weather data. It was tested on two adjacent reservoirs in the Netherlands with average depths of 5 m and 15 m, respectively. Similarly to de Bruin (1982), we used the 10-day mean values, because we are interested in the annual variations of the water temperature. Moreover, the 10-day mean values were found to better simulate the observed water surface temperature. Differences between the observed and modelled water temperature is typically ≤1 °C, except in July and December where discrepancies of up to 5 °C were observed (Fig. E1). This is likely because Lake A develops a thermal stratification over summertime and in wintertime. Potential uncertainties in isotopic mass balance models due to stratification in lakes up to 35 m were previously described and discussed by Gibson et al. (2017) and Gibson et al. (2019). They reported that sampling methods and lake stratification can lead to volume-dependent bias in the water balance partition. In this study, not accounting fully for thermal stratification will lead to overestimation of evaporation fluxes, and groundwater exchange will potentially be underestimated.

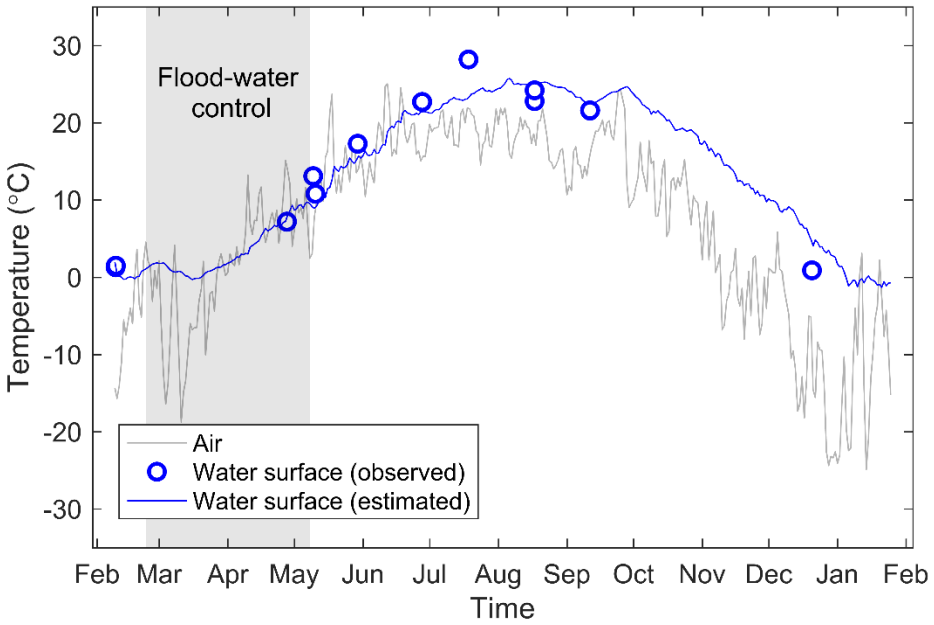

Figure F1. Temporal evolution of air temperature and observed and estimated water surface temperatures at Lake A. Water surface temperature estimations were computed according to the equilibrium method described by de Bruin (1982).

APPENDIX G ISOTOPIC COMPOSITION ALONG VERTICAL PROFILES IN LAKE A

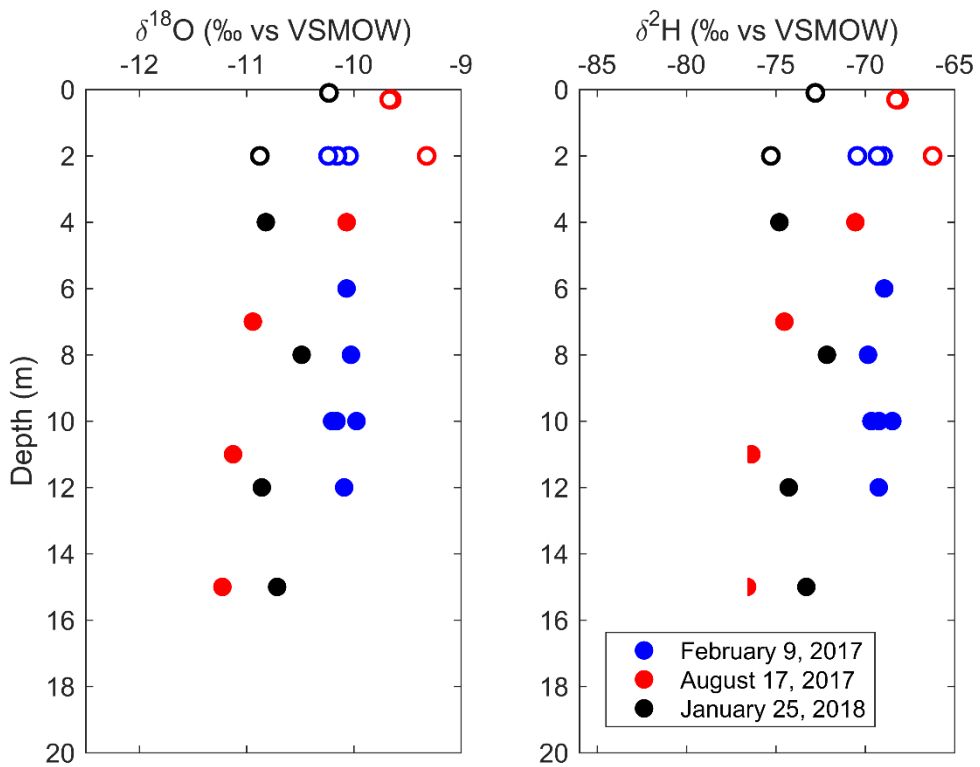

Figure G1. Isotopic composition of Lake A water samples against depth on February 9, 2017, August 17, 2017 and January 25, 2018. The hollow circles and solid circles represent samples collected at ≤2 m depth and >2 m, respectively.

APPENDIX H RESULTS OF THE SENSITIVITY ANALYSIS FOR REFERENCE SCENARIOS A AND B

Table H1. Sensitivity analysis on the input parameters of the isotopic mass balance model. Q is the output flux from Lake A, I the input flux and t_f the mean flushing time.

Scenario		Maximum Q	Minimum Q	Mean Q		Mean I		t_f
				Flooding	Annual	Flooding	Annual	
		(x 10^4 m^3/day)	(x 10^4 m^3/day)	(x 10^4 m^3/day)		(x 10^4 m^3/day)		(days)
A	Reference	8.0	3.7	5.64	4.77	6.61	4.86	97
A01	V + 3% (slope 30°)	8.0	3.7	5.64	4.77	6.61	4.86	100
A02	V - 8% (slope 20°)	7.8	3.7	5.55	4.72	6.51	4.81	93
A03	δ_{Is} ^{18}O + 0.5 ‰ δ_{Is} ^{2}H + 4.06 ‰	25.0	1.0	11.82	6.99	12.79	7.08	66
A04	δ_{Is} ^{18}O - 0.5 ‰ δ_{Is} ^{2}H - 4.06 ‰	4.3	4.2	4.25	4.22	5.21	4.31	109
A05	δ_G ^{18}O + 0.5 ‰ δ_G ^{2}H + 4.06 ‰			Not possible to fit data				
A06	δ_G ^{18}O - 0.5 ‰ δ_G ^{2}H - 4.06 ‰	10.0	1.0	5.06	3.25	6.02	3.34	141
A07	δ_A minimum			Not possible to fit data				
A08	δ_A maximum	8.0	4.0	5.80	5.00	6.77	5.09	92
A09	E + 20%	8.0	4.8	6.24	5.60	7.22	5.72	82
A10	E - 20%	8.0	2.7	5.09	4.02	6.05	4.09	115
A11	RH + 10%			Negligible change				
A12	RH - 10%							
A13	T_{air} + 10%	8.0	3.9	5.75	4.92	6.71	5.01	94
A14	T_{air} - 10%	8.0	3.5	5.53	4.62	6.50	4.71	100
A15	U + 10%	8.0	3.9	5.75	4.92	6.72	5.01	94
A16	U - 10%	8.0	3.6	5.58	4.70	6.55	4.78	98
A17	P + 10%			Negligible change				
A18	P - 10%							
A19	$T = T_{air}$	10.0	2.9	6.10	4.67	7.07	4.73	100
A20	Rs + 10%	8.0	3.9	5.75	4.92	6.72	5.02	94
A21	Rs - 10%	8.0	3.6	5.58	4.70	6.55	4.78	98
A22	LMWL (PWLSR method)	7.0	1.6	4.04	2.95	5.00	3.03	155

Table H2. Sensitivity analysis on the input parameters of the isotopic mass balance model for the reference scenario B. Q is the output flux from Lake A, I the input flux and t_f the mean flushing time.

	Scenario	Maximum Q	Minimum Q	Mean Q		Mean I		t_f
				Flooding	Annual	Flooding	Annual	
		(x 10^4 m^3/day)	(m^3/day)	(x 10^4 m^3/day)		(x 10^4 m^3/day)		(days)
B	Reference	28.0	1.0E+03	12.68	7.07	13.65	7.16	66
B01	V + 3% (slope 30°)	28.0	1.0E+01	12.63	6.99	13.59	7.07	69
B02	V - 8% (slope 20°)	26.0	1.0E+01	11.73	6.49	12.69	6.57	68
B03	δ_{Is} ^{18}O + 0.5 ‰ δ_{Is} ^{2}H + 4.06 ‰			Not possible to fit data				
B04	δ_{Is} ^{18}O - 0.5 ‰ δ_{Is} ^{2}H - 4.06 ‰	12.0	2.5E+04	6.78	4.87	7.75	4.95	95
B05	δ_G ^{18}O + 0.5 ‰ δ_G ^{2}H + 4.06 ‰			Not possible to fit data				
B06	δ_G ^{18}O - 0.5 ‰ δ_G ^{2}H - 4.06 ‰			Not possible to fit data				
B07	δ_A minimum	26.0	1.0E+01	11.73	6.49	12.69	6.57	72
B08	δ_A maximum			Negligible change				
B09	E + 20%	28.0	1.0E+04	13.18	7.74	14.15	7.84	60
B10	E - 20%	27.0	1.0E+01	12.18	6.74	13.13	6.80	69
B11	RH + 10%			Negligible change				
B12	RH - 10%							
B13	T_{air} + 10%			Negligible change				
B14	T_{air} - 10%							
B15	U + 10%	28.0	2.0E+03	12.74	7.14	13.70	7.23	65
B16	U - 10%	28.0	1.0E+01	12.63	6.99	13.59	7.08	66
B17	P + 10%			Negligible change				
B18	P - 10%							
B19	T = T_{air}	28.0	1.0E+01	12.63	6.99	13.60	7.05	67
B20	Rs + 10%	28.0	3.0E+03	12.79	7.22	13.76	7.31	64
B21	Rs - 10%	28.0	1.0E+01	12.63	6.99	13.59	7.07	67
B22	LMWL (PWLSR method)	16.0	1.0E+01	7.22	4.00	8.18	4.08	115

APPENDIX I ARTICLE 4: BANK FILTRATION FROM FLOOD-AFFECTED QUARRY LAKES: ISSUES AND SOLUTIONS IN A COLD CLIMATE (CANADA)

This chapter was submitted as a research paper in the special issue *Managed aquifer recharge (MAR)* in the journal *Groundwater* in September 2021.

Masse-Dufresne, J., Baudron, P., & Barbecot, F. (submitted). Bank filtration from flood-affected quarry lakes: issues and solutions in a cold climate (Canada)

ABSTRACT

We present a synthesis of knowledge obtained from 9 years of operation of a 2-lake bank filtration (BF) drinking water plant located in the floodplain of a snowmelt-affected 1300 km long river in the province of Quebec (Canada). Raw water is extracted by eight wells installed in a narrow sandbar separating two 20 m deep quarry lakes that frame the width and depth of the aquifer in a seasonally flooded paleo-channel. This unique hydrological and hydrogeological context induces several specific features: insignificant direct contribution from regional groundwater to the wells; high sensitivity to surface water quality due to short travel distances; substantial impact of springtime freshets to surface water quality and groundwater flow pattern; microbiological blooms and biogeochemical reactions driven by springtime and autumn turnovers in the lakes. In addition to these natural features, fluctuating operating conditions confer a highly transient groundwater flow. To cope with the challenge of maintaining high quality drinking water, several state-of-the-art monitoring, operational and/or post-treatment solutions have been tested and implemented, some of them within research projects, in the last decade. Post-treatment includes biological filtration (Mangazur®) and nanofiltration (NF90 FilmtecTM) technologies, while research projects including isotopic, geochemical and microbial approaches helped quantifying the importance of surface water renewal from yearly recurring floods at the scale of the ungauged floodplain, anticipating water quality changes with spatiotemporal-resolved water quality monitoring, highlighting the role of pumping schemes on maintaining high raw water quality and to anticipating microbial blooms and breakthrough.

Introduction

In cold climate regions, the hydrological cycle is strongly influenced by snow precipitations and snowmelt waters (Barnett et al., 2005). In fact, peak discharge of rivers and streams is typically observed during spring thaw, in response to snowpack melting over watersheds. These events, known as freshets, often result in the inundation of floodplains in the vicinity of watercourses. As the intensity and the timing of these inundations are hard to predict, operating bank filtration (BF) systems in these regions can be challenging. In the province of Quebec (Canada), 74% of groundwater-sourced drinking water is supplied by municipal wells located at < 500 m from a surface water body, thus potentially performing BF (Patenaude et al., 2020). In this context, the operation of numerous drinking water production plants could benefit from the lessons learnt at a reference BF site.

Located 50 km from the city of Montreal, the studied BF system combines several noteworthy hydrological and geological settings, including two 20-m deep quarry lakes as source waters which develop thermal stratification and experience springtime and autumn turnovers, a paleo-channel constraining the geometry of the aquifer and limiting the contribution of direct regional groundwater, and a yearly recurring surficial hydraulic connection with a 1300 km-long river that causes flooding during springtime freshets. These aspects, added to evolving operational conditions through space (i.e., along the wellfield) and time (varying water demand), end up setting highly transient groundwater flow.

A thorough monitoring program of the source waters and raw abstracted water, together with a proactive investment strategy and a tight collaboration with researchers, allow the town to produce high-quality drinking water year-round. This paper aims at highlighting the main characteristics of this BF facility, to emphasize on its unique and noteworthy aspects and illustrate the lessons learnt from one decade of operation and research projects.

Project Overview

Project timeline

The planning of a multiple-well BF system for the town was initiated in 2006. At this time, the inhabitants were supplied surface-sourced drinking water produced in a neighbouring town. Recurring water pressure issues during summertime, frequent consumption restrictions, boil

advisories and rapid demographic growth motivated the construction of a new drinking water production system. With the objective of producing high-quality drinking water at low-cost, the town opted for a two-lake BF system as a promising solution. The pumping wells were constructed in 2010 and the system became operational as of October 2012 (Figure I1).

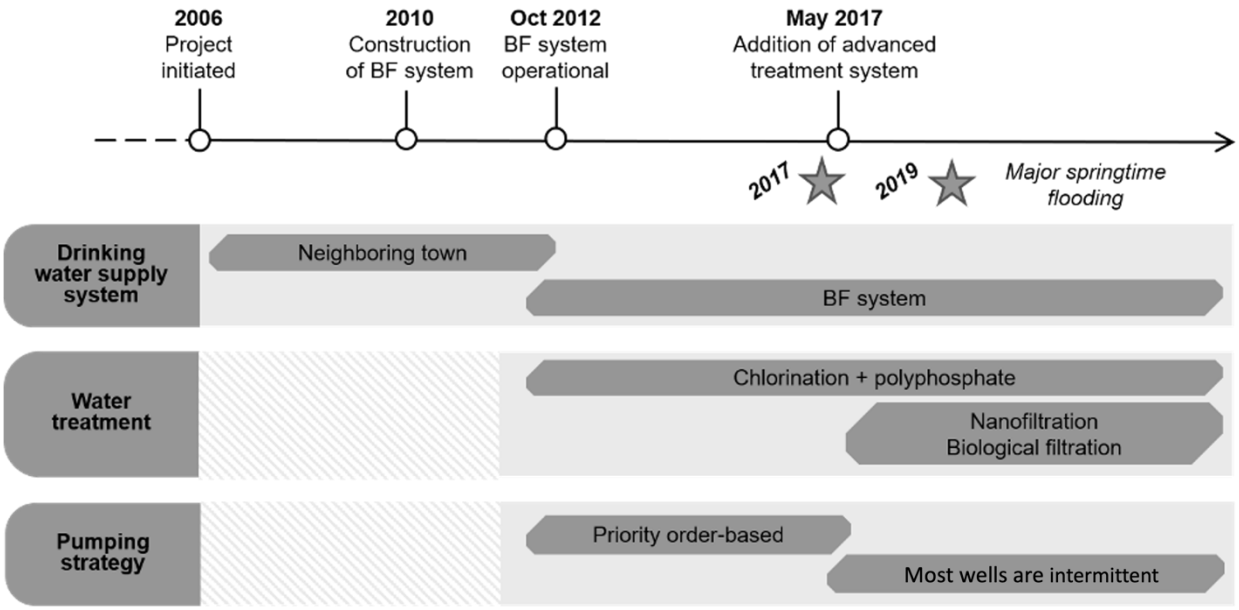

Figure I1. Timeline of the drinking water supply and treatment solutions

Design and operation of the pumping wells

The drinking water production system relies on seven pumping wells, plus an eighth to ensure system redundancy. They are spaced 30 m to 60 m apart and are located at 70 m to 80 m and 30 m to 35 m from two quarry lakes (Figure I2). Hydraulic conductivity is estimated at 2.7×10^{-3} m/s (Ageos, 2010). Mean annual distributed drinking water volume is 2.2 x 10^6 m^3 and daily pumped volume fluctuates from 4.6 x 10^3 m^3 (in November) to 7.5 x 10^3 m^3 (in June). Up to April 2017, the pumping wells were operated according to a quality-based priority order. Typically, the same two wells were solicited continuously, and one to four other wells were used intermittently to fulfill the daily or seasonal peak water demand. The two remaining wells were only activated monthly to perform the routine sampling program. Since May 2017 (see next sub-section), most wells are solicited intermittently, with less weight given to priority order strategies.

Raw water treatment solutions

On the initiation of the BF plant, the raw pumped water was only chlorinated, and a polyphosphate treatment was used to stabilize iron and manganese in the distribution system. On May 2017, with the objective of lowering Fe and Mn concentrations and total hardness in the distributed drinking water, an advanced treatment system consisting of biological filtration (Mangazur®) and nanofiltration (NF90 FilmtecTM) technologies was added to the post-BF treatment sequence.

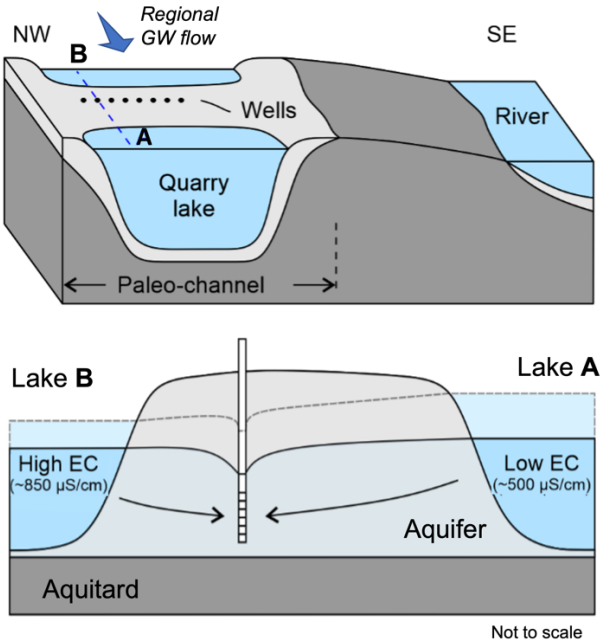

Figure I2. Schematic representation of the hydrogeological setting of the bank filtration system

Project Highlights

Unique hydrological and hydrogeological context

At the location of the BF system, the aquifer consists in a narrow (100m wide) sandy bar that roughly matches the depth and width of the two quarry lakes (i.e., Lake A and Lake B), thus framing the extent of the wellfield (Figure I2). In this context, the pumping wells are fed with the recently infiltrated water from Lake A and Lake B. The short travel distances provide a high sensitivity to surface water quality (Masse-Dufresne et al., 2019b). As opposed to the majority of existing BF sites, direct contribution from regional groundwater is believed to be not significant. Groundwater fluxes, together with precipitation and evaporation, contribute to the water balance

of both lakes. Direct surface water inputs, described thereafter, only contribute to Lake A. As a result, the two lakes have distinct geochemistry. Lake A is characterized by bicarbonate-calcium facies and low EC (~500 µS/cm), and Lake B has a chloride-sodium facies and high EC (~850 µS/cm).

Seasonality of source water quality

Source water quality in both quarry lakes evolves at different timescales and depending on both external and internal drivers. Firstly, the river water level rises during the springtime freshets. When a topographic threshold is attained, a hydraulic connection establishes with Lake A and surface water from the river can flow to Lake A. During the more intense events, part of the floodplain, including lake A, is inundated and the contribution of floodwater inputs to Lake A are significant. Secondly, internal processes favorized by the depth of the quarry lakes regularly drive seasonal evolution of their quality. Firstly, thermal stratification establishes (Masse-Dufresne et al., 2019b) and limits the exchange between the epilimnion and hypolimnion and stimulate depth-dependent water quality, as found in similar contexts (Diao et al., 2017). Secondly, twice a year (during springtime and autumn), this thermal stratification is disrupted by turnovers of the water column. Such mixing of the water column can favorize microbiological blooms and drive redox-dependant geochemical reactions (Diao et al., 2017). Note that at the studied BF site, the quality of distributed drinking water is independent from these natural processes, although they can affect the raw groundwater. Still, anticipating and predicting such processes, particularly in sensible periods of the year, is useful to optimize the post-treatment characteristics.

Transience of the BF system

The spatiotemporal variability of several physico-chemical indicators at the pumping wells testifies for a high transience of groundwater flow at the wellfield, related to seasonal variability of the lakes' water levels and daily variability of pumped volumes. Groundwater temperature at the pumping wells show a strong temporal evolution. Minimum (3°C to 4.1°C) and maximum (14.1°C and 17.9°C) values being observed during springtime and autumn, respectively (Figure I3a), illustrate the rapid infiltration of surface water. Such values also vary spatially along the wellfield, with temperature differences reaching up to 14°C between two wells located at only tenths of meters of distance and during one sampling campaign. EC also varies largely through space and time at the pumping wells, and typically ranges between ~500 µS/cm and ~850 µS/cm (Figure I3b).

These low-EC and high-EC values are representative of the measurements made in the two quarry lakes, revealing a variability of the contribution of each one to the pumped groundwater (Masse-Dufresne et al., 2019b). Additional insights of the spatiotemporal variability of the origin of water can be provided by stable isotopes of water (Figure I3c), as further discussed in the Lessons Learnt section.

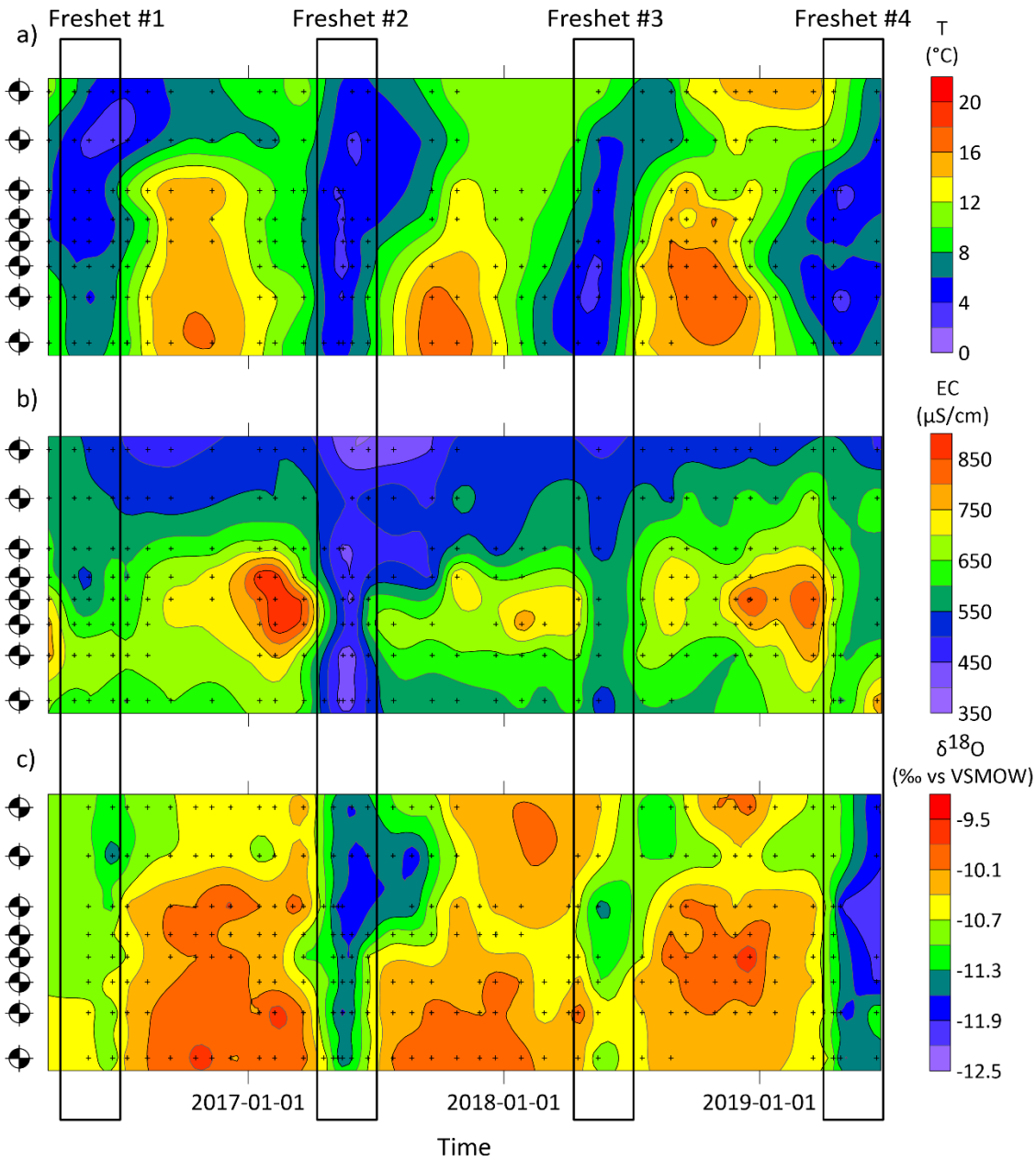

Figure I3. Spatiotemporal variability of a) temperature (T), b) electrical conductivity (EC), and c) δ18O from March 2016 to June 2019. Ordinary kriging was used to interpolate between the observed

data, which is represented by the cross symbols (+). On the y-axis are the 8 pumping wells, as positioned at the study site.

Lessons Learned

Resilience of surface water reservoirs

In order to examine the control of flooding on the surface water quantity and quality of Lake A, i.e. the larger surface water reservoir of the BF system, floodwater inputs to the lake were quantified using an isotopic mass balance model (Masse-Dufresne et al., 2021a). Both direct floodwater inputs and delayed floodwater inputs (i.e., due to bank storage and/or floodplain recharge) were determined, and their sum was found to represent nearly 50% of the annual lake water budget. This has important implications for the renewal of this surface water resource and for maintaining the actual lake water quality. In fact, floodwater inputs contribute to maintain lower salinity and hardness in comparison to Lake B (Masse-Dufresne et al., 2021a). Performing such balance for Lake B, where groundwater discharges from Lake A through the bank as evidenced with dissolved ^{222}Rn (Masse-Dufresne, unpublished data) would be a great output to complete an integrated water balance of the whole hydrosystem.

Low-cost EC monitoring helps to anticipate the origin of water

Given that the two quarry lakes are characterized by distinct EC values, a transient EC-based binary mixing model, based on data from the periodic monitoring program, demonstrated that the contributions from each quarry lake can range from 0% to 100% spatially and temporally across the BF system (Masse-Dufresne et al., 2019b). Such information was unexpected and of high importance for the managers, as previous studies rather proposed a single value for the whole wellfield. Differences between continuously, intermittently, and occasionally active wells were also found, with less variable mixing ratios for the first (mixed origin) and the last ones (mostly Lake A), respectively. The spatiotemporal variability of mixing ratios is thus both controlled by the pumping schemes (i.e., pumping rates and frequency of in-service) and the hydrological conditions (i.e., water level differences between the two quarry lakes) as deciphered by (Masse-Dufresne et al., 2019b).

Timescale of floodwater contribution to abstracted groundwater

The spatiotemporal evolution of the geochemical facies, EC and $\delta^{18}O$ of the bank filtrate proved to be complementary to understand the role of springtime floods on the BF system (Masse-Dufresne et al., 2021b). Indeed, during the beginning of the 2017 springtime flood event, the geochemical facies of the abstracted water at the pumping well P1 evolved within a few weeks from a mixture between the two lakes (respectively blue and red for Lakes A and Lake B, in Figure I4a), to the water type observed at Lake A (Figure I4b). On the flood peak, one month later (Figure I4c), the same water type was observed at all sampling locations across the sandy bank, meaning that Lake A water completely overpassed the hydraulic barrier established by pumping between the two lakes. After the flood, geochemical facies evolved globally towards normal conditions within a 1-month timescale (Figure I4d and e), although pumped water remained only composed of bank filtrate from Lake A.

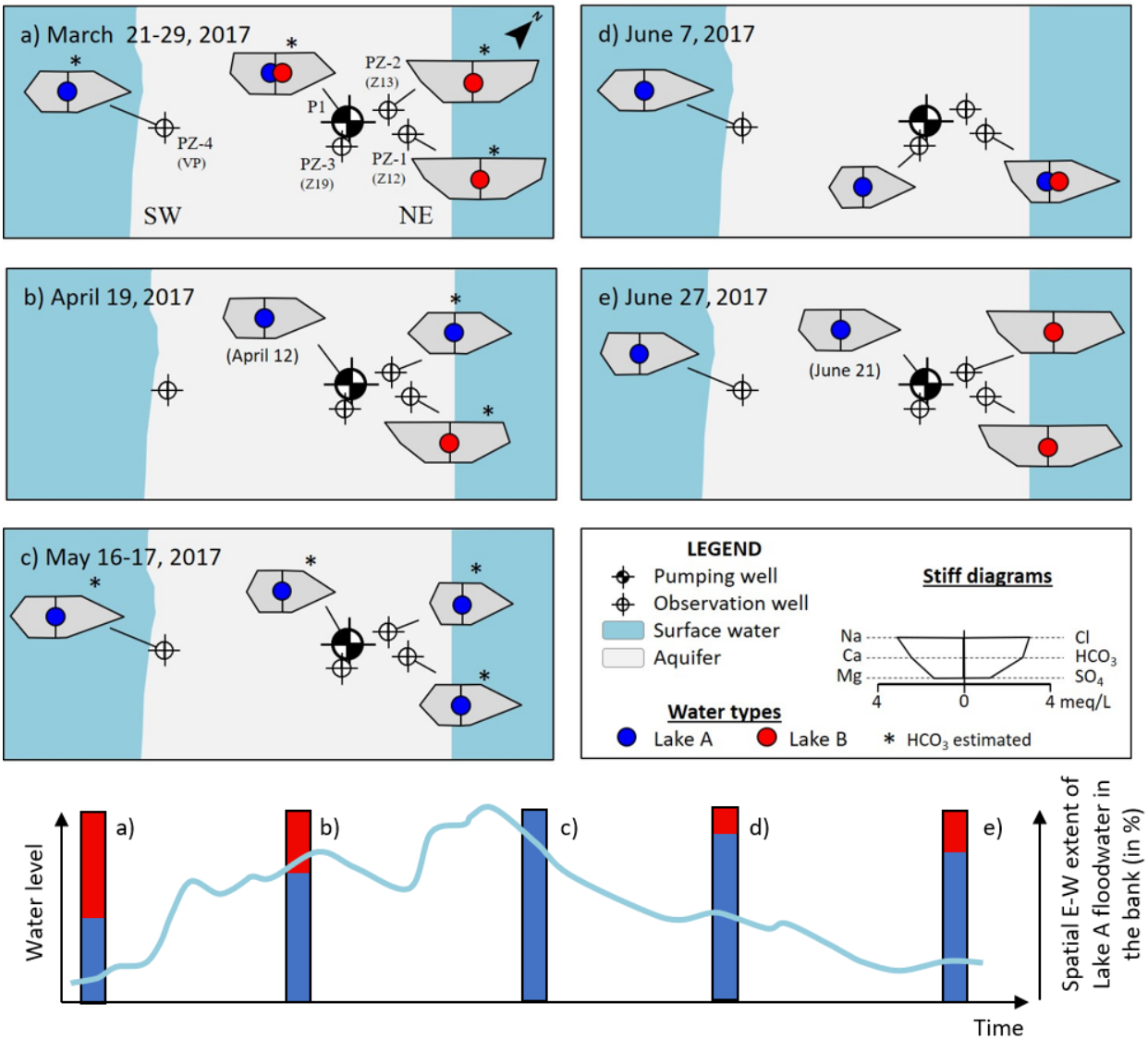

Figure I4. Temporal evolution of the bank filtrate and pumped water geochemical facies from pre- to post-flood event in 2017 at a transversal cross section passing by pumping well P1.

Post-flood recovery dependence on pumping schemes

The timescale of groundwater water post-flood recovery was shown to be dependent on the respective pumping regime of each well (Masse-Dufresne et al., 2021b), as illustrated by stable isotopic composition in Figure I3c: during the 2017 springtime freshet, groundwater from the upper part of the Figure (mostly occasional pumping) remained marked by relatively depleted snowmelt-originated water (blue color) months after the spring freshet, while groundwater from the lower part of the Figure (mostly continuous pumping), rapidly returned to a relatively enriched mean lake

composition water (orange to red color). Despite apparent recovery, snowmelt-originated groundwater storage can therefore remain months later in the aquifer matrix depending on pumping schemes. Isotopic monitoring also revealed that not all flooding events have an important contribution and rapid travel of floodwater to the pumping wells: depleted signatures ($\delta^{18}O$ = -11.5 ‰ to -12.5 ‰) were only observed during two major springtime flooding events illustrated by Figure I3b (freshets 2 and 4).

Anticipating microbial blooms and breakthrough

Pazouki et al. (2016) demonstrated that both quarry lakes at the studied BF system are prone to cyanobacteria blooms, and that rapid travel times (< 2 days) allow for the passage of cyanobacteria cells through the aquifer. Automated and low-cost depth-resolved continuous measurements of the lake's water temperature (Masse-Dufresne et al., 2019a) allowed to examine thermal stratification and the timing and duration of the autumnal turnovers. This knowledge concerning the lake stratification and water column turnover helped the water managers anticipate microbial contamination risks.

Tracer-based pumping strategies to control Fe and Mn concentrations

To limit the concentrations in Fe and Mn in the pumped water, specific pumping schemes were designed according to a concentration-based priority order, and then strengthened with a tracer-based monitoring approach (Masse-Dufresne et al., 2019b). The operation of the pumping wells on a continuous basis was shown to lower (at best) the total Fe and total Mn concentrations. Such pumping strategy likely allowed to limit the mobilization of particulate Fe in the vicinity of the pumping wells and to benefit from the mixing between Lake A and Lake B to lower the dissolved Mn concentrations and hardness. Wells operating on an occasional basis initially had the highest total Fe concentration, while operation of wells on an intermittent basis were associated with the highest total Mn concentration. The onset of an advanced post-treatment in May 2017 (biological filtration and nanofiltration) to better control the Fe and Mn concentrations and hardness was accompanied with a more intermittent operation of the wells (Masse-Dufresne, unpublished data). Interestingly, it resulted in an increase of dissolved Fe and Mn at the pumping wells. Also, the operation of a well on an occasional or intermittent basis stopped to be discriminant to predict total Fe and total Mn concentrations on the long term. A proposed explanation is that the more transient

pumping conditions from May 2017 likely induced a bias regarding the representativity of the groundwater samples.

Future Prospects

The studied BF site was shown to significantly benefit from a tracer-based approach, usually restricted to researchers, to provide deeper insights on the hydrological and hydrogeological processes controlling surface water availability and bank filtrate quantity. Time series of environmental tracers were proved to be essential to characterize such a highly transient hydrosystem. We recommend their application at the planning and operational phases in other BF sites. A more discrete monitoring would have led to limited representativity of the data and in some cases, to erroneous interpretations affecting the outputs provided to the managers. The approach was also found to be cost-effective to monitor the evolution of groundwater at the wellfield, to anticipate water quality changes and contribute to its daily management. Spatiotemporal resolved monitoring of environmental tracers is still on-going at the studied BF site. It will help anticipate future groundwater flow pattern, as a flood-proof dyke was recently constructed across the wellfield to prevent the inundation of residential area, northeastwards of Lake B. Also, new collaborative projects are being designed and developed by researchers in relation to the post-treatment system. More specifically to the groundwater part, the biotic processes that could influence the quality of the pumped water are being investigated into detail to anticipate post-treatment costs. Indeed, the important spatiotemporal variability of physico-chemical parameters are likely influencing the activity and metabolism of microbial communities in the bank filtrate and sediments. Particular attention will be paid to the spatial and temporal distribution of metal-reducing and metal-oxidizing bacteria and redox conditions in the stratified lakes and the aquifer, as it will help to better anticipate the evolution of Fe and Mn in the raw pumped water. Overall, the studied BF site can be considered as a reference site for the development of specific hydrogeological approaches on transient systems.